N°d'ordre NNT : 2017LYSE1052

THESE de DOCTORAT DE L'UNIVERSITÉ DE LYON
opérée au sein de
l'Université Claude Bernard Lyon 1

École Doctorale : Matériaux ED34

Spécialité de doctorat : Matériaux
Discipline : Matériaux innovants

Soutenue publiquement le 23/03/2017, par :
(Martha Margarita Rueda)

Rhéologie et Mise en œuvre de formulations polymères hautement chargées

---

Devant le jury composé de :

Prof. Paula Moldenaers	University of Leuven	Examinatrice
Dr. Edith Peuvrel-Disdier	Mines ParisTech - CEMEF	Rapporteure
Prof. Gilles Regnier	Art et Métiers ParisTech de Paris	Rapporteur
Dr. Philippe Sonntag	Centre de recherche Hutchinson	Examinateur
Prof. Philippe Cassagnau	Université de Lyon 1 – IMP@Lyon1	Directeur de thèse
Dr. René Fulchiron	Université de Lyon 1 – IMP@Lyon1	Co-directeur de thèse

UNIVERSITE CLAUDE BERNARD - LYON 1

Président de l'Université	**M. le Professeur Frédéric FLEURY**
Président du Conseil Académique	M. le Professeur Hamda BEN HADID
Vice-président du Conseil d'Administration	M. le Professeur Didier REVEL
Vice-président du Conseil Formation et Vie Universitaire	M. le Professeur Philippe CHEVALIER
Vice-président de la Commission Recherche	M. Fabrice VALLÉE
Directrice Générale des Services	Mme Dominique MARCHAND

COMPOSANTES SANTE

Faculté de Médecine Lyon Est – Claude Bernard	Directeur : M. le Professeur G.RODE
Faculté de Médecine et de Maïeutique Lyon Sud – Charles Mérieux	Directeur : Mme la Professeure C. BURILLON Directeur : M. le Professeur D. BOURGEOIS
Faculté d'Odontologie	Directeur : Mme la Professeure C. VINCIGUERRA
Institut des Sciences Pharmaceutiques et Biologiques	Directeur : M. X. PERROT
Institut des Sciences et Techniques de la Réadaptation	Directeur : Mme la Professeure A-M. SCHOTT
Département de formation et Centre de Recherche en Biologie Humaine	

COMPOSANTES ET DEPARTEMENTS DE SCIENCES ET TECHNOLOGIE

Faculté des Sciences et Technologies	Directeur : M. F. DE MARCHI
Département Biologie	Directeur : M. le Professeur F. THEVENARD
Département Chimie Biochimie	Directeur : Mme C. FELIX
Département GEP	Directeur : M. Hassan HAMMOURI
Département Informatique	Directeur : M. le Professeur S. AKKOUCHE
Département Mathématiques	Directeur : M. le Professeur G. TOMANOV
Département Mécanique	Directeur : M. le Professeur H. BEN HADID
Département Physique	Directeur : M. le Professeur J-C PLENET
UFR Sciences et Techniques des Activités Physiques et Sportives	Directeur : M. Y.VANPOULLE
Observatoire des Sciences de l'Univers de Lyon	Directeur : M. B. GUIDERDONI
Polytech Lyon	Directeur : M. le Professeur E.PERRIN
Ecole Supérieure de Chimie Physique Electronique	Directeur : M. G. PIGNAULT
Institut Universitaire de Technologie de Lyon 1	Directeur : M. le Professeur C. VITON
Ecole Supérieure du Professorat et de l'Education	Directeur : M. le Professeur A. MOUGNIOTTE
Institut de Science Financière et d'Assurances	Directeur : M. N. LEBOISNE

Doctoral thesis

R

Rheology and processing of highly filled materials

From fundamental understanding to elaboration process

Martha Margarita Rueda

Materials Doctoral school ED 34
University Claude Bernard, Lyon 1
Lyon, France

Supervisors

Philippe Cassagnau and René Fulchiron

January, 2017

A mis padres…

Life is like riding a bicycle. To keep your balance, you must keep moving…

-Albert Einstein-

Acknowledgements

Even though the heaviest burden of this work was on my shoulders it still would not have been possible without the support from many others. I would like to take this opportunity to acknowledge them.

First, I would like to express my sincere gratitude to my supervisors Philippe Cassagnau and René Fulchiron for their constant guidance and support throughout these three years. They have taught me, both consciously and un-consciously, how good experimental rheology is done. Thanks for encouraging and supporting my attendance at various conferences and workshops, engaging me in new ideas, nourishing my scientific culture and allowing me to discover different people and places in Europe. I am also deeply thankful for their high reactivity, in particular during this demanding last writing period. They were always available for me at any time. Thanks for sharing with me a little part of your broad knowledge in this matter, and especially for teaching me to always be focused on what is important.

I would like to acknowledge the Hutchinson Research Center for funding this work. I am very grateful to Philippe Sonntag and Nicolas Garois who give me the opportunity to do this thesis thanks to the joint-laboratory between Hutchinson and the IMP. Thanks for their precious remarks, advice, directive lines and support after each meeting. I would like also to thank Grégory Martin and Arnaud Prebé for their industrial guidance especially at the moment at which I needed it the most, during my first year of thesis. It was a real pleasure, each one of our scientific or non-scientific discussions. Special thanks to Arnaud Prebé and David Aymme-Perrot with whom I made my first step in the Hutchinson family. Thanks for believing in me and giving me the opportunity to work with you, I really appreciated this first experience of internship. The latter opens up to me the possibility to pursue the study of highly filled materials. Thanks to Aurélie Bergeron-Vanhille for always being available for any question, for their accurate remarks, advice and for her investment in consolidating the Hutchinson team inside of the lab.

I would also take this opportunity to thank Alvaro Ramirez who introduced me to the polymer science and whose enthusiasm and love for the science has had a lasting effect. I would like also to acknowledge Lionel Choplin who has always offered me his support, leading to new opportunities. They both were the major players on this journey to France, a place which has become home. My sincere thanks to Paula Moldenaers and her research team; Ruth Cardenaels and Pieter de Bruyn who also made part of my scientific training, demanding from me a high quality in my work and all my other endeavors. I am deeply grateful to Ruth and Pieter who

introduced me to the polymer research, consolidating my foundations in rheology, as well as giving to me solid basis on how to write scientific English which has greatly facilitated this work.

I would like to thank the IMP@Lyon1 members with whom I had the opportunity to work. This work would not have been possible without the help and technical support of Flavien and Adrien. They were available for me at any time, providing me with all of their experience in polymer processing and technical issues. Unconditionally supportive people as them were the pillar of my work and I am very grateful for that. Special thanks to Nathalie, Olivier and Guillaume for their technical support in light diffraction, TGA analysis and Infra-red techniques, for their guidance and availability. Thanks to Catherine who introduced me to the MALDI-TOF technique and performed for me some characterizations. I would also like to thank Thierry and Pierre for their technical support in SEM microscopy, as well as, all the members of the Technological Centre of Microstructures, especially Béatrice and Xavier for providing me all their assistance. I would also like to acknowledge Florian and Laurent Cavetier for their constant availability to immediately solve any of my technical problems. Thanks also to Gisèle, Sylvie and Sabine for their support, help and kindness. Finally, thanks to all the permanent staff, only some of whom it was possible to mention here.

I would also like to thank my old and current office mates: Seb; Nico, Fab, Fatima, Imed, Baptiste, Romina, Amira and Orianne with whom I shared most of my work time. I feel really lucky to have shared our office with them during the past three years. Second, special thanks go to Nico, Seb, Mélanie, Fab, Pierre, Antoine, Alice, Cyril, Kévin, Jingping, Danjun, Aurélie, Sofiane and of course Gautier, for receiving me in such a warm and kind way when I arrived at the lab. I am also thankful to those who went beyond the role of colleague with whom I shared unforgettable moments and with whom any date was an excuse to make an “apéro”, a dinner or a party. Thanks to them for making each day of this thesis, a different day! Thank them all for teaching me so many things, including the expansion of my French vocabulary, for always being there to explain to me the missing words, for your smile and help at any time. Special thanks to Marie-Camille with whom I performed a complete state of the art of the rheology of highly filled materials without her this arduous work would not have been possible. Finally, thanks to all the PhD students for their friendship and cooperative atmosphere at work and also useful feedback and insightful comments on my work.

Special thanks to my friends: Maria Paula, Silvia, Laura, Shanez and Marwa who always supported me, contributing to my personal equilibrium. Last, I would like to express my heartfelt gratitude to my companion Gautier, my family in Colombia and my family in Dijon for their constant support, love and encouragement. Special thanks to my parents whose efforts and love had made the person who I am.

Abstract

We present in this work a complete study of the melt rheological behavior of highly filled polymers. We study the rheological behavior of two model systems, ferrite particles and short-glass fibers dispersed in polypropylene. We investigate the structural features of such complex materials by linear and non-linear rheological behavior. Under different flow conditions, we show the close relationship between the variation in the microstructure, the formulation and the flow properties. We evaluate the effect of the main parameters related to the filler (*e.g.,* particle size distribution, aspect ratio, surface chemistry) on the viscosity of the mixture. This work shows that the addition of fillers fundamentally changes the linear and non-linear viscoelasticity of the molten composite. Under dynamic flow, we are able to quantify the particle-particle and matrix-particle interactions. Therefore, we study the creation of the filler network with increasing the particulate phase. On the one hand, ferrite/polypropylene systems presented a network structure that evolves over time which manifests by a solid-like behavior accentuation at very low deformations. On the other hand, fibers/polypropylene composites showed that the higher is the aspect ratio and the interparticle interactions, the higher is the probability to create a network structure. Under steady state flow, the non-linear behavior is studied. Wall slip effects were found to be negligible under the flow conditions studied in this work. In particular, ferrite/polypropylene showed an attenuation of the shear-thinning behavior at high shear rates. Thus, this experimental work has contributed to the understanding of the flow properties of these complex materials.

Key words: highly filled polymers, rheology, fillers, ferrites, short-glass fibers

Résumé

Nous présentons dans ce travail une étude approfondie de la rhéologie à l'état fondu de composites très chargés en particules inorganiques. Les systèmes modèles étudiés sont composés de particules de ferrites ou de fibres de verre dispersées dans une matrice polypropylène. Le comportement rhéologique linéaire et non-linéaire ainsi que la morphologie des composants du mélange ont été étudiés. Sous différentes conditions d'écoulement, nous avons pu mettre en évidence la relation étroite qu'il existe entre la microstructure du matériau, sa formulation et ses propriétés rhéologiques. Nous avons ainsi évalué les principaux paramètres liés à la charge (*e.g.,* distribution de taille, facteur de forme, chimie de surface) sur la viscosité du mélange. Ces travaux ont montré que l'ajout de charges dans une matrice thermoplastique change fondamentalement la rhéologie linéaire et non-linéaire du mélange. Sous écoulement dynamique, nous avons pu quantifier les interactions entre les charges (force de contact) et charges-polymère. D'une part, les systèmes ferrites/polypropylène ont montré une forte structuration dans le temps, ce qui se traduit par un comportement type réseaux à très faibles déformation. D'autre part, les systèmes fibres/polypropylène ont montré qu'un facteur de forme plus élevé et de meilleures interactions fibre-fibre favorisaient la création du réseau de particules. Sous écoulement permanent, les phénomènes non-linéaires ont été également étudiés. Nous n'avons pas mis en évidence de phénomènes de glissement pour l'ensemble de ces systèmes. Plus particulièrement, le système ferrites/polypropylène a montré une atténuation du comportement pseudo-plastique à haute vitesse de cisaillement. Ainsi, ce travail expérimental a contribué à la compréhension des propriétés d'écoulement de ces systèmes complexes.

Mots clés : polymères, rhéologie, charges, ferrites, fibres de verre

Présentation synthétique des travaux

Actuellement, les formulations polymères hautement chargés trouvent des applications dans de nombreuses industries, notamment dans le domaine de l'énergie (*e.g.,* batteries, pâtes thermiques, propergols solides), du biomédical (*e.g.,* des matériaux pour la restauration dentaire), des céramiques (*e.g.,* moulage par injection de pièces complexes), des matériaux magnétiques, des emballages électroniques, des adhésifs, etc. Dans la plupart de ces produits, le taux de charge est optimisé près de la fraction maximale d'empilement de solides (ϕ_m), pour obtenir ainsi les meilleures propriétés possibles intrinsèques à la charge. A taux de charge élevés, les particules sont en contact direct et ainsi ces interactions fortes se traduisent par une dissipation d'énergie. Il en résulte une très forte augmentation de la viscosité du mélange rendant très difficile la transformation de ces matériaux. De ce fait, la compréhension de la rhéologie de ces systèmes complexes constitue un véritable défi au niveau scientifique.

Ce sujet de thèse se positionne dans une problématique industrielle de la société Hutchinson. Ce groupe se positionne essentiellement sur la transformation du caoutchouc et plus généralement de formulations polymères pour des applications industrielles dans les domaines de l'automobile, l'aérospatial et l'aéronautique. Une partie de ces matériaux nécessite l'ajout de particules rigides à des concentrations très élevées comme par exemple : le matériau constituant la cathode dans une batterie Li-ion où la charge active plus les charges conductrices constituent >85 wt% de la cathode, des encodeurs magnétiques constitués des particules de ferrites (>90 wt%) incorporées dans une matrice élastomère pour des systèmes de contrôle ABS et ESP et des matériaux thermoplastiques renforcés (*e.g.,* fibres de verre, fibre de carbone) pour des applications dans le domaine des composites. Ainsi, tous ces matériaux utilisés pour des applications très diverses se rejoignent autour d'une même problématique : la transformation de ces matières par de procédés conventionnels dans l'industrie plastique (*e.g.,* extrusion, mélangeur interne, calandreuse, presse à injecter), avec pour objectif, la création d'une pièce finie, homogène et avec les propriétés souhaitées.

En conséquence, ces travaux de thèse ont été développés autour de la compréhension des paramètres qui définissent l'écoulement des polymères thermoplastiques chargés comme par exemple, les caractéristiques de la charge (taille, facteur de forme, traitements de surfaces), la viscoélasticité de la matrice ainsi que les différentes interactions entre les composants. Cette étude purement expérimentale a pour but de déterminer, quantifier et hiérarchiser les relations étroites entre tous ces paramètres qui contrôlent la rhéologie de ces matériaux à l'état fondu.

Pour ce faire, nous avons choisi d'utiliser pour cette étude une matrice polypropylène ainsi que deux types de charges bien distinctes (particules de ferrite et des fibres de verre broyées) de par leur nature (taille et facteur de forme) et de leurs applications potentielles.

Ce manuscrit de thèse est organisé en trois parties. La première partie est basée sur les développements du chapitre 1 : Etat de l'art et du chapitre 2 : Matériaux et Méthodes. La deuxième partie relate les travaux expérimentaux publiés et/ou en cours de soumission (trois chapitres). Enfin, la dernière partie concerne des résultats additionnelles non-publiés. Ce manuscrit se décompose donc en cinq chapitres et deux annexes de résultats additionnels.

Le premier chapitre est une synthèse bibliographique dont le but principal est l'étude des paramètres mis en jeux dans l'écoulement des systèmes chargés. Dans un deuxième objectif, nous avons décrit le procédé de mélange, ainsi que les méthodes utilisées pour étudier la dispersion et distribution de charges dans une matrice polymère. Enfin, le comportement rhéologique de ces systèmes concentrés a été analysé dans le domaine linéaire et non-linéaire. Pour conclure, ce chapitre bibliographique donne un état de l'art complet des applications visées par ces matériaux très chargés.

Dans le second chapitre nous présentons une synthèse des matériaux utilisés pour ce travail, ainsi que les techniques de mise en œuvre et caractérisation rhéologique de ces matériaux. Etant donné que les travaux expérimentaux de cette thèse ont été rédigés en format publication, chaque article comprend toutefoisune explication détaillée des matériaux et des méthodes utiliséss. En résumé, les composites ont été mis en œuvre par des techniques conventionnelles (mélangeur interne, extrusion bi-vis) et mis en forme par des presses de laboratoire (presse à plateaux chauffants et à injecter) et ont été ensuite caractérisés par rhéologie (viscoélasticité linéaire et écoulements permanents).

Le troisième chapitre traite de la structuration sous faibles déformations des charges de ferrite dans une matrice polypropylène (PP). L'effet de l'ajout d'un dispersant dans la formulation a été particulièrement étudié. Cette étude détaillée sur la rhéologie de ces systèmes, nous a permis de mettre en évidence le fort réarrangement de ces charges sous un écoulement quasi-linéaire. Nous avons pu voir que l'ajout d'un dispersant (acide gras commercial Solplus DP310) stabilisait les propriétés rhéologiques et donc la morphologie du composite à l'état fondu. Ce phénomène a été attribué à la différence de nature entre la charge et la matrice. Etant donné que le PP est de nature non-polaire et que les particules de ferrites sont très polaires, un gradient entropique local peut y avoir lieu favorisant ainsi la structuration de ce matériau vers un état de plus faible énergie. Par conséquence, quand le dispersant est ajouté à la formulation, celui-ci migre et se localise à l'interphase charge-polymère. Ce phénomène réduit l'énergie interfaciale, stabilisant ainsi le système dans un état plus favorable.

Dans un quatrième chapitre nous avons étudié le comportement rhéologique de ces mêmes composites ayant des taux de charges plus élevés (jusqu'à 40 vol%). Ces travaux ont porté sur la nature du comportement linéaire et non-linéaire. Dans le domaine linéaire, le comportement rhéologique a été étudié après structuration. Nous avons montré que l'ajout du dispersant écrante les interactions particule-particule et permet donc une diminution considérable du module de la viscosité complexe. Il est aussi capable d'augmenter le domaine de viscoélasticité linéaire du matériau composite. Le module ainsi que la déformation critique ont montré une variation en loi

puissance avec la fraction de solide. Dans le domaine non-linéaire, les phénomènes de glissement et changement microstructuraux ont été étudiés. A partir d'une analyse rhéologique conventionnelle, nous avons tout d'abord montré que les phénomènes de glissement à la paroi de la filière capillaire étaient parfaitement négligeables. D'autre part, la viscosité de composites chargés de 10 à 40 vol% a été mesurée. Les courbes d'écoulement ont montré trois domaines bien distincts à faible, modérée et haute vitesse de cisaillement. A faible cisaillement ($\dot{\gamma} < 10^1$ s^{-1}), la viscosité à cisaillement nul tend vers l'infini, ce qui est attribué à un comportement type réseaux. A vitesses de cisaillement intermédiaires ($10^1 < \dot{\gamma} < 10^3$ s^{-1}), cette structure type réseau est détruite. Les particules sont orientées dans le sens de l'écoulement et donc la contribution à la viscosité de cisaillement est plus faible dans cette région de cisaillement. A haute vitesse de cisaillement ($\dot{\gamma} > 10^3$ s^{-1}), une nouvelle microstructure est créée, conduisant ainsi à la création des obstacles à l'écoulement. Ainsi, la viscosité tend de nouveau vers l'infini en raison de ces interactions entre particules. Ce résultat correspond en effet à un phénomène original qui a été très peu observé dans la littérature dans le cas des polymères chargés.

Le chapitre cinq porte sur l'étude du système fibres de verres broyées également dispersées dans une matrice polypropylène. Deux types de fibres commerciales ont été étudiés. Nous avons caractérisé la taille de ces particules par deux méthodes (diffraction de lumière et traitement d'images issues de microscopie optique). Ainsi, nous avons pu observer que ces deux méthodes nous conduisaient à des diamètres moyens équivalents très proches, ce qui n'est pas forcément en accord avec les conclusions de la littérature. A partir de la taille caractéristique de fibres, nous avons pu calculer différents régimes de concentration (*e.g.,* dilué, semi-dilué, concentré et nématique) et les avons comparés aux changement de régimes observés dans le domaine linéaire. Nous avons ainsi pu observer un rapport étroit entre les régimes de concentration et la nature de l'écoulement. De plus, cette étude nous a aussi permis de montrer qu'un facteur de forme plus élevé, ainsi que des meilleurs interactions charge-charge provoque une diminution du taux de percolation de charges. Nous avons pu mettre encore en évidence les relations étroites qui existent entre la morphologie de charges (*e.g.,* distribution de taille, facteur de forme, chimie de surface) et le comportement rhéologique de ces matériaux composites.

La dernière partie de ce travail se compose de deux annexes de résultats additionnels. Dans la première, il s'agit d'une continuation du chapitre cinq où les composites à base de fibres de verre ont été préparés par le procédé d'extrusion. Ainsi, l'effet de certaines conditions opératoires a été abordé comme, par exemple, le profil de la vis, sa vitesse de rotation ou le débit massique. Nous avons pu observer une légère influence de ces conditions sur la distribution de taille de particules par rhéologie dynamique. En revanche, par rhéologie capillaire, l'influence de la distribution de taille est plus difficile à distinguer à cause de l'alignement des fibres dans le sens de l'écoulement. Finalement, l'analyse de la distribution de taille de particules avant et après mise en œuvre nous a montré que ce sont les particules les plus longues qui sont les plus affectées par le procédé.

De même, nous avons proposé une méthode purement expérimentale pour quantifier la quantité maximale de compactage à l'aide d'un mélangeur interne. Ainsi, nous avons pu établir deux zones de mélange, en mesurant la température matière et le couple qui s'exerce sur les pales. Ces deux paramètres augmentent drastiquement avec le taux de charge. Ces observations traduisent d'une part, un autoéchauffement dû à la dissipation visqueuse provoquée par la friction entre les particules et entre particules et chaines polymères, et d'autre part, une consommation plus

importante d'énergie pour réaliser le mélange. Ainsi, la première zone correspond à la zone où le matériau est « processable » alors qu'au-delà d'une valeur critique de fraction solide, le matériau final perd toute cohésion mécanique. Nous avons aussi évalué l'effet de l'ajout d'un dispersant dans le système ferrite/PP. L'ajout de ce troisième composant à faible teneur améliore considérablement la processabilité de ces matériaux, diminuant notamment le couple de pales pendant le procédé de mélange. De plus, la limite de compactage (limite de processabilité) est décalée de 5 vol% vers les concentrations les plus élevées. Ce gain de processabilité est extrêmement favorable d'un point de vue industriel.

Notre recherche a été donc motivée par l'étude des relations étroites entre la nature de l'écoulement et la structure du matériau composite chargé. Ce travail a montré que chaque système d'étude est très différent, cependant, leurs comportements rhéologiques sont gouvernés par des lois communes.

D'un point de vue scientifique, l'évaluation des propriétés rhéologiques des polymères chargés révèle un grand nombre de phénomènes intéressants qui peuvent varier en fonction de la nature de la charge et de la matrice. Une approche expérimentale est donc nécessaire pour établir ces tendances physiques qui peuvent être décrites de façon phénoménologique, avec pour objectif, la prédiction d'un comportement rhéologique à partir de paramètres liés aux interactions physiques. Pour aller plus loin, il faudrait maintenant formuler des modèles mathématiques robustes qui prennent en compte l'effet de la nature des particules, de leurs facteurs de forme et distributions de taille sur la viscosité du mélange. Cela serait une tâche indispensable pour envisager des simulations réalistes des procédés de mise en œuvre de systèmes à base de polymères très chargés.

Nomenclature

AIN	Aluminum Nitride
BN	Boron Nitride
BSED	Back-Scattered Electron detector
CB	Carbon Black
CIM	Ceramic Injection Molding
CNF	Carbon Nanofibers
CNT	Carbon Nanotubes
CTE	Coefficient of Thermal Expansion
EDX	Energy-dispersive X-ray spectroscopy
EVA	Ethylene-Vinyl Acetate Block Copolymer
FTIR-ATR	Fourier Transform Infrared-Attenuated Total Reflectance Spectroscopy
GFRP	Glass Fiber Reinforced Polymers
GRT	Ground Rubber Type
hBN	Hexagonal Boron Nitride
HDPE	High Density Polyethylene
HF	Highly Filled
HP	Hot Pressing
HTPB	Hydroxyl Terminated Polybutadiene
IA	Image Analysis
IM	Internal Mixer
iPP	Isotactic Polypropylene
KCl	Potassium Chloride
LDPE	Low-Density Polyethylene
LF	Long glass Fibers (VS 1320 K)
LLDPE	Linear Low Density polyethylene
LPIM	Low Pressure Injection Molding
LS	Light Scattering
LTEG	Low Temperature Expandable Graphite
LVR	Linear Viscoelastic Region
MI	Mixing Index
MR	Magnetic Resonance
OMMT	Organically Modified Montmorillonite
PBAN	Polybutadiene acrylonitrile
PBT	Polybutylene Terephthalate
PDMS	Polydimethylsiloxane
PEG	Polyethylene Glycol
PIB	Polyisobutene
PIM	Powder Injection Molding

PIV	Particle Image Velocimetry
PM	Particle Migration
PMMA	Polymethyl Methacrylate
PP	Polypropylene
PPI	Stabilized matrix (1 wt% Irganox)
PS	Polystyrene
PSD	Particle Size Distribution
PVA	Poly(Vinyl Alcohol)
PVDF	Polyvinylidene Fluoride
SEM	Scanning Electron Microscopy
SF	Short glass Fibers (VS 1304)
SGF	Short Glass Fibers
Solplus DP310	SDP310
Solsperse 3000	S3000
SSA	Specific surface area
TEM	Transmission Electron Microscopy
TGA	Thermogravimetric analysis
TGA/GC-MS	TGA coupled to Gas Chromatography-Mass Spectrometry
UHMWPE	Ultra-High-Molecular-Weight Polyethylene

Symbols in Arabic letters

a	transition index [-]
A_p	projected area [μm^2]
A_r	aspect ratio equal to d_{max}/d_{min} [-]
c^{**}	concentrated regime for disk-like platelets
$\overline{D}$	particle mean diameter [m]
D	diameter of the die [mm]
D_L	diameter of the population of large particles [m]
D_F	diameter of the population of fines particles [m]
D_{ro}	rotary diffusivity [s^{-1}]
d_{max}	particle longest characteristic distance [m]
d_{min}	particle smallest characteristic distance [m]
d	diameter [μm]
D_{eq}	equivalent diameter [μm]
D^i	inter-particle spacing parameter [m]
$D_n(0.5)$	median diameter by number [μm]
$D_s(0.5)$	median diameter by surface [μm]
$D_v(0.5)$	median diameter by volume [μm]
g	gravity [m s^{-2}]
G'	storage modulus [Pa s]
G''	loss modulus [Pa s]
G_0	modulus at the plateau [Pa]
$G_{0,m}$	matrix plateau modulus [Pa]
Ga	Galileo number [-]
K	particle shape factor [-]
k_b	Bolztmann constant [-]
l	length of the particle[μm]
L	length of the die [mm]
L/D	length over diameter of the capillary die [-]
M_w	Molar mass [g mol^{-1}]

n	pseudoplasticity index [-]
N	rotor speed [rpm]
n	particle density (number of particles/total volume) [m^{-3}]
p	aspect ratio according to the axis of symmetry [-]
Pe	Peclet number = $\dot{\gamma}/D_{r0}$ [-]
q_0	number-weighted distribution [-]
Q_3	volume-weighted distribution [-]
Re	Reynolds number [-]
s	standard deviation[u]
s_o	maximum variance for a completely segregated system [u]
T	temperature [°C]
V_s	terminal velocity [m s^{-1}]

Greek symbols

$\dot{\gamma}$	shear rate [s^{-1}]
γ_c	critical strain value [-]
γ	deformation amplitude [-]
δ	apparent wall slip layer thickness [m]
δ_b	clearance between the flight tip and the barrel [mm]
$\Delta\rho$	difference between filler density and matrix density [kg m^{-3}]
ρ_p	density of the particulate phase [kg m^{-3}]
ρ_m	density of the matrix [kg m^{-3}]
$\lvert\eta^*\rvert$	the absolute value of the complex viscosity[Pa s]
$\lvert\eta_r^*(\omega)\rvert$	viscosity of the suspension over the viscosity of the matrix as a function of ω [-]
$\eta_{0,c}$	zero-shear viscosity of the composite [Pa s]
$\eta_{0,pp}$	zero-shear viscosity of the matrix [Pa s]
$\eta_{r,0}$	relative viscosity, $\eta_{0,c}/\eta_{0,pp}$ [-]
$[\eta]$	intrinsic viscosity [-]
λ	characteristic time [s]
λ	diameter ratio between large and fine particles (D_L/D_f) [-]
λ	the mean interparticle spacing
λ_{pp}	average relaxation time of the polypropylene [s]
ξ	volume ratio between coarse (large) and fine particles [-]
$\sigma_{ij,m}$	hydrodynamic (matrix) contribution [Pa]
$\sigma_{ij,p}$	interparticle interactions contribution [Pa]
σ_{ij}	total stress [Pa]
σ_y	yield stress [Pa]
ϕ_c	percolation threshold [-]
ϕ	filler volume fraction [-]
ω	angular frequency [rad s^{-1}]

Contents

Acknowledgements i
Abstract iii
Résumé iv
Présentation synthétique des travaux v
Nomenclature ix
Contents xiii
Introduction 1
Part I 3
Chapter 1 5
State of the art 5
1.1 Introduction 5
1.2 Structural description of fillers 7
1.2.1 Particle geometry 9
1.2.2 Maximum packing fraction and percolation threshold 11
1.2.3 Particle size distribution 15
1.2.4 Interaction forces 17
1.3 Mixing process 19
1.3.1 Dispersants and coupling agents 19
1.3.2 Analysis tools 21
1.3.3 Dispersion: important factors 24
1.4 Rheological behavior: Major factors 25
1.5 From linear to non-linear rheology 28
1.5.1 Linear rheology 30
1.5.2 Non-linear rheology 32
1.6 Applications 40

1.7 Conclusions 44
References 45
Chapter 2 60
Materials and Methods 60
1.1 Materials 60
2.1.1 Matrix 60
2.1.2 Ferrites 60
2.1.3 Dispersant 62
2.1.4 Short-glass fibers 62
2.2 Elaboration process 63
2.2.1 Batch mixing: internal mixer 63
2.2.2 Continuous mixing: extrusion process 64
2.3 Rheological characterization 66
2.3.1 Rotational rheometer 66
2.3.2 Capillary rheometer 66
References 68
Part II 69
Chapter 3 70
Ferrite composites under quiescent conditions 70
I. Introduction 71
II. Materials and Methods 73
III. Results and Discussion 78
IV. Conclusions 90
References 91
Chapter 4 94
Ferrite composites: linear and non-linear nature of the flow 94
I. Introduction 95
II. Materials and Methods 97
III. Results and Discussion 102
IV. Conclusions 115
References 116

Chapter 5 120
Short glass fiber composites rheology 120
I. Introduction 121
II. Materials and Methods 123
III. Results and Discussion 130
IV. Conclusions 140
References 141
Part III 144
Additional Results N°1 145
Extrusion process: short-glass fibers 145
I. Materials and Methods 145
II. Results and Discussion 145
Additional Results N°2 149
Limit of processability: Batch mixing process study 149
I. Materials and Methods 149
II. Results and Discussion 149
Conclusions and Outlooks 153

Introduction

Nowadays, highly filled polymers are found in many industries including energetic industries (*e.g.,* batteries, solid propellants), biomedical (*e.g.,* dental restorative materials), ceramics, composites, magnetics, electronics packaging, and adhesives. Most of these products require the incorporation of rigid solid particles at concentration which attempt to approach the maximum packing of solids (ϕ_m). At such high filler levels, the viscosity of the mixture increases which makes very difficult the process elaboration of these materials. Deeper knowledge on the rheology of highly filled polymers is fundamental in order to optimize their processing. The understanding of composite flow properties enables us to control, predict and model the elaboration process, as well as design the processing equipment.

This work is positioned in an industrial context encountered by Hutchinson, a major player in the rubber processing for industrial applications such as automobile, aeronautics and aerospace. Hutchinson combines his know-how in polymer processing with product engineering, offering to the market new composites materials the more and more performant. Indeed, some of its composite products require highly filled levels of the particulate phase, in order to increase the intrinsic properties that the filler confers to the whole material. Some examples are: the material constituting the cathode in a Li-ion battery where the active charge together with the conductive particles include filler levels >85 wt%, magnetic encoders made of ferrite particles (>90 wt%) incorporated in an elastomer matrix for ABS and ESP braking systems and reinforced thermoplastic materials (*e.g.,* glass and carbon fibers) for automobile and aeronautics applications. Hence, all these materials for a wide variety of applications meet the same industrial issue: their transformation by conventional processes in the plastic industry (*e.g.,* internal mixer, extrusion, injection molding) with the common goal of creating a finished part with homogenous and desired properties.

Consequently, this thesis is devoted to the study of the flow and the processing of highly filled polymers. Flow properties are affected by numerous parameters such as size, shape and concentration of the filler, the matrix behavior as well as the interactions between the components. This experimental study aims to determine, quantify and prioritize the close relations between all these parameters which control the flow of such materials in the molten state.

In order to achieve this, we use for this study a polypropylene (PP) matrix, as well as two different types of fillers. They are different by their nature (size, shape factor and surface) and by their potential application. On the one hand, we use ferrite particles which are used to perform magnetic materials and on the other hand, we use short-glass fibers which are commonly used as reinforcing fillers.

This thesis work is organized into three parts which are made of five chapters. The first part corresponds to the state of the art and the materials and methods used in this work. The second part gathers the experimental works performed during these three years of thesis. It is constituted of three papers (chapters) published or in submission process. Lastly, the third part is composed of two supplementary results sections.

The first chapter is a complete state of the art of the issue. We will cover all the parameters which are involved in the rheology of highly filled materials. We will describe the mixing process and the problematics related to the mixing. Then, we will describe the flow in the linear and the non-linear regime for concentrated systems. Finally, we present a synthesis of applications targeted by these materials. In the second chapter, the materials, elaboration process and experimental methods used in this work will be presented. The third chapter deals with the structuring of ferrite particles suspended in a polypropylene (PP) under low deformations. The fourth chapter is dedicated to the study of the same system (ferrite/PP and ferrite/dispersant/PP) at higher filler levels in the linear and the non-linear domain. The last chapter was dedicated to study the rheological dynamic properties for the system short-glass fibers/PP.

Each one of these experimental studies brought to light original aspects of the rheology of highly filled polymers. We brought out phenomena such as the structuring of fillers, the creation of a filler network when increasing the filler level, the effect of adding a dispersant into the formulation, wall slip phenomena, among others. We highlight the close relationship between all the characteristics of the filler with the material flow properties. Under static, dynamic or steady conditions, we correlate the microstructural changes with the rheological flow properties. Therefore, the follow experimental work definitely contributes to gain more insight on the behavior of such complex materials, giving reliable data and understanding to the open scientific community.

Part I

Reformatted and shortened version of paper:

Rheology and Applications of Highly Filled Polymers: A review of current understanding

Originally published in:

Prog Polym Sci doi:10.1016/j.progpolymsci.2016.12.007

Authors

Martha Margarita Rueda[1,2], Marie-Camille Auscher[1,3], René Fulchiron[1], Thomas Périé[3], Grégory Martin[2], Philippe Sonntag[2], Philippe Cassagnau[1]

[1)] Univ-Lyon, Université Lyon 1, Ingénierie des Matériaux Polymères, CNRS, UMR 5223, 15 Bd Latarjet, 69622 Villeurbanne Cedex, France.

[2)] HUTCHINSON Research Center, Rue Gustave Nourry – B.P. 31, 45120 Chalette-sur-Loing, France.

[3)] Saint-Gobain CREE, Grains et Poudres, 550 Avenue Alphonse Jauffret, BP 20224, 84306 Cavaillon, France.

Chapter 1

State of the art

1.1 Introduction

For decades, the incorporation of inorganic and organic fillers into a polymer matrix has been of significant industrial importance, as this is one of the most effective ways to develop new materials with desirable properties adapted to specific applications. The combination of a suspended solid phase in a continuous one opens the way to a vast field of applications ranging from suspensions with clay particles in water, polymer particles in water (latex) and inorganic and organic particles in polymer, metal or ceramic matrices (composites) [1]. Therefore, suspensions cover an innumerable amount of materials that can be catalogued by the nature of the filler, the nature of the matrix and the size of the particles. Concerning the nature of the particles, two kinds of suspensions can be considered: Brownian and non-Brownian suspensions. On the one hand, Brownian suspensions are composed of small particles (<< 1 μm). These can be disturbed by thermal fluctuations (Brownian motion), which represents a driving force in the system. On the other hand, when the particle size increases, the typical timescale for particles to diffuse becomes larger and Brownian thermal forces can be totally neglected. The transition between Brownian and non-Brownian particles in a flowing suspension is indicated by the Peclet number ($Pe \equiv \dot{\gamma}/D_{ro}$), where $\dot{\gamma}$ is the shear rate and D_{r0} is the rotary diffusivity of the particle [2]. Regarding the size of the particles, two principal types of composites are distinguished in the literature: micro-composites and nanocomposites. A micro-composite consists of a micro-filler between 1–100 μm, incorporated in a polymer matrix, while nanocomposites contain nanoparticles (at least one dimension less than 100 nm). Nanofillers can be generally associated with Brownian particles and so micro-sized fillers to non-Brownian particles; however it also depends on the flow conditions. Indeed, particles can be considered as non-Brownian when $Pe \gg 1$.

During the last two decades, it was generally believed that nanocomposites could overcome micro-composite limitations. Including fewer fillers in the matrix with nanometer-size fillers was a revolutionary fact to enhance the properties. The literature indeed contains a number of examples where nanocomposites present a larger bonding strength between fillers and matrices, as well as smaller inter-filler spaces than micro-composites [3–5]. However, in recent years, this tendency has

been changing due to the high content of solids that is needed to impart filler properties to the material [6]. Nanocomposites with particle size of about a few nanometers cannot achieve very high filler levels due to the ultra-large interfacial area per volume between the components, which leads to nanostructured fractal networks, drastically reducing the maximum packing fraction. Therefore, particles whose size is about or higher than several 100s nm are necessary to achieve highly filled (HF) formulations. Particles much smaller than 1 µm bring some conceptual and technical difficulties, such as time dependencies during flow deformation and difficulties to disperse the fillers during the mixing process [6].

Nowadays, HF polymers are found in many industries including biomedical (*e.g.,* dental restorative materials), batteries, ceramics, composites, magnetics, electronics packaging, solid propellants and adhesives [1,6,7]. It was demonstrated that filled polymeric materials result in a system that combines the properties of its constituents. Hence, the developments in this field attract great interest in combining the advantages of both components, expanding polymer applications. For instance, the intrinsic properties of polymers like corrosion resistance, lightness and ease of processability can be combined with the unique properties of fillers, covering up some of the drawbacks of polymers such as their relative low strength and low stiffness [1]. The incorporation of different fillers can considerably modify properties like mechanical strength [8,9], thermal [10–13] and electrical conductivity [12,14], thermal stability [3], magnetic characteristics [15–17], flame retardancy [18–21], electromagnetic wave absorption (shielding) [22], dielectric [23] and barrier properties [24,25]. It is important to note that the addition of particles decreases some mechanical properties beyond a critical value of a solid level; in particular, the impact strength, elongation to break, tensile strength and flexural strength [9,19,26,27]. Indeed, material cohesion is reduced when high filler content is added to the matrix. However, the rigidity of the material increases by increasing the solid content, resulting in higher storage, tensile and flexural moduli.

The properties of such composites are also dependent on different factors such as the size, shape and nature of the particles, interactions between their constituents, orientation, dispersion and distribution of the particles in the matrix and notably the filling level [6,18,24,25]. It is generally known that bimodal and multimodal systems can achieve higher solid levels than mono-modal systems [28,29].

Filled polymer composites are mainly processed under complex operating conditions. High temperatures and high shear rates are needed to transform these materials. There are several drawbacks that result from mixing hard particles with polymers at high filler concentration, principally due to the huge difference in densities. Adding solid particles into a molten polymer changes the viscoelastic behavior, the viscosity and the elasticity of the mixture [30]. In fact, when particles are added into a matrix, they act as impediment agents that alter the flow lines of the continuous phase, restricting the mobility of the chains [26]. At high filling level, particles are closely packed together, making particle-particle interactions predominate over matrix-particle interactions [31]. The constant friction between particles results in energy dissipation, and thus a greater viscosity mixture is obtained [16,32–34]. Hence, the specific area of particles has a major impact on the mixture viscosity [35]. The area increases with decreasing particle size, leading to a potential increase in the probability of agglomeration of individual particles [36].

Linear and non-linear flows of filled molten polymers are commonly characterized by respective rotational flows (dynamic and steady) and capillary rheometry. Capillary rheometry correlates directly with common production processes and allows the study of flow properties at high shear rates. Rotational rheology is limited to relatively low shear rates, but it enables a more fundamental understanding of dispersion, structure and interactions between the components [30,37]. Understanding the rheological properties is of great importance because it gives us an overview of the material's internal structure and allows the determination of processing conditions for real polymer processing, such as extrusion and injection molding. Therefore, the main challenge is to find the optimum balance between improvements in properties while also being able to process these materials.

Many studies have been carried out concerning filled polymers; however, a detailed study of the rheology of HF systems is still lacking: only a few studies show evidence of highly filled level experimental data (> 40 vol%). Hence, it is important to compile the results of previous studies, and the limiting factors behind this field of research. Here, we focus on the study of the rheology of particles with sizes of around 1 μm, suspended in a molten polymer. Additionally, attention will be paid to the theory of concentrated suspensions in low viscous fluids. Concentrated suspensions of particles in a low viscous matrix have been heavily studied and are well known in the literature [1,2,6,38–51]. This field of study is of great importance to understand HF polymers' behavior; however, when considering a molten polymer matrix, new physical phenomena arise because of the synergism between properties of the filler and those of the highly viscous polymer matrix [2]. In short, we attempt to summarize the most recent published works about the rheology of polymers with high content of fillers, giving an overview of concentrated suspension theory, mixing process and the most important parameters that affect the process of those materials.

1.2 Structural description of fillers

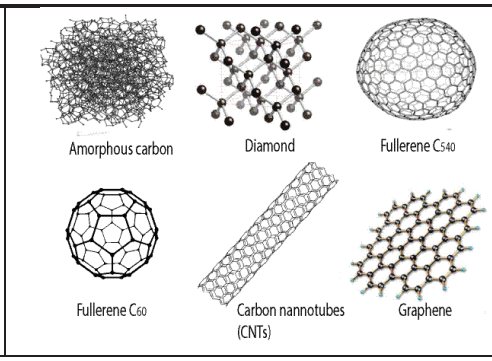
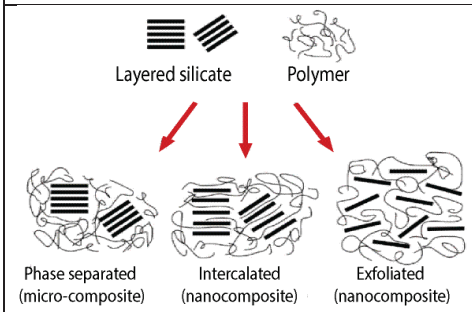
In Table 1.1, we give a general description of the nature of fillers in order to contextualize the topic of the present review. Here, we consider the range from Brownian to non-Brownian particles, including a short description of latex suspensions.

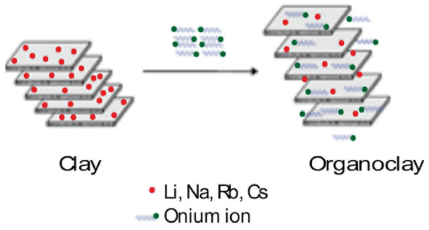
The Brownian motion of particles strongly depends on their aspect ratio and flow conditions. When increasing the size, other interplay forces take place and become of the first order. For instance, latex suspensions are mostly controlled by colloidal interactions such as steric and electrostatic forces. During a flow process, micrometric particles suspended in a matrix are mostly controlled by viscous hydrodynamic forces; however, when considering HF systems, interparticle forces become predominant. All these forces are evoked in Section 1.2.4 and are reviewed at the end of this section.

Table 1.1. Filler description from Brownian particles to non-Brownian particles, including fabrication process and traditional filler examples [2,37,52–54]. Illustrations: Carbon allotropes, Layered silicate [55], Copyright 2000, reprinted with permission from Elsevier Ltd. Scheme of the modification of clay layers by organic onium cations [56], Copyright 2011, reprinted with permission from InTech. Open access: http://oers.taiwanmooc.org.

<table>
<tr><th>Particle type</th><th>Size</th><th>Fillers</th><th>Examples</th></tr>
<tr><td rowspan="3">Brownian particles</td><td>Nanostructured</td><td>Nanofillers can be obtained by:
• Sol-gel method
• reducing reactions

Carbonaceous materials:
• arc discharge
• laser ablation
• high-pressure carbon monoxide disproportionation
• chemical vapor deposition (CVD)


</td><td>• Wollastonite ($CaSiO_3$)
• fumed silica (SiO_2)
• carbon nanotubes (CNT)
• carbon nanofibers (CNF)
• carbon black
• graphene</td></tr>
<tr><td rowspan="2">Micro-sized to nanometric particles</td><td colspan="2">The mixing process could lead to a certain level of exfoliation, moving from tactoids (μm) to exfoliated platelets (nm). Therefore, processing conditions and surface treatment are fundamental to attain exfoliation and consequently nanostructuration</td><td rowspan="2">• Organoclays: organo-montmorillonite (OMMT)
• laponite
• bentonite
• sepiolite
• graphite</td></tr>
<tr><td>

By the process: from micro-composites to nano-composites [55]</td><td>

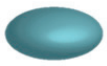
Surface treatment of clay layers by organic alkylammonium cations via ion exchange process (bifunctional molecules) [56]</td></tr>
<tr><td>Between Brownian and non-Brownian particles</td><td>Latices: (0.01–1 μm)</td><td>Latices are suspensions of polymer spheres in a continuous aqueous phase. These concentrated suspensions are possible due to the high concentration of the surfactant, stabilized by either electrostatic or steric forces. Particles are generally obtained by aqueous emulsion polymerization</td><td>They can be considered as deformable particles, where there is a thick layer of stabilizer surrounding the polymer particle. Mostly, we found:
• polystyrene
• polyurethane
• acrylate particles</td></tr>
<tr><td>Non-Brownian particles in molten polymers</td><td>Micro-sized particles (>>0.1 μm)</td><td>Traditional fillers are obtained by standard ceramic techniques, in which heating a mixture of solids produces a desired phase or they are simply obtained in their natural state, extracted by mining or quarrying. Then the mineral is normally milled, powdered and sintered to increase the density of the grain. Other methods found in the literature are:
• Melting process: raw materials in solid form
• Co-precipitation
• Sol-gel process (e.g., Pechini)
• Spray pyrolysis
• Hydrothermal synthesis
• Combustion method</td><td>• Fibers as a common example of non-Brownian suspensions: They are composed of glass, carbon, nylon, kevlar. Typically several μm long, with p = 6–100s.
• Calcium carbonate: $CaCO_3$ (plates and acircular forms)
• Talc (plate-like)
• Ferrites (Hexagonal plate-like)
• Clays, mica (layered silicates, plate-like)
• Silica (beads)
• Zirconia* (spheres)
• Boron Nitride (BN)* (plate-like)
• Aluminum Nitride (AIN)* (polygonal)
* These particles may also be used as nanofillers, according to their application</td></tr>
</table>

1.2.1 Particle geometry

According to their shape, particles are typically divided into three groups: spheres, needles (tube, fiber) and sheets (layer, lamellae, platelet) [3,8]. Regarding nano-fillers, carbonaceous material composites have been the focus of many studies for decades. Such ubiquitous fillers exist in several ways like diamond, graphite, carbon black (CB), nano-tubes, graphene, fullerenes and more. Each of these allotropes presents different structural configurations, which confer specific characteristics to the composite due to its shape. Among traditional fillers, the following can be found: calcium carbonate, mica, talc, ferrites, clays, glass fibers and so on. Table 1.1 gives a schematic representation of several nano, nano-structured and micro fillers with different shapes found in the literature, as well as some allotropes of carbon.

Spherical particles are commonly used as the basic shape for mathematical models. However, this approach is in most of the cases a vague approximation. The particle shape is generally described in mathematical models by the aspect ratio (A_r). The aspect ratio represents the deviation of the filler shape from the ideal spherical shape and can be found in many forms, according to characteristic parameters of the particle like its volume, surface area, projected area, related to the equivalent sphere. The aspect ratio is also considered as the largest characteristic length (*i.e.,* the diameter for platelet or length for fibers) divided by the opposite length (thickness or diameter) [57,58], so $A_r=d_{max}/d_{min}>1$ It has been also defined in terms of the axis of symmetry and flow orientation. Table 1.2 shows the particle rotary diffusivity as a function of the aspect ratio (p), which is defined as the ratio of the length of the particle along its axis of symmetry to its length perpendicular to this axis [2]; indeed $p < 1$ for platelets and $p > 1$ for fibers.

Table 1.2. Particle size geometry and their rotary diffusivities in the case of Brownian particles [2].

Aspect ratio (p)		**Rotary diffusivity (D_{ro})**
	Particles nearly spherical shape $p \approx 1$	$D_{ro} = \frac{k_b T}{\pi \eta_s d^3}$
	Circular disk-like particle $p < 1$	$D_{ro} = \frac{3k_b T}{4\eta_s d^3}$
	Prolate spheroids $p > 1$	$D_{ro} = \frac{3k_b T(\ln 2p - 0.5)}{\pi \eta_s L^3}$
	Fibers, rods $p \gg 1$	$D_{ro} = \frac{3k_b T(\ln(p - 0.8)}{\pi \eta_s L^3}$

Experimental data have demonstrated that the maximum packing fraction (ϕ_m) decreases as A_r of the suspended particles increases [59,60]. The mixture viscosity increases with increasing aspect ratio for a given filler content [60]. Fig. 1.1 shows the viscosity as a function of the content level for particles with different A_r. It can be seen from the figure that, for rod particles of length L and diameter D,

A_r>>1 and the viscosity drastically increase with the filler content compared to the spherical particle suspension viscosity. Indeed, when A_r increases, their effective volume fraction also increases. As a result, the friction between particles increases, increasing energy dissipation; thus, higher melt viscosity is obtained [22,60].

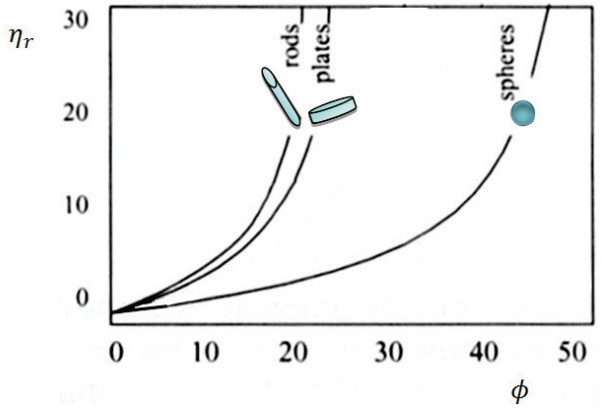


Fig. 1.1. Schematic representation of the effect of particle shape on the relative viscosity. Adapted from [61].

Particle geometry plays an important role in final composite properties and processing. Well defined and characterized specific particle lengths are fundamental in industry. For example, the thickness of plate-like particles such as mica and talc is important in the paper and paint industries. Thinner particles can overlap more easily and produce a more opaque coating. Furthermore, the use of high aspect ratio particles in composites has certain advantages over low aspect ratio particles. Indeed, high aspect ratio particles reduce the maximum packing fraction and consequently the percolation threshold (*i.e.,* the critical solid concentration level) where interparticle interactions become important. Therefore, it is possible to improve properties such as magnetization, thermal and electrical conductivity with the same quantity of particles by using irregularly shaped particles [62,63].

Another remarkable example of how particles properties interplay is for instance the powder injection molding process (PIM), in which the combination effect of particle shape and size is imperative to allow the transformation process to succeed [33,34,64]. We consider PIM technology, in which materials are filled as much as possible in order to reduce possible structural defects [64]. These materials consist of a very high content of ceramic or metallic powders compounded with a binder (matrix) to obtain, in most cases, complicated shape products. In this regard, it is important to point out the four stages of this process. First, the filler is mixed with the binder formulation (often a mix of thermoplastic polymers with additives) and compounded to obtain a feedstock that is then injected into a mold. Then, a debinding step is performed where all the polymeric phase needs to be removed. Finally, the sintering stage is carried out. The particle size, particle-size distribution and particle shape are the key parameters that have a strong influence on every single step of the process. For instance, spherical particles present higher packing density and lower mixture viscosity, which is required for injection. However, during debinding, they have a lower compact strength than asymmetric particles.

Then, a compromise can be found to combine hybrid fillers (spherical and irregular shape particles) in order to achieve the benefits of both. Regarding the particle size, small particle size has some advantages: it allows faster sintering and has fewer molding defects. However, such particles notably increase the mixture viscosity, making injection control more difficult. A broader particle size distribution (PSD) exhibits higher packing density; however, it results in slower debinding and an inhomogeneous micro-structure can be obtained.

1.2.2 Maximum packing fraction and percolation threshold

The determination of the maximum packing fraction (ϕ_m) of particles has been the topic of research of hundreds of studies, and continues to be of great fundamental, practical and industrial interest. Physically, ϕ_m defines the maximum packing arrangement of particles while still retaining a continuous cohesive material. This parameter is a property of the geometry of the filler, independent of its size [65,66]. For instance, spherical unimodal size particles, no matter what their size is, can achieve a typical value of $\phi_m = 0.64$ for random close packing. This value can be calculated theoretically for different types of packing [67] and can be increased by using particles with bimodal or multimodal size distributions [40,41,48,51,68]. This can be expected because fine particles can be placed in the interstices of coarse particles, allowing a higher packing density, as shown in Fig. 1.2.

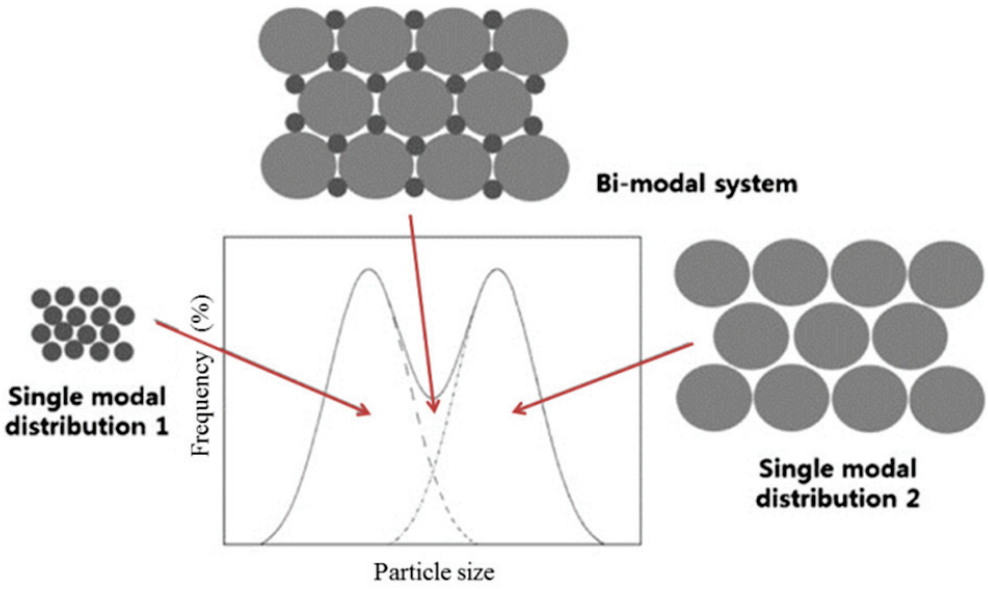


Fig. 1.2. Schematic representation of a bimodal population in which fine particles fulfill the interstice of coarse particles. Reprinted from [53], Copyright 2012, with permission from Elsevier Ltd.

The maximum packing fraction has been defined as [41,69]:

$$\phi_m = \frac{Bulk\ density\ of\ particles}{True\ density\ of\ particles} \tag{1.1}$$

Experimentally, bulk density is estimated as the dry weight of the filler divided by its occupied volume, which includes the volume of the filler and the void spaces. It can be estimated using different methods such as sedimentation methods [41,70], from the volume occupied by a given weight of fillers [67] and by mechanical vibration methods in well-defined containers [69,71]. Bulk density is thus an indicator of the filler compaction. The true density of particles can be estimated by the classical method of using a pycnometer and different solvents [69], and is an indication of the true density of a solid grain.

Rheological measurements can be also used to estimate the value of ϕ_m by plotting $\phi\eta_r/(\eta_r - 1)$ versus ϕ (the method proposed by Chong et al. [39]), or by fitting model predictions of the relative viscosity η_r as a function of solid level ϕ (as further explained below).

Many other attempts to calculate ϕ_m have been oriented to mathematical simulations *e.g.,* Milewiski and Macropack simulation used in Lee et al. [63] for HF polymer composites. Torquato et al. [72,73] gave fundamental insight into jammed hard-particle packing simulations. In particular, they defined three different jammed configurations: (1) locally jammed configuration where all the particles are locally jammed, (2) collectively jammed configuration in which there is no collective motion and so the system cannot unjam, and (3) strictly jammed configuration in which the system is collectively jammed and remains totally fixed even under global deformation of the system boundary. They found that the particular classification of random packing depends on the shape of the boundary and the type of the imposed boundary condition. Later [74], they demonstrated that the response of jammed hard-particle packing to global deformations cannot be described by linear elasticity, but requires another theoretical description. In fact, the nature of highly concentrated systems leads to the breakdown of linear elasticity. They proposed a conical non-linear theory as a description for hard-sphere packing using simple examples. Monte Carlo simulations allowed their group to model maximum packing arrangements in two and three dimensions for binary disk mixtures [75], identical non-overlapping spheres in two [76] and three dimensions [77], polyhedral [78] and truncated tetrahedral [79] fillers.

The great importance of determining ϕ_m is that this parameter appears in most mathematical models that attempt to predict the viscosity of highly concentrated suspensions in the form ϕ/ϕ_m. However, an inverse approach can also be considered. The rearrangement of these predictions, together with experimental datasets, can lead to finding the missing coefficients, including ϕ_m.

At this point of the discussion, it is necessary to define the relative viscosity (η_r). As already evoked in the introduction, the presence of particles together with a flowing fluid represents an increase in the viscous dissipation. The mixture viscosity is always higher than that of the neat matrix (η_o). Therefore, in order to isolate the effect of the filler phase, a relative viscosity is defined as follows:

$$\eta_r = \frac{\eta}{\eta_o} \tag{1.2}$$

Where the viscosity of the suspension (η) is mainly dependent on the solid level ϕ:

$$\phi = \frac{V_{particle}}{V_{particle} + V_{matrix}} \tag{1.3}$$

It is important to remark that, when the filler level is high, the viscosity becomes more sensitive to small variations in particle properties; thus, ϕ_m aside from the particle size distribution, also depends on particle shape, as shown in Fig. 1.1, and surface roughness [2,42,65].

Mooney [80] developed one of the most frequently used equations that predicts the dependency of the zero shear viscosity of a particles suspension having spherical or other aspect ratios (Eq. (1.4)). This semi-empirical equation was developed for hard and mono-dispersed particles, and has been used as a basis for other more sophisticated predictions.

$$\eta_r = \left(\frac{\kappa\phi}{1 - \frac{\phi}{\phi_m}} \right) \tag{1.4}$$

Where κ is an empirical parameter. From Eq. (4), it can be deduced that when ϕ tends to ϕ_m the relative viscosity tends to infinity and the suspension exhibits a yield stress behavior [2,67,70] (see Section 1.4). At this point the suspension "jams up" or blocks, resulting in a continuous close-packed structure in which the flow is totally hindered [2,42,70].

Eq. (4) can be rearranged in the following form:

$$\frac{\phi}{\eta_r} = \frac{1}{\kappa} - \frac{1}{\kappa\phi_m}\phi \tag{1.5}$$

Therefore, the coefficients ϕ_m and κ can be calculated from the slope and the intercept using experimental data. It is worth noting that ϕ_m is a constant parameter for a given suspension at given flow conditions [81].

Taking this into consideration, two important parameters can be distinguished: the percolation threshold (ϕ_c) and the maximum packing fraction of solids (ϕ_m). From a rheological point of view, ϕ_c is also defined as the limit where the zero shear viscosity tends to infinity, as well as ϕ_m has been defined before, which can lead to confusion. However, the flow conditions within the state of dispersion are paramount to distinguish between both parameters.

The percolation threshold ϕ_c has been also widely investigated, especially for conductive fillers such as carbon black (CB), graphite, CNT, CNF and metal powders [82]. ϕ_c is commonly denoted as the point where filler particles would start to be in contact with their closest neighbors, thus increasing

the viscosity and hindering the flow properties control. In other words, particles start to form a three-dimensional contact network with bridges or paths throughout the material. In practice ϕ_c and ϕ_m do not have the same physical meaning. In fact, ϕ_m is the limit above which it is not possible to continue loading the polymer matrix with solid powders [47].

This is actually very subtle in some systems and depends on the filler nature and the physical phenomena that govern the suspension. Actually, dispersion is the key word to define such a difference. In the hypothetic ideal case when the dispersion and distribution (see Section 1.3) of particles through the matrix are "totally" attained, ϕ_c would converge to ϕ_m values.

From a process point of view, dispersion is closely linked to particle size. As the size of the filler decreases, the capacity that particles have to form a network increases [10,66,70] and dispersion becomes more difficult [25]. For this reason, nanostructured fillers present very low values of ϕ_c. Most studies have reported that very low quantities of such fillers are necessary to attain the percolation threshold (less than 5 vol% [82,83]). Generally, particles less than 1 µm in size are propitious to form agglomerates and thus a filler network [66]. However, the interparticle network depends on the flow conditions. Higher shear rates provoke ruptures of this network; thus, more powder can be incorporated into the mixture.

Fig. 1.3 shows the effect of agglomeration on the zero-shear viscosity for two systems: carbon black/mineral oil and TiO_2/linseed oil. Carbon black has a very strong tendency to agglomerate [67] and presents higher values of η_r for the same level of solids compared to the TiO_2 suspension. This can be attributed to the state of dispersion. Same trends have been seen for HF suspensions in the molten state [66]. Composites with agglomerates have a higher effective filler level. The effective volume occupied by the agglomerate includes the volume occupied by the filler plus the volume of the polymer arrested in between the filler. The trapped matrix cannot deform as the rest of the matrix does, leading to higher viscosity [67].

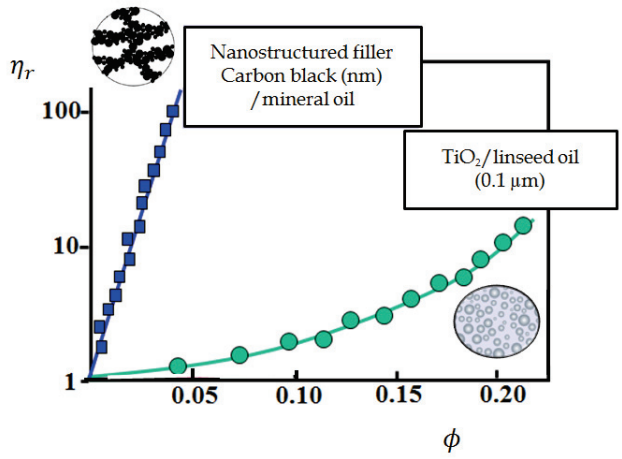


Fig. 1.3. Relative viscosity as a function of filler level for TiO_2/linseed oil and CB/mineral oil suspensions. Adapted from [43,84].

Latices represent another good example at this point in the discussion. Such systems are generally governed by steric and electrostatic interactions. The agglomeration process can be considered as totally arrested principally due to physical interactions. When the suspension is sterically stabilized and/or the ionic strength of the suspending phase is high enough to screen the charges, particles do not agglomerate but rather remain suspended, enabling higher values of ϕ_c. Therefore, in those cases, it would be possible to consider $\phi_c \equiv \phi_m$, in order to make a rheological description [47,85]. Good agreements have been found between the percolation model ($\eta_r \sim (\phi_c - \phi)^{-s}$) correlated with the dynamic zero shear viscosity and ϕ_m predicted by Krieger and Dougherty model for those systems [47].

In this review, we focus on systems for which solid levels are much higher than the percolation limit *i.e.,* where $\phi_c < \phi < \phi_m$ and $\phi \to \phi_m$. Nevertheless, ϕ_c is an important rheological parameter to consider in order to understand the internal organization process.

1.2.3 Particle size distribution

The particle size distribution (PSD) strongly affects the viscosity of the mixture, especially when the solid level becomes closer to the maximum packing of solids [40]. In fact, it has been observed that bi- or multi-modal fillers can decrease the mixture viscosity and attain higher values of ϕ_m compared to the unimodal filler distribution at a given solid level. It has been also found that dilute systems ($\phi < 0.2$) do not seem to be affected by PSD [40].

Bimodal suspensions have been characterized in terms of diameter or size ratio (λ) defined as the ratio between the large particle diameter (D_L) to the fine particle diameter (D_f), $\lambda = D_L/D_f$ as well as by the volume ratio between each population $\xi = \phi_L/\phi_f$. Some works have shown [71,86] that the size ratio should be greater than 7; others have stated [39,87] that it should be around 10 to optimize the blend viscosity. The maximum recommended volume fraction of fine particles oscillates around 30% to obtain lower viscosity mixture and higher filler levels [39,71,88]. Farris [89] was one of the first to predict these trends, developing models for bimodal, trimodal and tetramodal suspensions. According to him, the best processing and least particle attrition are obtained by adding particles at different stages, from the finest to the coarsest.

Later, Chong [39] found similar trends for highly concentrated suspensions. The dependence of flow properties of HF suspensions (glass beads/PIB up to 74 vol%) on filler level, particle size and PSD was studied by using an orifice viscometer, proposing an empirical equation to predict such effects. In the case of dilute systems and spherical particles, this equation is reduced to the well-known Einstein equation ($\eta_r = 1 + 2.5\phi$) at dilute solid concentrations. In a similar matrix, Poslinski et al. [41] studied the effect of a bimodal size distribution on four rheological properties: shear viscosity, dynamic viscosity, first normal stress coefficient and storage modulus. Their bimodal size distribution system consists of glass spheres of 15 and 78 μm, mixing into polybutene (a Newtonian liquid at room temperature). As a result, they found that all four rheological properties were reduced compared to a unimodal size distribution suspension. The lowest values of η_r were obtained with the volume fraction of fines (ϕ_f) between 10–30%.

Ouchiyama and Tanaka [28,90] proposed a mathematical model to estimate the porosity of a bed of randomly distributed spherical bimodal particles. Such a theory has been widely used for the prediction of ϕ_m and has been verified experimentally by [88,91] and theoretically corrected by [92]. Furthermore, their model was adapted by Pishvaei et al. [48] who studied the effect of a bimodal size distribution on the zero shear viscosity of high solid content latex. They drew a master curve of viscosity (η) versus polymer concentration (ϕ/ϕ_m) using the concept of reduced volume fraction. They showed that up to 20 vol% of solid content, there is no significant effect of PSD on the zero shear viscosity, as Metzner et al. [40] predicted before. The origin of this effect can be attributed to the fact that in a dilute system, particle-particle interactions are negligible compared to particle-matrix interactions. Fig. 1.4 shows their experimental results in which a bimodal distribution gives higher maximum packing fraction compared to the related monomodal population. The Krieger-Dougherty equation was used to fit experimental data for two different particle sizes: 79 and 452 nm. As can be seen, low-size particles result in a more pronounced increase in viscosity, due to stronger interparticle interactions. They also demonstrated that the complex rheological behavior of polydispersed lattices can be easily predicted by the corresponding monomodal lattices [49].

Kaully et al. [29,31] studied $CaCO_3$ particles of various PSD in poly(di-methyl siloxane) of $M_w = 45000\ g/mol$. Lower viscosity was always obtained by using a bimodal size distribution, as long as the coarse particles form the majority of the powder population. This is in agreement with experimental data obtained by previous mentioned research. The viscosity of coarse unimodal particles suspensions was found to be lower compared to the fine particle unimodal suspension for solid levels higher than 0.4. Other studies have been carried out concerning bimodal fillers suspended in an epoxy resin in order to obtain higher packing density and therefore enhance properties such as thermal conductivity [53,93–96] (Section 1.6).

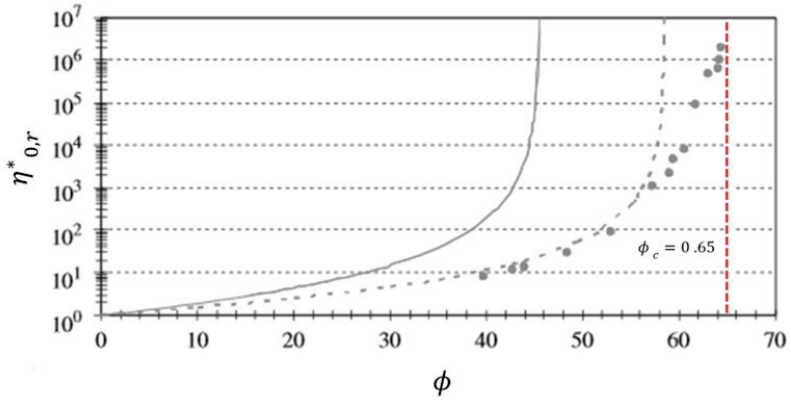


Fig. 1.4. Variation of the relative zero shear viscosity of a PS latex versus volume fraction. Solid and dashed lines represent the curve of a monomodal population viscosity using the Krieger-Dougherty equation for two different particle sizes: 79 and 452 nm. Circles represent experimental data for a bimodal size population of a mixture of such monomodal lattices at [$\xi = 4$]. *Reprinted from [48], Copyright 2006, with permission from Elsevier Ltd.*

Very few experimental studies are found for fillers suspended in molten polymers. This can be attributed to some technical drawbacks. For example, particle attrition during the process provokes a broader PSD [97], making more difficult the study or simulation. Among the available studies, Honek et al. [34] examined HF unimodal and bimodal hard-metal carbide powder up to 60 vol% incorporated into a binder composed of paraffin wax, EVA and LDPE. The maximum fraction of solids was attained by the bimodal suspensions (69 vol%).Concerning the unimodal populations, the maximum loading level was achieved with the broadest PSD powder and the lowest value with the powder population with the greatest part of fine particles. Mayudenne et al. [69] studied the effect of PSD of Ground Rubber Type (GRT) particles incorporated to LDPE. Fig. 1.5 shows the relative viscosity for a bidispersed system at size ratio λ=4.6, for concentrations up to 50 vol%. Similar trends have been found between HF molten polymers and highly concentrated studies [98]. For low concentrations, the behavior seems to be independent of the blend ratio; however, when the solid level increases, noticeable improvements in viscosity can be made by choosing the proper blend ratio. For the HF system at 50 vol%, the minimum viscosity was observed for 80% of coarse particles.

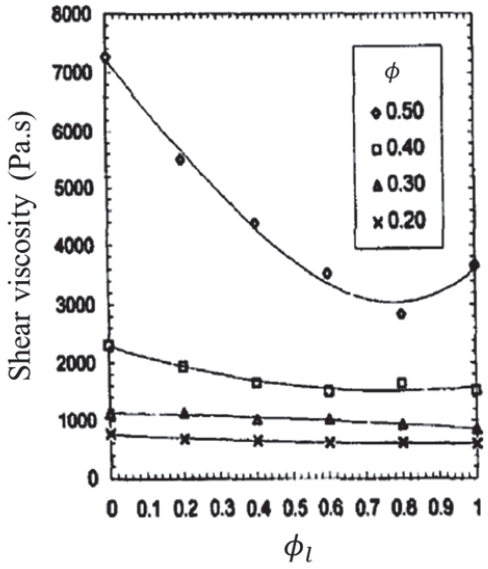


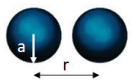
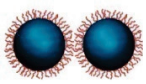
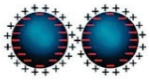
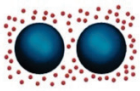
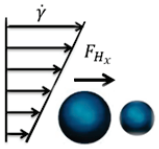
Fig. 1.5. Evolution of the relative viscosity in bimodal composite of Ground Rubber Type (GRT) particles suspended in LDPE for different blend ratios and concentrations. Reprinted from [69], Copyright 1996, with permission from Elsevier Ltd.

1.2.4 Interaction forces

HF polymers are complex systems to define in terms of interaction forces. There are many factors to take into account, which makes a systematic description of all the phenomena that take place during the processing very difficult. Understanding how this interplay of forces works has huge implications for interpreting flow properties during processing conditions. Table 1.3 shows the different interactions that affect Brownian and non-Brownian suspensions. Three kinds of forces coexist in a suspended system: colloidal interactions, Brownian and viscous forces [42,84].

First, colloidal forces arise from interparticle interactions. These occur either by direct contact between the particles or by indirect contact between the particles and the polymer chains, which are absorbed onto the surface of the particle [37]. The interparticle forces that take place in suspended systems are well documented [2,35,37,42]. The same interactions can be inferred for filled molten polymers. Those are: London-van der Waals attracting forces, which occur when particles are close enough (some nm), steric forces when absorbed chains on the particle surface hinder agglomeration, electrostatic forces when particles are charged, and depletion forces between large colloidal particles suspended in a solution of non-adsorbing smaller species, for example: polymers, polyelectrolytes or fine colloidal particles. The characteristic length scale of such interactions is said to be up to several nm [37,99].

Table 1.3. Colloidal and viscous interaction forces for particles suspended in a continuous medium. Reprinted from [37]. Copyright 2000, with permission from John Wiley and Sons.

Interaction force		**Schematic representation**
Colloidal interactions	Van der Waals	
	Steric	
	Electrostatic	
	Depletion	
Viscous interactions	Hydrodynamic	

In general, interparticle interactions dominate when the suspending matrix is a low viscosity phase; when the matrix phase viscosity exceeds 100 Pa s, interparticle interactions can be hindered [40]. Molten polymers satisfy this condition; however, when particles are close enough, they can definitely experience colloidal forces with their closest neighbors [2], which is the case for HF polymers. Therefore, particle-particle interactions become important above a certain value of filler level, depending on the particle size, surface chemistry and particle shape [6,100]. It has been found that interparticle interactions are present when the solid level exceeds 20% by volume [40,48]. Colloidal forces can thus result in either repulsion or attraction between particles. If the net result of all the

forces is an attraction, the particles agglomerate; overall repulsion means that they remain separate [2].

Second, the viscous forces acting on the particles during a flow experiment must be considered. Viscous hydrodynamic interactions are mostly present for large particle sizes (> 1 μm). The friction between the particles and the surrounding matrix is the origin of this force. In other words, hydrodynamic interactions are present when two particles are close enough to perceive and be affected by the dragging of one particle nearby [2]. Generally in molten filled polymers, viscous forces prevail over interparticle interactions during a flow process. Nevertheless, when the volume fraction ϕ is sufficiently high, interparticle interactions must be taken into account [66,101].

Finally and less importantly in micro-composites systems are Brownian (thermal) forces. Those forces are strongly size-dependent and are mostly considered for very small particles in low viscous phases in the dilute and semi-dilute regimes [2,42,57]. HF polymers present a high viscosity which largely impedes particle movement [2], and thus diffusion can be normally neglected in micro-composites in common shear rate ranges ($10^{-3}\ s^{-1} < \dot{\gamma} < 10^{3}\ s^{-1}$).

In most of the cases, only two primary forces are considered, which govern the rheological behavior of highly viscous suspensions: particle-particle interactions and particle-matrix interactions [35,37,102]. Polymer-particle interactions have been studied in order to improve the material performance [103,104]. Such interactions basically depend on particle size, matrix nature and surface chemistry of the fillers. Coupling agents are used either to increase polymer-particle interactions over interparticle interactions or to increase the interparticle repulsive forces, avoiding in this way particle aggregation (Section 1.3.1).

1.3 Mixing process

1.3.1 Dispersants and coupling agents

Effective methods have been developed to improve the state of dispersion. Table 1.1 shows how some micro-fillers can be spread to nano-fillers either by the process or by surface chemistry modification. Regarding surface chemistry modification, intercalation and exfoliation are often used for particles such as flakes and sheets. For example, the intercalation and exfoliation of clay layers in branched polyol and polyurethane were found to correlate with changes in the dispersion state and in the rheological behavior [112]. Graphite exfoliated to graphene, which has caught researchers' attention in the last decade because of the numerous applications of this material [113].

In this manner, coupling agents and dispersants play a key role in suspension pseudo-stabilization *i.e.,* suspensions that are stable long enough to be processed, without mechanical stirring, and therefore reducing particle aggregates. Their role has been investigated with the development of demanding processing techniques like extrusion, Ceramic Injection Molding (CIM), screen printing, slip-casting and tape-casting, which require stable suspensions [64].

As described in Section 1.2.4, three types of forces interact in polymeric suspensions. The dominating interparticle forces for HF suspensions are the van der Waals, electrostatics, and steric forces [114]. Increasing the last two forces is the most common method for stabilizing a suspension. For example, this can be performed by creating an electrostatic double layer at the solid-polymer interface or by adsorbing a dispersant agent on the particle surface.

The use of dispersants is therefore preferred in many cases. They become even more significant with increasing the solid loading of the composite and therefore need to be adjusted to the process. Indeed, these amphiphilic molecules can promote a steric stabilization. The stability of the dispersion is achieved when the repulsive forces are high enough to overcome the attractive van der Waals forces. The conformation of the adsorbed layer depends on several factors (*e.g.,* the number of anchoring groups, molecular length, surface chemistry and so on), and may adopt the configurations represented in Fig. 1.6.

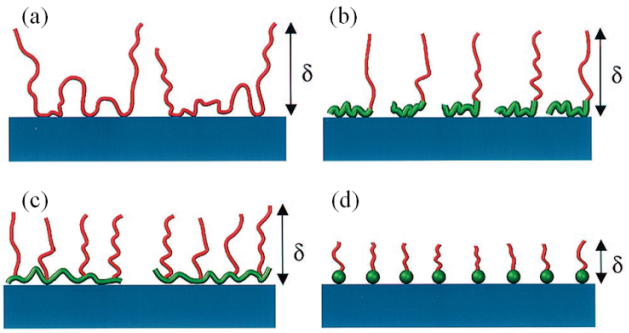


Fig. 1.6. Schematic representations of steric stabilization depending on the molecular configuration: (a) homopolymer, (b) diblock copolymer with a short anchor block and an extended chain block, (c) comb-like copolymer with extended segments attached to an anchored backbone and (d) dispersant. Reprinted from [37], Copyright 2000, with permission from John Wiley and Sons.

The mechanisms are not yet perfectly understood. To be effective, the two following conditions need to be met [115]. First, the adsorbed polymer layer should be thick and dense enough to avoid a close contact where attractive van der Waals forces are dominant; the thickness should be at least greater than 10–20 nm [64]. If the coverage is not complete, agglomeration may occur [116]. Second, the dispersant should be strongly anchored to the filler surface to prevent desorption during particle collision.

Four mechanisms can be found for this adsorption: ligand exchange, ionic interaction with an acid-base reaction, hydrogen bonding and chemisorption [64]. Usually it entails quasi-chemical bonding with Lewis acid-base pair [35]. Stearic stabilization can therefore be used by optimizing the following interplaying parameters: the thickness of the adsorbed layers and the affinity of the polymer to the surface [114]. A combination of electrostatic repulsion and steric repulsion is also possible, and is called electrosteric stabilization.

Many types of dispersants have been used to investigate the efficiency of different groups to reduce the mixture's viscosity. Recently, 12 dispersants with different structural features were evaluated as dispersants for fine zirconia powders (40 vol%) in five different organic media [64]. It was concluded that –OH and $–NH_2$ were not good anchoring groups compared to chelating anchoring groups like $-COOH$ (ligand exchange).

Fatty acids are dispersants commonly used in highly filled polymer processing [117,118]. The most cited ones in increasing chain length order are oleic, lauric, stearic and behenic acids. Hanemann et al. [119,120] determined an optimum dispersant concentration of around 2.2 mg/m² based upon mixing torque measurements at equilibrium, for suspension with small particles zirconia. An interfacial layer is rapidly formed, because of the strong driving force between the amphiphilic acid with its polar carboxylic moiety and the hydroxyl groups on the surface of the fillers, contrasting with the pronounced non-polar behavior of the matrix. The powder surface changes from hydrophilic to hydrophobic, which increases its affinity to the polyolefin matrix and enhances the bonding strength. In addition, Hanemann et al. [120] reported that 30 vol% of fillers could not be achieved without a dispersant agent.

1.3.2 Analysis tools

Quantitative analysis of filler dispersion has been extensively performed based on microscopic local studies and other global methods. The analysis of the degree of mixedness of the ingredients in a polymer matrix is of great industrial interest. However, obtaining the dispersion quality in a composite is far from trivial, and the degree of mixing has been difficult to describe on a quantitative basis. For this reason, tools need to be continuously developed to assess the processing ability of mixing. The practical question is: when can one really know if the filled polymer is sufficiently well mixed? Then, responses can be found on properties requirements. It is accepted that a fully dispersed and stable state will lead to optimal properties. On the contrary, the presence of particle agglomerates will lead to loose material performance [21,121,122].

Some methods have been used to analyze the state of dispersion of concentrated suspensions such as: light scattering, X-ray diffraction, SEM and SEM-EDX techniques. An initial approach by SEM microscopy is suitable for composites. These observations can reveal whether particles are well dispersed throughout the sample or not. In the case of surface modification, whether intercalation or exfoliation was attained can be observed. One needs however to be very critical when using microscopic observations, and make sure that they are representative of the whole material. This can be performed by coupling microcopy results to other techniques such as rheology, image analysis (*e.g.,* ImageJ software), multifractal studies and statistics. Microscopic analysis drawbacks are the very local morphology observation and the requirement of cost-intensive machines.

In 1993 Yazici and Kalyon [123] studied the degree of mixing of concentrated suspensions (76.5 vol% of aluminium and ammonium sulfate in a hydroxyl terminated polybutadiene matrix) by energy dispersive x-ray (EDX) and wide angle X-ray diffraction (WAXD) techniques. Both methods could be successfully used to determine the relative volume fraction of the solid fillers and were

sensitive to the examination of the scale. Some years after, their research group [124] focused on the degree of mixing of silica glass beads/PDMS up to 60 vol% based on experimental and simulation data. The mixing was performed by means of a co-rotating twin-screw extruder. Experimental data were compared to a mathematical model using the Finite Element Method, resulting in a successful description. The largest difference between experimental and theoretical data was observed for high screw speed rotation (210 rpm), due to the high viscous dissipation effect. The distributive degree of mixing was characterized by the WAXD. A distributive Mixing Index (MI) was used to characterize the state of dispersion. Eq. (1.6) defines MI as the ratio between the standard deviation (s) of the concentration of one of the ingredients of the formulation over the standard deviation (s_o) of the completely segregated sample for the same ingredient:

$$MI = 1 - \frac{s}{s_o} \tag{1.6}$$

MI would be equal to 0 for a completely segregated system, and its value would approach 1 for a completely random distribution of particles. The mixing index, as calculated in this example for WAXD data, can be calculated with other methods measuring the particle concentration, such as SEM/EDX and TGA. However, it is worth noting that the mixing index depends on the number of samples analyzed. This index can be considered as a good preliminary indicator of the quality of the mixing; however, it is a quantitative analysis rather for distribution than for dispersion.

Mills et al. [21] used the X-ray mapping (SEM-EDX) method for visualizing high loading composites combined with multifractal image analysis, which is used to analyze and mathematically describe irregular figures with infinitely repeated patterns. They described the dispersion quality of $Mg(OH)_2$/EVA composites up to 60% by weight. However, EDX analysis is limited by the acquisition time. Later, this group [125] used the backscattered electron detector (BSED) to study the dispersion assessment of HF aluminium and magnesium hydroxide particles in an EVA polymer. This has an extremely rapid image acquisition, overcoming EDX problems. It is important to note that the success for assessing the dispersion quality depends on a sufficient atomic number contrast between individual filler components and the matrix.

Tomography is another imaging technique that implies imaging by sections using penetrating waves. It allows dispersion quality investigations on a macroscopic level, using micro-computer tomography [126], and can be coupled with a TEM to reach up to nanoscale imaging. In the first case only aggregates can be visualized, the spatial resolution being 5–10 μm. Tomographic techniques are not often used for HF polymers in the literature; however, they are still in development and could be very useful in the coming years to obtain 3D representations of HF materials easily.

More recently, Carrot's research group [18,65,127] implemented SEM-EDX analysis to study the effect of matrix viscosity on the state of dispersion. They presented a complete description at the fractal dimension of a composite made of $Mg(OH)_2$/Poly(ethylene-co-octene) filled up to 60 wt% (34 vol%). They also used SEM-EDX to analyze the effect of the mixing time on the dispersion with the same components, however only for composites with 10 wt% fillers (see Fig. 1.7).

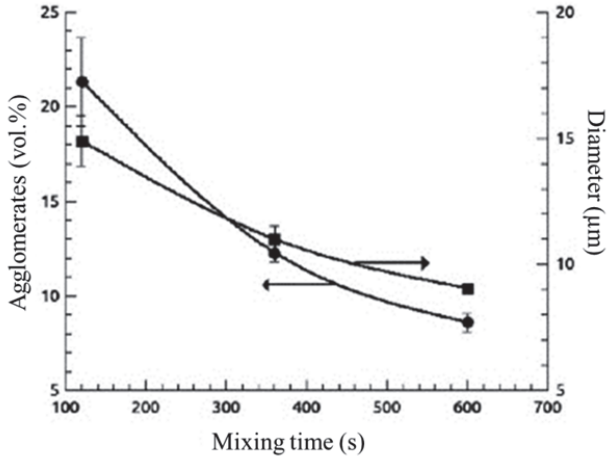


Fig. 1.7. Influence of mixing time on the dispersion studied by SEM coupled with EDX in a suspension of $Mg(OH)_2$ in Poly(ethylene-co-octene) loaded at 3.6 vol%. Reproduced from [127], Copyright 2012, with permission from Elsevier Ltd.

Other methods have been used to qualitatively characterize the dispersion state during the mixing process. The mixing torque rheology is for example commonly used to follow the state of dispersion [117,128–132]. The evolution of the torque with time gives an insight into the physical state of the mixture (*e.g.,* melt, dough) so that the addition of components can be better controlled. The totalized torque over a certain mixing period (*i.e.,* the area under the torque curve) reflects the total energy put into the system during this period, and allows the estimation of the relative network strength in suspensions [130]. This method has also been used to correlate the torque response and the viscosity to the de-agglomeration phenomena [128].

The latter methods can be useful to study the dispersion state; however, a microscopic study is generally unavoidable to confirm the results. However, in general, the quality of the dispersion and the distribution of a mixture remain difficult to quantify especially for highly filled polymers in which the particles are in direct contact. When $\phi \rightarrow \phi_m$, a whole block of particles is observed and the matrix wettability is mostly measured thanks to the final properties of the product. However, different attempts to analyze the state of dispersion of concentrated suspensions were reviewed in this section and summarized in Table 1.4.

Table 1.4. Summary chart of the analysis tools used to study the quality of dispersion and distribution for highly filled systems.

Analysis tool		Remarks	Ref.
Imaging techniques	SEM	• Qualitative method • Quantitative, if coupled with image-analysis software • From micro- to nano-scopic level • In BSED mode, faster acquisition than SEM-EDX	[18,21,105,123,124,127]
	TEM	• Qualitative method • Quantitative, if coupled with image-analysis software • From nano- to angstrom-level	[126]
	Tomography	• Quantitative method • Macroscopic level	[126]
X-ray diffraction techniques	SEM-EDX	• Quantitative method • Limited to the acquisition time	[18,21,65,123,124,127]
	WAXD	• Quantitative method • Not very precise	[105,123,124]
Global analysis	TGA	• Quantitative method for distribution • Complementary but not sufficient	[105]
	Mixing torque rheology	• Qualitative method • Complementary but not sufficient	[117,128–132]

1.3.3 Dispersion: important factors

All results tend to prove that there is an intimate relationship between the rheological behavior and the thermo-mechanical history that concentrated suspensions experience during the processing stage [105]. Concerning the effect of solid levels on dispersion, some disagreements have been found. Dispersion is hindered when the filler level is increased [65], since it promotes the formation of agglomerates during the process. However, some studies claim the contrary, arguing that fewer agglomerates have been found for highly concentrated composites [125]. It is also known that aggregates must be avoided, since they lead to catastrophic degradation of the final mechanical properties of the final product, and negatively impact the flow behavior of concentrated suspensions in general.

Carrot's research group [18,65,127] concluded that the most influential factor in dispersion is the matrix viscosity; the higher this parameter is, the better the state of dispersion [65], in agreement with Tadmor and Gogos [106]. In fact, a higher matrix viscosity results in an increase in the hydrodynamic dispersing forces. However, there is a mechanical limitation from a processing point of view.

Increasing the mixing time and the shear rate has been found to improve the dispersion [127]. They also found evidence that the number of agglomerates increases with filler level; this effect was more visible for the low viscosity matrix system. Similarly, Saini et al. [16] found that particles tend to agglomerate in systems with lower matrix viscosity compared to those with higher matrix viscosity. A mixture of a low molar mass polymer and a viscous polymer has been found as strategy to; on the one hand, decrease the viscosity of the mixture by adding a low viscous polymer, acting as a plasticizer. On the other hand, the viscous phase would ensure the shear forces necessary to disperse fillers and break-up agglomerates [34].

Yang et al. [117] achieved a better dispersion by optimizing the temperature and the mixing time. The latter had to be long enough for the agglomerates to break apart. Song and Evans [133,134] developed a test for the estimation of agglomerate strength, confirming that the maximum shear stress during mixing should be 5–10 times greater than the agglomerate strength in order to disperse the powder in an organic vehicle in the case of $Zr0_2$ and $Ti0_2$ powders in polystyrene. They thus concluded that the dispersive mixing of agglomerated powder is dominated by the agglomerate strength and shear rate imposed, rather than the mixing time.

In general, higher homogeneity induces lower elastic modulus and shear viscosity as a result of network rupture [105]. It is important to note that the latter is only true in the case of non-colloidal particles. When nanoparticles are considered, the opposite is observed. The break-up of nano-particle agglomerates leads to a sharp increase in the surface area between the components, resulting in a higher shear viscosity and elasticity [135].

1.4 Rheological behavior: Major factors

In general during a flow experiment, a change in viscosity implies a structural reorganization of particles and polymer chains *e.g.,* orientation of components, formation of a filler network, interlocking of particles and so on. Consequently, filled materials present significant changes in the rheological behavior beyond a certain value of solids. HF molten polymers commonly exhibit shear thinning behavior [16,33,34,98,136,137]. Shear thickening behavior for filled-molten polymers has been rarely evidenced [32]. In contrast, concentrated suspensions such as inorganic fillers [29,138–141], cement [142], latex [47,143] and cornstarch [144,145] suspensions in low viscous liquids (*e.g.,* PBAN) and polymers (*e.g.,* PDMS) have been found to be shear thickening under specific conditions. For such suspensions, shear thickening was found to be a reversible phenomenon. It should also be noted that shear thickening can be masked due to the presence of wall slip effects that are not corrected [141]. In this manner, concentrated suspensions' behavior gives a fundamental understanding to study the rheological behavior of HF polymers due to common rheological characteristics.

Three different regimes have been observed for highly concentrated suspensions at different shear rate levels [2,42,45]. Each regime depends on the type of filler and suspending phase nature. Fig. 1.8 describes the dependence of the shear viscosity as a function of shear rate for a latex suspension at different concentrations. It can be clearly seen that no rheological behavior changes are perceived for

low particle concentrations ($\phi \leq 0.18$). Therefore, the latex suspension exhibits a completely Newtonian behavior. Beyond this point, the suspension exhibits a Newtonian plateau up to $\phi = 0.43$ at low shear rate values. However, the viscosity seems to diverge to infinity for higher solid levels ($\phi > \phi_c$) at low shear rates. This indicates that the particles have attained the contact percolation threshold in which a filler network is noticed for low shear rates. This point is often known as a yield stress [146], designed as σ_y.

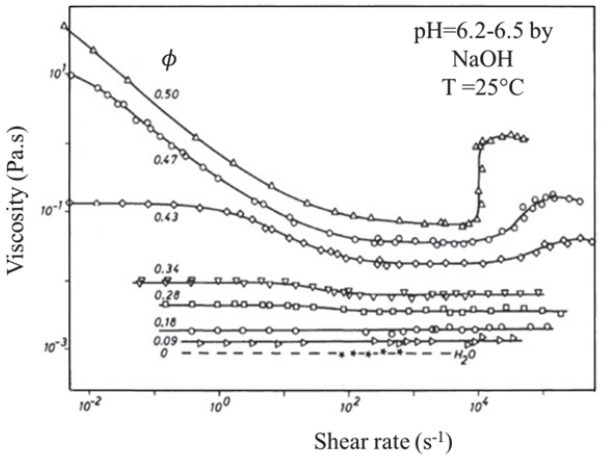


Fig. 1.8. Viscosity versus shear rate for styrene-ethylacrylate-copolymer latex particles of d=0.25 μm at various particle concentrations over the range 0–0.50 vol%. Conditions: T=25°C, pH: 6.2–6.5 by NaOH. Reproduced from [143,147], Copyright 1988, with permission from Springer Science and Business media.

The yield stress phenomenon has been widely studied for concentrated suspensions in low viscous fluids and less studied for HF molten polymers. Indeed, some studies have revealed the real existence of such behavior in HF viscous [118,144,148–150] and molten [33,66,98,136,151] polymers. This behavior has been attributed to a three-dimensional structure in which particles reversely form at the beginning of the flow experiment, suggesting that HF systems respond in a highly non-linear behavior. Suspensions in low viscous phases and with a high quantity of solids have been reported to exhibit a value of σ_y that must be exceeded in order to bring the suspension to flow [98].

Yield stress can be visually determined on the flow curve or through using a fitting model *e.g.,* Bingham, Casson. Recently, Bonn et al. [146] reviewed different rheological techniques for determining σ_y. It is worth highlighting that time-dependent phenomena and wall slip may strongly impact the estimation of the yield stress [152,153].

It can also be observed from Fig. 1.8 that beyond $\phi = 0.28$, the viscosity decreases with increasing shear rate, resulting in shear thinning behavior. The shear rate or stress transmitted through the matrix is high enough to disturb from the equilibrium the spacing distances between the particles, breaking the 3D formed structure [47]. In other words, when the suspension is brought to flow, the particle distance in the normal direction increases and decreases in the flow direction. This results in a layered

structure that offers less resistance to flow and is dominated by hydrodynamic forces [2,38,140]. Suspensions that tend to form a network at rest would present a more severe shear thinning behavior [2].

Again from Fig. 1.8 at volume fractions greater than 43%, the viscosity increases when the applied shear rate exceeds a critical value. This increase in the viscosity would lead to cessation of the flow, exhibiting a shear thickening behavior. The increase in viscosity becomes more pronounced for HF suspensions. This behavior is in general a history-dependent phenomenon that corresponds to the physical interlocking of particles. Actually, shear may induce hydrodynamic clusters, leading to the creation of a jammed network [144] Fig. 1.9). This phenomenon has also been confused with dilatancy, whose physical meaning has been elucidated and differentiated from shear thickening during recent years. Dilatancy is mostly considered for unconfined particles (*e.g.,* dry grains), in which an applied shear may increase the interparticle interactions, so that the packing volume expands [45,154]. On the other hand, hard fillers suspended in a molten matrix can be considered as a confined system in which confinement can provide an opposite restoring force that frustrates dilation. Thus, it is expected that fillers in a molten polymer jam before they dilate. Recently, Brown et al. [45,145] presented different mechanisms and models to describe shear thickening; the difference between dilatancy and shear thickening was also discussed.

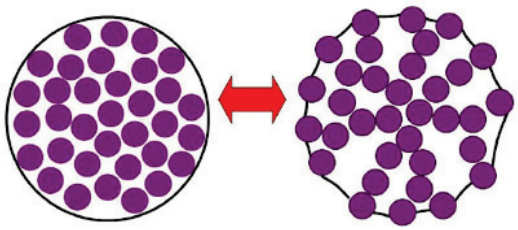


Fig. 1.9. Schematic representation of hydrodynamic clusters induced by shearing. After [154], Copyright 2014, with permission from Springer Science and Business media.

It is important to note that not all suspensions exhibit all regimes, and it basically depends on the material parameters. Fig. 1.10 shows some results for HF molten polymers in (a) steady and (b) dynamic state. Fig. 1.10(a) illustrates the flow curve for glass spheres suspended in a thermoplastic polymer at 150 °C at different solid levels. It can be clearly seen that the Newtonian plateau becomes shorter when increasing the filler level. Shear thinning is exhibited for all concentration levels. Yield stress and shear thickening were not observed at least in the domain of the concentrations and the range of shear rates investigated here. This could be due to the geometry of the particles. Fig. 1.10(b) shows the variation of the absolute complex viscosity as a function of frequency for bamboo charcoal particles suspended in EVA. Here, it can be observed that the yield stress and shear thinning behavior become the more and more visible when increasing the filler content.

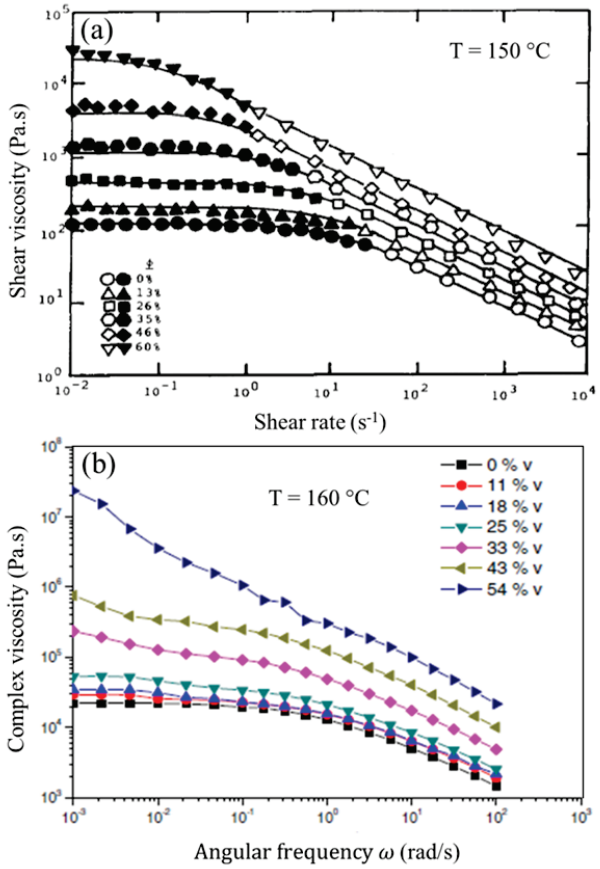


Fig. 1.10. Shear viscosity of glass spheres suspended in a molten TP polymer as a function of shear rate at 150 °C. Solid and open symbols represent data set obtained by cone-plate geometry and capillar rheometer, respectively (a) and complex viscosity as a function of frequency for bamboo charcoal particles suspended in EVA matrix (b) for different filler concentrations. Reprinted from [98,137] (a) Copyright 2015, with permission from The Society of Rheology (b) Copyright 2012, with permission from Springer Science and Business media.

As a final example, Gulmus et al. [155] studied the rheological behavior of PMMA (polymethyl methacrylate) particles suspended in a low viscous HTPB (hydroxyl-terminated polybutadiene) matrix. They drew some interesting conclusions based on the maximum packing fraction of solids: 1) when the solid level was lower than 81% of ϕ_m, the suspension showed a Newtonian behavior; 2) when the solid level ranged from 81–90% of ϕ_m, the suspension exhibited shear-thinning behavior; and 3) when the solid level was 90% of ϕ_m , the suspension exhibited shear thinning followed by shear-thickening behavior.

1.5 From linear to non-linear rheology

As expressed in Section 1.1, HF molten polymers are mostly characterized by means of rotational (dynamic and steady flows) and capillary rheometry to study respectively linear and non-linear flow

behavior. Some of the most common drawbacks of using rotational rheometers are the short linear visco-elastic domain and the impossibility of deforming HF systems. As a result, rectangular slit and squeeze flow rheometers have also been used to study the rheological behavior of such suspensions [156,157]. Capillary rheometry is also a powerful tool to reproduce high shear conditions that commonly occur in mixing, extrusion and injection molding processes [158]. Linear and non-linear rheology of HF systems have been discussed in detail in Section 1.5.1 and 1.5.2 and summarized in Table 1.5.

Table 1.5. Summary chart of the of most recent works about highly filled systems: from linear to non-linear rheology.

Field of study		Analysis methods	General trends	Ref.
Linear rheology	Dynamic viscoelastic properties	• Rotational rheometer • plate-plate	• $\phi \nearrow \Rightarrow$ LVR $\searrow$ • $\phi \nearrow \Rightarrow G', G'', \eta^* \nearrow$ • $\phi \longrightarrow \phi_m \Rightarrow G', G''$ are independent of ω • $\omega \nearrow \Rightarrow$particle-matrix interactions • $\omega \searrow \Rightarrow$particle-particle interactions	[18,31, 65,159]
Non-linear rheology	Particle migration (PM)	• Capillary rheometer • Slit rheometer	• Filler depleted region near the wall • Length/Diameter of the die $\nearrow \Rightarrow$ PM $\nearrow$ • $\phi \nearrow, D \searrow, \eta \nearrow \Rightarrow$ PM $\searrow$ • Addition of a surfactant $\Rightarrow$ PM $\searrow$	[160–166]
	Particle orientation	• Polymer shaping (injection molding, hot press) combined with analysis tools (SEM, tomography)	• $\dot{\gamma} \nearrow \Rightarrow$ particle orientation $\nearrow$ with respect to the flow direction • Final properties depend on particle orientation	[12,13, 54,167]
	Wall slip	• Capillary rheometry • Rotational rheometry • Squeeze flow rheometer • Slit rheometer • combined with: • Particle Image Velocimetry • SEM-EDX • Magnetic resonance velocity imaging	• $\phi \nearrow \Rightarrow U_s \nearrow$ or may $U_s \searrow$ • $D \nearrow \Rightarrow U_s \nearrow$ • $\sigma < \sigma_y \Rightarrow$ plug flow • Entrapped air may$\Rightarrow U_s \nearrow$ • Normal stress, Pressure $\nearrow \Rightarrow U_s \searrow$ • Coupling agents may strongly modify the slip behavior	[6,153, 155,168–173]
	Extrudate distortions	• Capillary rheometry	• $\phi \nearrow \Rightarrow$ extrudate distortions$\searrow$	[44, 174]
	Swell	• Capillary rheometer coupled to laser analytical devices	• $\phi \nearrow \Rightarrow$ elastic recovery$\searrow$ and thus die swell$\searrow$	[175, 176]

1.5.1 Linear rheology

Linear rheology gives insight into the structure-properties relationship and the state of dispersion. In the linear viscoelastic region, the observed moduli are not a function of the deformation amplitude. Therefore, the sample must be excited at very low values of deformation amplitude, which implies low torque values that are difficult to measure. If the aforementioned condition is fulfilled, the molecular behavior can be observed without significant modification of the relative position of the structure from the equilibrium. All filled materials exhibit non-linear behavior after a certain amount of strain (γ_c). Indeed, the higher the filler level, the shorter the linear viscoelastic domain becomes [26,30,31]. It has also been shown that the incorporation of particles will systematically increase the storage modulus *(G')* and the loss modulus (*G''*) of the composite [33,65,136]. Adding a more rigid material would definitely increase the response of *G',* which reflects the elasticity of the material; while, *G''* is increased due to the more pronounced dissipation processes that occur at higher filler level *e.g.,* more pronounced friction between particles.

During a strain sweep, *G'* and *G''* present a drastic decrease when the deformation amplitude (γ) increases beyond a critical point (γ_c). The dependence of the moduli on the amplitude deformation is known as the Payne effect [30]. To characterize the linear domain, the dynamic test must be carefully performed at $\gamma < \gamma_c$. Some authors [65,177] have shown that when γ exceeds γ_c, *G'* drastically decreases, while, *G"* displays a maximum, indicating a maximum rate of energy dissipation that corresponds to the break of the filler network, deagglomeration of clusters or other dissipation process. Fig. 1.11(a) shows the evolution of the moduli with the strain for a sample filled at 25.2 vol%, in which the maximum of energy dissipation can be observed.

Regarding frequency sweep tests, *G'* is almost independent of angular frequency for HF polymers. Fig. 1.11(b) shows the storage modulus as a function of the frequency for different concentrations. It can be seen that *G'* increases by increasing the filler level. At low frequencies, *G'* presents a plateau for the sample filled at 12.6 vol%. This critical concentration value is therefore close to the percolation threshold, since the observed plateau reflects a percolated network [18,33,65]. The highest concentrated composite presents a solid-like behavior, whose moduli do not depend on the applied frequency. It can be clearly seen that ϕ_c can already be observed at 12.6 vol%, but higher concentrations can still be reached.

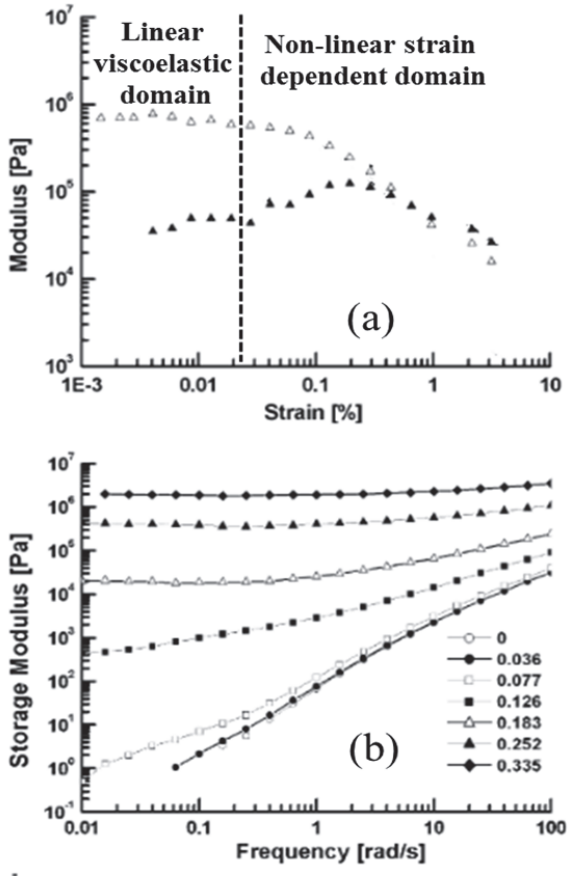


Fig. 1.11. Dynamic test for $Mg(OH)_2$/ Poly(ethylene-co-octene) system (a) Results of strain sweep for sample of 25.2 vol% of fillers, storage (opened symbols) and loss (filled symbols) modulus at 0.1 rad/s (b) Storage modulus as a function of frequency for different filler levels. Reprinted from [65], Copyright 2010, with permission from Springer Science and Business media.

It is also very important to note that the particle-particle interactions govern the composite behavior at low frequencies or shear rates, while particle-matrix interactions govern at high frequencies or shear rates. Therefore, the total stress (σ_{ij}) in a composite can be written as:

$$\sigma_{ij} = \sigma_{ij,p} + \sigma_{ij,m} \tag{1.7}$$

Where $\sigma_{ij,p}$ is due to the interparticle interactions and $\sigma_{ij,m}$ is due to hydrodynamic forces (matrix contribution). In order to isolate the particle-particle contribution, one can normalize the moduli response by a function $\psi(\phi)$ that only describes the hydrodynamic interactions. Further information is given by Carrot et al. [65].

1.5.2 Non-linear rheology

Concentrated suspensions of particles in a suspending liquid or molten polymer that are subjected to strong shear strain beyond the critical point (γ_c) exhibit a non-linear rheological behavior. In fact, harsh conditions affect the suspensions, leading to structural modification such as shear thinning, shear thickening or viscoplasticity, and concentration gradients may arise. These changes are of particular interest for industrial applications, since most shaping methods imply high shear rates like extrusion and injection molding. Elongational flow may also take place during processing; however, it only prevails over shear flow in processes such as vacuum forming, blow molding, film blowing and melt spinning [158].

Different problems arise like particle migration and orientation, wall slip, extrudate deformations and swelling. Even though these effects are commonly observed in concentrated suspensions, most underlying mechanisms have not yet been solved. Non-linear phenomena occurring during processing in HF suspensions of non-Brownian hard spherical particles will be described in the following section.

1.5.2.1 Particle migration

Particle migration is particularly important in pressure-driven viscometric flows such as extrusion [178] and injection molding [115,162]. In fact, filler-matrix separation in mixtures is responsible for many defects such as heterogeneities and cracks, voids and distortions in the final product [161]. It has been observed that pressure-driven flows lead to a filler-depleted region near the wall [160,164,165]. Plug flow, which often occurs in HF suspensions, reduces the filler-binder segregation [6]. Particle migration depends upon the processing parameters and the experiment design; in fact, the binder of HF suspensions can more easily filter out and separate from particles during converging or squeezing flows [6].

Shivashankar et al. [161] used the inter-particle spacing parameter D^i as a predictor of powder-binder separation that they observed, for example, during the injection of tensile bars (see Fig. 1.12).

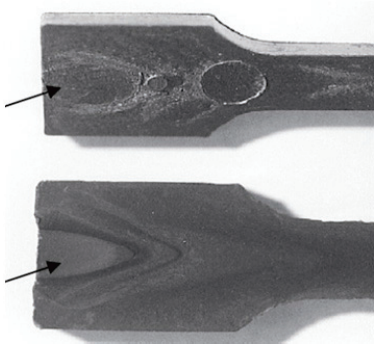


Fig. 1.12. Example of binder-filler separation occurring during injection, as indicated by arrows. Reprinted from [161], Copyright 2013, with permission from Elsevier Ltd.

This parameter brings three independent powder characteristics together: the powder volume fraction ϕ, the maximum powder volume fraction ϕ_m and the mean diameter D:

$$D^i = D\left[\left(1+\frac{1}{\phi}+\frac{1}{\phi_m}\right)^{1/3}-1\right] \tag{1.8}$$

In addition, a negative affinity between powder and binder is said to come along with a low bonding strength that facilitates the powder-matrix separation during the injection process, *i.e.*, when the mixture is submitted to high shear rates and pressures [166]. Consequently, adding coupling agents or surfactants is an effective way to increase the affinity and therefore reduce the demixing effect.

1.5.2.2 Particle orientation

High shear rates may induce orientation of rigid particles with an asymmetric shape in a suspending molten polymer with respect to the flow direction [179]. The final properties of filled materials strongly depend on particle orientation and filler loading level. Magnetic permeability [167], mechanical properties [54,180] (such as tensile strength and modulus), dielectric conductivity [13] and thermal conductivity along the axis of the heat flow [12,181] were reported to increase by promoting the orientation of asymmetric particles in HF materials. In general, the injection molding process induces high orientation of particles with a high aspect ratio [179]; whereas mixing the powders together with the polymer by internal mixers and then using hot press molding (HP) may exhibit a random orientation [13].

Fiske et al. [167] studied the influence of orientation during the injection molding process on magnetic permeability for ferromagnetic particles with different aspect ratios incorporated into a HDPE matrix. The most important results were: the higher the filler level, the better the magnetic properties obtained. Composites with high aspect ratios showed higher permeability for all filler levels. This can be explained by particles with higher A_r presenting a high degree of orientation. It was shown that different processing conditions (*e.g.,* injection rate, mold temperature) and die diameters influence the orientation distributions, hence the permeability.

The properties of thermally conducting filled polymers strongly depend on the orientation and distribution of the particles in the final product. A system composed of aluminum fibers incorporated into PBT was studied during a molding process by Danes et al. [12]. They found that the shape of the gate and the mold geometry alter the orientation of particles, and hence the final properties. Possible solutions to attain a further increase in the average thermal conductivity (along the injection axis) were increasing the filler level and changing the mold design to orient the fillers better. More recently, two different fabrication processes for HF hexagonal Boron Nitride (hBN)/PP composites were studied and compared by Takahashi et al. [13]. Fig. 1.13 shows that hBN/PP filled at 40 vol% performed either by injection molding or hot-press. On the one hand, hot pressing leads to random distribution of particle orientation. This was found to enhance the thermal conductivity of the material along the thickness direction. On the other hand, injection molding samples lead to an alignment of particles in the direction perpendicular to the thickness, leading to higher heat conduction due to the continuous percolated path.

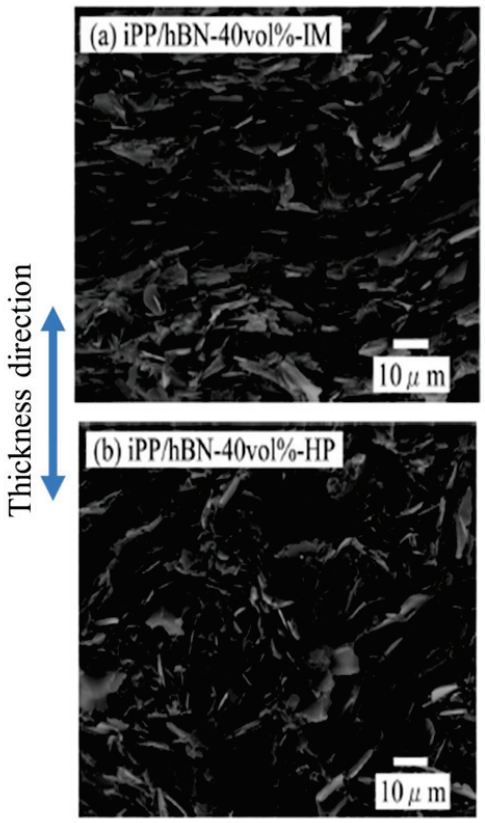


Fig. 1.13. SEM observation of samples filled at 40 vol% of hBN/isotactic PP performed by means of (a) injection molding (IM) and (b) mixing by batch process and then pressed (HP). Reprinted from [13], Copyright 2014, with permission from Elsevier Ltd.

Wang et al. [54] studied the morphology and the properties of HF talc and $CaCO_3$ in PVA composites prepared by melt processing. The talc particles orient in the flow direction due to their asymmetric lamellar structure, in contrast to $CaCO_3$ particles, whose regular shape results in a random orientation. Consequently, talc/PVA composites showed a higher tensile strength and modulus than $CaCO_3$/PVA at the same filler level. This has been explained as a consequence of better interactions between talc and PVA and more orientation of particles. However, a lower elongation at break has been observed for talc composites than for $CaCO_3$ composites. This was attributed to the larger confinement effect of anisotropic talc particles, which hinders the mobility of PVA molecules.

Up until now, few studies focus on the orientation of HF systems. Deeper understanding of this topic could lead to the development of interesting new materials, whose properties could be varied according to the considered direction.

1.5.2.3 Wall slip

Slip at the wall is a common processing problem that was initially reported a long time ago, however, many contradictions were found in literature. As expressed by Larson [2], a no-slip condition is supposed for simple small molecule liquids like water. When the fluid is set in motion by moving the solid boundary, the small molecules closer to the wall, may present the same velocity of the boundary. On the contrary, HF polymers exhibit a complex rheological behavior and are likely to undergo slip phenomena at a certain deformation rate. In fact, it has been claimed that slip at the wall is the controlling phenomenon of the rheological behavior of highly concentrated suspensions [105,155,170]. However, some studies give evidence where wall slip does not necessarily correlate with flow properties [29].

Indications of this phenomenon are abrupt slope changes in curves of shear stress versus shear rate, or oscillations in stress or pressure at fixed apparent flow rates. Visual observations and Mooney analysis are often used as evidence for wall slip, where the slip velocity U_s is expected to depend on the shear stress and on the gap height or capillary die [153,182].

In 1922, Bingham [183] observed a layer of liquid between the shearing surface and the main body of the suspension. This fact was ascribed to a lack of adhesion between the material and the shearing surface. Later on, Vand [184] explained the formation of a thin but always present layer, called the apparent slip layer, of fluid adjacent to the wall as the physical impossibility of the rigid particles to occupy the space adjacent to the wall as efficiently as they can away from the wall. Schematic representations of the velocity distributions of a viscoplastic fluid subjected to wall slip are depicted in Fig. 1.14. A plug flow region zone is observed. In this zone, the suspension remains undeformed. This would only be possible if wall slip occurs simultaneously and if the shear stress imposed is lower than the yield stress of the suspension.

Barnes [182] attributed the wall slip phenomenon or wall depletion effect to steric, hydrodynamic, viscoelastic and chemical forces and constraints acting on the disperse phase immediately adjacent to the wall. The filler concentration was claimed to be practically nil at a distance of approximately one-tenth of a particle radius of the wall; it takes up to five particle diameters before the filler concentration reaches the bulk concentration.

Microscopic studies coupled with energy dispersive X-ray analysis (EDX) are often used to measure the wall slip layer [29,153], while magnetic resonance (MR) velocity imaging can be used to measure the wall slip velocity in capillaries directly [185]. Particle Image Velocimetry (PIV) has also been employed to assess this phenomenon [186].

The apparent slip layer thickness can be calculated to a first approximation using the following linear fit:

$$\frac{\delta}{\bar{D}} = 1 - \frac{\phi}{\phi_m} \tag{1.9}$$

with δ the apparent slip layer thickness, $\overline{D}$ the particle mean diameter. For example a wall slip layer of 2–30 μm for KCl particles of 121 μm mean diameter in an elastomeric matrix could be measured *i.e.,* providing a ratio of about 0.09 between the mean particles diameter and the wall slip layer [153]. Yilmazer et al. [171] found the value of the ratio $\delta/\overline{D}$ of 0.06 for ammonium sulfate fillers in a PBAN matrix, which is in the range found by Soltani et al. [173] 0.04–0.07 for glass beads and aluminum respectively in polybutadiene [171,173].

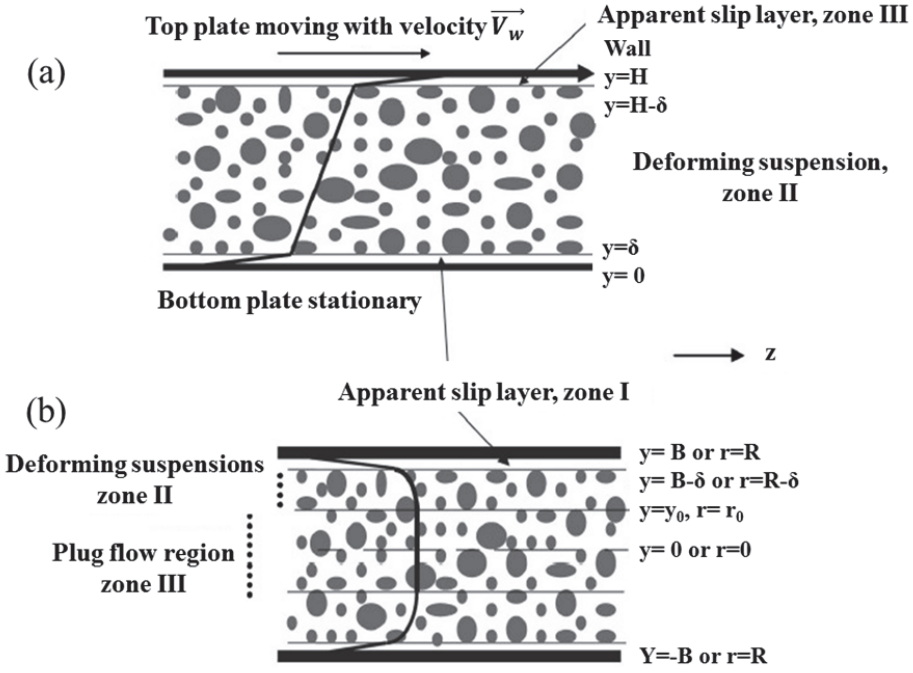


Fig. 1.14. Schematics of the apparent slip flow: a) in plane Couette (pure drag) flow; b) in capillary (radius R) or rectangular slit (gap 2B) dies. Reprinted from [153], Copyright 2005, with permission from The Journal of Rheology.

Suwardie et al. [170] studied the capillary flow behavior of a ceramic suspension consisting of a wax/stearic acid binder filled with 50 vol% of silicon carbide (SiC) particles. The factors affecting the flow were investigated by employing capillaries with varied diameters and length/diameter ratios. Ceramic suspension was found to exhibit viscoplasticity, plug flow, wall slip and axial binder migration.

Direct velocity measurements of the particles in a suspension became possible in the mid-1990s, for example through the adaptation of laser Doppler anemometry (LDA) techniques. This allowed Jana et al. [172] to study the apparent wall slip velocity in concentrated suspensions of non-colloidal monodisperse PMMA particles in a viscous Newtonian fluid. They noticed that the wall slip velocity increases with the solid filler ranging from $0.45<\phi<0.52$.

Gulmus et al. [155] investigated the true rheological behavior of model concentrated suspensions by using a parallel disk rheometer. They confirmed that as the solid level increases, the wall slip velocity and the viscosity corrected for slip effects also increase. Furthermore, as the particle size increases, the wall slip velocity was observed to increase, and the true viscosity was observed to decrease. This is explained by enhanced steric hindrance with higher particle size, which increases the wall slip layer and therefore favors wall slip. It is important to note that, at low solid levels, the wall slip layer was not significant.

The effect of filler level on the wall slip velocity is however contradicted by other studies. Haworth et al. [169] studied polypropylene suspensions filled with talc particles having an acicular, platelet or pseudo-spherical shape. They concluded that, as the filler content increases, the wall slip velocity is decreased. The particle size and geometry only have a marginal contribution to the occurrence and development of wall slip. They emphasized the role of coupling agents in wall slip, in particular once the concentration exceeds the monolayer coverage of the particles, with the example of organo-silane coatings. They also underlined that unreacted coating (amphiphilic molecules) are likely to migrate to the wall during dynamic flow. This is true at high shear stresses at which their presence at the wall may increase the wall slip velocity. Thus, the dispersant or coating efficiency, the affinity between the particles and polymer chains, as well as between the additives are key parameters to take into account in slip phenomena.

Finally, Kalyon et al. [6] suggested that air entrapment may increase the wall slip velocity when the solid content is close to the maximum packing fraction.

1.5.2.4 Extrudate distortions

Surface instabilities have been reported and their understanding is of industrial importance. In fact, the appearance of sharkskin or periodic “stick-slip” effects from extrudate mixtures arise with increasing production rates and represent an upper limit to the manufacturing rate in most extrusion-based processing techniques of polymers and suspensions [44]. Wall slip is commonly considered as being one of the major factors responsible for extrudate distortions; but the onset mechanisms are still not completely understood [44].

The increase of solid concentration strongly reduces the occurrence of extrudate distortion so that highly filled suspensions seem to be less concerned by this type of defects. Only a few studies focus on this topic considering high filler contents [44,174], whereas much work has been done in unfilled suspensions [187–192].

In the case of HF suspensions, the transition from weak to strong slip in simple shear is supposed to arise at a critical wall shear stress value that is material-dependent, since the value varies with the surface density of surface-anchored chains and the molar mass of the polymer melt [44]. PDMS filled with rigid spherical hollow glass particles showed a drastic improvement by increasing the filler content. The neat polymer exhibits four stages with increasing apparent shear rate from 0 to 50 s^{-1}: no distortion, sharkskin region, thread-like sharkskin and non-uniform irregularities. By adding 10% by

volume of fillers, extrudates could be obtained without bulk or surface distortions at low (below 10 s^{-1}) and high shear rates (above 1000 s^{-1}), as depicted in Fig. 1.15.

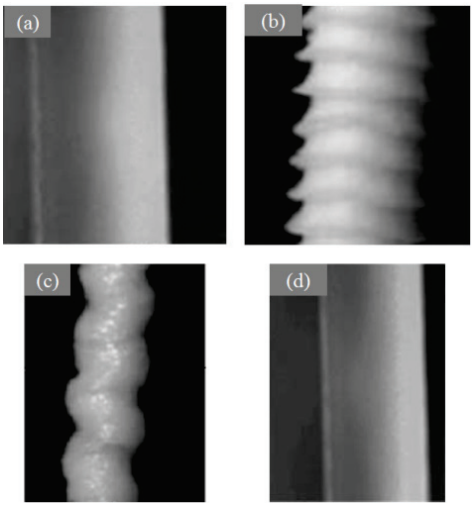


Fig. 1.15. Examples of extrudate distortions in a PDMS matrix filled with 10 vol% glass beads at a) low, b) & c) middle and d) high shear stress. Reprinted with permission from [44], Copyright 2006, from The Society of Rheology.

The shear rate range where distortions are observed becomes narrower with increasing filler content and disappears for filler concentrations above 40% by volume for all capillary diameters. In this case, the wall boundary condition is a wall slip condition over the entire range of apparent shear rates. It was assumed that the addition of rigid particles leads to an apparent wall slip mechanism that has a stabilizing effect on the flow boundary conditions. This is in agreement with another study [174] focusing on glass filled PDMS suspensions. In this case, increasing the particle concentration reduced the apparent shear rate range over which flow instabilities and bulk distortions occurs.

Slight changes in powder size or PSD may result in major changes that cannot be detected by rheological analysis. EVA suspensions were filled with 30 vol% zirconia powders having a monomodal or bimodal particle distribution. The latter case gave rise to larger stick-slip defects compared to the former one. This is illustrated in Fig. 1.16, from capillary experiments at shear strains close to 650 s^{-1}.

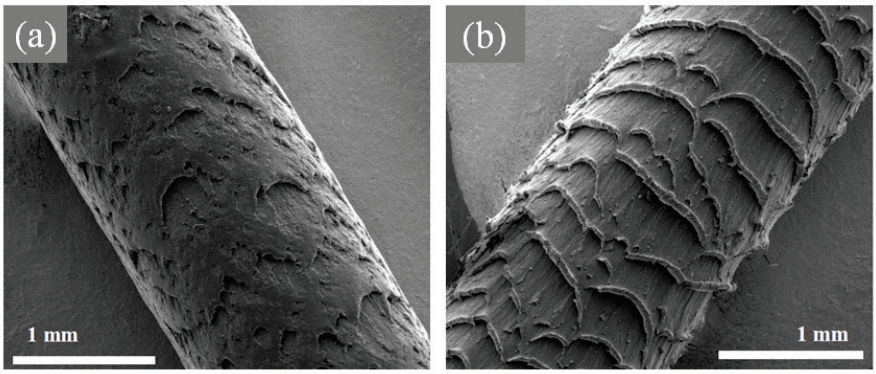


Fig. 1.16. Examples of extrudate distortions in EVA filled with 30 vol% sub-micrometric zirconia powders whose size and distribution are (a) d_{50}=0.18 µm, monomodal (b) d_{50}=0.25 µm, bimodal. Courtesy of Saint-Gobain.

Numerical simulations have been successfully used to support the analysis of wall slip in filled suspensions. Tang et al. [174] showed by numerical simulations that under stable flow conditions, the flow at the exit plane of the capillary die is plug flow. In addition, the mathematical model for predicting instabilities was in agreement with the observations.

1.5.2.5 Swell

Another non-linear phenomenon is the swelling of polymeric suspensions, for example at the die exit of an extruder. Extrudate swell, also called die swell or the Barus Effect, is one of the most important viscoelastic responses of polymer melts that plays a key role in processability [193]. It has therefore to be taken into account in the die design, since it determines the size and quality of the extrudate products [194]. Like extrudate distortions, swell issues seem to be less encountered when increasing the solid content. Many studies dealing with swell focus on unfilled [195] or filled suspensions with nano- or microparticle [176,193,194,196–198] but only a few with highly filled polymers [175].

The degree of swelling and the mechanisms often refer to the effect of residence time on the applied stresses and elastic recovery. In fact, polymer molecules tend to uncoil during converging flows when forced to pass through the die, and part of the shear deformational energy is stored in the molecules. On the contrary, the polymer molecules try to re-equilibrate the internal energy in the form of elastic recovery by coiling again to some extent at the die exit, causing swell [194].

Concerning intermediate solid contents, Dangtungee et al. [196] evaluated the extrudate swell of different systems. Isotactic polypropylene filled with 5 to 25 wt% of $CaCO_3$ and 5 to 30 wt% of TiO_2 nanoparticles. Such systems showed non-linearly increasing swell with increasing shear rates until reach a plateau value. Indeed, swell was reduced with increasing particle concentration [196–198]. This could be explained first by the simple volumetric reduction of polymers. Second explanation consider the limited mobility caused by the addition of fillers, so that the elastic recovery at the exit of the die is to some extent blocked.

Regarding highly filled suspensions, Aral and Kalyon [175] studied suspensions of PDMS filled with holly glass spheres up to 60 vol%. In low filled systems, they noticed that N_1 was positive. Nevertheless, once particles are incorporated at high concentrations (ϕ>30 vol%), it turned to be negative [175]. They suggested that it was due to microstructural changes happening during the shear flow despite the non-colloidal nature of the suspension. Besides, the swell was nearly suppressed over the whole shear rate range when the solid content was increased to 60 vol%.

Therefore, swelling problems seem to be less important in the case of HF suspensions. Furthermore, several studies agree that wall slip reduces the amount of swell to such an extent that it has to be taken into account for extrusion simulations [199].

1.6 Applications

HF particulate composite materials have been developed and investigated for different applications. The solid levels of such materials tend to be very high, often close to the maximum packing fraction of solids. High filler levels are obtained by tailoring the particle size distribution, shape and different interactions (particle-particle and particle-matrix).

During the last twenty years, heat management applications involve many industrial developments in HF materials. Thermal conductivity can be imparted to polymers by adding thermal conductive particles. The higher the filler level, the closer the contact between particles and thus the more efficient thermal conducting paths [10]. The continuous demand on achieving greater computer speeds and miniaturization of electronic devices conduce to the increment of the heat transfer rate. For this reason, the packaging for heat managing applications requires the highest thermal conductivity as possible [200]. Table 1.6 summarizes the most recent works carried out in order to increase the overall heat transfer material by increasing the filler level. Here, the thermal conductivity obtained for the composite at its maximum filler loading is shown. In this context, the coefficient of thermal expansion (CTE) has been also largely studied. In general, CTE of the composites decreases with increasing filler level [63,201].

Particle size distribution and shape has been studied to maximize the ~~affect~~ thermal conductivity properties. Boudenne et al. [10] compared two filler sizes of HF copper/PP micro-composites. As a result, the highest thermal conductivity was found for the smallest particles that also show the broadest distribution at 40 vol%. Regarding shape, it has been found that mixing two kinds of shape distributions (hybrid fillers) [63] and also increasing the filler orientation parallel to the heat transport direction, may increase thermal conductivity [12,205]. Zhou et al. [205] developed a model to determine the effective thermal conductivity of HF composites as a function of volume fraction. This model considered the effect of the orientation and distribution of the filler on the thermal conductivity, representing a good approximation up to 50 vol% of fillers.

Adding conductive particles to an insulating matrix leads to the transition from an electrical insulator material to a conductor material. Percolation theory forms the basis for electrical conductivity properties of filled polymers. After the percolation limit, conducting paths are formed, allowing

electricity to pass through the matrix [207]. It was demonstrated that above the percolation limit, both thermal and electrical conductivity would increase; however, electrical percolation has been reported to be attained at much lower values than the thermal limit [12].

*Table 1.6. Summary of recent works about thermal conductivity at 25 °C enhanced by filler content. The highest thermal conductivity is obtained for the highest filler level obtained in each work. *LTEG: Low Temperature Expandable Graphite.*

Year	Filler/Polymer	Highest level reported	Thermal conductivity [W/mK]	Ref
1998	Boron nitride (BN)/ polybenzoxazine	78.5 vol%	32.5	[96]
2003	Aluminum fibers/PBT	43.5 vol%	2.2	[12]
2005	Copper powder/PP	44 vol%	2.25	[10]
2005	Spherical aluminum nitride/Epoxy resin	74 vol%	8	[93]
2005	BN/HDPE	50 vol%	3.66	[63]
2008	AIN/Epoxy resin	57 vol%	3.39	[201]
2009	Diamond Powder/Epoxy	68 vol%	4.10	[202]
2012	BN/PP	70 wt%	1.20	[203]
2012	Hybrid filler: AIN-BN/Epoxy resin	80 vol%	8	[53]
2013	Graphite/polybenzoazine	68 vol%	10.20	[204]
2013	LTEG*/PA6	70 wt%	32.33	[205]
2013	MgO/Epoxy	56 vol%	3	[11]
2013	Alumina/Epoxy	39 vol%	1.13	[206]
2014	hBN/iPP	40 vol%	2.1	[13]

Depending on the type of application, thermal and electric conductivity can be either maximized or minimized. For instance, thermal pastes are highly filled compounds consisting of thermally conductive particles (*e.g.,* Cu, diamond, Al, Al_2O_3, BN, AIN, MgO, Ag, SiC, among others) suspended in a liquid matrix (*e.g.,* hydrocarbons, silicone oils) and stabilized by a dispersant agent (*e.g.,* fatty acids) [159,200,208]. Such application requires very high thermal conductivity and high electrical resistivity. The paste is applied onto the surface of a heat generating device (*e.g.,* CPU, microprocessors or integrated circuit chip). The main role of such material is to allow heat dissipation from the heat source to the heat-sink, by eliminating air gaps or spaces in between them. Therefore, air included in the paste during the mixing process highly reduces the material performance [159]. Epoxy polymer composites are also widely used in heat management applications due to their relatively low viscosity, this facilitates the coating onto the silicon integrated circuit chip [201]. Table 1.6 clearly shows such tendency.

On the contrary, low thermal conductivity can also be the target to form a thermal barrier. To this end, rare-earth zirconates can be used, since they are one of the ceramics with the lowest thermal conductivity, even at high temperatures [209,210]. Possible industrial uses for thermal barrier applications are coatings used to insulate and protect metal surfaces (*e.g.,* gas-turbine aircraft) exposed to high temperatures. Such barrier improves the durability of the metal component and the engine efficiency [210]

Inorganic particles are also well known to enhance some mechanical properties [8,24,203]. Liang et al. [8] reviewed four theories that describe the reinforcement of polymers by adding particles. First,

the interfacial adhesion as a reinforcing mechanism was studied. It has been shown that the better the composite interfacial adhesion between the particles and the matrix, the better the reinforcing effect [8,24] (based on a higher yield strength). When the composite is bearing load, the stress is transmitted from the matrix phase to the particulate phase, and hence interfacial adhesion strength between the phases is crucial to improve the homogenous stress transfer. The second theory is about the crystallization reinforcing effect. It was found that adding particles into the matrix could lead to a heterogeneous nucleation. This can therefore result in an increase in the crystallinity degree of the composite [203]. Nevertheless, more nucleation processes do not systematically contribute to an increase in the degree of crystallinity. The third theory evokes the natural effect of inorganic particles into the matrix. Particles have much higher modulus than polymers: their contribution increases the rigidity of the whole material. Finally, a synergistic reinforcing effect theory was also discussed.

Among different industrial applications, electrode materials for lithium-ion batteries constitute a good example in which a high quantity of active material is needed to increase the capacity of the battery. The formulation is generally composed of 90 wt% of fillers and 10 wt% of binder [211,212]. Other energetic materials such as gun and solid rocket propellants used for the propulsion of rockets, projectiles and launchers are also examples of HF materials commonly encountered in the industry. Their filler volume fraction is maximized and generally attains 80% [7,152]. In the magnetic composite industry, continuous demand for higher magnetic properties and particularly higher storage densities also contributes to increasing the filler level. Thermoplastic 3-D printing has been also found as a promising elaboration process of HF composites with a high geometric complexity [213]. Globally, to improve properties, the incorporation of a high level of fillers is required; however, this leads to a decrease in the material mechanical properties, reducing the field of applications. Table 1.7 shows some recent works with very high solid content levels and their corresponding industrial applications.

Table 1.7. Recent works concerning HF systems as a source for different industrial applications. The maximum solid level reached for the different applications is given.

Year	filler/matrix	Filler %	Applications	Ref
1986	Ferrite/thermoplastic matrix	85 wt%	magnetic polymer composites	[16]
1993	Aluminum and ammonium sulfate/HTPB	76.5 vol%	solid rocket fuel	[152]
1993	Nickel powder/PE	67 vol%	electrical and magnetic composites	[62]
1993	Iron and Nickel-Iron/thermoplastic elastomer	50 vol%	magnetic polymer composites	[214]
1997	Ferromagnetic powder/LDPE	70 vol%	electrical and magnetic properties	[215]
1998	Silicon carbide/wax binder	50 vol%	CIM	[170]
2000	Zirconia/wax	68 vol%	CIM	[216]
2002	$Mg(OH)_2$/PP	60 wt%	flame retardancy	[19]
2004	Alumina / paraffin	67 vol%	PIM	[217]
2005	Wood/HDPE	70 wt%	natural fiber composites	[218]
2005	hard-metal carbide powders/binder (LDPE-EVA)	60 vol%	PIM	[34]
2005	Aluminum and Alumina/hydrocarbon oil	72 vol%	thermal pastes	[159]
2010	$Mg(OH)_2$/poly(ethylene-co-octene)	60 wt%	flame retardancy	[18]
2010	Fe_2O_3, CB/PVDF	90 wt%	lithium-ion batteries	[211]
2011	Zirconia/wax-HDPE	89 wt%	CIM	[219]
2012	Sulfur and conductive carbon fillers/four different binders	90 wt%	lithium batteries	[212]
2012	Zirconia/PMMA-PEG	57 vol%	CIM	[111]
2012	$LiFePO_4$/PVDF binder	75 wt%	lithium batteries	[220]
2013	FePt/ionic liquid	70 wt%	ferromagnetic fluids	[177]
2014	Al_2O_3 /polyvinyl butyral	78 vol%	ceramic polymer composites	[221]
2014	Ferroelectric powder/PDMS	50 vol%	flexible piezoelectric composites	[222]
2014	Kaolinite/ EVA	60 wt%	fire retardancy	[20]
2014	$BaTiO_3$ /epoxy	50 vol%	dielectric properties	[223]
2014	Bamboo charcoal powder/UHMWPE	80 wt%	mechanical properties	[224]
2014	Ammonium perchlorate and Aluminum /elastomers	86–90 wt%	solid propellants	[7]
2014	$BaTiO_3$ / PVDF binder	60 vol%	electrical and electromechanical properties	[225]
2014	Zirconate titanate power/thermoplastic binder	58 vol%	piezoelectric fibers	[226]
2014	Zirconia toughened alumina / PE-PEG	57.5 vol%	CIM	[115]
2015	Alumina/paraffin, beeswax	67 vol%	3D printing	[213]
2015	Zirconia/paraffin, beeswax	45 vol%	3D printing	[213]

1.7 Conclusions

We have reviewed the current understanding of the rheology of high filled systems. The filler shape, size and size distribution, orientation of the filler, different interactions, filler content and nature of the constituents directly affect the final properties and processability of the material.

Concentrated suspensions (low viscosity matrix phase) have been widely studied and are largely encountered in daily life, especially in personal care, paints, and the pharmaceutics and food industries. This review has shown that their behavior can be used to explain highly filled polymers due to common rheological behaviors. However, processability could strongly differ.

The viscosity is a key parameter that has to be optimized to be low enough for the suspension to be processed, and high enough to improve the dispersion process. Size polydispersity on fillers allows both higher filling level and a decreased melt viscosity for a given filler content. It has been also shown that adding fillers with different shapes can enhance the properties.

High-quality dispersion and distribution are imperative to achieve desirable and homogeneous properties of the material. Furthermore, process and formulation should be taken into account in parallel in order to obtain desirable properties. Low molar mass polymers and fatty acids have been successfully used as dispersants in order to decrease the melt mixture viscosity. Indeed, particle surface modification can improve the dispersion or enhance particle-matrix interactions, hence reinforcing the composite. Mixing methods and the use of dispersants to improve the dispersion, as well as tools to characterize the degree of mixedness, have been discussed.

The processing of these HF composites can be very difficult. High temperatures and shear rates are generally needed to process these materials. The filled molten polymers present non-linear rheological behaviors, such as wall slip, particle-binder segregation and to less extent swelling and surface instabilities. All these phenomena have been reviewed. Strategies should therefore be found in order to control flow properties and reduce nonlinearities during the mixing and elaboration processes. Non-linear behavior should be taken into account in order to design and optimize technological apparatus.

This is why rheological studies gives fundamental insight into the flow behavior, helping to determine the optimum processing conditions, in the case of polymer processing such as extrusion and injection molding. Much has already been done; however, further experimental studies coupled with numerical data need to be carried out, to fully understand the mechanism that govern such complex behaviors. Then, there is still a lack of reliable fundamental concepts to describe completely how all these parameters interplay in flow properties.

Finally, HF systems open a vast possibility to improve final product properties such as magnetic, thermal, and electrical conductivity. Batteries, adhesives, solid propellants, composites and electronic packaging are also examples of HF polymers available nowadays in the market. HF polymers offer a new possibility to elaborate such products using polymer processing. Moving from conventional

methods to melt polymer processing would break a technological barrier, increasing production rates and reproducibility, while also reducing dead times and process operators. For instance, electrodes in Li-ion batteries are conventionally made by the classic coating process (batch process) which is nowadays being changed by continuous melt polymer processing (dry process, without solvent) [227]. HF suspensions also have the potential to improve the shaping process of the Powder Injection Molding industry. Such manufacturing operation has been used during the last few decades to achieve complicated material shapes using very high concentration levels, which continue to be developed. Additive manufacturing also opens a vast field of industrial applications for HF polymers. This technique would undoubtedly change and facilitate the elaboration of complex-shaped objects, reducing fabrication costs and thus increasing the implementation of such composite pieces.

References

[1] Pal R. Rheology of Particulate Dispersions and Composites. Waterloo: CRC Press; 2006.

[2] Larson RG. The Structure and Rheology of Complex Fluids. New York: OUP USA; 1999.

[3] Bikiaris D. Can nanoparticles really enhance thermal stability of polymers? Part II: An overview on thermal decomposition of polycondensation polymers. Thermochim Acta 2011;523:25–45. doi:10.1016/j.tca.2011.06.012.

[4] Iyer G, Gorur RS, Krivda A. Understanding electrical discharge endurance of epoxy micro- and nano-composites through thermal analysis. IEEE Trans Dielectr Electr Insul 2014;21:225–9. doi:10.1109/TDEI.2013.003466.

[5] Kozako M, Kido R, Fuse N, Ohki Y, Okamoto T, Tanaka T. Difference in surface degradation due to partial discharges between polyamide nanocomposite and microcomposite. Ann Rep Conf Electr Insul Dielect Phenom 2004:398–401.

[6] Kalyon DM, Aktaş S. Factors Affecting the Rheology and Processability of Highly Filled Suspensions. Annu Rev Chem Biomol Eng 2014;5:229–54. doi:10.1146/annurev-chembioeng-060713-040211.

[7] Azoug A, Nevière R, Pradeilles-Duval R-M, Constantinescu A. Influence of crosslinking and plasticizing on the viscoelasticity of highly filled elastomers. J Appl Polym Sci 2014;131:40392(1-9). doi:10.1002/app.40392.

[8] Liang J-Z. Reinforcement and quantitative description of inorganic particulate-filled polymer composites. Compos Part B Eng 2013;51:224–32. doi:10.1016/j.compositesb.2013.03.019.

[9] Aghazadeh Mohandesi J, Refahi A, Sadeghi Meresht E, Berenji S. Effect of temperature and particle weight fraction on mechanical and micromechanical properties of sand-polyethylene terephthalate composites: A laboratory and discrete element method study. Compos Part B Eng 2011;42:1461–7. doi:10.1016/j.compositesb.2011.04.048.

[10] Boudenne A, Ibos L, Fois M, Majesté JC, Géhin E. Electrical and thermal behavior of polypropylene filled with copper particles. Compos Part Appl Sci Manuf 2005;36:1545–54. doi:10.1016/j.compositesa.2005.02.005.

[11] Wereszczak AA, Morrissey TG, Volante CN, Farris PJ, Groele RJ, Wiles RH, et al. Thermally Conductive MgO-Filled Epoxy Molding Compounds. IEEE Trans Compon Packag Manuf Technol 2013;3:1994–2005. doi:10.1109/TCPMT.2013.2281212.

[12] Danes F, Garnier B, Dupuis T. Predicting, Measuring, and Tailoring the Transverse Thermal Conductivity of Composites from Polymer Matrix and Metal Filler. Int J Thermophys 2003;24:771–84. doi:10.1023/A:1024096401779.

[13] Takahashi S, Imai Y, Kan A, Hotta Y, Ogawa H. Dielectric and thermal properties of isotactic polypropylene/hexagonal boron nitride composites for high-frequency applications. J Alloys Compd 2014;615:141–5. doi:10.1016/j.jallcom.2014.06.138.

[14] Tanaka T, Kozako M, Okamoto K. Toward High Thermal Conductivity Nano Micro Epoxy Composites with Sufficient Endurance Voltage. J Int Counc Electr Eng 2012;2:90–8. doi:10.5370/JICEE.2012.2.1.090.

[15] Peinado F, Medel E, Silvestre R, Garcia A. Open-grade wearing course of asphalt mixture containing ferrite for use as ferromagnetic pavement. Compos Part B Eng 2014;57:262–8. doi:10.1016/j.compositesb.2013.10.008.
[16] Saini DR, Shenoy AV, Nadkarni VM. Melt rheology of highly loaded ferrite-filled polymer composites. Polym Compos 1986;7:193–200. doi:10.1002/pc.750070402.
[17] Hunyek A, Sirisathitkul C. Electromagnetic and Dynamic Mechanical Properties of Extruded Cobalt Ferrite-Polypropylene Composites. Polym-Plast Technol Eng 2011;50:593–8. doi:10.1080/03602559.2010.543743.
[18] Olalla B, Carrot C, Fulchiron R, Boudimbou I, Peuvrel-disdier E. Analysis of the influence of polymer viscosity on the dispersion of magnesium hydroxide in a polyolefin matrix. Rheol Acta 2011;51:235–47. doi:10.1007/s00397-011-0580-z.
[19] Mai K, Qiu Y, Lin Z. Mechanical properties of Mg(OH)2/polypropylene composites modified by functionalized polypropylene. J Appl Polym Sci 2003;88:2139–47. doi:10.1002/app.11762.
[20] Batistella M, Otazaghine B, Sonnier R, Caro-Bretelle A-S, Petter C, Lopez-Cuesta J-M. Fire retardancy of ethylene vinyl acetate/ultrafine kaolinite composites. Polym Degrad Stab 2014;100:54–62. doi:10.1016/j.polymdegradstab.2013.12.026.
[21] Mills SL, Lees GC, Liauw CM, Lynch S. Dispersion assessment of flame retardant filler/polymer systems using a combination of X-ray mapping and multifractal analysis. Polym Test 2002;21:941–7. doi:10.1016/S0142-9418(02)00038-7.
[22] Qin F, Brosseau C. A review and analysis of microwave absorption in polymer composites filled with carbonaceous particles. J Appl Phys 2012;111:061301. doi:10.1063/1.3688435.
[23] Moučka R, Vilčáková J, Kazantseva NE, Lopatin AV, Sáha P. The influence of interfaces on the dielectric properties of MnZn-based hybrid polymer composites. J Appl Phys 2008;104:103718. doi:10.1063/1.3028272.
[24] Fu S-Y, Feng X-Q, Lauke B, Mai Y-W. Effects of particle size, particle/matrix interface adhesion and particle loading on mechanical properties of particulate–polymer composites. Compos Part B Eng 2008;39:933–61. doi:10.1016/j.compositesb.2008.01.002.
[25] Bhattacharya SK, Tummala RR. Next generation integral passives: materials, processes, and integration of resistors and capacitors on PWB substrates. J Mater Sci Mater Electron 2000;11:253–68. doi:10.1023/A:1008913403211.
[26] Barnes HA. Review of the rheology of filled viscoelastic systems, Rheology Reviews, The British Society of Rheology. Br Soc Rheol 2003:49.
[27] Landel RF, Nielsen LE. Mechanical Properties of Polymers and Composites, Second Edition. New York: CRC Press; 1993.
[28] Ouchiyama N, Tanaka T. Porosity of a mass of solid particles having a range of sizes. Ind Eng Chem Fundam 1981;20:66–71. doi:10.1021/i100001a013.
[29] Kaully T, Siegmann A, Shacham D. Rheology of highly filled natural CaCO3 composites. I. Effects of solid loading and particle size distribution on capillary rheometry. Polym Compos 2007;28:512–23. doi:10.1002/pc.20308.
[30] Cassagnau P. Melt rheology of organoclay and fumed silica nanocomposites. Polymer 2008;49:2183–96. doi:10.1016/j.polymer.2007.12.035.

[31] Kaully T, Siegmann A, Shacham D. Rheology of highly filled natural CaCO3 composites. II. Effects of solid loading and particle size distribution on rotational rheometry. Polym Compos 2007;28:524–33. doi:10.1002/pc.20309.
[32] Hojczyk M, Weichold O. Melt-Rheological Behavior of High-Solid Cement-in-Polymer Dispersions. J Appl Polym Sci 2011;119:565–71. doi:10.1002/app.32676.
[33] Hausnerova B, Honkova N, Kitano T, Saha P. Superposed flow properties of ceramic powder-filled polymer melts. Polym Compos 2009;30:1027–34. doi:10.1002/pc.20645.
[34] Honek T, Hausnerova B, Saha P. Relative viscosity models and their application to capillary flow data of highly filled hard-metal carbide powder compounds. Polym Compos 2005;26:29–36. doi:10.1002/pc.20067.
[35] Yin X, Hong L, Liu Z. A study on the fundamental ceramic–polymer interactions in the high CeO2-loading polyethylene glycol blend. J Eur Ceram Soc 2005;25:3097–107. doi:10.1016/j.jeurceramsoc.2004.09.018.
[36] Fu J-F, Shi L-Y, Zhong Q-D, Chen Y, Chen L-Y. Thermally conductive and electrically insulative nanocomposites based on hyperbranched epoxy and nano-Al2O3 particles modified epoxy resin. Polym Adv Technol 2011;22:1032–1041. doi:10.1002/pat.1638.
[37] Lewis JA. Colloidal Processing of Ceramics. J Am Ceram Soc 2000;83:2341–59. doi:10.1111/j.1151-2916.2000.tb01560.x.
[38] Krieger IM, Dougherty TJ. A Mechanism for Non-Newtonian Flow in Suspensions of Rigid Spheres. Trans Soc Rheol 1957-1977 1959;3:137–52. doi:10.1122/1.548848.
[39] Chong JS, Christiansen EB, Baer AD. Rheology of concentrated suspensions. J Appl Polym Sci 1971;15:2007–21. doi:10.1002/app.1971.070150818.
[40] Metzner AB. Rheology of Suspensions in Polymeric Liquids. J Rheol 1985;29:739–75. doi:10.1122/1.549808.
[41] Poslinski AJ, Ryan ME, Gupta RK, Seshadri SG, Frechette FJ. Rheological Behavior of Filled Polymeric Systems II. The Effect of a Bimodal Size Distribution of Particulates. J Rheol 1988;32:751–71. doi:10.1122/1.549991.
[42] Barnes HA, Hutton JF, Walters K. An Introduction to Rheology. 1st ed. Amsterdam: Elsevier Science; 1989.
[43] Mewis J, Spaull AJB. Rheology of concentrated dispersions. Adv Colloid Interface Sci 1976;6:173–200. doi:10.1016/0001-8686(76)80008-5.
[44] Birinci E, Kalyon DM. Development of extrudate distortions in poly(dimethyl siloxane) and its suspensions with rigid particles. J Rheol 2006;50:313–26. doi:10.1122/1.2184312.
[45] Brown E, Jaeger HM. Shear thickening in concentrated suspensions: phenomenology, mechanisms and relations to jamming. Rep Prog Phys 2014;77:046602. doi:10.1088/0034-4885/77/4/046602.
[46] Denn MM, Morris JF. Rheology of Non-Brownian Suspensions. Annu Rev Chem Biomol Eng 2014;5:203–28. doi:10.1146/annurev-chembioeng-060713-040221.
[47] Pishvaei M, Graillat C, McKenna TF, Cassagnau P. Rheological behaviour of polystyrene latex near the maximum packing fraction of particles. Polymer 2005;46:1235–44. doi:10.1016/j.polymer.2004.11.047.

[48] Pishvaei M, Graillat C, Cassagnau P, McKenna TF. Modelling the zero shear viscosity of bimodal high solid content latex: Calculation of the maximum packing fraction. Chem Eng Sci 2006;61:5768–80. doi:10.1016/j.ces.2006.04.024.
[49] Pishvaei M, Graillat C, McKenna TF, Cassagnau P. Experimental investigation and phenomenological modeling of the viscosity-shear rate of bimodal high solid content latex. J Rheol 2007;51:51–69. doi:10.1122/1.2391069.
[50] Tsai SC, Botts D, Plouff J. Effects of particle properties on the rheology of concentrated noncolloidal suspensions. J Rheol 1992;36:1291–305. doi:10.1122/1.550260.
[51] Faroughi SA, Huber C. Crowding-based rheological model for suspensions of rigid bimodal-sized particles with interfering size ratios. Phys Rev E 2014;90:052303. doi:10.1103/PhysRevE.90.052303.
[52] Pullar RC. Hexagonal ferrites: A review of the synthesis, properties and applications of hexaferrite ceramics. Prog Mater Sci 2012;57:1191–334. doi:10.1016/j.pmatsci.2012.04.001.
[53] Hong J-P, Yoon S-W, Hwang T, Oh J-S, Hong S-C, Lee Y, et al. High thermal conductivity epoxy composites with bimodal distribution of aluminum nitride and boron nitride fillers. Thermochim Acta 2012;537:70–5. doi:10.1016/j.tca.2012.03.002.
[54] Wang B, Wang Q, Li L. Morphology and properties of highly talc- and CaCO3-filled poly(vinyl alcohol) composites prepared by melt processing. J Appl Polym Sci 2013;130:3050–7. doi:10.1002/app.39557.
[55] Alexandre M, Dubois P. Polymer-layered silicate nanocomposites: preparation, properties and uses of a new class of materials. Mater Sci Eng R Rep 2000;28:1–63. doi:10.1016/S0927-796X(00)00012-7.
[56] Reddy B. Advances in Diverse industrial Applications of Nanocomposites. Rijeka: inTech; 2011.
[57] Cassagnau P. Linear viscoelasticity and dynamics of suspensions and molten polymers filled with nanoparticles of different aspect ratios. Polymer 2013;54:4762–75. doi:10.1016/j.polymer.2013.06.012.
[58] Godovskiĭ IK, Privalko VP. Thermal and electrical conductivity of polymer materials. Berlin Heidelberg: Springer; 1995.
[59] Kitano T, Kataoka T, Shirota T. An empirical equation of the relative viscosity of polymer melts filled with various inorganic fillers. Rheol Acta 1981;20:207–9. doi:10.1007/BF01513064.
[60] Genovese DB. Shear rheology of hard-sphere, dispersed, and aggregated suspensions, and filler-matrix composites. Adv Colloid Interface Sci 2012;171–172:1–16. doi:10.1016/j.cis.2011.12.005.
[61] Barnes HA. A Handbook of Elementary Rheology. Aberystwyth: University of Wales, Institute of Non-Newtonian Fluid Mechanics; 2000.
[62] Göktürk HS, Fiske TJ, Kalyon DM. Effects of particle shape and size distributions on the electrical and magnetic properties of nickel/polyethylene composites. J Appl Polym Sci 1993;50:1891–901. doi:10.1002/app.1993.070501105.
[63] Lee G-W, Park M, Kim J, Lee JI, Yoon HG. Enhanced thermal conductivity of polymer composites filled with hybrid filler. Compos Part Appl Sci Manuf 2006;37:727–34. doi:10.1016/j.compositesa.2005.07.006.

[64] Zürcher S, Graule T. Influence of dispersant structure on the rheological properties of highly-concentrated zirconia dispersions. J Eur Ceram Soc 2005;25:863–73. doi:10.1016/j.jeurceramsoc.2004.05.002.
[65] Carrot C, Majesté J-C, Olalla B, Fulchiron R. On the use of the model proposed by Leonov for the explanation of a secondary plateau of the loss modulus in heterogeneous polymer–filler systems with agglomerates. Rheol Acta 2010;49:513–27. doi:10.1007/s00397-010-0432-2.
[66] Bigg DM. Rheological behavior of highly filled polymer melts. Polym Eng Sci 1983;23:206–10. doi:10.1002/pen.760230408.
[67] Nielsen LE. Polymer rheology. New York: M. Dekker; 1977.
[68] Guyot A, Chu F, Schneider M, Graillat C, McKenna TF. High solid content latexes. Prog Polym Sci 2002;27:1573–615. doi:10.1016/S0079-6700(02)00014-X.
[69] Mayadunne A, Bhattacharya SN, Kosior E. Modelling of packing behavior of irregularly shaped particles dispersed in a polymer matrix. Powder Technol 1996;89:115–27. doi:10.1016/S0032-5910(96)03155-5.
[70] Lewis TB, Nielsen LE. Viscosity of Dispersed and Aggregated Suspensions of Spheres. Trans Soc Rheol 1957-1977 1968;12:421–43. doi:10.1122/1.549114.
[71] McGeary RK. Mechanical Packing of Spherical Particles. J Am Ceram Soc 1961;44:513–22. doi:10.1111/j.1151-2916.1961.tb13716.x.
[72] Torquato S, Stillinger FH. Multiplicity of Generation, Selection, and Classification Procedures for Jammed Hard-Particle Packings†. J Phys Chem B 2001;105:11849–53. doi:10.1021/jp011960q.
[73] Kansal AR, Torquato S, Stillinger FH. Diversity of order and densities in jammed hard-particle packings. Phys Rev E Stat Nonlin Soft Matter Phys 2002;66:041109.
[74] Torquato S, Donev A, Stillinger FH. Breakdown of elasticity theory for jammed hard-particle packings: conical nonlinear constitutive theory. Int J Solids Struct 2003;40:7143–53. doi:10.1016/S0020-7683(03)00359-7.
[75] Uche OU, Stillinger FH, Torquato S. Concerning maximal packing arrangements of binary disk mixtures. Phys -Stat Mech Its Appl 2004;342:428–46. doi:10.1016/j.physa.2004.05.082.
[76] Hopkins AB, Stillinger FH, Torquato S. Densest local sphere-packing diversity: General concepts and application to two dimensions. Phys Rev E 2010;81:041305. doi:10.1103/PhysRevE.81.041305.
[77] Hopkins AB, Stillinger FH, Torquato S. Densest local sphere-packing diversity. II. Application to three dimensions. Phys Rev E 2011;83:011304. doi:10.1103/PhysRevE.83.011304.
[78] Torquato S, Jiao Y. Dense packings of polyhedra: Platonic and Archimedean solids. Phys Rev E 2009;80:041104. doi:10.1103/PhysRevE.80.041104.
[79] Chen D, Jiao Y, Torquato S. Equilibrium Phase Behavior and Maximally Random Jammed State of Truncated Tetrahedra. J Phys Chem B 2014;118:7981–92. doi:10.1021/jp5010133.
[80] Mooney M. The viscosity of a concentrated suspension of spherical particles. J Colloid Sci 1951;6:162–70. doi:10.1016/0095-8522(51)90036-0.
[81] Dörr A, Sadiki A, Mehdizadeh A. A discrete model for the apparent viscosity of polydisperse suspensions including maximum packing fraction. J Rheol 2013;57:743–65. doi:10.1122/1.4795746.

[82] Bauhofer W, Kovacs JZ. A review and analysis of electrical percolation in carbon nanotube polymer composites. Compos Sci Technol 2009;69:1486–98. doi:10.1016/j.compscitech.2008.06.018.
[83] Huang J-C. Carbon black filled conducting polymers and polymer blends. Adv Polym Technol 2002;21:299–313. doi:10.1002/adv.10025.
[84] Macosko CW. Rheology: Principles, Measurements, and Applications. 1 edition. New York: New York: Wiley-VCH; 1994.
[85] Raynaud L, Ernst B, Vergé C, Mewis J. Rheology of Aqueous Latices with Adsorbed Stabilizer Layers. J Colloid Interface Sci 1996;181:11–9. doi:10.1006/jcis.1996.0351.
[86] Brouwers HJH. Viscosity of a concentrated suspension of rigid monosized particles. Phys Rev E 2010;81:051402. doi:10.1103/PhysRevE.81.051402.
[87] Dames B, Morrison BR, Willenbacher N. An empirical model predicting the viscosity of highly concentrated, bimodal dispersions with colloidal interactions. Rheol Acta 2001;40:434–40. doi:10.1007/s003970100171.
[88] Fiske TJ, Railkar SB, Kalyon DM. Effects of segregation on the packing of spherical and nonspherical particles. Powder Technol 1994;81:57–64. doi:10.1016/0032-5910(94)02862-1.
[89] Farris RJ. Prediction of the Viscosity of Multimodal Suspensions from Unimodal Viscosity Data. Trans Soc Rheol 1957-1977 1968;12:281–301. doi:10.1122/1.549109.
[90] Ouchiyama N, Tanaka T. Estimation of the Average Number of Contacts between Randomly Mixed Solid Particles. Ind Eng Chem Fundam 1980;19:338–40. doi:10.1021/i160076a002.
[91] Gupta RK, Seshadri SG. Maximum Loading Levels in Filled Liquid Systems. J Rheol 1986;30:503–8. doi:10.1122/1.549856.
[92] Song M, Chuang KT, Nandakumar K. A Theoretical Correction of the Ouchiyama and Tanaka Formula for Predicting Average Porosity of Packed Beds Consisting of Nonuniform Spheres. Ind Eng Chem Res 1998;37:3490–6. doi:10.1021/ie980036o.
[93] Ohashi M, Kawakami S, Yokogawa Y, Lai G-C. Spherical Aluminum Nitride Fillers for Heat-Conducting Plastic Packages. J Am Ceram Soc 2005;88:2615–8. doi:10.1111/j.1551-2916.2005.00456.x.
[94] Xu J, Moon K-S, Tison C, Wong CP. A novel aluminum-filled composite dielectric for embedded passive applications. IEEE Trans Adv Packag 2006;29:295–306. doi:10.1109/TADVP.2006.874701.
[95] M. Inoue JL. Effects of Multi-modal Filler Size Distributions on Thermal Conductivity of Electrically Conductive Adhesives Containing Ag Micro and Nanoparticles. Trans Jpn Inst Electron Packag 2009;2:125–33. doi:10.5104/jiepeng.2.125.
[96] Ishida H, Rimdusit S. Very high thermal conductivity obtained by boron nitride-filled polybenzoxazine. Thermochim Acta 1998;320:177–86. doi:10.1016/S0040-6031(98)00463-8.
[97] Gupta VB, Mittal RK, Sharma PK, Mennig G, Wolters J. Some studies on glass fiber-reinforced polypropylene. Part I: Reduction in fiber length during processing. Polym Compos 1989;10:8–15. doi:10.1002/pc.750100103.
[98] Poslinski AJ, Ryan ME, Gupta RK, Seshadri SG, Frechette FJ. Rheological Behavior of Filled Polymeric Systems I. Yield Stress and Shear-Thinning Effects. J Rheol 1988;32:703–35. doi:10.1122/1.549987.

[99] Cao X-Z, Merlitz H, Wu C-X, Sommer J-U. Polymer-induced entropic depletion potential. Phys Rev E 2011;84. doi:10.1103/PhysRevE.84.041802.
[100] Makled MHM, Washiya H, Tsuda H, Matsui T. Effect of coprecipitated barium ferrite on the cure characteristics and dynamic properties of natural rubber–ferrite composites around percolation. J Appl Polym Sci 2009;113:3294–9. doi:10.1002/app.30263.
[101] Ohshima H. Effective viscosity of a concentrated suspension of uncharged spherical soft particles. Langmuir 2010;26:6287–94. doi:10.1021/la904121p.
[102] Kango S, Kalia S, Celli A, Njuguna J, Habibi Y, Kumar R. Surface modification of inorganic nanoparticles for development of organic–inorganic nanocomposites—A review. Prog Polym Sci 2013;38:1232–61. doi:10.1016/j.progpolymsci.2013.02.003.
[103] Chen X, Gug J, Sobkowicz MJ. Role of polymer/filler interactions in the linear viscoelasticity of poly(butylene succinate)/fumed silica nanocomposite. Compos Sci Technol 2014;95:8–15. doi:10.1016/j.compscitech.2014.01.025.
[104] Ning N, Fu S, Zhang W, Chen F, Wang K, Deng H, et al. Realizing the enhancement of interfacial interaction in semicrystalline polymer/filler composites via interfacial crystallization. Prog Polym Sci 2012;37:1425–55. doi:10.1016/j.progpolymsci.2011.12.005.
[105] Kalyon DM, Dalwadi D, Erol M, Birinci E, Tsenoglu C. Rheological behavior of concentrated suspensions as affected by the dynamics of the mixing process. Rheol Acta 2006;45:641–58. doi:10.1007/s00397-005-0022-x.
[106] Tadmor Z, Gogos CG. Principles of Polymer Processing. John Wiley & Sons; 2006.
[107] Liang JZ, Li RKY. Prediction of tensile yield strength of rigid inorganic particulate filled thermoplastic composites. J Mater Process Technol 1998;83:127–30. doi:10.1016/S0924-0136(98)00051-X.
[108] Seyvet O, Navard P. Collision-induced dispersion of agglomerate suspensions in a shear flow. J Appl Polym Sci 2000;78:1130–3. doi:10.1002/1097-4628(20001031)78:5<1130::AID-APP220>3.0.CO;2-I.
[109] Yamada H, Manas-Zloczower I, Feke DL. Observation and analysis of the infiltration of polymer liquids into carbon black agglomerates. Chem Eng Sci 1998;53:1963–72. doi:10.1016/S0009-2509(98)00043-8.
[110] Kryachek VM. Injection Moulding (Review). Powder Metall Met Ceram 2004;43:336–48. doi:10.1023/B:PMMC.0000048127.24809.d3.
[111] Liu W, Xie Z, Jia C. Surface modification of ceramic powders by titanate coupling agent for injection molding using partially water soluble binder system. J Eur Ceram Soc 2012;32:1001–6. doi:10.1016/j.jeurceramsoc.2011.11.017.
[112] Xia H, Song M. Intercalation and exfoliation behaviour of clay layers in branched polyol and polyurethane/clay nanocomposites. Polym Int 2006;55:229–235. doi:10.1002/pi.1948.
[113] Asghar HMA, Hussain SN, Sattar H, Brown NW, Roberts EPL. Environmentally friendly preparation of exfoliated graphite. J Ind Eng Chem 2014;20:1936–41. doi:http://dx.doi.org/10.1016/j.jiec.2013.09.014.
[114] Sigmund WM, Bell NS, Bergström L. Novel Powder-Processing Methods for Advanced Ceramics. J Am Ceram Soc 2000;83:1557–74. doi:10.1111/j.1151-2916.2000.tb01432.x.

[115] Sommer F, Walcher H, Kern F, Maetzig M, Gadow R. Influence of feedstock preparation on ceramic injection molding and microstructural features of zirconia toughened alumina. J Eur Ceram Soc 2014;34:745–51. doi:10.1016/j.jeurceramsoc.2013.09.020.
[116] Liu D-M, Tseng WJ. Influence of Powder Agglomerates on the Structure and Rheological Behavior of Injection-Molded Zirconia–Wax Suspensions. J Am Ceram Soc 1999;82:2647–52. doi:10.1111/j.1151-2916.1999.tb02136.x.
[117] Yang SY, Huang CK, Lin BC, Wei WCJ. Kneading and molding of ceramic microparts by precision powder injection molding (PIM). J Appl Polym Sci 2006;100:892–9. doi:10.1002/app.23010.
[118] Liu D-M. Effect of Dispersants on the Rheological Behavior of Zirconia-Wax Suspensions. J Am Ceram Soc 1999;82:1162–8. doi:10.1111/j.1151-2916.1999.tb01890.x.
[119] Hanemann T, Heldele R. Fatty Acid Surfactant Structure–Feedstock Flow Properties: Correlation for High-Pressure Ceramic Injection Molding. Int J Appl Ceram Technol 2011;8:1296–304. doi:10.1111/j.1744-7402.2011.02612.x.
[120] Hanemann T, Heldele R, Mueller T, Hausselt J. Influence of Stearic Acid Concentration on the Processing of ZrO2-Containing Feedstocks Suitable for Micropowder Injection Molding. Int J Appl Ceram Technol 2011;8:865–72. doi:10.1111/j.1744-7402.2010.02519.x.
[121] Galindo-Rosales FJ, Moldenaers P, Vermant J. Assessment of the Dispersion Quality in Polymer Nanocomposites by Rheological Methods. Macromol Mater Eng 2011;296:331–40. doi:10.1002/mame.201000345.
[122] Vermant J, Ceccia S, Dolgovskij MK, Maffettone PL, Macosko CW. Quantifying dispersion of layered nanocomposites via melt rheology. J Rheol 2007;51:429–50. doi:10.1122/1.2516399.
[123] Yazici R, Kalyon DM. Degree of Mixing Analyses of Concentrated Suspensions by Electron Probe and X-Ray Diffraction. Rubber Chem Technol 1993;66:527–37. doi:10.5254/1.3538325.
[124] Kalyon DM, Lawal A, Yazici R, Yaras P, Railkar S. Mathematical modeling and experimental studies of twin-screw extrusion of filled polymers. Polym Eng Sci 1999;39:1139–51. doi:10.1002/pen.11501.
[125] Mills SL, Lees GC, Liauw CM, Lynch S. An Improved Method for the Dispersion Assessment of Flame Retardant Filler/Polymer Systems Based on the Multifractal Analysis of SEM Images. Macromol Mater Eng 2004;289:864–71. doi:10.1002/mame.200400138.
[126] Ziadeh M, Fischer B, Schmid J, Altstädt V, Breu J. On the importance of specific interface area in clay nanocomposites of PMMA filled with synthetic nano-mica. Polymer 2014;55:3770–81. doi:http://dx.doi.org/10.1016/j.polymer.2014.05.063.
[127] Carrot C, Olalla B, Fulchiron R. Relaxation of loose agglomerates of magnesium hydroxide in a polymer melt. Polymer 2012;53:5560–7. doi:10.1016/j.polymer.2012.10.004.
[128] Wu R-Y, Wei W-CJ. De-Agglomeration Kinetics of Feedstocks with Granule Tetragonal Zirconia Polycrystalline Powder. J Am Ceram Soc 2005;88:1734–9. doi:10.1111/j.1551-2916.2005.00282.x.
[129] Sakr WF, Ibrahim MA, Alanazi FK, Sakr AA. Upgrading wet granulation monitoring from hand squeeze test to mixing torque rheometry. Saudi Pharm J 2012;20:9–19. doi:10.1016/j.jsps.2011.04.007.

[130] Hidalgo J, Jiménez-Morales A, Torralba JM. Torque rheology of zircon feedstocks for powder injection moulding. J Eur Ceram Soc 2012;32:4063–72. doi:10.1016/j.jeurceramsoc.2012.06.023.
[131] Takahashi M, Suzuki S, Nitanada H, Arai E. Mixing and Flow Characteristics in the Alumina/Thermoplastic Resin System. J Am Ceram Soc 1988;71:1093–9. doi:10.1111/j.1151-2916.1988.tb05797.x.
[132] Kalyon DM, Gotsis AD, Yilmazer U, Gogos CG, Sangani H, Aral B, et al. Development of experimental techniques and simulation methods to analyze mixing in co-rotating twin screw extrusion. Adv Polym Technol 1988;8:337–53. doi:10.1002/adv.1988.060080401.
[133] Song J-H, Evans JRG. A Die Pressing Test for the Estimation of Agglomerate Strength. J Am Ceram Soc 1994;77:806–14. doi:10.1111/j.1151-2916.1994.tb05369.x.
[134] Song JH, Evans JRG. The effect of undispersed agglomerates on the relative viscosity of ceramic moulding suspensions. J Mater Sci Lett 1994;13:1642–4. doi:10.1007/BF00704527.
[135] Küçük I, Gevgilili H, Kalyon DM. Effects of dispersion and deformation histories on rheology of semidilute and concentrated suspensions of multiwalled carbon nanotubes. J Rheol 2013;57:1491–514. doi:10.1122/1.4819745.
[136] Chae DW, Kim BC. Thermal and rheological properties of highly concentrated PET composites with ferrite nanoparticles. Compos Sci Technol 2007;67:1348–52. doi:10.1016/j.compscitech.2006.09.018.
[137] Belaïd S, Boiteux G, Cassagnau P. Rheological and electrical properties of EVA copolymer filled with bamboo charcoal. Rheol Acta 2013;52:75–84. doi:10.1007/s00397-012-0669-z.
[138] Kaully T, Siegmann A, Shacham D. Mechanical behavior of highly filled natural CaCO3 composites: Effect of particle size distribution and interface interactions. Polym Compos 2008;29:396–408. doi:10.1002/pc.20435.
[139] Bender J, Wagner NJ. Reversible shear thickening in monodisperse and bidisperse colloidal dispersions. J Rheol 1996;40:899–916. doi:10.1122/1.550767.
[140] Ianni F, Lasne D, Sarcia R, Hebraud P. Aggregates relaxation in a jamming colloidal suspension after shear cessation. Phys Rev E 2006;74. doi:10.1103/PhysRevE.74.011401.
[141] Yilmazer U, Kalyon DM. Dilatancy of concentrated suspensions with Newtonian matrices. Polym Compos 1991;12:226–32. doi:10.1002/pc.750120403.
[142] Murray LR, Erk KA. Jamming rheology of model cementitious suspensions composed of comb-polymer stabilized magnesium oxide particles. J Appl Polym Sci 2014;131:40429(1-11). doi:10.1002/app.40429.
[143] Laun HM. Rheological properties of aqueous polymer dispersions. Angew Makromol Chem 1984;123:335–59. doi:10.1002/apmc.1984.051230115.
[144] Fall A, Bertrand F, Ovarlez G, Bonn D. Shear thickening of cornstarch suspensions. J Rheol 2012;56:575–91. doi:10.1122/1.3696875.
[145] Brown E, Jaeger HM. The role of dilation and confining stresses in shear thickening of dense suspensions. J Rheol 2012;56:875–923. doi:10.1122/1.4709423.
[146] Bonn D, Paredes J, Denn MM, Berthier L, Divoux T, Manneville S. Yield Stress Materials in Soft Condensed Matter. ArXiv150205281 Cond-Mat 2015.

[147] Laun DHM. Rheological properties of polymer dispersions with respect to shear-induced particle structures. In: Giesekus PDH, D MFHP, editors. Prog. Trends Rheol. II, Steinkopff; 1988, p. 287–90.
[148] Kaully T, Siegmann A, Shacham D. Rheology of highly filled natural CaCO3 composites: IV. Effect of surface treatment. Polym Adv Technol 2007;18:696–704. doi:10.1002/pat.977.
[149] Magnin A, Piau JM. Shear rheometry of fluids with a yield stress. J Non-Newton Fluid Mech 1987;23:91–106. doi:10.1016/0377-0257(87)80012-5.
[150] Piau J-M, Dorget M, Palierne J-F, Pouchelon A. Shear elasticity and yield stress of silica–silicone physical gels: Fractal approach. J Rheol 1999;43:305–14. doi:10.1122/1.550989.
[151] Kataoka T, Kitano T, Sasahara M, Nishijima K. Viscosity of particle filled polymer melts. Rheol Acta 1978;17:149–55. doi:10.1007/BF01517705.
[152] Kalyon DM. Rheological behavior of a concentrated suspension: A solid rocket fuel simulant. J Rheol 1993;37:35. doi:10.1122/1.550435.
[153] Kalyon DM. Apparent slip and viscoplasticity of concentrated suspensions. J Rheol 2005;49:621–40. doi:http://dx.doi.org/10.1122/1.1879043.
[154] Cates ME, Wyart M. Granulation and bistability in non-Brownian suspensions. Rheol Acta 2014;53:755–64. doi:10.1007/s00397-014-0795-x.
[155] Gulmus SA, Yilmazer U. Effect of volume fraction and particle size on wall slip in flow of polymeric suspensions. J Appl Polym Sci 2005;98:439–48. doi:10.1002/app.21928.
[156] Kalyon DM, Gevgilili H, Kowalczyk JE, Prickett SE, Murphy CM. Use of Adjustable-Gap On-Line and Off-Line Slit Rheometers for the Characterization of the Wall Slip and Shear Viscosity Behavior of Energetic Formulations. J Energ Mater 2006;24:175–93. doi:10.1080/07370650600791080.
[157] Kalyon DM, Tang HS, Karuv B. Squeeze Flow Rheometry for Rheological Characterization of Energetic Formulations. J Energ Mater 2006;24:195–212. doi:10.1080/07370650600791148.
[158] Evans JRG, Greener J. Elongational flow processing of ceramics. J Mater Process Technol 1999;96:143–50. doi:http://dx.doi.org/10.1016/S0924-0136(99)00325-8.
[159] Feger C, Gelorme JD, McGlashan-Powell M, Kalyon DM. Mixing, rheology, and stability of highly filled thermal pastes. IBM J Res Dev 2005;49:699–707. doi:10.1147/rd.494.0699.
[160] Allende M, Kalyon DM. Assessment of particle-migration effects in pressure-driven viscometric flows. J Rheol 2000;44:79–90. doi:http://dx.doi.org/10.1122/1.551074.
[161] Shivashankar TS, Enneti RK, Park S-J, German RM, Atre SV. The effects of material attributes on powder–binder separation phenomena in powder injection molding. Powder Technol 2013;243:79–84. doi:http://dx.doi.org/10.1016/j.powtec.2013.03.037.
[162] Fang W, He X, Zhang R, Yang S, Qu X. The effects of filling patterns on the powder–binder separation in powder injection molding. Powder Technol 2014;256:367–76. doi:10.1016/j.powtec.2014.01.065.
[163] Mannschatz A, Höhn S, Moritz T. Powder-binder separation in injection moulded green parts. J Eur Ceram Soc 2010;30:2827–32. doi:http://dx.doi.org/10.1016/j.jeurceramsoc.2010.02.020.
[164] Yaras P, Kalyon DM, Yilmazer U. Flow instabilities in capillary flow of concentrated suspensions. Rheol Acta 1994;33:48–59. doi:10.1007/BF00453463.

[165] Yilmazer U, Gogos CG, Kalyon DM. Mat formation and unstable flows of highly filled suspensions in capillaries and continuous processors. Polym Compos 1989;10:242–248. doi:10.1002/pc.750100406.
[166] Liu W, Xie Z, Bo T, Yang X. Injection molding of surface modified powders with high solid loadings: A case for fabrication of translucent alumina ceramics. J Eur Ceram Soc 2011;31:1611–7. doi:10.1016/j.jeurceramsoc.2011.03.003.
[167] Fiske T, Gokturk HS, Yazici R, Kalyon DM. Effects of flow induced orientation of ferromagnetic particles on relative magnetic permeability of injection molded composites. Polym Eng Sci 1997;37:826–37. doi:10.1002/pen.11725.
[168] Krauss VA, Pires EN, Klein AN, Fredel MC. Rheological properties of alumina injection feedstocks. Mater Res 2005;8:187–9. doi:10.1590/S1516-14392005000200018.
[169] Haworth B, Khan SW. Wall slip phenomena in talc-filled polypropylene compounds. J Mater Sci 2005;40:3325–37. doi:10.1007/s10853-005-0424-2.
[170] Suwardie H, Yazici R, Kalyon DM, Kovenklioglu S. Capillary Flow Behaviour of Microcrystalline Wax and Silicon Carbide Suspension. J Mater Sci 1998;33:5059–67. doi:10.1023/A:1004423411227.
[171] Yilmazer U, Kalyon DM. Slip Effects in Capillary and Parallel Disk Torsional Flows of Highly Filled Suspensions. J Rheol 1989;33:1197–212. doi:http://dx.doi.org/10.1122/1.550049.
[172] Jana SC, Kapoor B, Acrivos A. Apparent wall slip velocity coefficients in concentrated suspensions of noncolloidal particles. J Rheol 1995;39:1123–32. doi:http://dx.doi.org/10.1122/1.550631.
[173] Soltani F, Yilmazer Ü. Slip velocity and slip layer thickness in flow of concentrated suspensions. J Appl Polym Sci 1998;70:515–522. doi:10.1002/(SICI)1097-4628(19981017)70:3<515::AID-APP13>3.0.CO;2-#.
[174] Tang HS, Kalyon DM. Time-dependent tube flow of compressible suspensions subject to pressure dependent wall slip: Ramifications on development of flow instabilities. J Rheol 2008;52:1069–90. doi:http://dx.doi.org/10.1122/1.2955508.
[175] Aral BK, Kalyon DM. Viscoelastic material functions of noncolloidal suspensions with spherical particles. J Rheol 1997;41:599–620. doi:http://dx.doi.org/10.1122/1.550841.
[176] Ariffin A, Jikan SS, Samsudin MSF, Ariff ZM, Ishak Z a. M. Melt Elasticity Phenomenon of Multicomponent (Talc and Calcium Carbonate) Filled Polypropylene. J Reinf Plast Compos 2006;25:913–23. doi:10.1177/0731684406063550.
[177] Dallas P, Kelarakis A, Sahore R, DiSalvo FJ, Livi S, Giannelis EP. Self-suspended permanent magnetic FePt ferrofluids. J Colloid Interface Sci 2013;407:1–7. doi:10.1016/j.jcis.2013.06.024.
[178] Wilson DI, Rough SL. Exploiting the curious characteristics of dense solid–liquid pastes. Chem Eng Sci 2006;61:4147–54. doi:10.1016/j.ces.2005.10.032.
[179] Krug S, Evans JRG, ter Maat JHH. Differential sintering in ceramic injection moulding: particle orientation effects. J Eur Ceram Soc 2002;22:173–81. doi:10.1016/S0955-2219(01)00259-X.
[180] Tarfaoui M, Choukri S, Neme A. Effect of fibre orientation on mechanical properties of the laminated polymer composites subjected to out-of-plane high strain rate compressive loadings. Compos Sci Technol 2008;68:477–85. doi:10.1016/j.compscitech.2007.06.014.

[181] Zhou H, Zhang S, Yang M. The effect of heat-transfer passages on the effective thermal conductivity of high filler loading composite materials. Compos Sci Technol 2007;67:1035–40. doi:10.1016/j.compscitech.2006.06.004.
[182] Barnes HA. A review of the slip (wall depletion) of polymer solutions, emulsions and particle suspensions in viscometers: its cause, character, and cure. J Non-Newton Fluid Mech 1995;56:221–51. doi:http://dx.doi.org/10.1016/0377-0257(94)01282-M.
[183] Bingham EC. Fluidity and plasticity. New York: McGraw-Hill; 1922.
[184] Vand V. Viscosity of Solutions and Suspensions. I. Theory. J Phys Colloid Chem 1948;52:277–99. doi:10.1021/j150458a001.
[185] Barker DA, Wilson DI. Rheology of a thermoplastic paste through the mushy state transition. Chem Eng Sci 2008;63:1438–48. doi:http://dx.doi.org/10.1016/j.ces.2007.12.004.
[186] Aktas S, Kalyon DM, Marín-Santibáñez BM, Pérez-González J. Shear viscosity and wall slip behavior of a viscoplastic hydrogel. J Rheol 2014;58:513–35. doi:10.1122/1.4866295.
[187] Mackley MR, Rutgers RPG, Gilbert DG. Surface instabilities during the extrusion of linear low density polyethylene1. J Non-Newton Fluid Mech 1998;76:281–97. doi:10.1016/S0377-0257(97)00122-5.
[188] Kalika DS, Denn MM. Wall Slip and Extrudate Distortion in Linear Low-Density Polyethylene. J Rheol 1987;31:815–34. doi:10.1122/1.549942.
[189] Taliadorou E, Georgiou GC, Alexandrou AN. A two-dimensional numerical study of the stick–slip extrusion instability. J Non-Newton Fluid Mech 2007;146:30–44. doi:10.1016/j.jnnfm.2006.11.005.
[190] Kim S, Dealy JM. Gross melt fracture of polyethylene. I: A criterion based on tensile stress. Polym Eng Sci 2002;42:482–494. doi:10.1002/pen.10965.
[191] Denn MM. Extrusion Instabilities and Wall Slip. Annu Rev Fluid Mech 2001;33:265–87. doi:10.1146/annurev.fluid.33.1.265.
[192] Vergnes B. Extrusion Defects and Flow Instabilities of Molten Polymers. Int Polym Process 2015;30:3–28. doi:10.3139/217.3011.
[193] Saadat A, Nazockdast H, Sepehr F, Mehranpour M. Linear and nonlinear melt rheology and extrudate swell of acrylonitrile-butadiene-styrene and organoclay-filled acrylonitrile-butadiene-styrene nanocomposite. Polym Eng Sci 2010;50:2340–9. doi:10.1002/pen.21769.
[194] Dangtungee R, Yun J, Supaphol P. Melt rheology and extrudate swell of calcium carbonate nanoparticle-filled isotactic polypropylene. Polym Test 2005;24:2–11. doi:10.1016/j.polymertesting.2004.08.006.
[195] Fulchiron R, Revenu P, Kim B., Carrot C, Guillet J. Extrudate swell and isothermal melt spinning analysis of linear low density polyethylene using the Wagner constitutive equation. J Non-Newton Fluid Mech 1997;69:113–36. doi:10.1016/S0377-0257(96)01527-3.
[196] Dangtungee R, Supaphol P. Melt rheology and extrudate swell of titanium (IV) oxide nanoparticle-filled isotactic polypropylene: Effects of content and surface characteristics. Polym Test 2008;27:951–6. doi:10.1016/j.polymertesting.2008.08.005.
[197] Dangtungee R, Supaphol P. Melt rheology and extrudate swell of sodium chloride-filled low-density polyethylene: Effects of content and size of salt particles. Polym Test 2010;29:188–95. doi:10.1016/j.polymertesting.2009.10.009.

[198] Wagner A, Yazici R, Kalyon DM. Extrudate swell behavior of glass fiber filled polyamide 6. Polym Compos 1996;17:840–849. doi:10.1002/pc.10677.
[199] Phan-Thien N. Influence of wall slip on extrudate swell: a boundary element investigation. J Non-Newton Fluid Mech 1988;26:327–40. doi:10.1016/0377-0257(88)80024-7.
[200] Iruvanti S, Gupta RK, Ruckenstein E. Stable high solids, high thermal conductivity pastes. US5098609 A, 1992.
[201] Lee E-S, Lee S-M, Shanefield DJ, Cannon WR. Enhanced Thermal Conductivity of Polymer Matrix Composite via High Solids Loading of Aluminum Nitride in Epoxy Resin. J Am Ceram Soc 2008;91:1169–74. doi:10.1111/j.1551-2916.2008.02247.x.
[202] Zhang Y, Hu X, Zhao JH, Sheng K, Cannon WR, Wang X, et al. Rheology and Thermal Conductivity of Diamond Powder-Filled Liquid Epoxy Encapsulants for Electronic Packaging. IEEE Trans Compon Packag Technol 2009;32:716–23. doi:10.1109/TCAPT.2009.2029701.
[203] D S Muratov DVK. Thermal conductivity of polypropylene filled with inorganic particles. J Alloys Compd 2014;586:S451–4. doi:10.1016/j.jallcom.2012.11.142.
[204] Dueramae I, Pengdam A, Rimdusit S. Highly Filled Graphite Polybenzoxazine Composites for an Application as Bipolar Plates in Fuel Cells. J Appl Polym Sci 2013;130:3909–18. doi:10.1002/app.39661.
[205] Zhou S, Lei Y, Zou H, Liang M. High thermally conducting composites obtained via in situ exfoliation process of expandable graphite filled polyamide 6. Polym Compos 2013;34:1816–23. doi:10.1002/pc.22586.
[206] Poostforush M. Superior thermal conductivity of transparent polymer nanocomposites with a crystallized alumina membrane. Express Polym Lett 2013;8:293–9. doi:10.3144/expresspolymlett.2014.32.
[207] Gulrez SKH, Ali Mohsin M e., Shaikh H, Anis A, Pulose AM, Yadav MK, et al. A review on electrically conductive polypropylene and polyethylene. Polym Compos 2014;35:900–14. doi:10.1002/pc.22734.
[208] Iruvanti S, Olsen KS, Sachdev KG. Polyester dispersants for high thermal conductivity paste. US5591789 A, 1997.
[209] Moulin G, Favergnon J, Béranger G. Zircone- Céramique fonctionnelle. Tech Ing 2008:1–13.
[210] Wu J, Wei X, Padture NP, Klemens PG, Gell M, García E, et al. Low-Thermal-Conductivity Rare-Earth Zirconates for Potential Thermal-Barrier-Coating Applications. J Am Ceram Soc 2002;85:3031–5. doi:10.1111/j.1151-2916.2002.tb00574.x.
[211] Zhou G, Wang D-W, Li F, Zhang L, Li N, Wu Z-S, et al. Graphene-Wrapped Fe3O4 Anode Material with Improved Reversible Capacity and Cyclic Stability for Lithium Ion Batteries. Chem Mater 2010;22:5306–13. doi:10.1021/cm101532x.
[212] Schneider H, Garsuch A, Panchenko A, Gronwald O, Janssen N, Novák P. Influence of different electrode compositions and binder materials on the performance of lithium–sulfur batteries. J Power Sources 2012;205:420–5. doi:10.1016/j.jpowsour.2011.12.061.
[213] Scheithauer U, Schwarzer E, Richter H-J, Moritz T. Thermoplastic 3D Printing—An Additive Manufacturing Method for Producing Dense Ceramics. Int J Appl Ceram Technol 2015;12:26–31. doi:10.1111/ijac.12306.

[214] Gokturk HS, Fiske TJ, Kalyon DM. Electric and magnetic properties of a thermoplastic elastomer incorporated with ferromagnetic powders. IEEE Trans Magn 1993;29:4170–6. doi:10.1109/20.280866.
[215] Fiske TJ, Gokturk HS, Kalyon DM. Percolation in magnetic composites. J Mater Sci n.d.;32:5551–60. doi:10.1023/A:1018620407013.
[216] Liu D-M. Particle packing and rheological property of highly-concentrated ceramic suspensions: φm determination and viscosity prediction. J Mater Sci 2000;35:5503–7. doi:10.1023/A:1004885432221.
[217] Novak S, Olhero SMH, Ferreira JMF, Zupančič A. Rheological properties of paraffin suspensions of surface-modified alumina powder for low-pressure injection moulding. Rheol Acta 2004;43:559–66. doi:10.1007/s00397-004-0401-8.
[218] Li T q., Wolcott M p. Rheology of wood plastics melt. Part 1. Capillary rheometry of HDPE filled with maple. Polym Eng Sci 2005;45:549–559. doi:10.1002/pen.20308.
[219] Liu G, Xie Z, Wang W, Wu Y. Fabrication of ZrO2–CoAl2O4 Composite by Injection Molding and Solution Infiltration. Int J Appl Ceram Technol 2011;8:1344–52. doi:10.1111/j.1744-7402.2011.02621.x.
[220] Yim C-H, Baranova EA, Abu-Lebdeh Y, Davidson I. Highly ordered LiFePO4 cathode material for Li-ion batteries templated by surfactant-modified polystyrene colloidal crystals. J Power Sources 2012;205:414–9. doi:10.1016/j.jpowsour.2012.01.042.
[221] Wolff MFH, Salikov V, Antonyuk S, Heinrich S, Schneider GA. Novel, highly-filled ceramic–polymer composites synthesized by a spouted bed spray granulation process. Compos Sci Technol 2014;90:154–9. doi:10.1016/j.compscitech.2013.11.006.
[222] Babu I, de With G. Highly flexible piezoelectric 0–3 PZT–PDMS composites with high filler content. Compos Sci Technol 2014;91:91–7. doi:10.1016/j.compscitech.2013.11.027.
[223] Huang X, Xie L, Yang K, Wu C, Jiang P, Li S, et al. Role of Interface in Highly Filled Epoxy/BaTiO3 Nanocomposites. Part I-Correlation between Nanoparticle Surface Chemistry and Nanocomposite Dielectric Property. Ieee Trans Dielectr Electr Insul 2014;21:467–79. doi:10.1109/TDEI.2013.004165.
[224] You Z, Li D. Highly filled bamboo charcoal powder reinforced ultra-high molecular weight polyethylene. Mater Lett 2014;122:121–4. doi:10.1016/j.matlet.2014.01.010.
[225] Vacche SD, Oliveira F, Leterrier Y, Michaud V, Damjanovic D, Månson J-AE. Effect of silane coupling agent on the morphology, structure, and properties of poly(vinylidene fluoride–trifluoroethylene)/BaTiO3 composites. J Mater Sci 2014;49:4552–64. doi:10.1007/s10853-014-8155-x.
[226] Lusiola T, Scharf D, Graule T, Clemens F. Low shear compounding process for thermoplastic fabrication of ferroelectric lead-free fibres. J Eur Ceram Soc 2014;34:2265–74. doi:10.1016/j.jeurceramsoc.2014.02.036.
[227] Voillequin B, Ayme-Perrot D, Dufour B, Sonntag P. Cathode for a Cell of a Lithium-Ion Battery, Its Manufacturing Process and the Battery Incorporating It. US20130183577 A1, 2013

Chapter 2

Materials and Methods

2.1 Materials

In this chapter the materials and the experimental methods that have been used in this work will be presented. As this thesis has been written in articles format, the materials and methods used in each one of the papers will be explained in each article. However, this chapter aims to compile the most important information of the materials and methods used in this study by including some additional information.

2.1.1 Matrix

The polymer matrix used in this work is a commercial grade of polypropylene (PPH 7060) supplied by Total refining & chemicals of density 0.905 g/cm^3, Melt Flow Index of 12 g/10 min (230°C/2.16 kg) and melting temperature of 165 °C. The polypropylene (PP) has been stabilized by using Irganox 1010 at 1 wt% based on the weight of the matrix (PPI: stabilized matrix). Irganox 1010 is a sterically hindered phenolic antioxidant whose function is to protect PP matrix against thermo-oxidative degradation. Such degradation was found to represent more than 20% loss in the absolute complex viscosity after the same process conditions as shown in Fig. 2.1. For this reason, this component was used in all our formulations. The zero-shear viscosity of the stabilized matrix is $\eta_0 = 3800$ Pa.s at T=190°C as depicted in Fig. 2.2.

2.1.2 Ferrites

The ferrite powder NK132 (F) was supplied by Toda Kogyo Corp., Japan. This powder is a solid solution of Strontium with a low quantity of Barium Ferrite. The chemical composition and other powder characteristics are given in Table 2.1. The aspect ratio (p) is defined as the diameter (D) to the thickness (L) ratio and has been estimated by Scanning Electron Microscopy (SEM) coupled to image analysis software (Image J). The average aspect ratio was estimated to be $p \sim 4$ and thus the average thickness has been calculated as the ratio of $D_s(0.5)/p \approx 0.5$ μm.

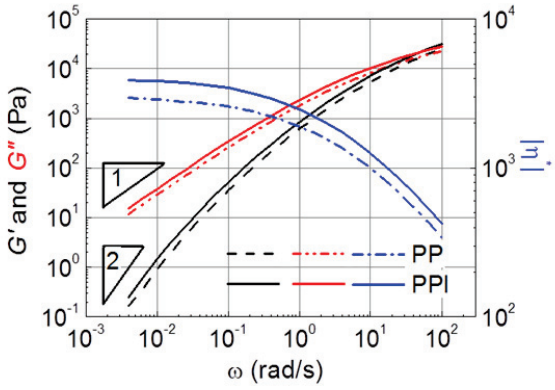


Fig. 2.1. Complex viscosity and storage and loss modulus as a function of angular frequency (190°C) for pure PP compared to the stabilized PP by adding 1 wt% of Irganox.

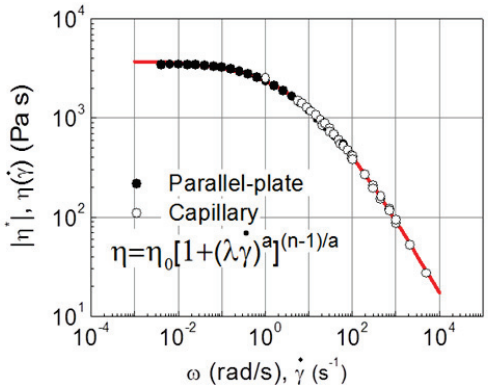


Fig. 2.2. Shear viscosity as a function of the shear rate and complex viscosity as a function of the angular frequency for the stabilized matrix (PPI). Carreau-Yasuda model, zero shear viscosity $\eta_0 = 3800$ Pa s, Pseudoplasticity index n=0.22, Characteristic time λ=0.092 s, transition index a=0.47.

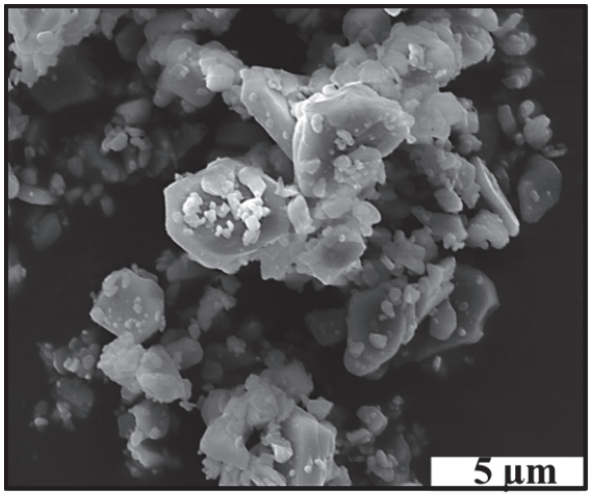


Fig. 2.3. Scanning electron image of dry ferrite particles under 15 kV, high vacuum, Hitachi S800.

Table 2.1. Powder characterization of Ferrite NK132 particles.

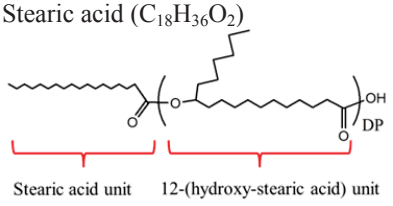
Powder characterization					**Method**
Chemical composition		$SrO.6Fe_2O_3$ (92-99 wt%)	$BaO.6Fe_2O_3$ (1-8 wt%)		Checked by SEM-EDX*
PSD	**D(i) (µm)**	D(0.1)	D(0.5)	D(0.9)	Light scattering: Mastersizer 2000(dry analysis, 2 bar gas flow)
	Surface area (D_s)	0.85	1.96	3.15	
Surface area (SSA)		1.80 m^2/g			BET
Density		4.45 ± 0.06 g/cm^3			Pycnometer (T=25°C)
Bulk density		3.20 g/cm^3			Compressed (1ton/cm^2)
Aspect ratio (*p=D/L*)		3.97 ± 1.40			SEM-Image J (based on 50 particles)
Shape		Hexagonal plate-like			SEM

**SEM-EDX: Scanning electron microscopy coupled to Energy-dispersive X-ray spectroscopy.*

2.1.3 Dispersant

A commercial dispersant supplied by Lubrizol, Advanced Materials was used in this work. Some of its most important characteristics are compiled in Table 2.2.

Table 2.2. Characteristics of the dispersant used in this work

Name	Solplus DP310 (SDP310)
Nature	fatty acid dispersant, carboxyl functional group
Repeated pattern	Stearic acid ($C_{18}H_{36}O_2$)
Structure	
Degree of Polymerization (DP)	1 to 10
Melting temperature (°C)	105.5
Density (g/cm3)	0.952

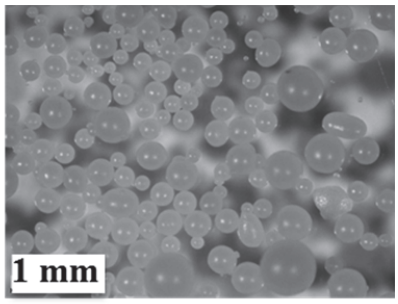


Fig. 2.4. Optic image of the commercial dispersant Solplus DP310

2.1.4 Short-glass fibers

Two commercial short-glass fibers were used in this work: VS 1304 and VS 1320 K, provided by Owens Corning. They are Vitrostrand milled fibers made from E-glass, Advantex® Glass (boron and fluorine-free). Table 2.3 compiles all the technical characteristics given by the supplier, as well as

some of our characterizations. The fibers will be named in this work as Short fibers (SF) for VS 1304 and Long Fibers (LF) for VS 1320 K.

Table 2.3. Technical characteristics given for the two commercial grades of fibers VS 1304 (SF) and VS 1320 K (LF).

Fiber name	VS 1304 (SF)	VS 1320 K[(2)] (LF)	Method
Nominal fiber diameter[(1)] (µm)	16	16	*Cross section of the strand*
Average fiber length[(1)] (µm)	80	160	*Optic-Image analysis*
Average fiber diameter (µm)	~12	~12	*Optic-Image analysis*
Measured length (µm)	97	112	*Light scattering*
Aspect ratio	8.1	9.3	*L/D*
Moisture content (wt%)	0.02	0.04	*TGA*
Bulk density[(1)] (g/cm^3)	1.2	0.65	-
density (g/cm^3)	2.73	2.73	*Experimentally-TGA*
Product appearance	Powdery	Lumpy powdery	-

[(1)]Technical characteristics given by the supplier
[(2)]K = lubricant in the formulation

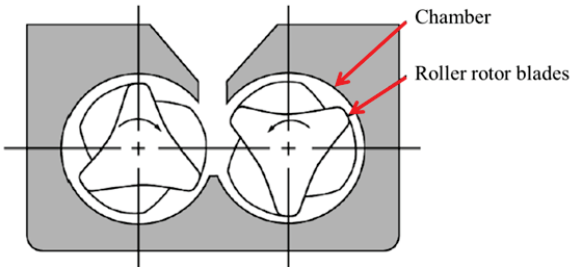
2.2 Elaboration process

2.2.1 Batch mixing: internal mixer

The composites were prepared using an internal mixer (HAAKE PolyLab Mixer Rheomix 600, Thermo Fisher Scientific). The total volume of the compounds was formulated to fill 62% of the volume of the mixer chamber. Table 2.4 presents the geometric dimensions of the internal mixer used in this work. All the compounding processes were performed at 190 °C.

Table 2.4. Geometric dimensions and schematic representation of the internal mixer used in this work. Figure adapted from [1].

Volume of the chamber (cm^3)	69
Largest rotor radius (R_e) (mm)	18
Smallest rotor radius (R_i) (mm)	11
Widest gap size (mm)	8.6
Smallest gap size (mm)	2



Therefore, in the narrow gap case, the average shear rate can be calculated by using the Couette analogy showed in Equation (2.1) [2]:

$$\dot{\gamma} = \frac{2\pi N}{\ln(R_e/R_i)} \quad (2.1)$$

Where N is the rotor speed (rpm), R_e and R_i the largest and smallest rotor radius. Thus, the average shear rate at 50 rpm is~10 s^{-1}. Subsequently, laminar flow is expected due to the high viscosity of the molten PP (Re~10^{-4}). Hence, laminar mixing is the only mechanism in this batch process [3]. Thus, in order to improve homogeneity and reduce particle agglomeration, the mixing was carried out by using different steps sequences.

On the one hand, ferrites were incorporated into PP by following 5 steps: melting (2 min, 50 rpm), incorporation (3 min, 15 rpm), pre-mixing (1 min, 50 rpm), incorporation (4 min, 15 rpm) and mixing (10 min, 50 rpm). During the melting step, the PP granules and the irganox powder were melted and blended. Dispersant was also added at the end of this step. Finally, all the components were mixed for 10 min. The variations of the measured torque and temperature with time for a sample filled with 30 vol% of ferrites are shown in Fig. 2.5(a).

On the other hand, the fibers-based composites compounding was divided into three steps: melting (1 min, 30 rpm), incorporation (2 min-15 rpm) and mixing (10 min-50 rpm). The mixing time was considerably reduced compared to the ferrite mixtures, even though the last mixing step was maintained the same. Fig. 2.5(b) shows the mixing process for a composite filled with 30 vol% of SF.

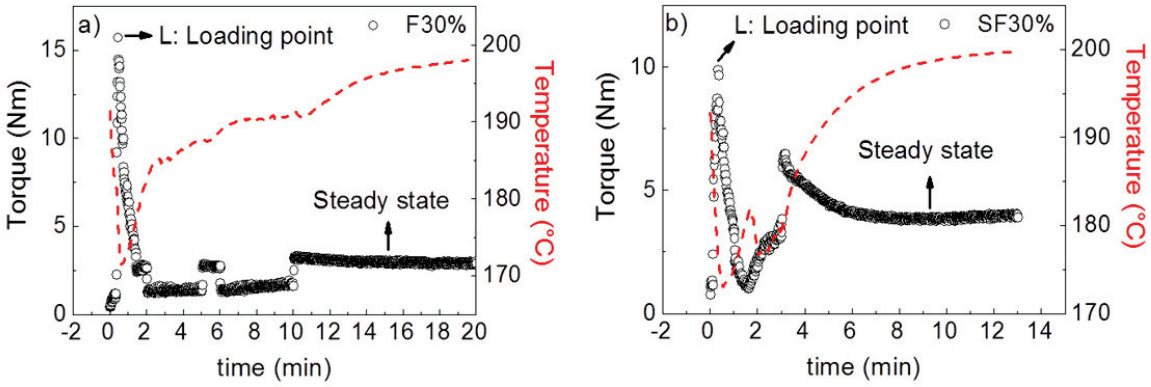


Fig. 2.5. Variation of the measured torque and temperature as a function of the mixing time for (a) ferrite/PP and (b) fibers/PP filled with 30 vol%, at a set temperature of 190 °C.

2.2.2 Continuous mixing: extrusion process

The mixing of the components was also performed by extrusion process by means of a Leistritz ZSE-18, fully intermeshing co-rotating twin-screw extruder. The barrel length over barrel diameter was L_b/D_b=60 and the D_b=18 mm.

In the case of ferrite/PP and ferrite/dispersant/PP, composites with filler levels from 10 to 40 vol% were compounded. The operating conditions were fixed at 190°C, a speed of 800 rpm and a mass flow rate of 3kg/h. The mean residence time under these conditions is estimated to be ~70 s. The global process steps consist in a manual pre-mixing of the components, then, the raw materials were

blended in the extruder, granulated and then shaped into rheometer disks by injection molding, Babyplast 610P, Alecop at 190 °C. Two kinds of samples were prepared by this process: samples without and with the dispersant agent. The concentration of dispersant was fixed at 2 wt% based on the weight of the filler. The screw profile used in this study is illustrated in Fig. 2.6(a). This is considered as a soft profile without reverse-conveying elements.

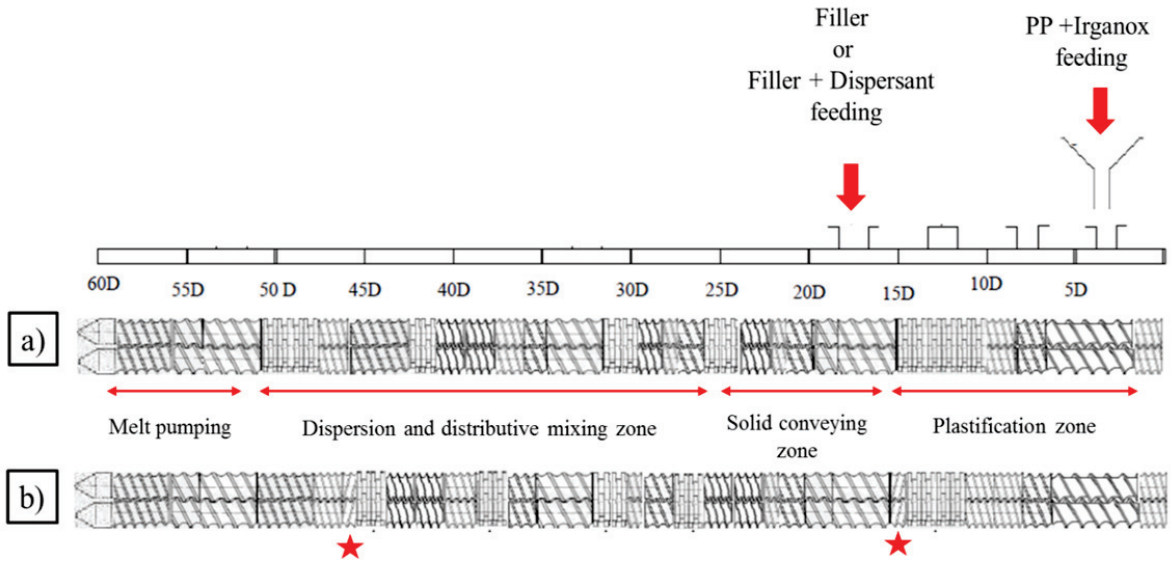


Fig. 2.6. (a) Soft and (b) hard screw profile used in this study and the zones of mixing. Two reverse-conveying elements were included in the hard screw profile. Leistritz ZSE18, $L/D_b = 60$.

In the case of fibers/PP composites, composites with 30 vol% were prepared for both types of composites (SF and LF).The temperature was fixed at 190 °C, while the rotation speed and the mass flow rate were varied as Table 2.5 shows. The raw materials were blended in the extruder, granulated and then shaped into rheometer disks by injection molding, Babyplast 610P, Alecop at 190 °C. The two screw profiles showed in Fig. 2.6 were used in this study. It is worth noting that, 30 vol% was the maximum filler level attained under these conditions for LF.

Table 2.5. Operating conditions studied for SF and LF

N (rpm)	200	400	600	800	400
Flow rate (kg/m^3)	3	3	3	3	5

2.3 Rheological characterization

2.3.1 Rotational rheometer

The rheological characterization of the different composites has been performed in oscillatory dynamic mode with a stress-controlled Discovery Hybrid Rheometer (DHR-2), TA instruments. This device is equipped with a torque transducer, ranging from 2 nN/m to 200 mN/m and a normal force

transducer, ranging from 0.005 to 50 N. The temperature was always fixed at 190 °C and controlled by the convection/radiant heating oven (Environmental Test Chamber, ETC) under Nitrogen atmosphere. Two different stainless steel geometries were used in this work: a cone-and-plate geometry with a diameter of 25 mm and a cone angle of 2° and parallel-plate geometry with the same diameter.

Time sweep experiments were performed in the case of ferrite/PP composites for samples filled up to 20 vol% in a cone-and-plate geometry. The protocol consisted in three steps. First, a pre-shear to the sample was applied at 1 s^{-1} for 160 s. Second, the sample was led under quiescent conditions for 1 min and finally, the oscillatory time sweep experiment at fixed frequency and strain was performed as shown Fig. 2.7.

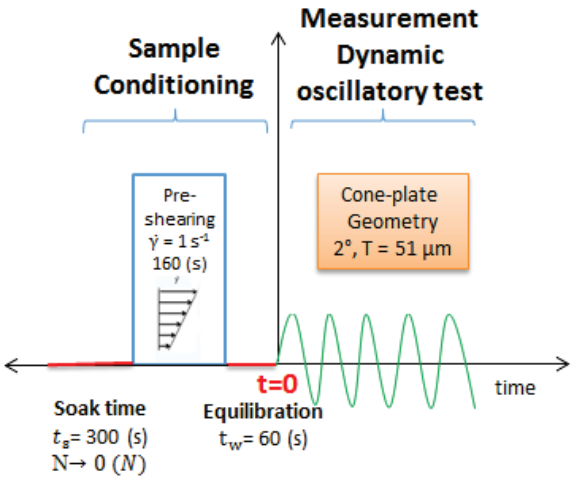


Fig. 2.7. Experimental protocol to study the evolution of the structure by oscillatory time sweep.

The linear viscoelastic domain was carefully measured for all the composites at 1 rad/s, before performing the oscillatory frequency sweep tests.

2.3.2 Capillary rheometer

A twin-bore capillary rheometer (RH7, Rosand, Malvern) was used to study the shear flow behavior of the composite melts. The diameter of the bore was 15 mm. A schematic representation of our set-up is displayed in Fig. 2.8. Steady shear flow properties were measured from 1 s^{-1} to 4×10^4 s^{-1} at 190 °C. To achieve this large range of shear rates, this device is equipped with different pressure sensors, ranging from 250 to 10000 psi. On the right bore, the Bagley correction is performed by means of a "zero length" die. On the left bore, the capillary die is positioned. To maintain consistency between the tests, a pre-conditioning was applied before running all the experiments. Such pre-conditioning enables a good contact between the piston and the melt composite, lets the whole sample to reach the thermal equilibrium and removes trapped air bubbles. It consisted in two cycles of

compression and soak times (5, 4 min). The compression steps were performed at a piston speed of 50 mm/min until reaching a limit pressure value at each one of the capillary entrance.

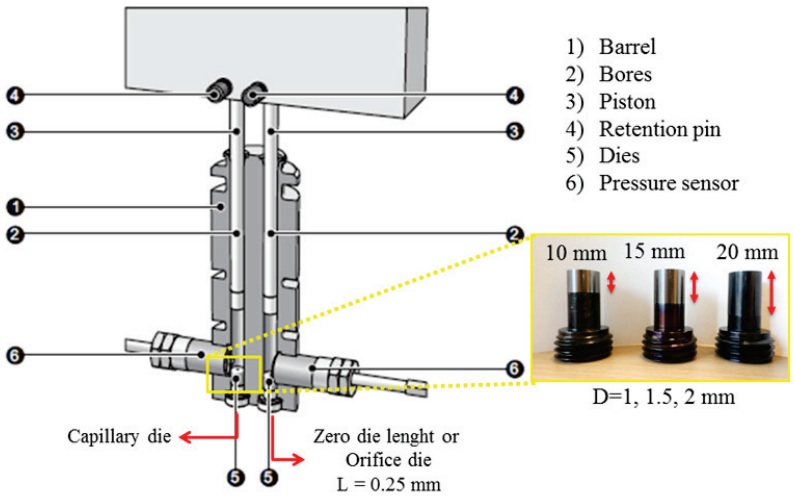


Fig. 2.8. Capillary rheometer components and picture of three capillary dies used in this work of dimensions: L/D=10/1; 1.5/15; 20/2. Adapted from [6]

Wall slip analysis was performed by the traditional Mooney method. Hence, slip at the wall was analyzed by using three different dies with same Length over Diameter ratio and entry angle of 180° (*L/D*=10/1, 15/1.5 and 20/2 mm/mm). The obtained data was further processed according to Bagley correction by deducing the entry pressure measured with the zero length die.

The shear viscosity of the composite was analyzed by using a die with L/D=20/1 and entry angle 180°. The Bagley correction was again applied. The Rabinowitsch correction did not change in any aspect the behavior of the filled composites but slightly enhanced the differences. We thus decided to show the apparent shear rate to be consistent with the wall slip analysis.

References

[1] Michen MI. Co-extrusion of Piezoelectric Ceramic Fibres. 2011.

[2] Bousmina M, Ait-Kadi A, Faisant JB. Determination of shear rate and viscosity from batch mixer data. J Rheol 1999;43:415–33. doi:10.1122/1.551044.

[3] Rauwendaal C. Mixing in Polymer Processing. CRC Press; 1991.

[4] Kohlgrüber K. Co-Rotating Twin-Screw Extruder. Carl Hanser Verlag GmbH & Company KG; 2012.

[5] Charrier J-M, Rieger J-M. Flow of short glass fibre-filled polymer melts. Fibre Sci Technol 1974;7:161–72. doi:10.1016/0015-0568(74)90014-1.

[6] Malvern instruments. User Manual Rosand-RH7-RH10 2006. http://www.malvern.com/en/support/resource-center (accessed October 20, 2016).

Part II

Chapter 3

Ferrite composites under quiescent conditions

Summary

This paper focuses on the relation between the structure and the rheological properties of non-Brownian ferrite particles suspended in a molten polypropylene (PP) matrix with and without the addition of a dispersant agent. The studied filler levels were 2, 15 and 20 vol%. Under low deformation, the measurement of the complex shear modulus over time showed that the material structure were not stable. Such evolution was, on the one hand, more visible at concentrations near the percolation threshold ($\phi_c \approx 0.25$) and on the other hand, less visible when adding a dispersant agent. Oscillatory time sweep experiments were performed after a pre-shearing. It was shown that the kinetics of the evolution strongly depends on the applied deformation. Such evolution has also been highlighted by optical microscopy, in which an agglomeration phenomenon was clearly observed after few hours, again less visible for formulations with dispersant agent. Under high deformations, no structure evolution was noticeable. Our results stress the important role of adding a dispersant into the formulation of highly filled materials. The dispersant agent acts therefore as a stabilizer and lubricating agent. The origin of such structuring process has been attributed to a favorable entropy gradient from the polymer chains between the particles to the polymer chains in the bulk.

Reformatted version of paper originally published in:

Journal of Rheology, Volume 60, Issue 6 (2016), Page 1245-1255

Structuring of non-Brownian ferrite particles in molten polypropylene: viscoelastic analysis

Martha Margarita Rueda[1,2], René Fulchiron[1], Arnaud Prebé[2], Grégory Martin[2], Philippe Cassagnau[1]

[1)] *Univ-Lyon, Université Lyon 1, Ingénierie des Matériaux Polymères, CNRS, UMR 5223, 15 Bd Latarjet, 69622 Villeurbanne Cedex, France.*

[2)] *HUTCHINSON Research Center, Rue Gustave Nourry – B.P. 31, 45120 Chalette-sur-Loing, France.*

I. Introduction

The elaboration process of highly filled materials remains very difficult in the industry and continuous technological developments need to be performed to attain higher filler levels [1,2]. Increasing the fraction of fillers leads to a strong increase of the viscosity which is clearly disadvantageous for mixing and extrusion processes. As a consequence, lack of dispersion together with low interfacial adhesion between the filler and the matrix get reflected in terms of poor properties and inhomogeneous products. To address this challenge, it is imperative to get insight into the flow properties and stability of filled polymers.

Particularly in terms of industrial applications, ferrites particles are extensively used in data storage media materials (*e.g.,* hard disk), magnetic recording media, magnetic encoder wheels, clutches and also in damping fluids (*e.g.,* shock absorbers, breaks) due to the ease of control of their rheological properties. Continuous demand for higher magnetic properties and particularly higher storage densities conduces to increase the filler level.

The common idea to develop high-performance filled polymers is, on the one hand, the particulate phase needs to be fully dispersed in the continuous phase [3–6], resulting in individual particles surrounded by a shell of polymer. On the other hand, melt rheological properties need to be stable over time in order to adequately characterize the material and thus control the final dispersion.

Particles suspended in a continuous phase are thermodynamically unstable and the suspension rheological behavior is determined by the structure that particles form during flow [7,8]. Therefore, interparticle interactions play a crucial role in the rheological properties and stability of the suspension [8–10]. In literature, many studies can be found about nanocomposites subjected to clustering mechanism under annealing. This agglomeration process has been clearly evidenced by rheological time measurements in which the structuring of particles results to an elastic network structure which manifests by a solid-like behavior. Even so, the mechanism controlling particle re-organization remains not completely clear. In the majority of cases, these studies perform a pre-conditioning (pre-shearing) to the sample before following the rheological properties with time [11–16]. The latter is performed to erase the emplacement and to impart an initial morphology to the

sample. Some authors [10,12,13] observed that after pre-shearing, the structure evolution presents a double kinetics depicted by two different time scales: a short one, in which particles relax from the alignment imposed by the pre-shear and a long one attributed to the slow aggregation of particles. Under quiescent conditions, organoclay/polypropylene nanocomposites has been reported to evolve with time [12,15–17]. Carbon black and Carbon nanotubes' suspensions are also common examples; these particles form a fractal network under annealing, phenomenon which is responsible of the augmentation of the electrical conductivity and elasticity [14,18–20]. Finally, silica suspensions have been also found to form a fractal arrangement, giving rise to a gel network at low concentrations [9,21]. Cao *et al.* [21] demonstrated the ability to tune the gelation process by changing the ionic strength of the dispersion. In general, such colloidal suspensions can be either dispersed or flocculated, depending on the magnitude of interparticle interactions and particle-matrix interactions [22]. It is important to note that the fractal dimension of the aggregates, commonly found between 1.8 $<d_f<2$, showed that the initial particles and agglomerates clump over time by creating flocs of few micrometers [9,10,21,23].

According to the above mentioned procedure, nanocomposites with particles size about a few nanometers cannot achieve very high filler levels due to the ultra-large interfacial area per volume between the components which lead to nanostructured fractal networks and thus very low percolation thresholds. Therefore, particles which size is about or superior to several hundred nanometers are necessary to achieve highly filled materials [3]. Particles much smaller than 1μm bring some conceptual and technical difficulties, such as time dependencies during flow deformation and difficulties to disperse the fillers during the mixing process [1].

In this work, the micro-structure of ferrite filled polymer has been studied under dynamic conditions. Generally, ferrite suspensions studies use dispersants to stabilize flow properties [24–27]. Therefore, this paper focuses on the relation between the structure and the rheological properties of ferrite particles suspended in molten polypropylene (PP) matrix with and without the addition of a dispersant agent. In fact, regarding polymer filled with micro-particles, stability has been rarely reported [28] and rheological studies normally consider no structure evolution over time under small deformation. An unexpected flow behavior has been found for such ferrite filled polymer and thus complicating effects when under dynamic flow will be reviewed in detail in this paper.

II. Materials and Methods

A. Materials

1. Polymer

The polymer matrix used in this study is a commercial grade of polypropylene (PPH 7060) supplied by Total refining & chemicals of density 0.905 g/cm^3 (ISO1183) and Melt Flow Index of 12 g/10 min (230°C/2.16 kg). The melting temperature is 165 °C and its melt density was assumed to be 0.7 g/cm^3. Irganox 1010 was used as a thermal stabilizer (I) at 1 wt% based on the weight of the matrix. It protects PP matrix against thermo-oxidative degradation. The zero-shear viscosity for the stabilized matrix was $\eta_0 = 3760$ Pa s at T=190°C.

2. Particles

The ferrite powder NK132 (F) was supplied by Toda Kogyo Corp., Japan. This powder is a solid solution of Strontium with a low quantity of Barium Ferrite. It belongs to the ferrimagnetic hard ferrites family with a near hexagonal flake shape as shown in Fig.1(a). The chemical composition and other powder characteristics are given in Table I. The particle size distribution (PSD) was characterized by laser diffraction, using a Malvern instrument Mastersizer 2000. Light scattering device averages various dimension as the particles flow randomly; however, when disk-like particles are considered, the influence of the thickness (z-axis) is smaller when compared to the x-y plan dimension. For this, volume distribution (3D) has been converted to surface distribution (2D) in order to minimize errors, thus $D_s(0.5)$ corresponds to the median diameter of the plate particles, while, $D_v(0.5)$ corresponds to the equivalent sphere with the same volume as the particle (also known as the nominal diameter [29]). Fig.1(b) shows the PSD by volume and the converted surface distribution. The aspect ratio (A_r) is defined as the diameter ($d=2a$) to the thickness (l) and has been estimated by Scanning Electron Microscopy (SEM) coupled to image analysis software (Image J). The calculated A_r was about $d/l \sim 4$ and thus the average thickness has been estimated as the ratio of $D_s(0.5)/A_r \approx 0.5$ µm.

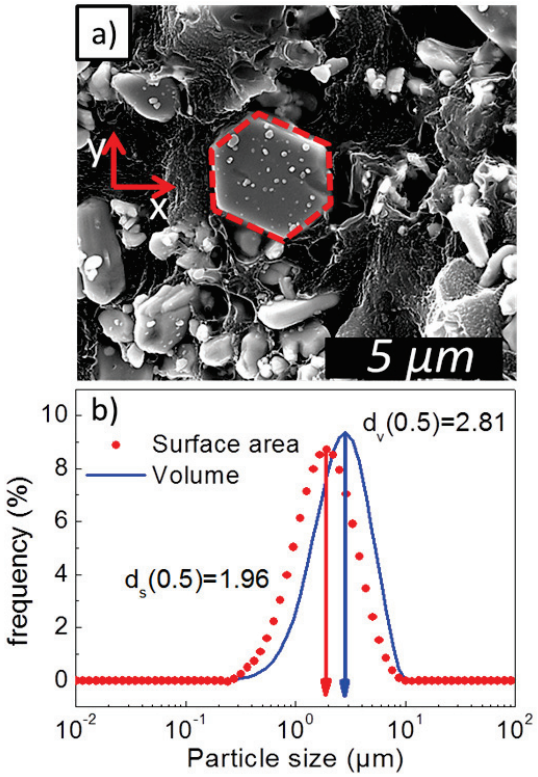


Fig.1. Ferrite particle characterization. (a) SEM image of ferrite/PP composite at 20 vol% of filler level, 10kV, (b) Particle size distribution by volume (3D) and by surface area (2D) for ferrite particles obtained by Master sizer 2000, dry measure, 2 bar.

Table I. Powder characterization of Ferrite NK132 particles.

Powder characterization					**Method**
Chemical composition		$SrO.6Fe_2O_3$ (92-99 wt%)		$BaO.6Fe_2O_3$ (1-8 wt%)	Checked by SEM-EDX*
PSD	D(i)	D(0.1)	D(0.5)	D(0.9)	Light scattering: Mastersizer 2000 (dry analysis, 2 bar gas flow)
	Volume (D_v)	1.25 µm	2.81 µm	5.58 µm	
	Surface area (D_s)	0.85 µm	1.96 µm	3.15 µm	
Surface area (SSA)		$1.80\ m^2/g$			BET
Density		$4.45 \pm 0.06\ g/cm^3$			Pycnometer (T=25°C)
Bulk density		$3.20\ g/cm^3$			Compressed ($1ton/cm^2$)
Aspect ratio (A_r=d/l)		3.97 ± 1.40			SEM-Image J (based on 50 particles)
Shape		Hexagonal plate-like			SEM

**SEM-EDX: Scanning electron microscopy coupled to Energy-dispersive X-ray spectroscopy.*

4. *Dispersant*

Solplus DP310 (SDP310) was kindly supplied by Lubrizol, advanced materials. SDP310 was selected for this study due to its high thermal stability and good compatibility with polyolefins and inorganic fillers. It comes as a white powder with a density of 0.952 g/cm^3 and a melting point of 105.5°C.

Matrix-assisted laser desorption/ionization time-of-flight (MALDI-TOF) mass spectrometry has been used to analyze the chemical composition of such dispersant. MALDI-TOF technique showed that the masses of the highest peaks increased at the distance of 282 uma, corresponding to one stearic acid unit. This fatty acid presented a high polydispersity which goes from one to ten stearic acid units. Fig.2(a) shows the molecule which has been found by this analysis. Nonetheless, results are not quantitative for samples with very large distribution, as in our case. This means that it cannot be possible to know which population is present in the largest amount. Proton Nuclear Magnetic Resonance spectroscopy (NMR) corroborated the latter results, without giving additional quantitative information again due to the high polydispersity of population.

On the basis of these results, it can be stated that SDP310 is a molecule with a carboxyl functional group, with a high dispersity index. In literature, those dispersants are widely used due to its ability of adsorbing onto the surface of inorganic powders. They are able to build chelate complexes via hydrogen bonding with the hydroxyl sites on the ferrite surface [26] as shown in Fig.2(b), leading to the reduction of the attractive forces either by steric barrier or by increasing the particle charge [30–32].

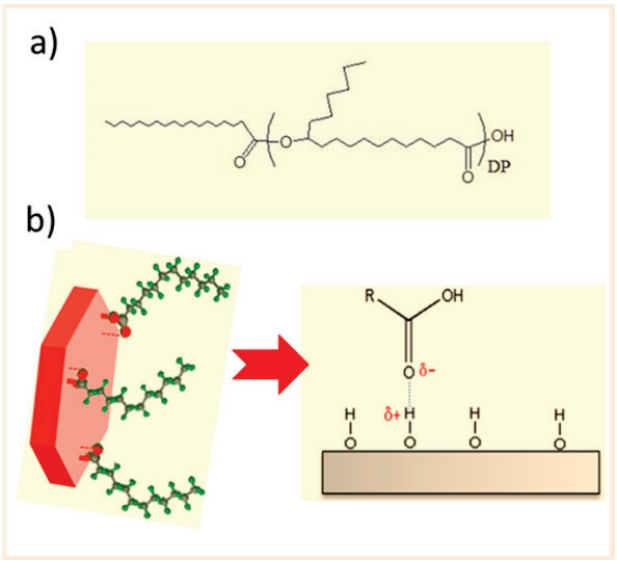


Fig.2. Chemical modification of the ferrite surface: (a) SDP310 molecule with a Stearic acid ($C_{18}H_{34}O_2$) repeat pattern found by MALDI-TOF technique, (b) Schematic representation of fatty acid reacting with the hydroxyl sites of ferrites surface (adapted from [33]).

B. Sample preparation

Ferrite particles were incorporated into PP by melt mixing using a Haake Rheomix 600 internal mixer (Thermo Fisher Scientific) at 190°C. The mixing unit contained a net volume of 69 cm^3 with the rotors. The filling level of the chamber was fixed at 62%. Roller rotor blades were used to blend the materials. The blending was divided into 5 steps: melting (2 min, 50 rpm), incorporation (3 min, 15 rpm), pre-mixing (1 min, 50 rpm), incorporation (4 min, 15 rpm) and mixing (10 min, 50 rpm). During the melting step, the PP granules and the Irganox powder were melted and blended. Dispersant was also added at the end of this step. Two incorporation steps were performed in order to be able to further fill the matrix, while maintaining the same operating conditions. Finally, all the components were mixed for 10 min. The reported kneading torque was always constant over the last 2 min of the mixing step, indicating that the mixtures were homogeneous and have reached the equilibrium under the present conditions. Samples containing 2, 15, 20 vol% (9, 46, 55 wt%) of fillers were prepared by this method. Finally, disks of 0.5 mm thickness and 25 mm diameter were prepared by hot-pressing at 190°C.

Two kinds of samples were prepared by the before-mentioned process: samples without dispersant and samples with dispersant. The concentration of dispersant was fixed at 2 wt% based on the filler weight.

C. Dynamic rheological tests

The rheological measurements were conducted on a Discovery Hybrid Rheometer (DHR), TA instruments. All measurements were performed at 190 °C under nitrogen atmosphere, using a cone-plate geometry (angle: 2°, D=25 mm, Truncation=51 μm). A sample conditioning was performed before all the experiments to minimize the effect of the sample loading and to control the initial state of dispersion. Such protocol consisted in three steps: 1. Soak time of 300 *s* in order to enable the sample to relax stresses due to the loading, 2. Pre-shearing of 1 s^{-1} for 160 s, 3. Equilibration step in which the sample was maintained under quiescent conditions for 60 *s*. The latter time is also known in literature as rest (t_w) or annealing time. Very low shear rates are preferred in the pre-shear step in order to avoid material expulsion from the cone-plate geometry. The linear viscoelastic deformation was carefully determined for each sample. As expected, the more the filler level, the shorter the linear viscoelastic domain (LVD). Oscillatory time sweeps were performed at fixed frequency of 1 rad/s and different deformations: 4×10^{-4}, 10^{-3}, 10^{-2}, 10^{-1}, even out of the LVD. Frequency sweeps measurements have been also performed by varying the frequency at fixed deformation. From an experimental point of view, the errors on the measurements of the complex shear modulus are lower than 10%.

D. Morphological measurements

The state of dispersion and powder characterization has been studied by SEM microscopy (Quanta 250, high vacuum) under an acceleration voltage of 10 kV, with an E-T detector. Prior to

observations, samples were cryo-cut and metallized with 80/20 Au/Pd coating by means of a Hummer RII sputtering system, for 3min ½ at 10 mA.

Larger scale observations were performed by means of an optical Leitz Orthoplan SM-POL microscope, with an objective lens UM 32/0.3. This microscope was coupled to a Linkam optical shearing cell (CSS450), in which the gap and the temperature can be controlled. Digital images were recorded by means of a QImaging Camera. Observations were performed at an exposure time of 2.5 s, 190 °C, 80 µm gap in a parallel quartz plate. It is important to note that the shearing optic cell enables us to maintain similar initial conditions to the dynamic rheological measurements. Image recording has been performed under quiescent conditions after same conditions of pre-shearing (1 s^{-1}, 160 s) and 60 s rest time.

III. Results and Discussion

SEM imaging has been performed as preliminary observations to study the state of dispersion. Fig.3 shows some SEM images from sample filled with 20 vol% obtained after internal mixing and pressing. Relative good dispersion was observed under the operating conditions used in this work. Some aggregates between 5<d<20 µm, equally to some cavities were observed. Cavities were produced either by the cutting in which particles were unstuck or by trapped air during the mixing process. Both types of cavities can be easily recognized by its shape. Despite of these heterogeneities, individual particles are quite well dispersed through the matrix and agglomerates are not representative from the whole sample. It can be also observed that at 20 vol%, particles are very close to the percolation threshold. Percolating paths, but also individual particles can be recognized in Fig.3.

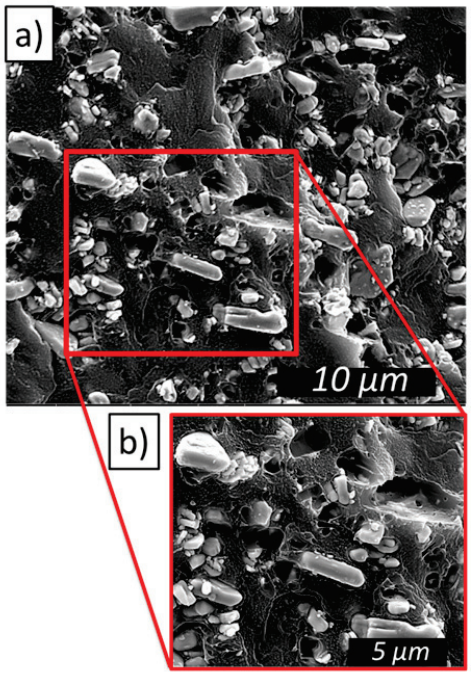


Fig.3. SEM observations of F20%/PP after hot pressing at (a) large magnification and (b) small magnification at 10 kV.

According to Larson [7], the transition between Brownian particles to non-Brownian particles in a flowing suspension is indicated by the Peclet number ($Pe \equiv \dot{\gamma}/D_{ro}$), where $\dot{\gamma}$ is the shear rate and D_{r0} is the rotary diffusivity of the particle. In oscillatory tests [34], the shear rate can be replaced by $\dot{\gamma} \rightarrow \gamma_0\omega$. Considering the following conditions, a dilute system at 190°C, for disks with d=1.96 µm (a=d/2) suspended in a molten matrix ($\eta_0 = 3760$ Pa s) under a dynamic oscillatory test at γ_0=10^{-3} and ω=1rad/s. We found $\dot{\gamma} \approx \gamma_0\omega \approx 10^{-3}\ s^{-1}$, the Pe number = $6\pi\eta\dot{\gamma}a^3/kT$ is then close to Pe $\approx 10^4$ which demonstrates the preponderance of viscous forces over the Brownian forces, thus, ferrite

particles can be considered as totally non-Brownian particles. The particle Reynolds number (Re_p) indicates that complications due to inertia can be totally neglected with $Re_p = 10^{-16}$. Furthermore, non-density matched suspensions ($\Delta\rho \approx 3750$ kg/m^3) can undergo buoyancy effects; however the high viscosity of the molten polymer drastically hinders such effect. Under low Reynolds number, Stokes' Law Eq. (1) can be used to estimate the single particle settling velocity.

$$V_s = \frac{K}{18}\frac{\rho_p - \rho_m}{\eta_0} {D_v}^2 g \tag{1}$$

Where K is the particle shape factor defined by Dietrich *et al*. [29]. The terminal velocity was found to be around: $V_s = 5\times10^{-12}$ m/s with K=1.16. The time during which a particle would move its own diameter is about 4×10^5 s, almost imperceptible in our scale of time. The latter considerations are very simplistic because they consider an individual average size particle suspended in a dilute medium. However regarding the settling velocity, even slower-moving particles are expected due to shape effects [35] and greater effective viscosity of the melt polymer [36]. Indeed, the competition between gravitational forces to viscous forces is given by Galileo (*Ga*) number which is in the order of magnitude of 10^{-9}. This means that viscous forces are again predominant over gravitational forces.

A. Time evolution of the rheological behavior

First, the samples were sheared according to the above-mentioned protocol and then the rheological properties were followed over 2 hours. It is important to remember that, pre-shearing has been performed before all the experiments and thus an initial totally de-structured network was assumed with a certain particle orientation in the flow direction.

Figs. 4(a) and 4(b) shows the variation of the storage and the loss moduli with time for a sample filled with 15 vol% (F15%) and 20 vol% (F20%) respectively. Lower values of moduli are obtained for sample filled with 15% (F15%), because of lower filler level, whereas, similar evolving behaviors were observed. On the one hand, the neat matrix behavior is stable over time, no degradation or structural changes are manifested during the experiment. On the other hand, the filled samples present a strong evolution of the moduli over time. This clearly means that the material evolution can be totally attributed to structural reorganization of particles. For the filled samples, the storage modulus strongly increases and overtakes the loss modulus at a certain characteristic time, resulting in a solid-like behavior at the end of the experiment. Such crossover point ($G' = G''$, $\tan(\delta) = 1$) can be considered as a "gel point" in the case that, G' changes in the same rate as G'' with a slope near 0.5 in the frequency domain. Such behavior, $G'(\omega) \propto G''(\omega) \propto \omega^{0.5}$, was already observed for filled polymer systems [20,37]. When both conditions are satisfied, it can be inferred that a gelling process occurs and it +might represents in our case the construction of paths of particles across the sample. This particles organization induces also a further rise in viscosity. Sample filled with 20 vol% attained the gel point faster than the sample filled with 15 vol%. It is important to note that at long time scales the structure seems to stabilize as will be shown in Section 3.3. This behavior suggests that the

suspension is gradually yielding with time. Here, log-log representations are preferred to give equal importance to either long or short time scales.

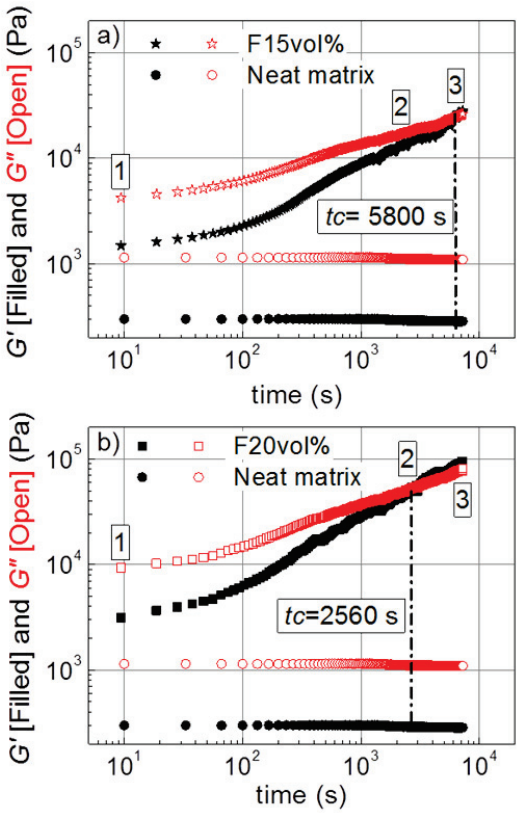


Fig.4. Time evolution of the storage and the loss modulus as a function of time for neat matrix and (a) F15%/PP and (b) F20%/PP, at 190°C, 1 rad/s, $\gamma=10^{-3}$.Dashed line corresponds to the moduli crossover.

Samples filled with 15 and 20 vol% were also studied in the frequency domain. Data were collected from 100 to 0.1 rad/s in order to make the measurement in a scale of time comparable or lower than the evolution kinetics. Fig.5 shows the variation of the moduli with the frequency for samples (a) F15% and (b) F20% under ten consecutive frequency sweeps. Each sweep took about 720 s to be performed. To simplify, Fig.5 only shows the sweeps at times: 0, 2200, 5000 s, points which are indicated respectively by numbers 1, 2, 3 in Fig.4.

From Fig.5, it can be observed that the storage modulus evolves and thus the materials becomes more and more rigid over time. At the lowest frequencies, the moduli slope declines when time increases. In fact, a flow regime is evidenced during the first frequency sweep for F15%, while, F20% presents already a gelling behavior. It can be also observed how *G'* gradually increases over *G"* with time which clearly indicates how particles build an energetically elastic filler network.

In Fig.5(b), a network behavior is indicated during the second sweep, as both moduli slopes are very close to~0.5, while, sample F15% (Fig.5(a)) shows the sol-gel transition during the 3th sweep showed in the figure which means that particles took more time to build up the network structure. It is important to remark that, frequency sweep behavior perfectly matches with reference times included in Fig.4. Therefore, a time sweep experiment (fixed ω, γ) is clearly depicted in the frequency window by a vertical line as arrows show in Fig.5.

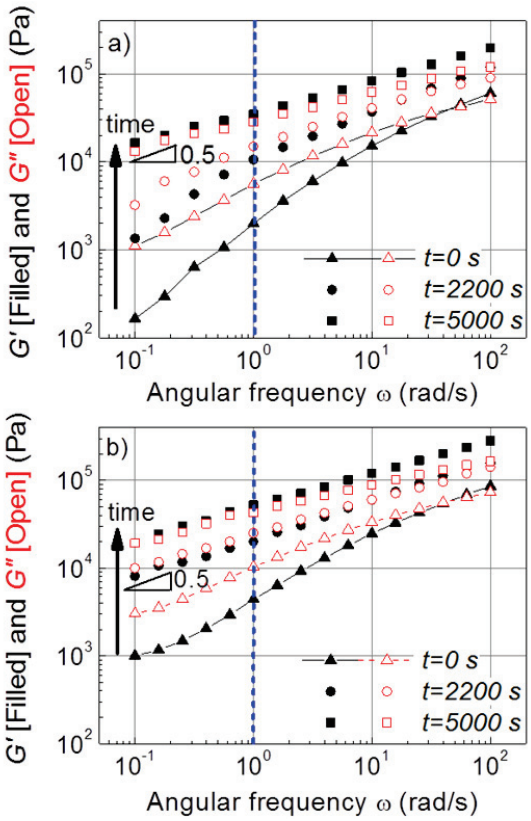


Fig.5. Storage G 'and loss modulus G" versus frequency for (a) F15% and (b) F20% at 190°C, $\gamma = 10^{-3}$. Data were collected from 100 to 0.1rad/s. Time increases from the bottom to the top of the graph. Dashed lines correspond to moduli in Fig.4.

Structural reorganization seems to be a time-dependent aggregation process in which structuring of particles occurs, leading to particles paths which explain the large enhancement in the storage modulus. The total viscoelastic response is caused by polymer-polymer, polymer-particle and inter-particle interactions. However, the strong increase of *G'* is principally due to particle-particle interactions.

This networking process is in direct relation with the percolation threshold (ϕ_c) and thus with the interparticle spacing. Indeed, the larger the interparticle spacing, the lower the influence by the presence of neighboring particles. Theoretically, the concentrated regime for disk-like platelets [11] is

given by $c^{**} = l/d \approx 0.25$, where l and d are thickness and particle diameter, respectively. Our previous experimental works showed that the critical volume fraction where particles start to touch their closest neighbors was near $\phi_c \sim 0.2$, defined as the divergence of the zero-shear viscosity. Therefore, it can be stated that the more the interparticle spacing, the slower the kinetics evolution is, as clearly shows Fig.4 and Fig.5.

For instance, composites filled at low concentrations (2 vol%) presented a very slight, almost not remarkable evolution in the structure under a time sweep experiment. Experiments for higher solids levels were not possible to perform in cone-plate geometry due to the quantity of solids.

It is important to mention that as the structuring process occurs, the linear viscoelastic domain (LVD) gets shorter over time. Fig.6 shows a strain sweep at $t = 0$ (the moment just after the pre-shearing and 60 s rest time) and after 2h time sweep experiment, $\gamma = 10^{-3}$, 1rad/s, Fig.4(b). The critical strain goes from $\gamma_c = 4\times10^{-3}$ to a shorter linear viscoelastic domain difficult to measure under the sensitivity of our machine. The author will consider, and further proved, the critical strain as closer to $\gamma_c \approx 10^{-3}$, after 2h experiment. The latter means that an oscillatory time sweep test performed at 10^{-3} of deformation goes from the linear domain to the limit of the non-linear viscoelastic domain. Such deformation was chosen to perform most of our experiments in order to record enough signal response.

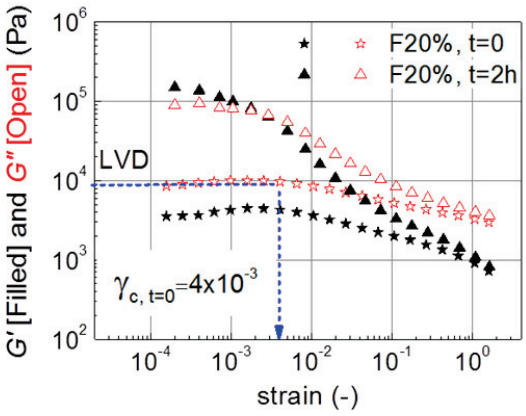


Fig.6. Strain sweep of sample F20% at t=0 and t=2h, 1 rad/s, 190°C.

In addition, the time evolution of the structure as a function of the applied strain has been investigated and shown in Fig.7 for sample F20%. Different deformations have been applied from 4×10^{-4} to 10^{-1}. The evolution under quiescent conditions has been also investigated: The sample was maintained at rest ($\gamma = 0$) and each 10 min the lowest possible strain was applied ($\gamma = 4\times10^{-4}$) for 30 s in order to follow the material evolution. Surprisingly, the behavior evolves as fast as at the low strain of $\gamma < 10^{-3}$, which clearly demonstrates that shear external forces are not responsible of the particle structuring.

Nevertheless, it can be stated that the behavior of ferrite composites strongly depends on the applied strain amplitude. The same trends, not shown for brevity, were found for F15%. Fig.7 clearly shows that the more the applied deformation, the less structuring of particles appears. At low strain amplitude, the storage modulus increases more than one decade and overtakes the loss modulus, showing an elastic filler network behavior, whereas, applying a sufficiently high strain amplitude leads to a homogenization of the system. Typically at $\gamma = 10^{-1}$, the amplitude deformation is sufficiently high that a very slight, almost nil, evolution was noticed. The crossover zone, indicated by the stripped square (*G'= G"*) in Fig.7, means the transition from viscous (liquid) to solid-like (elastic) regime and was observable below the critical deformation around $\gamma_c \sim 10^{-3}$. Beyond this point, the rebuilding of the microstructure leading to an elastic behavior cannot happen during the time of observation, indeed, above $\gamma_c > 10^{-3}$, hydrodynamic interactions predominate over filler-filler interactions. Based on this observation it can be stated that when $\gamma_c \leq 10^{-3}$, the LVD is respected. *G'* is independent of the deformation. The strong increase in *G'* might be attributed to particles interactions, forming percolating networks which evolve and break continuously throughout the system for $\gamma > \gamma_c$.

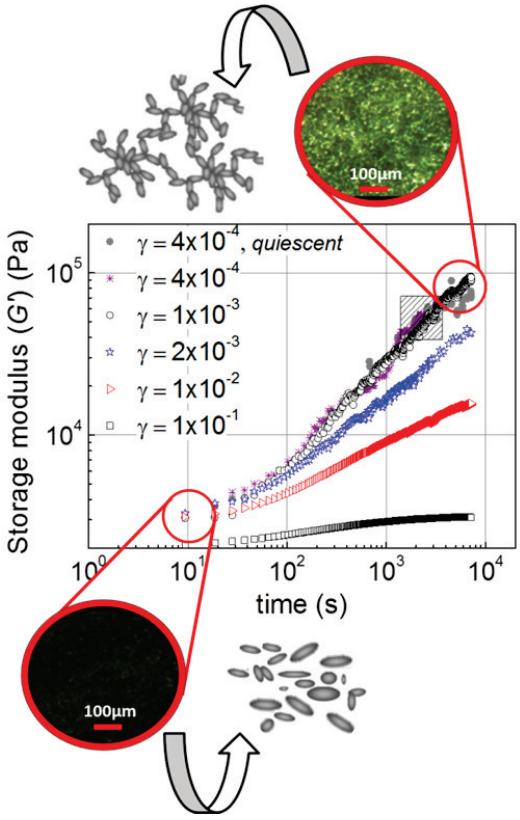


Fig.7. Time evolution of the storage modulus G' for F20% for different deformations at 190°C, 1 rad/s. The stripped square denotes the zone where the crossover occurs (G' = G", tanδ = 1). Optical micrographs of 2 vol% samples are shown at t=0 and t=2h, in the molten state at 190 °C and optical gap = 80µm.

The samples were also optically observed in the molten state under similar conditions to the oscillatory tests. A pre-shear (1 s^{-1}, 160 s) was performed and then the morphology was observed during some hours under quiescent conditions. However, it was necessary to filled the samples at very low loading levels (2 vol%), in order to make possible the observation through a sample of 80 µm thick. The samples were observed in the vertical axis, through two parallel quartz plates at 190°C. Fig.7 shows the initial picture and the observed structure after two hours observation. Undoubtedly, self-assembly of particles occurs over time under low strains or quiescent conditions, leading to the formation of a particle network with rich regions in ferrite and others completely free of particles. Indeed such evolution was not remarkable by rheological experiments for such low filler concentration, but the phenomenon is clearly noticed by optical observations.

Similar observations have been found in literature for Non-Brownian particles when the matrix density mismatched a lot from the suspended particles. Fall *et al*. [28] studied the rheological behavior of monodisperse, spherical polystyrene beads (40 µm) suspended in water+NaI. They have observed that at high shear rates, there was homogenization of the system, while, at low shear rates the system sediments (or creams, depending on the NaI quantity) and a viscosity bifurcation was observed. They demonstrated that the viscous stresses $\approx \eta\dot{\gamma}$ were balanced by the compressive stresses due to gravity and thus the critical shear rate can be estimated as shown in Eq (2), giving them a good approximation.

$$\dot{\gamma}_c = \Delta\rho g a/\eta_0 \tag{2}$$

By using $\dot{\gamma} \to \gamma_0\omega$, the critic amplitude strain was underestimated γ_c~9.6×10^{-6} by Eq (2). Admittedly, simple sedimentation of particles would not explain the current particular behavior. Sedimentation would produce a slight film in the top of the sample which may deform easily with time. The latter would certainly conduce to the decrement of the apparent viscosity of the system and not at all to the viscosity bifurcation observed in this work. Indeed, no proof of settling of ferrite particles has been observed by SEM microscopy even after several hours of observation. Thus, it can be concluded that the structuring of the material is governed by particle-particle interactions which are likely stronger than the polymer–particle compatibility but sufficiently weak to be easily broken by a very moderate strain

B. Structuring and rupture of the micro-structure

The effect of shearing the sample during structuring was investigated and is shown in Fig.8. During this test, four steps were performed: 1) pre-shearing the sample, 2) following of the rheological properties over time during a first time sweep, 3) shearing the sample again at the same conditions of the initial pre-shearing and 4) following again the behavior, Fig.8(a). Fig.8(b) shows the two time sweep steps overlapped in a log-log plot. As it can be noticed, initial structuring point is exactly the same for both sweeps. This result suggests that the de-structuring process is very fast and corroborates that low shear rates ($\dot{\gamma} = 1\mathrm{s}^{-1}$) are enough to completely erase the history of the sample by totally destroying the particle network, leading to reproducible measurements.

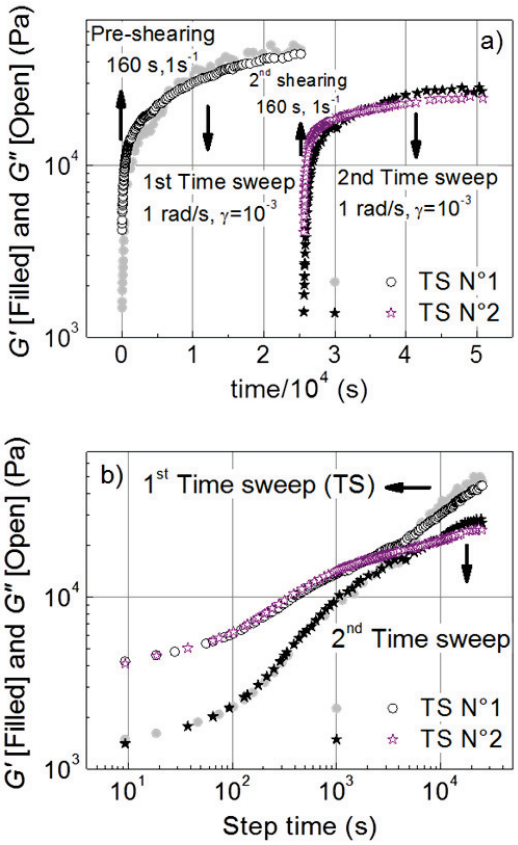


Fig.8. Structure build-up and break-down during a time sweep (TS) experiment for (a) F15% at 190°C, 1 rad/s, $\gamma = 10^{-3}$ and (b) overlapping of time sweep steps.

Another important aspect to notice is that the second time sweep leads to the same structure till a certain time (4670 s) in which the curves separated and thus the formed structure presents lower modulus but still elastic character at the end of the test. Rebuilding of the microstructure is a reversible and time dependent process, thus ferrite suspensions can be considered as complex rheological materials with a non-linear viscoelasticity.

C. Study of the morphological process by optical and SEM imaging

The structure formed under annealing has been investigated by optical microscopy and SEM microscopy. Fig. 9 shows a time sweep experiment performed over 14 hours under nitrogen at $\gamma = 10^{-3}$, 1 rad/s and 190 °C. As one has already seen, a sharp increase occurs in the moduli over the first three hours and then the system apparently reaches a saturated state. A slight decrease in the moduli is observed after 12 hours of observation which is possibly due to polymer chain degradation. The observation at different states of evolution has been performed at t = 0h, t = 2h and t = 14h. Optical images showed an agglomeration process in which some atypical pattern structures were evidenced. SEM microscopy was performed to elucidate such vast structure domains. Therefore,

different samples were recovered from the rheometer at the same annealing times and then, their fracture surface was observed at the solid state. The observation is performed perpendicular to the axial direction of the recovered disk. In spite of the efforts, there was no significant difference on dispersion at observed in Fig. 9. So, the non-trivial question is whether the SEM images are representatives from the molten state or not. It is worth to investigate then, the effect of crystallization on the melt-structure.

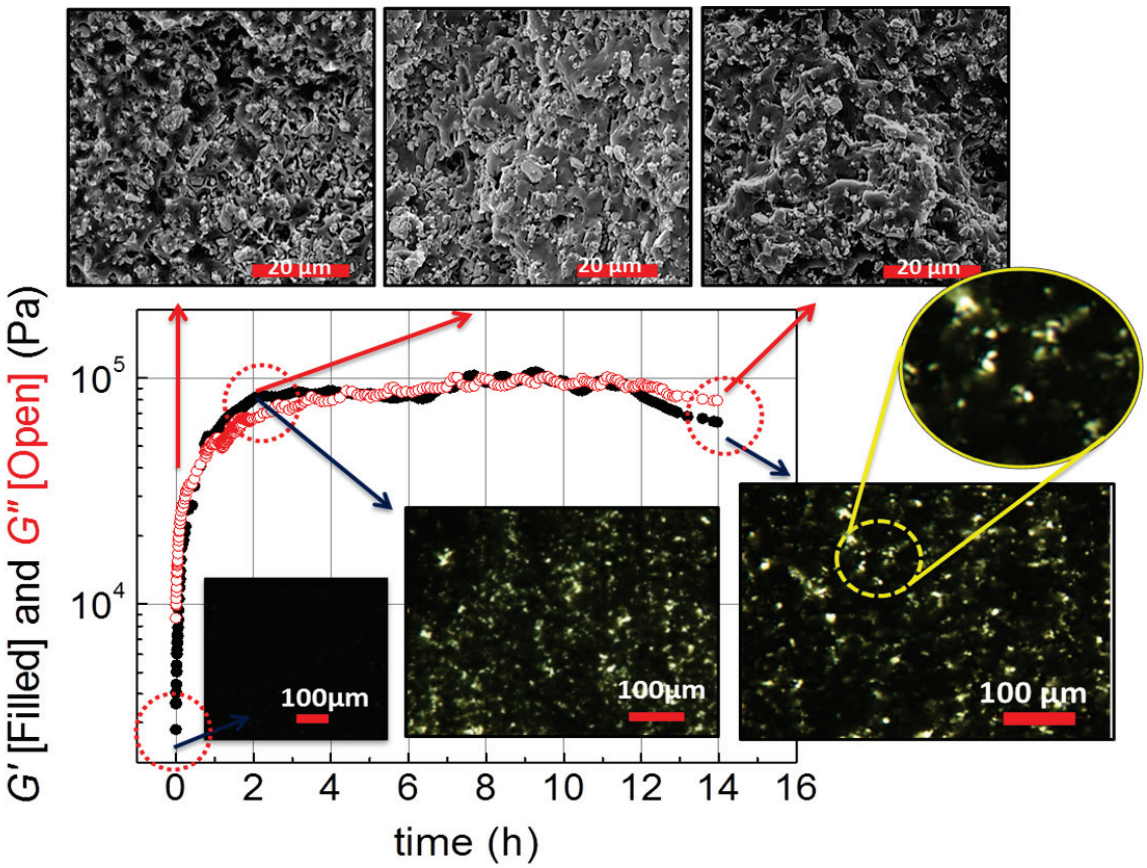


Fig. 9. Morphological analysis performed by scanning electron microscopy (solid state) after dynamic annealing for F20vol% and optical microscopic observation in the molten state, under quiescent conditions for sample filled with 2 vol%. Time sweep experiment for F20vol% performed over 14 hours at 1 rad/s, $\gamma = 10^{-3}$, 190 °C.

In this manner, two consecutive time sweep experiments were carried out. The first was interrupted and in-situ crystallization of the sample was performed. The normal force was manually maintained in the same range of values in order to protect the force sensor from damage. The shrinkage of the sample is quite important in such test, consequently, the fully loosen of the geometry was required. During this test, four steps were performed: (1) pre-shearing the sample, (2) following the rheological properties over 1h, (3) in situ crystallization/melting and (4) following the rheological behavior over several hours. It is important to note that there is no second pre-shear performed here so that the effect

of crystallization/melting is studied isolated from other variables. The experiment is shown in Fig.10. Unexpectedly, no dramatic difference in the behavior was noticed before and after crystallization. Structural rearrangements of ferrite particles start at the same initial point after crystallization/melting step. The obtained results suggested that crystallization may clearly destroy the already formed structure in the same manner that the pre-shear conditioning step does. In literature, there is evidence in which crystallization may conduce to the total recovery of the particle network, once destroyed by a strain sweep [38], here, on the contrary, it has been observed that crystallization destroys the particle network. So, it has been proved that the observation of the micro-structure at the solid state is not representative from the melt state structure. Subsequently, one might think that an amorphous matrix allows such observation.

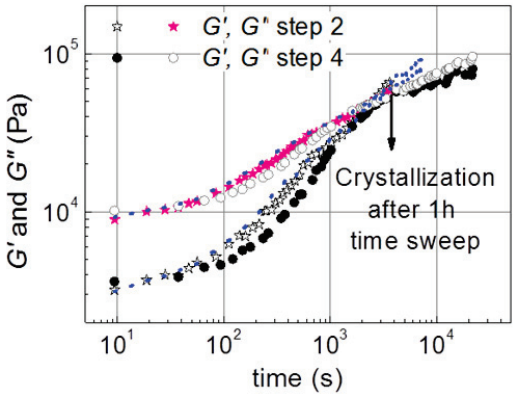


Fig.10. In situ crystallization/melting effect on the melt rheological properties. Two consecutive time sweeps were performed for F20%/PP at 190°C, 1rad/s, $\gamma = 10^{-3}$, one performed over 1h (step 2) and the second performed over several hours (step 4). Crystallization and melting step (step 3) was performed after the first time sweep. Dot line shows an experimental time sweep without interruption during 2h.

D. The effect of adding a dispersant on the rheological properties

The dispersant SDP310 (D) was added to the formulation. Its effectiveness has been studied by oscillatory time (Fig.11(a)) and strain sweeps (Fig.11(b)) measurements. Fig.11 shows the rheological behavior of a suspension filled with 20% of fillers with and without dispersant agent (D). As it can be evidenced, the rheological behavior is dramatically changed and stabilized in a metastable state by adding the dispersant. Fig.11.a shows how the building of the micro-structure is hindered by the fatty acid. It can be evidenced that during the last hour, sample FD20% stabilizes in a plateau, while sample F20% sharply evolves. Fig.11(a) also shows optical microscope images captured at t = 0h and t = 2h for samples F2% and FD2%. At t = 0, almost no light pass through the sample which means good initial dispersion. After that, agglomeration process occurs gradually with time and the optical observations show how particles had aggregated to form agglomerates and clusters, leaving big domains without fillers as it can be observed at t = 2h. The formulation with dispersant FD2% significantly hinders this phenomenon, showing more stable structure over time. Fig.11(b) shows the

LVD for sample FD20%, after a 2h experiment ($\gamma = 10^{-3}$, 1rad/s) compared to that of the sample F20% at t = 0 and t = 2h under the same conditions. Sample FD20% can be compared to the initial LVD of sample F20%, where particles are relatively well dispersed in the sample. The elastic character has been only slightly increased along the experiment. Only few connecting paths have been created. It is important to notice that all experiments converge to the same destroyed/oriented structure at high deformations. Strong shear thinning behavior is thus evidenced due to particles orientation.

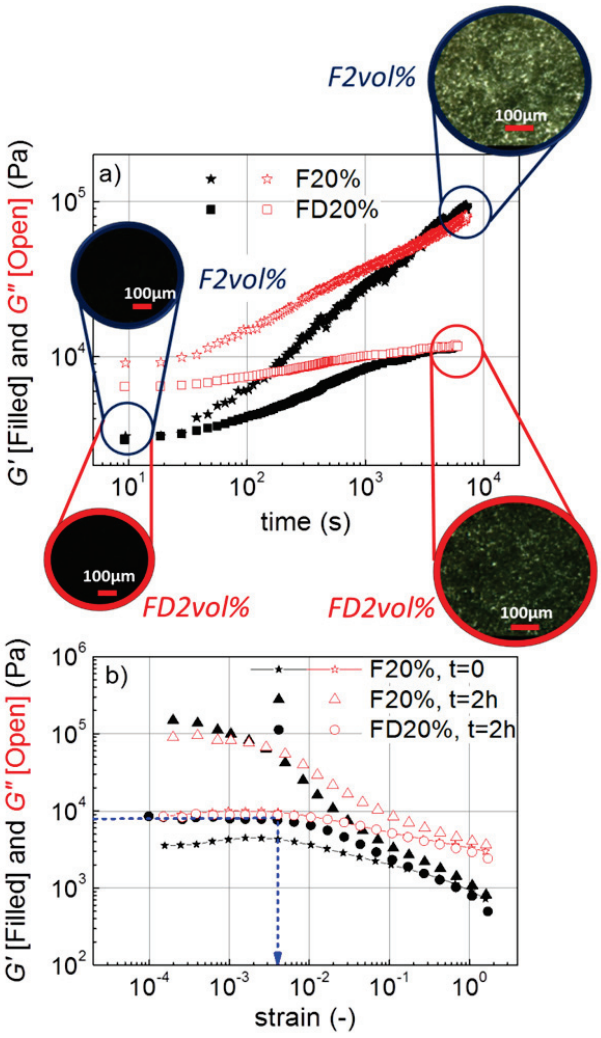


Fig.11. Rheological behavior of ferrite particles suspended in PP with and without dispersant agent (a) moduli variation over time during 2h, $\gamma = 10^{-3}$, 1rad/s, 190 °C. Optical images in the molten state at 190°C (b) strain sweep for F20% at t=0, t=2h and FD20% at t=2h.

The crucial question thus becomes: How do particles move under low deformations and even under quiescent conditions, provoking such a drastic increase in the storage modulus? Previous attempts to quantitatively describe the mechanism controlling the structural organization showed that neither

Brownian nor gravitational forces predominate in the system. Dimensionless numbers *Pe, Re_p, Ga* showed that viscous forces prevail during a flow experiment. Notwithstanding, it has been seen by time sweep tests that structuring also appears under quiescent conditions which implies that shearing forces were not the driving forces. Optic observations demonstrated that even at dilute conditions 2 vol%, agglomeration appears quite fast (2h). At 2 vol%, the mean interparticle spacing (λ) has been estimated by using $\lambda \sim 1/(n)^{1/3}$, with n the particle density = N/V (number of particles/total volume) and the effective volume fraction $\phi^* = NV_p/V$, where V_p is the volume of the sphere with the same diameter of the disk. Considering particles as hard spheres suspended in a cuboid box of dimensions A^3, the mean interparticle spacing is about $\lambda \sim 1/(N/V)^{1/3} \sim 5.8\ \mu m$, large enough to neglect neighboring particles [39,40].

These experiments demonstrated that, dense micro-fillers suspended in a polymer melt are structuring over time. Throughout this work, we have attributed networking to particle motion, however, what if motion comes from the suspended phase? In literature, it is known that PP chains present Brownian motion in the molten state [41]. It is also important to remember that polypropylene is a non-polar component, while ferrite particles are highly polar. The natural tendency of any material is to attain the lowest state of energy, thus leads to an evolution of the micro-structure over time. In colloidal systems with short-range interactions, the aggregation processes are quite well understood [42].

The latter results demonstrated that demixing of the phases is the origin of such phenomenon which is clearly impeded by the dispersant agent who decreases the surface energy between particles and polymer chains [43]. Complex interplay between enthalpic and entropic interactions between polymer chains and fillers are the origin of depletion forces [44]. So that, PP chains might be depleted from the gap in-between particles due to the low surface affinity, forming domains of matrix with less entropic restrictions (higher number of molecular conformations). Thus, when adding a fatty acid, a steric barrier around the particles is built due to its double nature [32]. The adsorbed chains interact with the PP chains and promote a screening effect, avoiding depletion forces. A direct measure of depletion forces is very difficult and it was out of the scope of this work. So, depletion forces together with interparticle interactions (magnetic, electrostatic, Van der Waals) at very short range might be the origin of such self-assembly process.

IV. Conclusions

In this work, we have studied the dynamics of ferrite suspensions near and below the percolation threshold. It was observed that ferrite suspensions exhibit a time and shear dependent Non-Newtonian behavior. The following are the main conclusions: Linear viscoelastic domain has been found to become shorter over time, which indicates the construction of an elastic but weak filler structure network. Structure evolution has been studied at different conditions. Reorganization of particles strongly depends on the applied deformation. When $\gamma \leq 10^{-3}$, depletion forces provoke a structuring of the micro-structure and the material showed a solid-like behavior at the end of the experiment, while, when $\gamma > 10^{-3}$ the networking is hindered by hydrodynamic interactions. At low strain amplitude, reversible rebuilding of the particle microstructure has been evidenced. The structure evolution was evidenced by optical microscopy, while, SEM microscopy did not conduce to any satisfactory conclusion. It was demonstrated that crystallization previous to SEM observation destroys the formed structure. Melt rheological properties seem not to be affected by crystallization step and finally it has been highlighted the importance of adding a dispersant agent into this filled polymer formulations.

References

[1] D. M. Kalyon and S. Aktaş, "Factors Affecting the Rheology and Processability of Highly Filled Suspensions," Annu. Rev. Chem. Biomol. Eng. 5, 229–254 (2014).

[2] M. F. H. Wolff, V. Salikov, S. Antonyuk, S. Heinrich, and G. A. Schneider, "Novel, highly-filled ceramic–polymer composites synthesized by a spouted bed spray granulation process," Compos. Sci. Technol. 90, 154–159 (2014).

[3] D. M. Bigg, "Rheological behavior of highly filled polymer melts," Polym. Eng. Sci. 23, 206–210 (1983).

[4] S. L. Mills, G. C. Lees, C. M. Liauw, and S. Lynch, "Dispersion assessment of flame retardant filler/polymer systems using a combination of X-ray mapping and multifractal analysis," Polym. Test. 21, 941–947 (2002).

[5] J. Vermant, S. Ceccia, M. K. Dolgovskij, P. L. Maffettone, and C. W. Macosko, "Quantifying dispersion of layered nanocomposites via melt rheology," J. Rheol. 51, 429–450 (2007).

[6] F. J. Galindo-Rosales, P. Moldenaers, and J. Vermant, "Assessment of the Dispersion Quality in Polymer Nanocomposites by Rheological Methods," Macromol. Mater. Eng. 296, 331–340 (2011).

[7] R. G. Larson, (New York: OUP USA, 1999).

[8] B. Cabane, K. Wong, P. Lindner, and F. Lafuma, "Shear induced gelation of colloidal dispersions," J. Rheol. 41, 531–547 (1997).

[9] F. Saint-Michel, F. Pignon, and A. Magnin, "Fractal behavior and scaling law of hydrophobic silica in polyol," J. Colloid Interface Sci. 267, 314–319 (2003).

[10] T. Domenech, R. Zouari, B. Vergnes, and E. Peuvrel-Disdier, "Formation of Fractal-like Structure in Organoclay-Based Polypropylene Nanocomposites," Macromolecules 47, 3417–3427 (2014).

[11] A. Franceschini, E. Filippidi, E. Guazzelli, and D. J. Pine, "Dynamics of non-Brownian fiber suspensions under periodic shear," Soft Matter 10, 6722–6731 (2014).

[12] R. Zouari, T. Domenech, B. Vergnes, and E. Peuvrel-Disdier, "Time evolution of the structure of organoclay/polypropylene nanocomposites and application of the time-temperature superposition principle," J. Rheol. 56, 725–742 (2012).

[13] F. Pignon, A. Magnin, and J.-M. Piau, "Thixotropic behavior of clay dispersions: Combinations of scattering and rheometric techniques," J. Rheol. 42, 1349–1373 (1998).

[14] L. Moreira, R. Fulchiron, G. Seytre, P. Dubois, and P. Cassagnau, "Aggregation of Carbon Nanotubes in Semidilute Suspension," Macromolecules 43, 1467–1472 (2010).

[15] M. J. Solomon, A. S. Almusallam, K. F. Seefeldt, A. Somwangthanaroj, and P. Varadan, "Rheology of Polypropylene/Clay Hybrid Materials," Macromolecules 34, 1864–1872 (2001).

[16] G. Galgali, C. Ramesh, and A. Lele, "A rheological study on the kinetics of hybrid formation in polypropylene nanocomposites," Macromolecules 34, 852–858 (2001).

[17] M. A. Treece and J. P. Oberhauser, "Soft Glassy Dynamics in Polypropylene−Clay Nanocomposites," Macromolecules 40, 571–582 (2007).

[18] I. Alig, P. Pötschke, D. Lellinger, T. Skipa, S. Pegel, G. R. Kasaliwal, and T. Villmow, "Establishment, morphology and properties of carbon nanotube networks in polymer melts," Polymer 53, 4–28 (2012).

[19] P. Cassagnau, "Linear viscoelasticity and dynamics of suspensions and molten polymers filled with nanoparticles of different aspect ratios," Polymer 54, 4762–4775 (2013).

[20] A. W. K. Ma, F. Chinesta, and M. R. Mackley, "The rheology and modeling of chemically treated carbon nanotubes suspensions," J. Rheol. 53, 547–573 (2009).

[21] X. J. Cao, H. Z. Cummins, and J. F. Morris, “Structural and rheological evolution of silica nanoparticle gels,” Soft Matter 6, 5425–5433 (2010).
[22] W.-H. Shih, W. Y. Shih, S.-I. Kim, J. Liu, and I. A. Aksay, “Scaling behavior of the elastic properties of colloidal gels,” Phys. Rev. A 42, 4772 (1990).
[23] J.-M. Piau, M. Dorget, J.-F. Palierne, and A. Pouchelon, “Shear elasticity and yield stress of silica–silicone physical gels: Fractal approach,” J. Rheol. 43, 305–314 (1999).
[24] S. Dasgupta, “Degree and stability of magnetic dispersions: Sedimentation, rheological, and magnetic properties,” J. Colloid Interface Sci. 121, 208–213 (1988).
[25] S. Dasgupta, “Interaction characteristics of magnetic particles with surfactants, solvents, and binder resins,” J. Colloid Interface Sci. 124, 22–27 (1988).
[26] R. C. Navarrete, L. E. Scriven, and C. W. Macosko, “Rheology and Structure of Flocculated Iron Oxide Suspensions,” J. Colloid Interface Sci. 180, 200–211 (1996).
[27] M.-C. Yang, L. E. Scriven, and C. W. Macosko, “Some Rheological Measurements on Magnetic Iron Oxide Suspensions in Silicone Oil,” J. Rheol. 30, 1015–1029 (1986).
[28] A. Fall, H. de Cagny, D. Bonn, G. Ovarlez, E. Wandersman, J. A. Dijksman, and M. van Hecke, “Rheology of sedimenting particle pastes,” J. Rheol. 57, 1237–1246 (2013).
[29] W. E. Dietrich, “Settling velocity of natural particles,” Water Resour. Res. 18, 1615–1626 (1982).
[30] V. M. B. Moloney, D. Parris, and M. J. Edirisinghe, “Rheology of Zirconia Suspensions in a Nonpolar Organic Medium,” J. Am. Ceram. Soc. 78, 3225–3232 (1995).
[31] P. C. Hidber, T. J. Graule, and L. J. Gauckler, “Influence of the dispersant structure on properties of electrostatically stabilized aqueous alumina suspensions,” J. Eur. Ceram. Soc. 17, 239–249 (1997).
[32] S. Zürcher and T. Graule, “Influence of dispersant structure on the rheological properties of highly-concentrated zirconia dispersions,” J. Eur. Ceram. Soc. 25, 863–873 (2005).
[33] I. V. Chernyshova, S. Ponnurangam, and P. Somasundaran, “Adsorption of Fatty Acids on Iron (Hydr)oxides from Aqueous Solutions,” Langmuir 27, 10007–10018 (2011).
[34] C. D. Cwalina and N. J. Wagner, “Rheology of non-Brownian particles suspended in concentrated colloidal dispersions at low particle Reynolds number,” J. Rheol. 60, 47–59 (2016).
[35] R. M. Turian, F.-L. Hsu, K. S. Avramidis, D.-J. Sung, and R. K. Allendorfer, “Settling and rheology of suspensions of narrow-sized coal particles,” AIChE J. 38, 969–987 (1992).
[36] A. J. Poslinski, M. E. Ryan, R. K. Gupta, S. G. Seshadri, and F. J. Frechette, “Rheological Behavior of Filled Polymeric Systems II. The Effect of a Bimodal Size Distribution of Particulates,” J. Rheol. 32, 751–771 (1988).
[37] P. Cassagnau, “Payne effect and shear elasticity of silica-filled polymers in concentrated solutions and in molten state,” Polymer 44, 2455–2462 (2003).
[38] P. Cassagnau and F. Mélis, “Non-linear viscoelastic behaviour and modulus recovery in silica filled polymers,” Polymer 44, 6607–6615 (2003).
[39] Y. N. Kryuchkov, “Concentration dependence of the mean interparticle distance in disperse systems,” Refract. Ind. Ceram. 42, 390–392 (2001).
[40] M. Mathew, T. Schilling, and M. Oettel, “Connectivity percolation in suspensions of hard platelets,” Phys. Rev. E 85, 61407 (2012).
[41] Y. Termonia, “Self-sustained entropy-driven flow in nano-confined polymer melts,” J. Polym. Sci. Part B Polym. Phys. 53, 869–875 (2015).
[42] J. A. Lewis, “Colloidal Processing of Ceramics,” J. Am. Ceram. Soc. 83, 2341–2359 (2000).
[43] B. Haworth, C. L. Raymond, and I. Sutherland, “Polyethylene compounds containing mineral fillers modified by acid coatings. 2: Factors influencing mechanical properties,” Polym. Eng. Sci. 41, 1345–1364 (2001).

[44] X.-Z. Cao, H. Merlitz, C.-X. Wu, and J.-U. Sommer, “Polymer-induced entropic depletion potential,” Phys. Rev. E 84 (2011).

Chapter 4

Ferrite composites: linear and non-linear nature of the flow

Summary

The flow behavior of a filled suspension consisting of ferrite particles suspended in a polypropylene matrix with and without the addition of a commercial dispersant (Solplus DP310) was studied. The composites were filled with 10, 20, 30 and 40 vol%. Both capillary and parallel disk rotational flows were employed. On the one hand, dynamic results confirm general trends found for highly concentrated systems. The higher is the filler level, the lower is the linear viscoelastic domain. When adding the dispersant agent, it was shown a larger linear viscoelasticity domain, lower moduli values and thus, lower viscosity. Also, the critical strain, G' and G" showed a power law dependency on the volume fraction. On the other hand, the capillary results showed no dependency of the flow properties on the die. Thus, no slip of the suspension at the wall was observed. Actually, this experimental finding elucidated that the significant decrease on viscosity produced by the addition of the dispersant agent at 40 vol% is principally due to lubricant effects and not at all to slip contributions. The results also reveal three distinct flow regimes. Low, moderate and high shear rates lead to different microstructure under flow.

Keywords: Highly filled polymers, rheology, dispersant, viscosity, ferrite particles

Reformatted version of paper submitted in:

Rheological Acta, Submission date: 15/01/17

Linear and Non-linear nature of the flow of polypropylene filled with ferrite particles: from low to concentrated composites

Martha Margarita Rueda[1,2], René Fulchiron[1], Grégory Martin[2], Philippe Cassagnau[1]

[1)] *Univ-Lyon, Université Lyon 1, Ingénierie des Matériaux Polymères, CNRS, UMR 5223, 15 Bd Latarjet, 69622 Villeurbanne Cedex, France.*

[2)] *HUTCHINSON Research Center, Rue Gustave Nourry – B.P. 31, 45120 Chalette-sur-Loing, France.*

I. Introduction

Understanding the rheological behavior of Highly Filled (HF) materials gain a lot of interest in many industrial applications such as magnetic materials [1,2], thermal pastes [3], batteries [4], solid propellants [5], electrically conductive compounds [6] and the elaboration of ceramic materials [7], among others applications [8]. The concentration of solids in such applications need to be maximized to be as close as possible to the maximum packing fraction of solids (ϕ_m), generally exceeding 60 vol% of the particulate phase [8,9]. Such high quantity of fillers strongly increases the mixture viscosity and thus the elaboration process becomes extremely difficult to control [8]. In addition, polymer-filler and filler-filler interactions may lead to agglomeration in the suspensions, defining the resultant morphology and thus the rheology of the materials [10]. For these reasons, most of these materials present dispersants (amphiphilic additives) in their formulations. They are claimed to avoid sedimentation of particles, to prevent agglomeration process and to produce low viscosity suspensions [10–14].

It is generally known that all metal and metalloids oxides particles are covered by hydroxyls (-OH) or ions groups which will determine the adsorption processes that take place onto the surface of particles [15,16]. The most common used dispersants in molten polymers are fatty acids, amine and amide acids. Fatty acids in particular, present a carboxyl functional group (COOH), which is able to being adsorbed onto the particle surface either by creating chelate complexes or hydrogen bonds [11,16,17]. Thus, dispersants coat and modify the interparticle potential by increasing the particle charge or by building up a steric barrier between particles [18]. In particular, a commercial dispersant, Solsperse 3000 (S3000) which principally consists in a penta-(12-hydroxystearic acid) oligomer, has been successfully used to disperse zirconia (YZS) [11,18], hydroxyapatite powder [19] and ferrite particles [20] in organic and semi-organic media (low molar mass liquids). Its efficiency has been demonstrated over a wide number of dispersants, including fatty acids *e.g.,* palmitic, stearic and oleic acid; fatty amines and molecules with hydroxyl groups [11,18,19]. This has been attributed to its effectiveness of the chelating anchoring group to bind on metal and oxide surfaces, in addition to the higher steric effect produced by its long carbon chain (66 carbon chain which is at least 10 nm long) [11,18]. Despite the efforts, the influence of these additives on the melt flow behavior is less well-known and has been less studied. Molten polymers are highly entangled in the melt which results in a

quite different behavior [21], as well as, different diffusion and mechanism of adsorption compared to what happen in a low molar mass medium.

In our recent work [10], we demonstrated that a similar dispersant, Solplus DP310 (SDP310), was able to stabilize the rheological properties of ferrite particles suspended in polypropylene. First, we have shown that the structure of such composites were not stable over time. Micro-structural changes were manifested by a sharp increase on the storage modulus (*G'*), resulting in a solid-like behavior at the end of the experiment. This manifestation was particularly important under very low shear deformations in the linear viscoelastic domain (LVD). When adding the dispersant, SDP310, it was shown that this drastically hinders the agglomeration process, impeding the creation of the particle network.

From a process point of view, HF polymers definitely need the addition of a dispersant agent to broaden the process window and facilitate the elaboration process, as long as it does not modify the final properties of the composite. The addition of particles, dramatically changes the viscoelasticity of polymer melts [22,23] and strongly increases the viscosity of the mixture [24]. All this recreates the perfect conditions for processing difficulties, resulting in flow instabilities. When considering quantitative analysis of polymer processing, the flow-boundary condition is a fundamental assumption to describe laminar flow (either no slip at the wall or slip condition) [9,25]. Wall slip phenomenon has been claimed to be ubiquitous and the controlling phenomenon of the flow behavior of highly concentrated suspensions [26–28]. In HF polymers field, the wall slip velocity has been found either to increase [28] or decrease [29–31], when adding particles. The slip at the wall has also been shown to appear at a certain value of ϕ/ϕ_m and then to remains relatively independent of such value [32]. There is also evidence of no correlation between flow properties and wall slip. Hence, the slip velocity was found in some studies negligible even at high shear rates in capillary tests (10^3, 10^4 s^{-1}) [24,33]. In addition, when adding a dispersant or a coupling agent, it is generally believe that unreacted dispersant is likely to migrate to the die wall. Hence, an accumulation of the dispersant agent may occur at the wall, resulting in slip effects, plug flow and, in some cases, the suppression of flow instabilities have been observed [30,34,35].

This paper presents experimental results of the rheological behavior of a filled polymer up to concentrated regimes. Generally, ferrite suspensions studies use dispersants to stabilize the flow properties [10,36–39]. Therefore, this work revisits important concepts of concentrated suspensions with and without the addition of a dispersant agent; by highlighting the important relationship between the microstructure and the flow.

II. Materials and Methods

A. Materials

1. Polymer

The matrix used in this study is a commercial homopolymer polypropylene PPH7060 (PP), provided by Total refining & chemicals. Table I summarizes some of its characteristics. A sterically hindered phenolic antioxidant, Irganox 1010 (I) was used as a thermal stabilizer at 1 wt% based on the weight of the polymer (it protects PP matrix against thermo-oxidative degradation).

Table I. Characteristics of polypropylene matrix (PPH 7060)

Properties	Method	Value	Unit
Density	ISO 1183	0.905	g/cm^3
Melting point (T_f)	ISO 3146	165	°C
Melt Flow Index	230°C/2.16 kg	12	g/10 min
η_0 (at 190 °C)	Viscosity at the plateau[a]	3800	Pa s

[a]*Carreau-Yasuda parameters: rate index (n)=0.22, Characteristic time (λ)=0.092 s, transition index (a)=0.47,* η_∞*=0 Pa s*

2. Particles

The ferrite powder NK132 (F) was supplied by Toda Kogyo Corp., Japan. These particles are a solid solution of Strontium with a low quantity of Barium Ferrite. The characterization of the particles has been discussed in detail in our recent work [10]. Ferrite particles have hexagonal plate shape with an average diameter (d) of 2 µm and 0.5 µm of thickness (l). The aspect ratio is around $p=d/l=4$.

3. Dispersant

Different works showed that the commercial dispersant, S3000, has a high potential to reduce the mixture viscosity in organic liquid media [11,18,19]. Based on these analyses, we compared and chose a new dispersant from its same family. In this work, SDP310 was used as an alternative to S3000. Both dispersants were kindly supplied by Lubrizol, Advanced Materials. SDP310 is a white powder (spheres of $\bar{d}$=150 µm) with T_f= 105.5 °C, while S3000 is a waxy paste at room temperature.

SDP310 characterization has been facilitated thanks to Moloney and coworkers [18]. They reported S3000 as a pentamer made up of one steric acid unit and four units of poly (12-hydroxy-stearic acid). This oligomer was compared to SDP310 by using thermogravimetric analysis (TGA), attenuated total reflection (ATR) spectroscopy, nuclear magnetic resonance (NMR) spectroscopy and matrix-assisted laser desorption/ionization time-of-flight (MALDI-TOF) mass spectrometry. Some of these results are shown in Fig. 1.

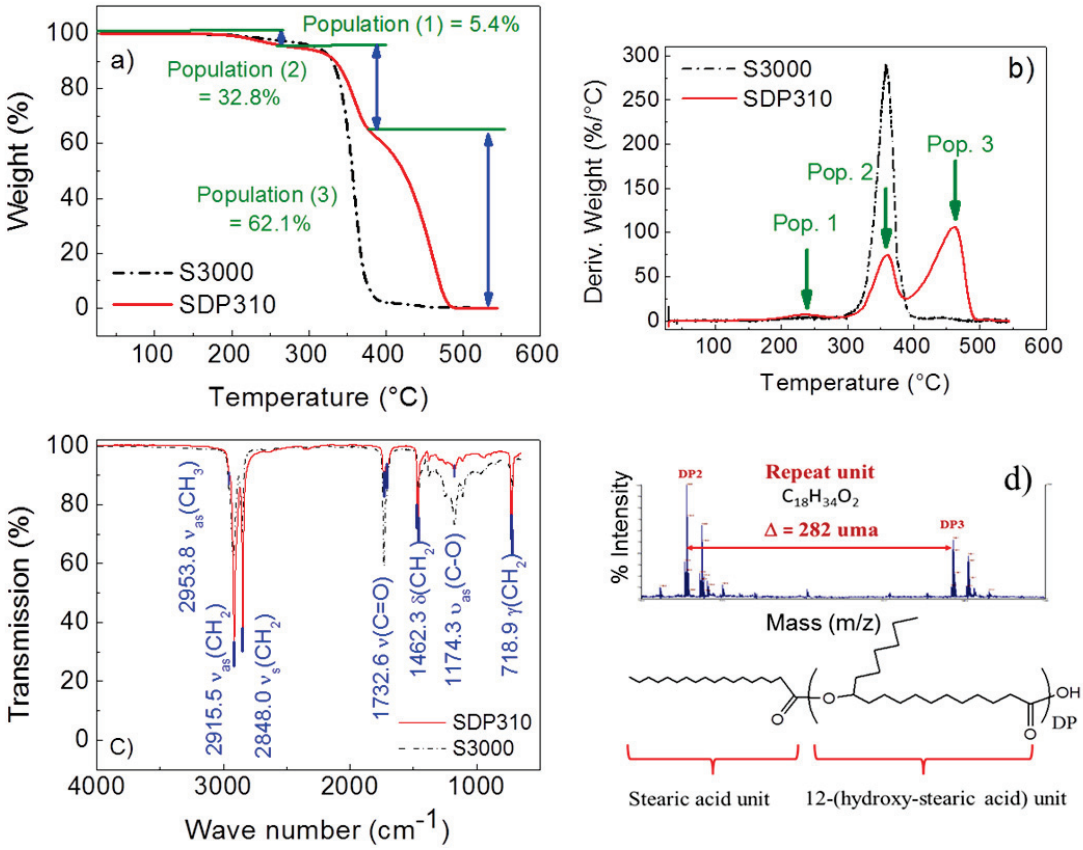


Fig. 1. Solplus DP310 (SDP310) dispersant characterization, considering as reference S3000 reported by [18]. (a) Normalized weight loss curves and (b) derivative weight loss curves of S3000 and SDP310. From 25 to 550°C at 10°C/min under Helium. (c) Infrared transmission spectra for both dispersants. Denoted peaks are shown only for SDP310 with their respective assignment, where: as: asymmetric, s: symmetric, υ: stretching, δ: bending and γ: rocking. (d) Repeat pattern ($C_{18}H_{34}O_2$), as well as the oligomer molecule found by Maldi-tof technique for both dispersants.

Fig. 1(a) and 1(b) show the TGA measurement performed for both dispersants. As it can be noticed, S3000 presents a monomodal distribution of population of oligomer chains, the population that is present in the largest amount is a penta (12-hydroxy-stearic acid) [18]. SDP310 presents three principal populations, one being a penta (12-hydroxy-stearic acid). Fig. 1(c) presents the transmission spectrum for both dispersants in which only SDP310 peaks are identified and attributed to the corresponding functional group. It can be clearly observed that S3000 and SDP310 present very similar chemical structures, despite the huge difference in their physical appearance. Infrared spectra reveal typical features from carboxylic acid with long carbonaceous chain described by the CH_2 stretching and rocking bands. Finally, the chemical composition has been studied by Maldi-tof mass spectroscopy. The waxy S3000 dispersant was easily dissolved in most common solvent compounds; whereas, SDP310 powder was not. A mixture $CHCL_3$/EtOH/H_2O (70/20/10 v/v/v) partially dissolves

SDP310; a white colour solution was obtained. THF and $CHCL_3$/EtOH/H_2O were chosen as solvents for S3000 and SDP310, respectively. Fig. 1(d) shows the molecule found by Maldi-tof based on [18]. The results demonstrated that both dispersants has exactly the same repeating unit ($C_{18}H_{34}O_2$). This technique also confirmed very exactly both extreme units: ($C_{18}H_{35}O_1$) and (OH). The degree of polydispersity (DP) goes from 1 to 10 for SDP310 and 1 to 12 for S3000. Nonetheless, results are not quantitative for samples with very large distribution, as in our case. NMR corroborated the latter results, without giving additional quantitative information again due to the high polydispersity of population.

On the basis of these results, it can be stated that SDP310 is a poly (12-hydroxy-stearic acid) with a high dispersity index (DP=1 to10). SDP310 powder was chosen for this study due to its high thermal stability and ease of use in extrusion process. The powder state facilitates the handle of the product, unlike, waxy physical state.

B. Mixing and sample preparation

The mixing of the components was performed by extrusion process by means of a Leistritz ZSE-18, fully intermeshing co-rotating twin-screw extruder. The barrel length over barrel diameter, L_b/D_b, was 60 and the barrel diameter was 18 mm. The operating conditions were fixed at 190°C, a speed of 800 rpm and throughput of 3kg/h.

A pre-mixing of the powders (Ferrite + 2 wt% SDP310) and the matrix (PP granulates + 1 wt% Irganox 1010) was manually performed. Then, composites with filler levels from 10 to 40 vol% were performed, granulated and then shaped into rheometer disks by injection molding by means of a Babyplast 610P, Alecop at 190 C. Collected disks and pellets were characterized by rotational and capillary rheometry, respectively. Samples with and without the dispersant agent were prepared. The dispersant concentration was fixed at 2 wt% based on the weight of fillers. The screw profile used in this study is illustrated in Fig. 2. This may be considered as a soft screw profile, principally because it does not present any reverse element and its kneading blocks are positioned with favorable feed angles.

C. Rheological characterization

1. Dynamic rheological test

Linear viscoelasticity characterization was performed by employing a stress-controlled Discovery Hybrid Rheometer (DHR), TA instruments. All measurements were performed at 190 °C under nitrogen atmosphere, using a plate-plate geometry (diameter=25 mm). The gap was fixed at 1800 µm. A sample conditioning was performed before all the tests to erase and impart an initial state of dispersion to the sample. The global protocol consisted in five steps: 1) Soak time of 300 *s* in order to enable the sample to relax stresses due to the loading, 2) pre-shearing of 0.5 s^{-1} for 160 s and 3) annealing step in which the sample was maintained under quiescent conditions for 1 hr. 4) a frequency sweep was performed, followed by 5) a strain sweep. The annealing step was performed to

enable the structuring of the material to certain equilibrium. Frequency sweeps were performed in the linear viscoelastic domain under the strain amplitude range between 10^{-3}–10^{-4} according to the filler level. Oscillatory strain sweeps were performed at fixed frequency of 1 rad/s, from 6×10^{-6} to 2 of deformation (γ).

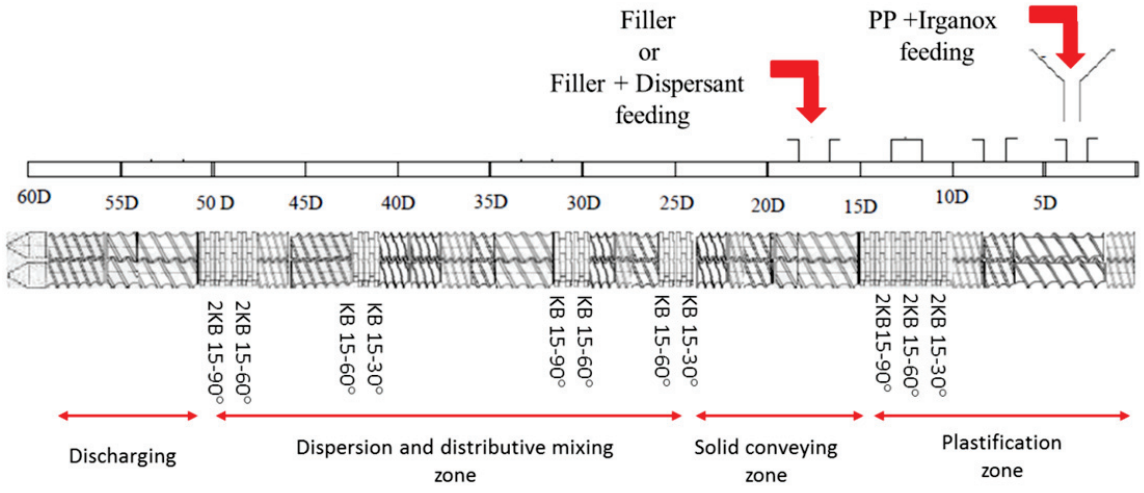


Fig. 2. Schematic representation of the soft screw profile used in this study. Leistritz ZSE18, L_b/D_b=60. Kneading blocks (KB) are characterized by 15 mm axial length and 30° stagger angle.

2. *Capillary rheometry*

A twin-bore capillary rheometer (RH7, Rosand, Malvern) was used to study the shear flow behavior of such composite melts. The diameter of the bore was 15 mm. Steady shear flow properties were collected from 1 s^{-1} to 4×10^4 s^{-1} at 190 °C. To maintain consistency between the tests, a pre-conditioning was applied before running the experiments. Such pre-conditioning principally enables a good contact between the piston and the melt composite, lets the whole sample reach the thermal equilibrium and removes trapped air bubbles. Such pre-conditioning principally enables a good contact between the piston and the melt composite, lets the whole sample reach the thermal equilibrium and removes trapped air bubbles. It consisted in two cycles of compression (according to the transducer) and soak time (5 and 4 min).

First, wall slip was analyzed by using three different dies with capillary length over diameter, L/D=10 and entry angle of 180° (L/D=10/1, 15/1.5 and 20/2 mm/mm). The obtained data were further processed according to Bagley correction. The orifice die was used to perform this correction (L=0.25, D=1, 1.5, 2). The pressure drops through this orifice was subtracted from the measured values of pressure. This is simultaneously performed during the measurement by using the double capillary system with orifice die. Second, the shear viscosity of the composite was analyzed by using a die with L/D=20/1 and entry angle 180°. The Bagley correction was again applied. The Rabinowitsch correction did not change in any aspect the behavior of the filled composites but rather

slightly enhance the differences. We thus decided to show the apparent shear rate to be consistent to the wall slip analysis.

D. Morphological characterization

The state of dispersion has been observed by Scanning Electron Microscopy (SEM) and Tomography. SEM observations have been performed by means of a Quanta 250 SEM under high vacuum, an acceleration voltage of 10 kV with an Electron Backscatter Diffraction (EBSD) detector. Prior to observations, the samples were cryo-cut and metallized by using a Bal-Tec MED 020 Coating System. Sputter coating was applied under 35 mA and a 10 nm layer copper was deposited. A quartz layer device was used for measuring the layer thickness.

Tomography (Nanotomography I-580) observations were also conducted to examine the state of dispersion. We were able to quantify the presence of agglomerates with a diameter >10µm for two samples. Composites filled with 20 vol% without and with the addition of the fatty acid were analyzed. The measurements were performed under 70 kV voltage, 90 µA intensity and 1250 ms of exposition time. The disk samples (diameter=25 mm, thickness =2mm) obtained by injection molding process were cut into rectangular sample. The dispersion analysis has been performed over an identical volume of 45.5 mm^3 for the two samples. The obtained 3D tomograms were threshold, binarized and the voxels which constitutes the agglomerates were quantified, giving as a result the agglomerate volume. Assuming spherical agglomerate shape, the equivalent diameter (D_{eq}) is calculated as $D_{eq}=(6V//\pi)^{1/3}$. According to this method, we are able to calculate the median diameter by number (D_n).

IV. Results and Discussion

In our recent work [10], we have covered the structuring over time of these materials at very low deformations, essentially in the linear viscoelastic domain (LVD) for samples filled with 15 and 20 vol%. Here, we will discuss different aspects on the linear and non-linear nature of the flow of more concentrated ferrite composites. Data were collected after 1h structuring in dynamic rheology and in the steady state in capillary rheology. No sign of structuring has been noticed in capillary rheometry.

Some abbreviations will be used in the following. Samples will be denoted by their process, their filler level and their formulation. For instance: EF20 and EFD20, whose letters mean E=Extrusion, F=ferrite, D=Dispersant and the number corresponds to the filler level in volume percentage.

A. Morphology observation

Agglomerates whose size ranges between 10 up to ~100 µm were quantified for a sample filled with 20 vol% with and without dispersant. Figs. 3(a-d) show some 2D images obtained by 3D tomographs. As a general observation, these images showed a homogenous gray zone with some dispersed white zones. The homogenous zones are represented by the Figs. 3(e-f), in which particles are well dispersed through the matrix, while, white zones are displayed by Fig. 3(g). Such white zones correspond to very dense zones of particles, thus to one agglomerate. Agglomerates seem to be uniformly distributed through the observed sample.

Table II sums up some important information obtained by image analysis provided by tomography method. First, for an identical volume, the average diameter of the agglomerates (D_{eq}) is about 26-27 µm for each one of the formulations (EF20, EFD20). Second, very few but huge agglomerates over 100 µm were found for both samples. Finally, there is not enough evidence to draw a significant conclusion to differentiate the state of dispersion between both formulations.

Moreover, it is also important to remark that extrusion-injection molding samples do not present entrapped air bubbles, unlike samples produced on a Haake melt blender and then shaped by hot-press [10]. This is extremely important because it has been shown that entrapped air may induce slip at the wall [9,40] and may affect the stability of HF suspensions [3]. In tomography, entrapped air would be indicated by a very low dense zone in black, according to the grayscale density.

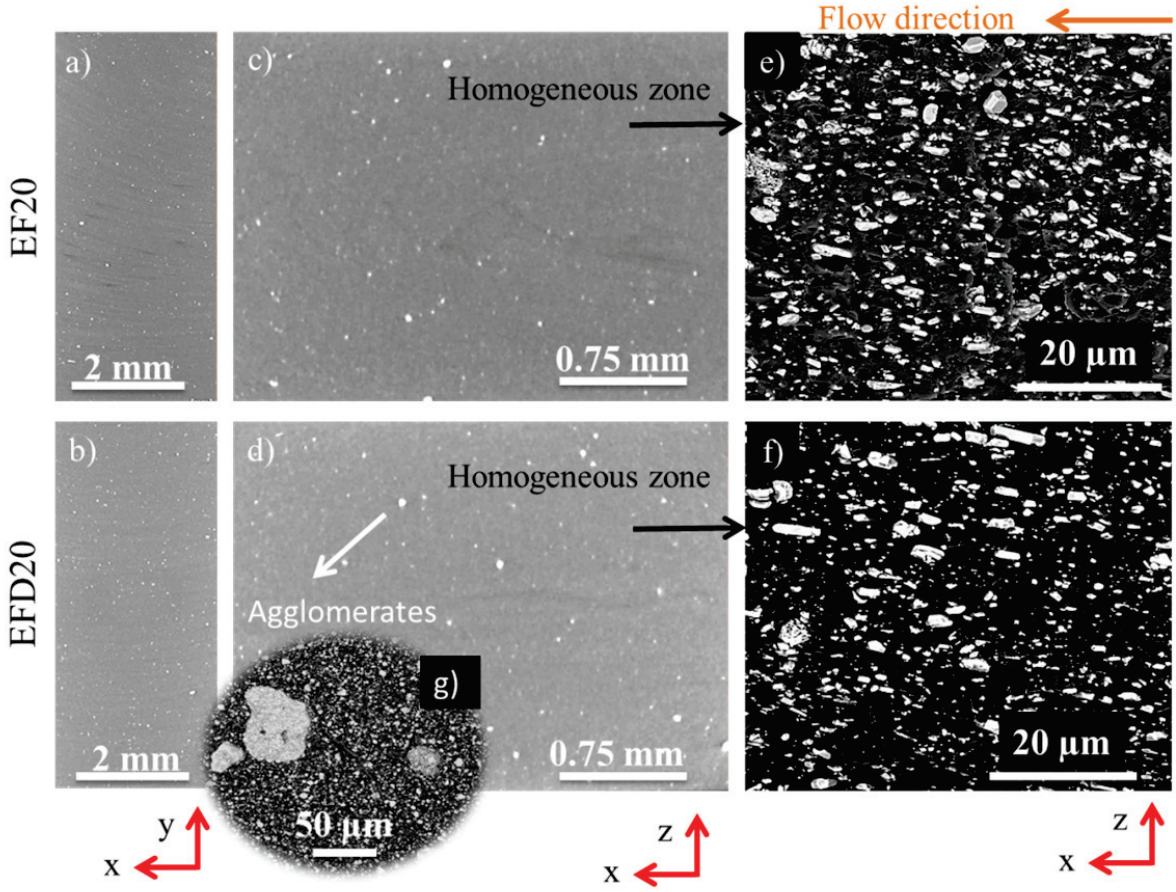
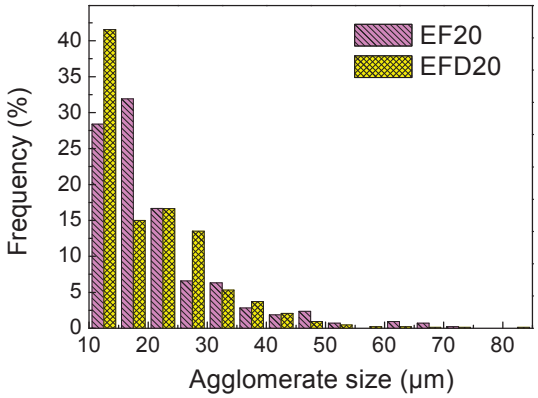


Fig. 3. State of dispersion observed either by tomography and SEM microscopy for samples EF20 (a, c, e) and EFD20 (b, d, f, g). Tomography (a, c, b, d) was performed over rectangular pieces of 3mm width, 2 mm height and 7.7 mm length under 55 kV and 150 µA. SEM microscopy (e, f, g) was performed under 10 kV, high vacuum (10^{-6}) and BSED detector. x, y and z axis represent width, length and height of the rectangular piece where z corresponds to the thickness and x the flow direction during the injection molding process.

Table II. Agglomerate size characterization by tomography method. Studied system=EF20 and EFD20, 45.5 mm^3 under 55 kV and intensity of 150 µA. D_n = median diameter by number.

Sample	EF20	EFD20
n	2821	2946
Maximum D_{eq} (µm)	132	102
Mean D_{eq} (µm)	27	26
D_n(0.2) (µm)	<20	<20
D_n(0.8) (µm)	<35	<35



B. Dynamic rheology

Fig. 4 displays frequency sweeps performed for the neat matrix (EPPI) and samples filled from 10 to 40 vol% with and without the addition of the dispersant agent. It is important to remember that these tests were obtained after a pre-shearing and 1 h of annealing time, in which the microstructure evolves [10]. The tests were performed in the linear viscoelastic domain (LVD) and further verified with a consecutive strain sweep.

From Fig. 4(a), the percolation threshold (ϕ_c) can be evidenced between 0.1< ϕ_c <0.2, due to the change in the flow regime. This means that a change in the plot curvature occurs, necessary passing by the moment which describes the material percolation ($G'(\omega) \alpha\ G''(\omega) \alpha\ \omega^{0.5}$) [10]. The percolation indicates the existence of strong links among particles, forming microscopic structures. For disk-like particles, ϕ_c has been shown as being inversely proportional to the aspect ratio, $\phi_c = l/d \approx 0.25$ [41,42]. Besides this, a geometric percolation obtained by two-dimension analysis is given by $\phi_c = \phi_m / p$ [43], where p is the aspect ratio and ϕ_m the maximum packing fraction defined as $\phi_m =$ bulk density/true density [44]. In our case, $\phi_m = 0.72$, and thus $\phi_c = 0.18$. We can indeed state that the physical percolation lies between 0.18< ϕ_c <0.25, which in fact supports our observation in Fig. 4(a). Saini et al. also reported similar percolation threshold (0.25< ϕ_c <0.30) for ferrite particles with comparable average particle size [2].

When the dispersant agent is added, the viscoelastic behavior is changed and the moduli values are highly reduced and thus the viscosity of the mixture (Fig. 4(b)). Fig. 4(c) shows the comparison between the highest filled materials. EF40 presents a completely solid-like behavior, while, EFD40 shows a gel behavior (*G' > G"* and log *G'* // log *G"*) which still has fluidity.

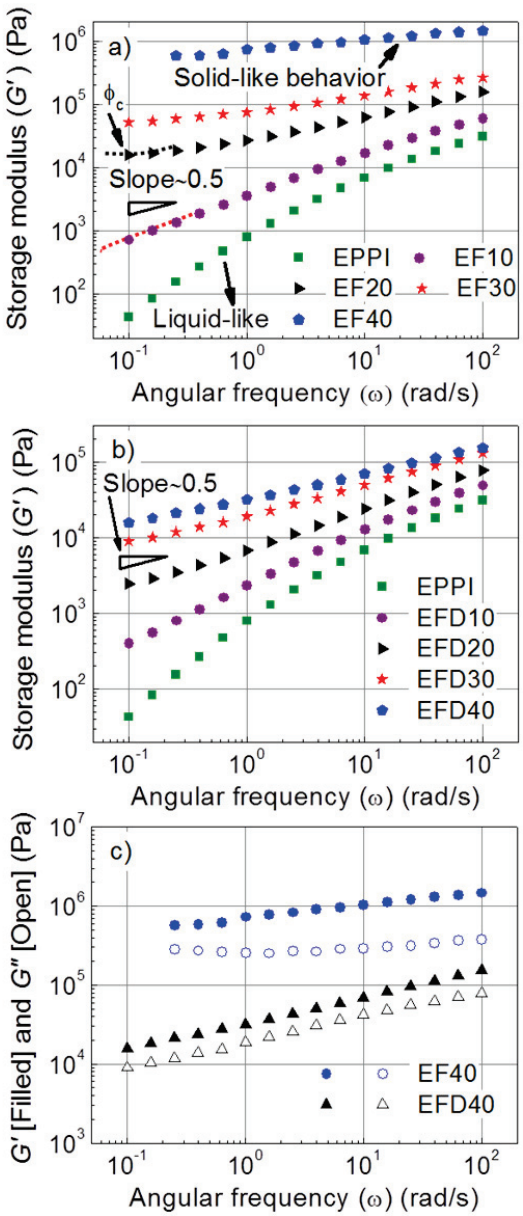


Fig. 4. Frequency sweep for samples filled with 0, 10, 20, 30, 40 vol% (a) without and (b) with the addition of 2 wt% of SDP310. Such tests were performed by using plate/plate geometry after 1 h annealing time, under nitrogen, 190 °C and (10^{-4}-10^{-3}) of strain. Dashed lines were put to guide the reader. (c) Comparison between EF40 and EFD40.

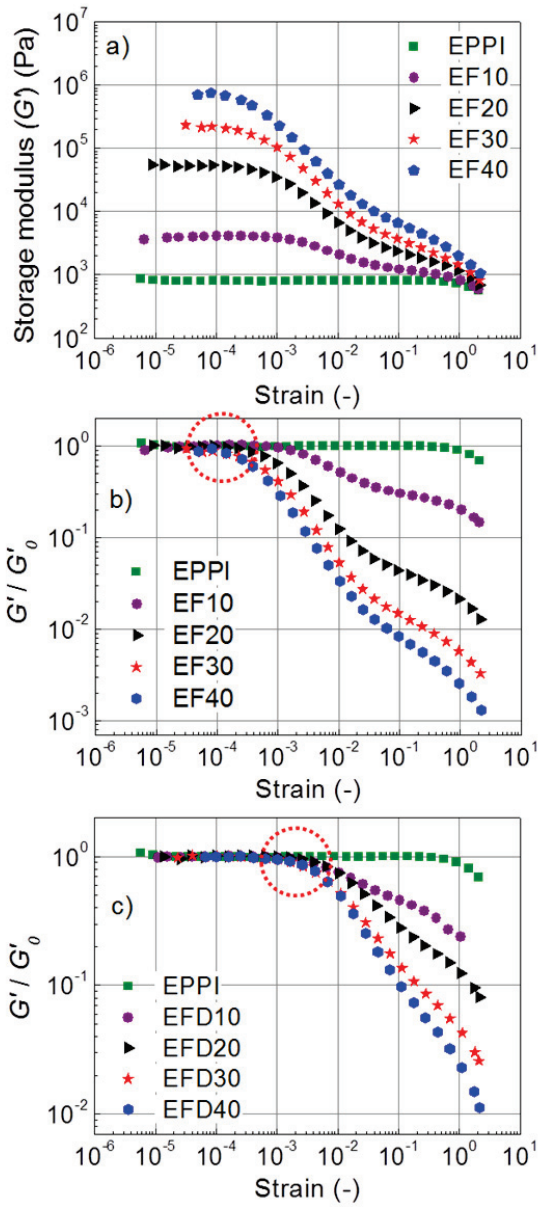


Fig. 5. Strain amplitude sweep from 6×10^{-6} to 2 of deformation (a) for composites filled up to 40 vol%. Normalized values of G'/G'$_0$ (b) without and (c) with the addition of the dispersant agent. Tests performed by using plate/plate geometry after frequency sweeps, under nitrogen, 190 °C and 1 rad/s. Circles depict the onset of non-linearity.

After each frequency sweep, a strain sweep was performed. Fig. 5 shows several important trends which are well-known in the HF suspension field. First, the maximum strain to which the LVD extends decreases with increasing the filler level (ϕ) [45] as shown Fig. 5(a). Such a decrease of the LVD is interpreted by considering that, when increasing the filler concentration, admittedly inter-

aggregate interactions become more abundant, leading to a higher modulus, however the probability of rupture is also increased so that the network becomes more brittle. This means that, very gentle deformations are transmitted by the connecting paths which in turn produce a particle rearrangement wherever is favorable, breaking the linearity. Thus, the mechanism that governs the onset of non-linearity can be interpreted by considering two regimes: above and below ϕ_c. Above ϕ_c, it can be understood as the rupture of the relatively weak bonds of the particle network [46]. Below this limit, matrix contribution dominates and so chain disentanglements together with rupture of filler interactions control the phenomenon [47]. Second, the addition of particles considerably increases both storage (*G'*) and loss modulus (*G"*), being the effect on *G'* greater than the effect on *G"* [48]. Finally, strong strain-dependence of the dynamic viscoelastic properties has been also reported in HF suspensions [3,49]. Such dependence is known as the Payne effect, in which the moduli drastically drop when increasing the deformation as it can be clearly evidenced in Fig. 5. The more the filler level is, the larger the amplitude of Payne effect is.

It is important to remember that, at low γ, particles interactions are more visible and at high γ, hydrodynamic interactions predominate over interparticle interactions. For this reason in Fig. 5(a), at high γ the behavior converges to the matrix flow behavior [50]. So, only very slight differences are visible in such zone (γ>1).

Fig. 5(b) and 5(c) shows the storage modulus (*G'*) normalized by the storage modulus at the plateau (G'_0) for all the composites. The addition of the dispersant agent drastically changes the viscoelastic behavior of the suspension, extending the limit of linearity for all concentrations as shown by the circle. This is attributed to the fact that lower interparticle interactions result from formulation with fatty acid, conducing to a screen effect between particles.

The critical strain value $\gamma_c = f(\phi)$ is in somehow difficult to determine. In order to observe the real decrease in the moduli, it is preferable to plot semi-log graphs of *G'* and *G"* vs log(γ). However, it is even better to establish a limit condition as proposed by [46], in which γ_c has been defined as the point beyond which *G'* deviates more than 5% from its maximum value. This condition has been used in this work for all samples, except for EF30 and EF40. Such composites presented almost no LVD at the lowest strain sensitive of the rheometer. Thus, γ_c and G'_0 were extrapoled from the semi-log plots.

Above the percolation threshold, the critical strain and the storage modulus exhibit a power-law behavior with respect to ϕ, in which $\gamma_c \sim \phi^{-3.4}$, $\gamma_c \sim \phi^{-1.3}$ for formulations EF and EFD respectively, Fig. 6(a). Such dependence is much stronger for samples without the dispersant. The power law exponents for the elastic character of the fractal network were obtained by plotting the modulus at the plateau (G_0) over the matrix plateau modulus ($G_{0,m}$) as a function of ϕ, thus $G'_0/G'_{0,m} \sim \phi^{3.9}$ and $G'_0/G'_{0,m} \sim \phi^{2.2}$ for formulations EF and EFD, displayed in Fig. 6(b). Scaling laws have been widely studied in literature especially for nanocomposites [51]. For instance, power law dependences of γ_c, *G'* and *G"* on ϕ coincide with filled-systems such as bohemite alumina particles/aqueous medium [46], clay suspended either in PMMA [50] or in PP [52], and also silica/polyol [53] suspensions. The power law exponent depends on the interparticle interactions [51]. Hence, the higher is the power law coefficient, the stronger are the interparticle interactions. Such coefficient has been also used to

discriminate the degree of exfoliation and thus the dispersion in clay/PP nanocomposites [50]. They also demonstrated that the sample with the lowest power law exponent presented a better exfoliation with a more open fractal structure. Here, it is shown again that the fatty acid compound actually reduces interparticle interactions, which may improve the dispersion. However, the latter could not be proven by the tomography analysis which shows very slight differences between the formulations.

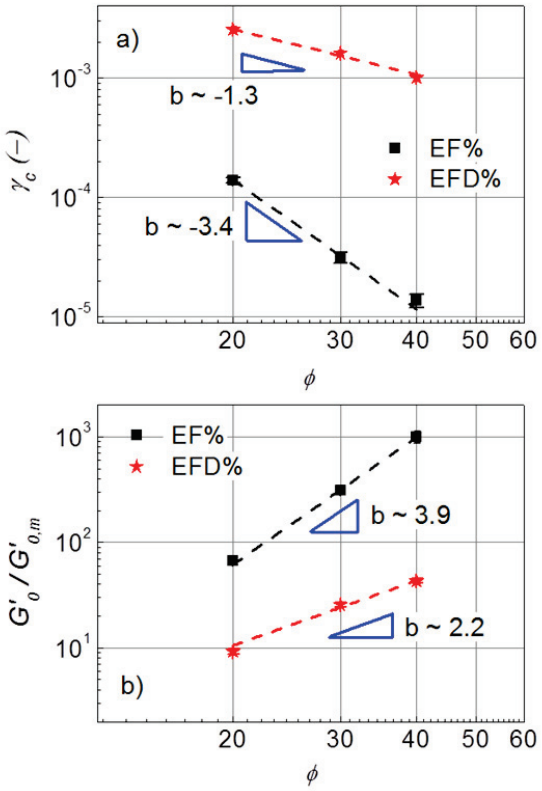


Fig. 6. Power laws relationship for concentrated ferrite suspensions (a) critical strain limit (γ_c) and (b) storage modulus at the plateau (G'_0) over matrix plateau modulus ($G'_{0,m}$) as a function of filler level (ϕ) for samples with and without the addition of fatty acid.

C. Non-linear rheology

Three different capillaries with the same L/D ratio were used to study the slip at the wall. According to the well-known Mooney method [54], wall slip is greater for capillaries with small diameters at same L/D, because of the larger contribution of the slippage on the total flow

Fig. 7(a) shows flow curves for the neat matrix, while Fig. 7(b) displays the results for the sample filled with the highest filler amount (40 vol%) with and without the addition of the dispersant agent. It is clearly shown that there is no contribution from the surface of the capillary to the flow properties. There is a complete superposition of the three flow curves either for the unfilled polymer or for the

concentrated composites. It must be added that EF20 and EFD20 have shown the same trend but these results were omitted in this work for sake of brevity. Additionally, Fig. 7(c), 7(d) and 7(e) display some axial observations from the extrudate. No concentration gradient is observed in these SEM images.

It must be pointed out that the possible flow surface instabilities were not easily observable, especially because our set-up obstructs the direct extrudate observation at the die exit. However, it can be asserted that the extrudates of the filled samples were smooth over all the range of shear rates studied here. This may not be the case for the unfilled matrix, particularly in the moderate and high shear rates range. Smooth surfaces are presented in Figs. 7(a-b) from the EPPI and EF40 extrudate. From these results, it can be thus concluded that either wall slip or surface wall instabilities do not interfere on the flow behavior of the ferrite composites.

Fig. 8 shows steady shear flow properties measured for samples at different solid fractions, as well as, the flow curve of PP matrix (EPPI), depicted by the line. The EPPI flow curve is continuous in all the range of shear rates. The matrix viscosity at low shear rates is purely Newtonian, while by increasing the shear rates, shear thinning behavior appears. Such a behavior is attributed to the exit from the linear to the non-linear domain, in which gradual relaxation of the physical entangled network occurs due to chain stretch and motion [55]. Fig. 8 compiles the filled flow curves for samples (a) with and (b) without the dispersant agent. First, it is noted that in the non-linear regime, very small differences among the flow curves are evidenced, as it has been observed in rotational flows at high shear rates. Next, it can be clearly seen that for $\dot{\gamma} \to 0$ or $\dot{\gamma} \to \infty$, $\eta(\dot{\gamma})$ displays higher deviation from the matrix behavior. On the one hand, at high shear rates, the slope decreases with increasing ϕ. On the one hand, at high shear rates, the absolute value of the slope decreases and the pseudoplasticity index (n) increases with increasing ϕ. On the other hand, at low shear rate, a deviation from the zero-shear viscosity appears, giving rise to an increase in the slope when increasing ϕ.

Figs. 9(a-d) display the shear viscosity at given filler level for samples with and without the dispersant in the formulation. Two process windows can be differentiated in these figures: 10^0 to 10^2 s^{-1} and 10^2 to 10^4 s^{-1}. In the first one, the dispersant agent acts as a lubricant, promoting slip between particles, decreasing particle interactions and thus, decreasing the shear viscosity [56]. On the second process window, almost no difference between both formulations was observed. Only EF40 and EFD40 showed a significant decrease in viscosity in both process windows, being more significant at low shear rates. Nevertheless, both formulations show similar power law behaviors at high shear rates. This means that the behavior at high shear rates is governed by the same mechanism. In the same way, lower filled composites show the same slope and thus similar behavior. A special attention should be taken when considering Fig 9(a). Surprisingly, at low shear rates, EFD10 presents a lower viscosity compared to that one of the pure matrix. However, it is important to remember that the reference matrix is only composed of PP+1 wt% of irganox. Hence, such decrement may be due to a small excess of dispersant that was not able to be adsorbed onto the particle surface. It may modify the matrix behavior, acting as a plasticizer. Therefore, when $\phi \geq 20\% \approx \phi_c$, the interparticle interactions suppress such effect.

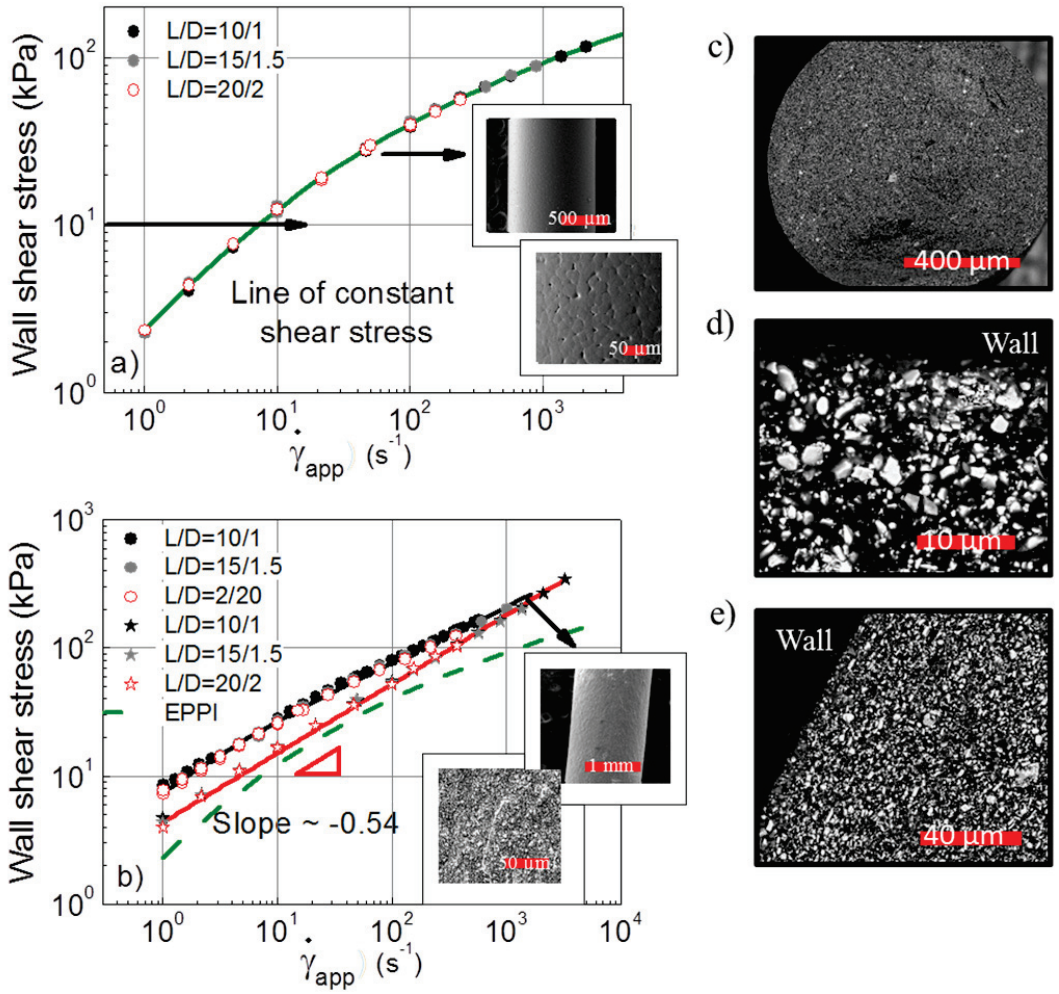


Fig. 7. On the left, wall shear stress versus apparent shear rate for (a) unfilled PP (EPPI) and (b) EF40 without (circle symbol) and with (star symbol) the addition of the fatty acid at 190 °C, the dashed line represents the EPPI matrix behavior, L/D=10/1, 1.5/15, 2/20 and radial SEM observations of the extrudate EPPI and EF40 at high and small magnification. On the right, axial SEM observations of the extrudate (c) (d) EF40 and (e) EFD40 at 3000 s^{-1}. EFD40 follows a power law model ($\sigma = K\dot{\gamma}^n$) in all the range of shear rates.

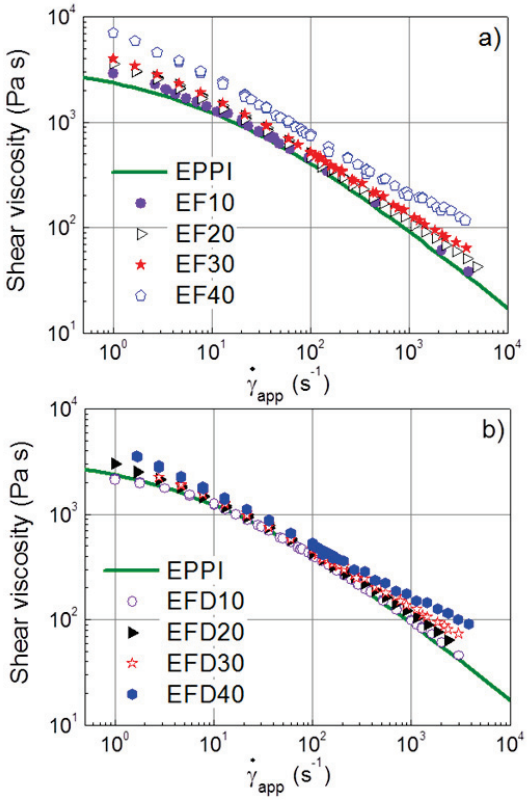
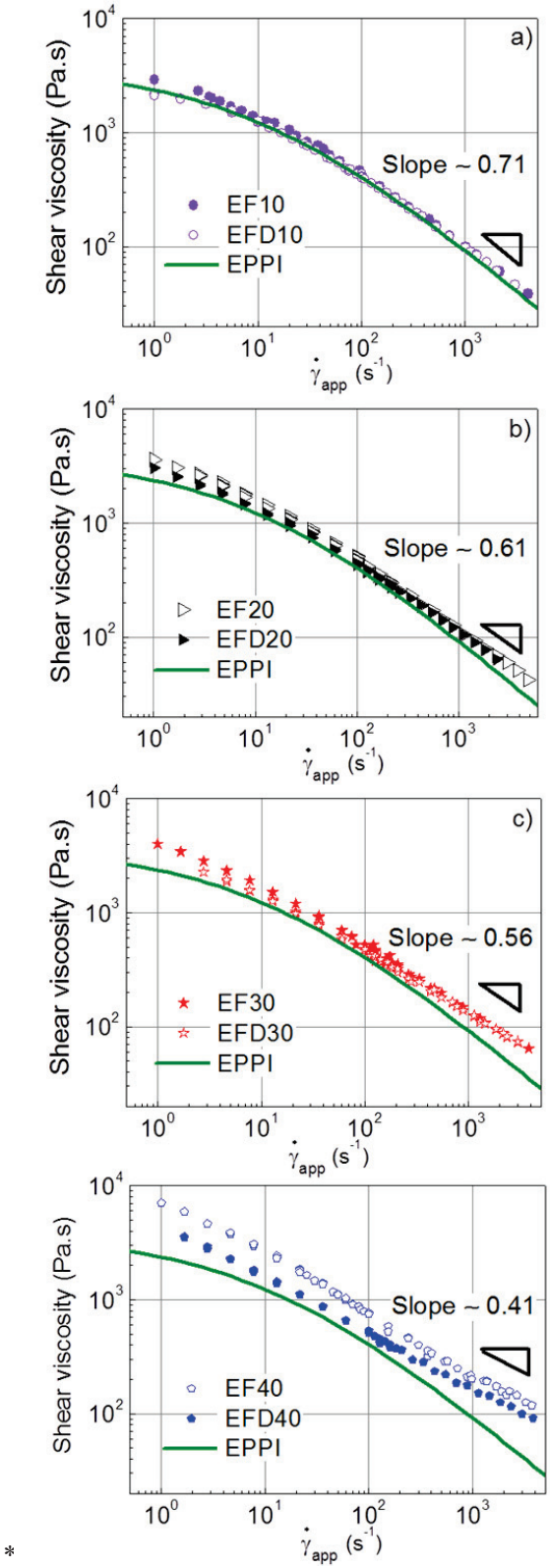


Fig. 8. Relationship between the shear viscosity and shear rate, $\dot{\gamma}$, of filled composites (a) without and (b) with the addition of the fatty acid. The line represents the unfilled matrix (EPPI). Steady state test performed at 190 °C, L/D=20/1.

To highlight the results, the viscosity of the suspension, $\eta_s(\dot{\gamma})$, has been divided by the viscosity of the melt polymer, $\eta_m(\dot{\gamma})$, at the given shear rate, in order to normalize by the matrix contribution. The results reveal that the dependency of $\eta_r(\dot{\gamma}) = \eta_s(\dot{\gamma})/\eta_m(\dot{\gamma})$ on $\dot{\gamma}$, exhibits three distinct regimes as Fig. 10 shown. Each of these regimes are associated to low, moderate and high shear rates. At low shear rates, the macrostructure is dominated by the particle interactions. The more is the filler amount, the higher is the deviation of the viscosity from the zero-shear viscosity. The microstructure is attributed to a particle network. Next, $\eta_r(\dot{\gamma})$ decreases to attain a minimum, revealing a shear thinning behavior which comes strictly from the ferrite phase. In fact, flow lines start to disturb ferrite particles orientation, which provokes an alignment and thus rupture of the network. In this zone, the filled composites present the closest behavior to that of the matrix. This evidences a completely destroyed structure, in which the viscosity contribution from the particles is the lowest. Finally, at high shear rates, $\eta_r(\dot{\gamma})$ starts to rise again. The higher is the filler level, the lower is the onset of non-linearity. Such a dramatic increase may be attributed to a new microstructure imposed by the high flow rate, thus an attenuation on the shear thinning behavior is clearly observed, which could indicate to the possible onset on shear thickening behavior.



*

Fig. 9. Comparison between samples with and without the addition of dispersant filled with (a) 10 vol% (b) 20 vol% (c) 30 vol% and (d) 40 vol%. Steady state test performed at 190 °C, L/D=20/1.

The later can be also observed by illustrating the normalized shear viscosity as a function of the wall shear stress (Fig. 11). In contrast to Fig. 10, this representation of the data presents a very slight deviation of the filled composites from the pure matrix at low shear rates.

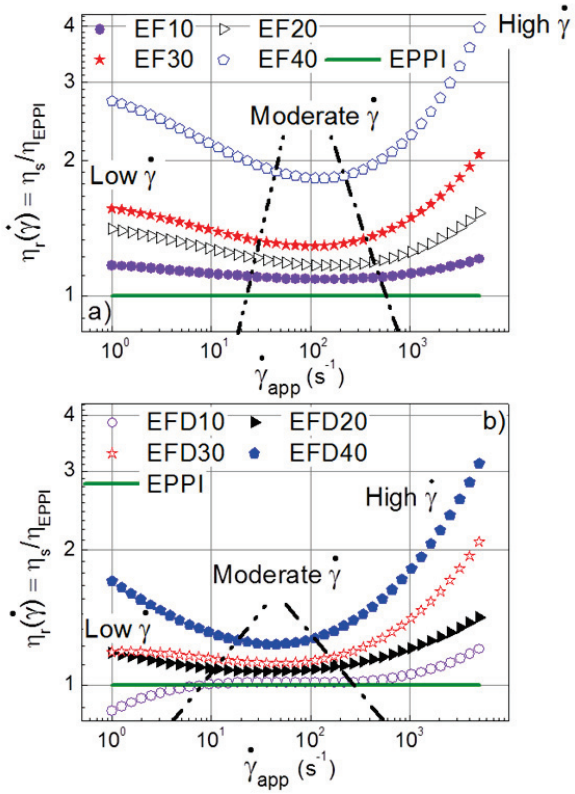


Fig. 10. Dimensionless shear viscosity as a function of the shear rate, normalized by the shear viscosity of the pure matrix at given shear rate. Formulations (a) without and (b) with the dispersant agent.

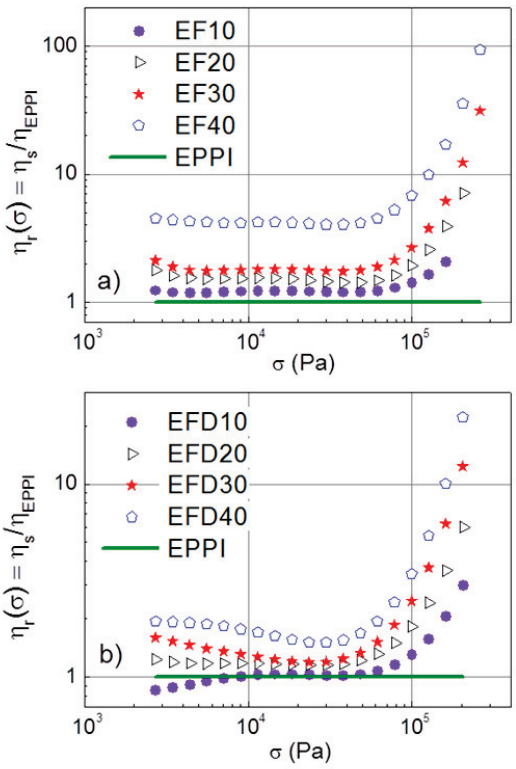


Fig. 11. Dimensionless shear viscosity as a function of the shear stress, normalized by the shear viscosity of the pure matrix at given wall shear stress. Formulations (a) without and (b) with the dispersant agent.

It has been evidenced that some concentrated colloidal suspensions and non-Brownian suspensions (suspended in a low molar mass liquid) shown an abrupt increase in the viscosity above a critical shear rate or wall shear stress [57]. However, analogous works on highly filled molten polymers reported that, at high shear rates, highly filled samples either converge to the matrix flow curve [58–61] or present the same power law behavior to that of the matrix [14,33,62–64] (same slope). It is generally believe that at very high shear rates (or shear stresses) the effect of the polymer matrix is much larger, totally suppressing the interparticle interactions. Here, we showed that, at high shear rates, the particle configuration change, leading to a new created micro-structure which opposes a certain restriction to flow. The same behavior was observed for particles covered by the fatty acid.

Based on these results, it can be concluded that the addition of the dispersant agent modifies the flow behavior (see Fig. 7(b)), decreases particles interactions and thus decreases the viscosity of the mixture (Fig. 9(d)). Such decrement is most important in the low shear rate process window. It can be expected that high shear rates induce fatty acid migration from the ferrite surface to the bulk, rather than to the die wall. The diffusion of the fatty acid to the wall might be restricted by the presence of the particles.

IV. Conclusions

In this work, we have studied the flow nature of ferrite suspensions in the linear and the non-linear regime for samples filled with 10, 20, 30 and 40 vol%, with and without the addition of a commercial dispersant SDP310. Under dynamic flows, it was observed that γ_c and $G'_0/G'_{0,m}$ follow power law dependencies with ϕ. Such dependency is most pronounced for samples without the fatty acid compound. The dispersant agent actually, reduces the moduli values and increases the linear domain. Under non-linear shear in capillary rheometer, the flow properties were found to do not depend on the diameter of the die. Wall slip contribution is negligible at the shear rates studied here. The nature of the flow was divided into three distinct sections: low, moderate and high shear rates. Such region presents very distinctive characteristics and has been attributed to distinct micro-structures formed due to flow. At low shear rates, a deviation from the zero-shear viscosity is observed which might correspond to a network structure. Moderate shear rates destroy particle network and thus particles are oriented in the flow direction, by increasing interparticle distances. In such region, the behavior is the closest to the unfilled polymer. Finally, high shear rates create a new micro-structure which attenuates the shear thinning behavior. Particles orient in the flow direction and may form local clusters which restrict the flow. A possible onset on shear thickening is put in evidence. When adding a dispersant agent, shear viscosity presented lower values at fixed ϕ, at low shear rates. At high shear rates, only the EF40% and EFD40% showed a remarkable decrease on viscosity. From this, it can be also concluded that by adding a fatty acid, particle interactions are decreased and thus the shear viscosity, which will improve the extrudability and the injection moldability of these materials.

References

[1] T. Fiske, H.S. Gokturk, R. Yazici, D.M. Kalyon, Effects of flow induced orientation of ferromagnetic particles on relative magnetic permeability of injection molded composites, Polym. Eng. Sci. 37 (1997) 826–837. doi:10.1002/pen.11725.

[2] D.R. Saini, A.V. Shenoy, V.M. Nadkarni, Melt rheology of highly loaded ferrite-filled polymer composites, Polym. Compos. 7 (1986) 193–200. doi:10.1002/pc.750070402.

[3] C. Feger, J.D. Gelorme, M. McGlashan-Powell, D.M. Kalyon, Mixing, rheology, and stability of highly filled thermal pastes, IBM J. Res. Dev. 49 (2005) 699–707. doi:10.1147/rd.494.0699.

[4] B. Voillequin, D. Ayme-Perrot, B. Dufour, P. Sonntag, Cathode for a Cell of a Lithium-Ion Battery, Its Manufacturing Process and the Battery Incorporating It, US20130183577 A1, 2013. http://www.google.com/patents/US20130183577 (accessed July 1, 2015).

[5] A. Azoug, R. Nevière, R.-M. Pradeilles-Duval, A. Constantinescu, Influence of crosslinking and plasticizing on the viscoelasticity of highly filled elastomers, J. Appl. Polym. Sci. 131 (2014) 40392(1-9). doi:10.1002/app.40392.

[6] A. Boudenne, L. Ibos, M. Fois, J.C. Majesté, E. Géhin, Electrical and thermal behavior of polypropylene filled with copper particles, Compos. Part Appl. Sci. Manuf. 36 (2005) 1545–1554. doi:10.1016/j.compositesa.2005.02.005.

[7] T. Lusiola, D. Scharf, T. Graule, F. Clemens, Low shear compounding process for thermoplastic fabrication of ferroelectric lead-free fibres, J. Eur. Ceram. Soc. 34 (2014) 2265–2274. doi:10.1016/j.jeurceramsoc.2014.02.036.

[8] M.M. Rueda, M.-C. Auscher, R. Fulchiron, T. Périé, G. Martin, P. Sonntag, P. Cassagnau, Rheology and applications of highly filled polymers: A review of current understanding, Prog. Polym. Sci. 66 (2017) 22–53. doi:10.1016/j.progpolymsci.2016.12.007.

[9] D.M. Kalyon, S. Aktaş, Factors Affecting the Rheology and Processability of Highly Filled Suspensions, Annu. Rev. Chem. Biomol. Eng. 5 (2014) 229–254. doi:10.1146/annurev-chembioeng-060713-040211.

[10] M. Rueda, R. Fulchiron, P. Cassagnau, A. Prebé, G. Martin, Structuring of non-Brownian ferrite particles in molten polypropylene: Viscoelastic analysis, J. Rheol. 60 (2016) 1245–1255. doi:10.1122/1.4963801.

[11] S. Zürcher, T. Graule, Influence of dispersant structure on the rheological properties of highly-concentrated zirconia dispersions, J. Eur. Ceram. Soc. 25 (2005) 863–873. doi:10.1016/j.jeurceramsoc.2004.05.002.

[12] A. Fall, H. de Cagny, D. Bonn, G. Ovarlez, E. Wandersman, J.A. Dijksman, M. van Hecke, Rheology of sedimenting particle pastes, J. Rheol. 57 (2013) 1237–1246. doi:10.1122/1.4809732.

[13] P. Ried, C. Lorenz, A. Brönstrup, T. Graule, N.H. Menzler, W. Sitte, P. Holtappels, Processing of YSZ screen printing pastes and the characterization of the electrolyte layers for anode supported SOFC, J. Eur. Ceram. Soc. 28 (2008) 1801–1808. doi:10.1016/j.jeurceramsoc.2007.11.018.

[14] M.A. Osman, A. Atallah, T. Schweizer, H.C. Öttinger, Particle–particle and particle-matrix interactions in calcite filled high-density polyethylene—steady shear, J. Rheol. 48 (2004) 1167–1184. doi:10.1122/1.1784782.

[15] C.G. Armistead, A.J. Tyler, F.H. Hambleton, S.A. Mitchell, J.A. Hockey, Surface hydroxylation of silica, J. Phys. Chem. 73 (1969) 3947–3953. doi:10.1021/j100845a065.

[16] A. Potanin, N.K.N. Jr, Formulation effects on magnetic mix microstructure based on rheological, magnetic susceptability, and particle size measurements, J. Rheol. 47 (2003) 389–412. doi:10.1122/1.1538607.
[17] P.C. Hidber, T.J. Graule, L.J. Gauckler, Influence of the dispersant structure on properties of electrostatically stabilized aqueous alumina suspensions, J. Eur. Ceram. Soc. 17 (1997) 239–249. doi:10.1016/S0955-2219(96)00151-3.
[18] V.M.B. Moloney, D. Parris, M.J. Edirisinghe, Rheology of Zirconia Suspensions in a Nonpolar Organic Medium, J. Am. Ceram. Soc. 78 (1995) 3225–3232. doi:10.1111/j.1151-2916.1995.tb07958.x.
[19] F. Gao, S. Yang, P. Hao, J.R.G. Evans, Suspension Stability and Fractal Patterns: A Comparison using Hydroxyapatite, J. Am. Ceram. Soc. 94 (2011) 704–712. doi:10.1111/j.1551-2916.2010.04149.x.
[20] D. Burnat, P. Ried, P. Holtappels, A. Heel, T. Graule, D. Kata, The Rheology of Stabilised Lanthanum Strontium Cobaltite Ferrite Nanopowders in Organic Medium Applicable as Screen Printed SOFC Cathode Layers, Fuel Cells. 10 (2010) 156–165. doi:10.1002/fuce.200900014.
[21] M.M. Denn, Extrusion Instabilities and Wall Slip, Annu. Rev. Fluid Mech. 33 (2001) 265–287. doi:10.1146/annurev.fluid.33.1.265.
[22] P. Cassagnau, Linear viscoelasticity and dynamics of suspensions and molten polymers filled with nanoparticles of different aspect ratios, Polymer. 54 (2013) 4762–4775. doi:10.1016/j.polymer.2013.06.012.
[23] A. Ariffin, S.S. Jikan, M.S.F. Samsudin, Z.M. Ariff, Z. a. M. Ishak, Melt Elasticity Phenomenon of Multicomponent (Talc and Calcium Carbonate) Filled Polypropylene, J. Reinf. Plast. Compos. 25 (2006) 913–923. doi:10.1177/0731684406063550.
[24] T. Kaully, A. Siegmann, D. Shacham, Rheology of highly filled natural CaCO3 composites. I. Effects of solid loading and particle size distribution on capillary rheometry, Polym. Compos. 28 (2007) 512–523. doi:10.1002/pc.20308.
[25] V.L. Bravo, A.N. Hrymak, J.D. Wright, Study of particle trajectories, residence times and flow behavior in kneading discs of intermeshing co-rotating twin-screw extruders, Polym. Eng. Sci. 44 (2004) 779–793. doi:10.1002/pen.20070.
[26] U. Yilmazer, D.M. Kalyon, Slip Effects in Capillary and Parallel Disk Torsional Flows of Highly Filled Suspensions, J. Rheol. 33 (1989) 1197. doi:10.1122/1.550049.
[27] D.M. Kalyon, Apparent slip and viscoplasticity of concentrated suspensions, J. Rheol. 49 (2005) 621–640. doi:10.1122/1.1879043.
[28] S.A. Gulmus, U. Yilmazer, Effect of volume fraction and particle size on wall slip in flow of polymeric suspensions, J. Appl. Polym. Sci. 98 (2005) 439–448. doi:10.1002/app.21928.
[29] V. Hristov, E. Takács, J. Vlachopoulos, Surface tearing and wall slip phenomena in extrusion of highly filled HDPE/wood flour composites, Polym. Eng. Sci. 46 (2006) 1204–1214. doi:10.1002/pen.20592.
[30] B. Haworth, S.W. Khan, Wall slip phenomena in talc-filled polypropylene compounds, J. Mater. Sci. 40 (n.d.) 3325–3337. doi:10.1007/s10853-005-0424-2.
[31] T. q. Li, M. p. Wolcott, Rheology of wood plastics melt. Part 1. Capillary rheometry of HDPE filled with maple, Polym. Eng. Sci. 45 (2005) 549–559. doi:10.1002/pen.20308.
[32] F. Soltani, Ü. Yilmazer, Slip velocity and slip layer thickness in flow of concentrated suspensions, J. Appl. Polym. Sci. 70 (1998) 515–522. doi:10.1002/(SICI)1097-4628(19981017)70:3<515::AID-APP13>3.0.CO;2-#.

[33] A.J. Poslinski, M.E. Ryan, R.K. Gupta, S.G. Seshadri, F.J. Frechette, Rheological Behavior of Filled Polymeric Systems I. Yield Stress and Shear Thinning Effects, J. Rheol. 32 (1988) 703–735. doi:10.1122/1.549987.
[34] S. Ahn, J.L. White, Wall effects on flow of polymer/particulate/(carboxylic acid) in dies and rheometers, J. Appl. Polym. Sci. 91 (2004) 651–658. doi:10.1002/app.13109.
[35] H. Suwardie, R. Yazici, D.M. Kalyon, S. Kovenklioglu, Capillary Flow Behaviour of Microcrystalline Wax and Silicon Carbide Suspension, J. Mater. Sci. 33 (1998) 5059–5067. doi:10.1023/A:1004423411227.
[36] S. Dasgupta, Degree and stability of magnetic dispersions: Sedimentation, rheological, and magnetic properties, J. Colloid Interface Sci. 121 (1988) 208–213. doi:10.1016/0021-9797(88)90424-9.
[37] S. Dasgupta, Interaction characteristics of magnetic particles with surfactants, solvents, and binder resins, J. Colloid Interface Sci. 124 (1988) 22–27. doi:10.1016/0021-9797(88)90320-7.
[38] R.C. Navarrete, L.E. Scriven, C.W. Macosko, Rheology and Structure of Flocculated Iron Oxide Suspensions, J. Colloid Interface Sci. 180 (1996) 200–211. doi:10.1006/jcis.1996.0290.
[39] M.-C. Yang, L.E. Scriven, C.W. Macosko, Some Rheological Measurements on Magnetic Iron Oxide Suspensions in Silicone Oil, J. Rheol. 30 (1986) 1015–1029. doi:10.1122/1.549892.
[40] B.K. Aral, D.M. Kalyon, Rheology and extrudability of very concentrated suspensions: effects of vacuum imposition, Plast. Rubber Compos. Process. Appl. 4 (1995) 201–210.
[41] A. Franceschini, E. Filippidi, E. Guazzelli, D.J. Pine, Dynamics of non-Brownian fiber suspensions under periodic shear, Soft Matter. 10 (2014) 6722–6731. doi:10.1039/c4sm00555d.
[42] H. Kim, A.A. Abdala, C.W. Macosko, Graphene/Polymer Nanocomposites, Macromolecules. 43 (2010) 6515–6530. doi:10.1021/ma100572e.
[43] A. Gassiot-Talabot, Renforcement d'un poly(oxyéthylène) par dispersion de whiskers de cellulose en voie fondue : contraintes et alternatives, Dissertation, Université Jean Monnet, 2015. http://www.theses.fr/s126251 (accessed December 12, 2016).
[44] A.J. Poslinski, M.E. Ryan, R.K. Gupta, S.G. Seshadri, F.J. Frechette, Rheological Behavior of Filled Polymeric Systems II. The Effect of a Bimodal Size Distribution of Particulates, J. Rheol. 32 (1988) 751–771. doi:10.1122/1.549991.
[45] H.A. Barnes, Review of the rheology of filled viscoelastic systems, Rheology Reviews, The British Society of Rheology, Br. Soc. Rheol. (2003) 49.
[46] W.-H. Shih, W.Y. Shih, S.-I. Kim, J. Liu, I.A. Aksay, Scaling behavior of the elastic properties of colloidal gels, Phys. Rev. A. 42 (1990) 4772.
[47] P. Cassagnau, Payne effect and shear elasticity of silica-filled polymers in concentrated solutions and in molten state, Polymer. 44 (2003) 2455–2462. doi:10.1016/S0032-3861(03)00094-6.
[48] J.A. Walberer, A.J. McHugh, The linear viscoelastic behavior of highly filled polydimethylsiloxane measured in shear and compression, J. Rheol. 45 (2001) 187–201. doi:10.1122/1.1332386.
[49] S. Merabia, P. Sotta, D.R. Long, A Microscopic Model for the Reinforcement and the Nonlinear Behavior of Filled Elastomers and Thermoplastic Elastomers (Payne and Mullins Effects), Macromolecules. 41 (2008) 8252–8266. doi:10.1021/ma8014728.
[50] J. Vermant, S. Ceccia, M.K. Dolgovskij, P.L. Maffettone, C.W. Macosko, Quantifying dispersion of layered nanocomposites via melt rheology, J. Rheol. 51 (2007) 429–450. doi:10.1122/1.2516399.
[51] P. Cassagnau, Melt rheology of organoclay and fumed silica nanocomposites, Polymer. 49 (2008) 2183–2196. doi:10.1016/j.polymer.2007.12.035.

[52] T. Domenech, R. Zouari, B. Vergnes, E. Peuvrel-Disdier, Formation of Fractal-like Structure in Organoclay-Based Polypropylene Nanocomposites, Macromolecules. 47 (2014) 3417–3427. doi:10.1021/ma5001354.
[53] F. Saint-Michel, F. Pignon, A. Magnin, Fractal behavior and scaling law of hydrophobic silica in polyol, J. Colloid Interface Sci. 267 (2003) 314–319. doi:10.1016/j.jcis.2003.07.018.
[54] M. Mooney, Explicit Formulas for Slip and Fluidity, J. Rheol. 2 (1931) 210–222. doi:10.1122/1.2116364.
[55] S.T. Milner, Relating the shear□thinning curve to the molecular weight distribution in linear polymer melts, J. Rheol. 40 (1996) 303–315. doi:10.1122/1.550742.
[56] R.G. Larson, The Structure and Rheology of Complex Fluids, New York: OUP USA, 1999.
[57] A. Fall, F. Bertrand, G. Ovarlez, D. Bonn, Shear thickening of cornstarch suspensions, J. Rheol. 56 (2012) 575–591. doi:10.1122/1.3696875.
[58] Y. Chan, J.L. White, Y. Oyanagi, A Fundamental Study of the Rheological Properties of Glass□ Fiber□Reinforced Polyethylene and Polystyrene Melts, J. Rheol. 22 (1978) 507–524. doi:10.1122/1.549486.
[59] P.R. Hornsby, A. Mthupha, Rheological characterization of polypropylene filled with magnesium hydroxide, J. Mater. Sci. 29 (1994) 5293–5301. doi:10.1007/BF01171538.
[60] K.-J. Kim, J.L. White, S. Eun Shim, S. Choe, Effects of stearic acid coated talc, CaCO3, and mixed talc/CaCO3 particles on the rheological properties of polypropylene compounds, J. Appl. Polym. Sci. 93 (2004) 2105–2113. doi:10.1002/app.20686.
[61] S. A. Ramazani, A. Ait-Kadi, M. Grmela, Rheology of fiber suspensions in viscoelastic media: Experiments and model predictions, J. Rheol. 45 (2001) 945–962. doi:10.1122/1.1378026.
[62] N. Minagawa, J.L. White, The influence of titanium dioxide on the rheological and extrusion properties of polymer melts, J. Appl. Polym. Sci. 20 (1976) 501–523. doi:10.1002/app.1976.070200222.
[63] L. Czarnecki, J.L. White, Shear flow rheological properties, fiber damage, and mastication characteristics of aramid-, glass-, and cellulose-fiber-reinforced polystyrene melts, J. Appl. Polym. Sci. 25 (1980) 1217–1244. doi:10.1002/app.1980.070250623.
[64] D.R. Saini, A.V. Shenoy, V.M. Nadkarni, Effect of surface treatments on rheological, mechanical and magnetic properties of ferrite-filled polymeric systems, Polym. Eng. Sci. 25 (1985) 807–811. doi:10.1002/pen.760251304.

Chapter 5

Short glass fiber composites rheology

Summary

Dynamic flow properties of two commercial short glass fiber reinforced polypropylene were carefully investigated. Rotational rheometry was employed to analyze the effect of the particle size distribution, the sizing and the fiber content on the flow properties. This experimental study allowed the examination of large fiber volume fractions up to 60 vol%, allowing the evidence of different phenomena. As generally known, the more the fiber level, the higher is the reinforcement effect on the matrix. The higher the average aspect ratio, the higher is the probability of creating a fiber network. Thus, higher aspect ratio leads to lower values of percolation threshold (ϕ_c). It was found that, small variations of the particle size distribution strongly affect the flow behavior of the composites. Dynamic frequency sweeps put in evidence the different concentration transitions regimes viz., dilute to semi-dilute and concentrated to nematic regimes. Finally, the elastic characteristic time has been found to increase when increasing the fiber content. This was in agreement with the behavior of the relative viscosity as a function of the filler level.

Keywords: dynamic flow properties, short-glass fibers, thermoplastic matrix, highly filled composites

Reformatted version of paper originally published in:

European Polymer Journal, Volume 93 (2017), Page 167-181

Rheology of Polypropylene filled with Short-Glass Fibers: from low to concentrated filled composites

Martha Margarita Rueda[1,2], René Fulchiron[1], Grégory Martin[2], Philippe Cassagnau[1]

[1)] *Univ-Lyon, Université Lyon 1, Ingénierie des Matériaux Polymères, CNRS, UMR 5223, 15 Bd Latarjet, 69622 Villeurbanne Cedex, France.*

[2)] *HUTCHINSON Research Center, Rue Gustave Nourry – B.P. 31, 45120 Chalette-sur-Loing, France.*

I. Introduction

Many industrial applications require the combination of materials with very high mechanical properties, while being lightweight. Glass fiber reinforced polymers (GFRP) combine both lightening and high performance [1]. Therefore, these materials have been largely used for replacing metallic and non-metallic parts, notably in aerospace, aviation, wind turbine blades and automobile applications [2]. Some specific examples are: structural parts, underbody shields and cockpit parts, which generally require highly filled (HF) levels of fibers (~ ≥40 vol%) [1,3,4]. In literature, most of the studies focus on dilute regimes up to 20 vol%, being far from the phenomena arising during the elaboration process of real engineering materials. Highly concentrated composites present some technical difficulties during the process elaboration, principally due to the high mixture viscosity [5]. Only few studies focus on the rheological properties of concentrated fiber composites (≥ 20 vol%) [6–10]. Therefore, there is still so much work to do in order to understand the flow properties of such complex materials.

GFRP can be reinforced either by short-fiber or continuous fibers. Short glass fibers (SGF) composites provide the possibility to tailor final properties and are easily manufactured by using conventional plastic machinery, such as extrusion and injection molding [11]. Such fillers can be encountered either in milled or chopped forms. They have diameters normally in between 10-20 μm [1]. On the one hand, chopped fibers have lengths between 3 to 4.5 mm or greater [12], which makes ~~strongly~~ more difficult a rheological study in small gaps. Chopped fibers are well known for their high reinforcement on the tensile and flexural modulus [13,14]. On the other hand, milled fibers present a wide particle length distribution with average lengths between 80-500μm [15,16]. They do not provide as strong reinforcement as chopped fibers do. However, such prolate fillers (aspect ratio, $p=L/D>1$) combine mechanical reinforcement with relative high $p\sim10$ to 50 compared to conventional micro-sized reinforcement fillers (*e.g.,* talc, calcium carbonate and clays). Hence, milled fibers are situated between both chopped fibers and conventional filler reinforcements.

The understanding of composite flow properties enables us to control, predict and model the elaboration process, as well as to design the processing equipment. Therefore, experimental works contribute to gain more insight on the behavior of such complex materials. The rheology of short-glass fibers

suspended in molten polymers depends on the characteristics of the fibers (p, sizing, stiffness), the characteristics of the matrix (viscosity, chemical nature), and the different interactions between the components [5,17]. Additionally, processing conditions affect the residual length distribution of the fibers [18]. However, such effect has been mostly encountered for chopped fibers rather than for milled fibers [19–23]. This is principally due to the fact that milled fibers present already a rather short initial length distribution compared to chopped fibers. Finally, the volume fraction (ϕ) determines the fiber-fiber interactions and thus the flow regime of the composite in the molten state [24,25].

Flow regimes have been well-established for Brownian rods and extended to Non-Brownian fibers [25]. Indeed, suspensions of short-glass fibers are always non Brownian. Four regimes can be found: dilute, semi-dilute, concentrated isotropic and nematic. In the dilute regime, the particles are not affected by hydrodynamic perturbations, providing from their neighbors. The transition between dilute to semi-dilute regimes occurs when the fibers begin to be affected each other hydrodynamically. Concentrated isotropic regime means that particles are still randomly oriented but start to be constraint by their neighbors, hindering the isotropic packing. Finally, nematic regime occurs when fibers achieve a certain filler level at which fibers are mostly oriented in parallel [16,25,26].

Rheological properties of fibers reinforced polymers were largely studied as a function of the already mentioned parameters. The most general trends are the following. The complex and shear viscosity increase when increasing ϕ and fiber aspect ratio (p) [15,27,28]. Hence, as expected, storage modulus (G') and loss modulus (G'') present the same trend [29,9,12,30]. Such effects are only visible when fibers have the probability to interact [16,31]. Typically, filler level lower than 10 vol% present no significant changes in the dynamic viscosity [9,27,30]. Short fibers composites with L<1mm can be assumed as rigid fillers at low shear deformations or in the linear viscoelastic domain [32]. Shear and complex viscosity ($|\eta^*|$) of filled systems present very small differences at high shear rates or frequencies, almost converging to the neat matrix behavior. In contrast, low shear rates or frequencies enable a better differentiation in the viscosity of the filled composites [7,9,10,28,29,32–34]. It is worth noting that, $|\eta^*|$ shows a much greater effect with ϕ at low frequencies than shear viscosity at low shear rates [6,35]. Complex viscosity was found to be much larger than shear viscosity (measured by capillary tests) at the same shear rate or frequency [6,9]. In addition, controlling orientation constitutes one of the most challenging problems for SGF systems. Indeed, final properties strongly depend on the orientation of the filler [5]. Fiber orientation is due to hydrodynamic interactions [24], thus at high shear deformations, for example in capillary flows, fibers are mostly aligned in the flow direction [9]. It was found out that, the viscosity of an aligned suspension is lower than a random dispersed suspension [36]. It has been also observed that the orientation and the anisotropy of fiber are strongly affected by the increase in glass fiber concentration [37].

Interesting controversial observations were also reported by some studies. Some authors [6,12] reported the presence of a secondary G' plateau at intermediate frequencies ($\omega = 10^0$-10^1 rad/s) for their highest filled composite (30 wt%, p=400 and 27 vol% p=19), which is not much common in the rheology of filled polymers. The latter results were in contrast to Guo et al. [9] work, in which G' and G'' do not present a secondary plateau even at very low frequency, $\omega = 0.1\, rad/s$. G' showed a

monotone decrease with decreasing ω, even for their highest filled system (35 vol%, p=14.5). No sign of mechanical percolation (plateau) was observed for any of their filled composites (0% to 35 vol%). Additionally, it has been seen that at fixed ϕ, shear thinning effects appear at lower shear rates for higher values of p. There is evidence that a more pronounced structure is formed by entangled fibers (fiber-fiber contact) as p increased [31]. Same trend was found for the effect of ϕ at fixed p [16]. On the contrary, Guo et al. [9] showed that the start on the shear thinning behavior was not affected by ϕ. Another interesting result concerns the orientation during an oscillatory dynamic test. It has been evoked that, in the linear viscoelastic domain, the low deformation imposed on the fiber suspension is too weak to induce significant fiber reorientation. Thus, the fibers preserve their original orientation and may vibrate at the corresponding frequency in equilibrium positions [9]. However, Kim and Song [38] showed that the $|\eta^*|$ decreases in consecutive frequency sweeps due to fiber orientation along the flow direction (parallel to the parallel plates).

Hence, this paper presents the result of measurements of the dynamic rheological properties of two commercial milled fibers suspended in a polypropylene matrix. We aim to elucidate the role of the particle size distribution, aspect ratio and sizing on the dynamic properties, covering all the regimes of concentration from dilute to nematic state. As far as we are aware, the effect of such a highly filled amount of fibers on the dynamic flow properties has not yet been considered. Therefore, the results of the present study are more relevant to practical applications in the industry of composite materials where high volume fractions are encountered.

II. Materials and Methods

A. Materials

1. Polymer

The polymer matrix used in this work is a commercial grade of polypropylene (PPH 7060) supplied by Total refining & chemicals of density 0.905 g/cm^3 and Melt Flow Index of 12 g/10 min (230°C/2.16 kg). It is a homopolymer with a melting temperature of 165 °C. The polypropylene (PP) has been stabilized by using Irganox 1010 at 1 wt% based on the weight of the matrix. Irganox 1010 is a sterically hindered phenolic antioxidant that protect PP matrix against thermo-oxidative degradation. The zero-shear viscosity of the stabilized matrix is $\eta_0 = 3900$ Pa.s at T=190°C.

2. Fibers

Two Vitrostrand milled fibers were used in this work: VS 1304 and VS 1320 K, provided by Owens Corning. This fibers are made from E-glass, Advantex® Glass (boron and fluorine-free). The initial state of each commercial grade is shown in Fig. 1. As it can be clearly observed, they present a broad length distribution. The diameter of the fibers (D) is fixed by the manufacturing process during the spinning step, while the length is less controlled. Such fibers were made from long fibers by milling process. Fibers VS 1304 undergoes two milling process, while, VS 1320 K undergoes only one. This is the reason why, VS 1304 seems to present a larger population of fragments.

Table I compiles all the technical characteristics given by the supplier, as well as some of our characterizations, whose explanation will be given below. According to the supplier, the fibers present the same *D* and their length differs from 80 to 160 µm. For this reason, the fibers will be denoted in this work as Short glass Fibers (SF).and Long glass Fibers (LF). LF presents half of the bulk density of SF, which may strongly reduce the flowability of the system. Consequently, a lubricant is added into the sizing formulation in order to improve such characteristic. According to the supplier, this is the principal difference in the sizing of both fibers.

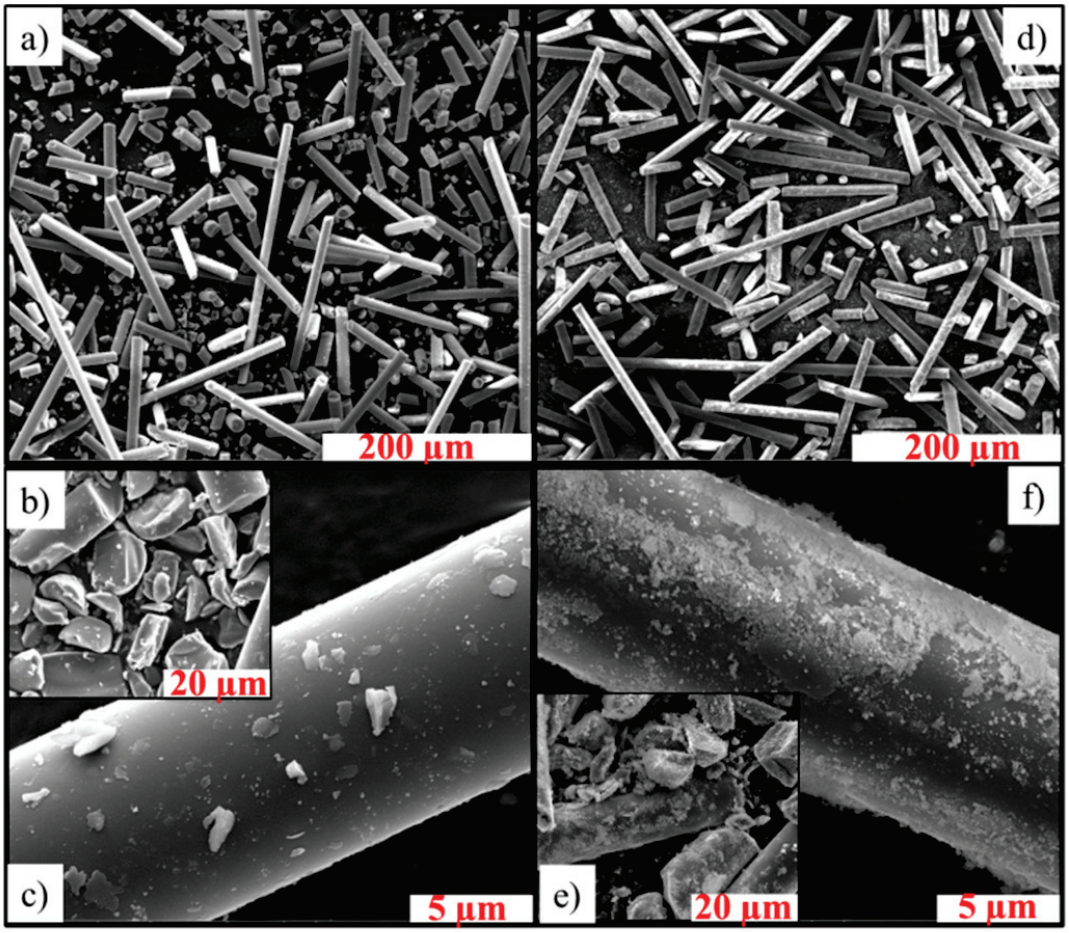


Fig. 1. Scanning electron microscopy (SEM) images of the glass fibers before processing taken with optical microscope: (a-c) VS 1304 and (d-f) VS 1320 K.

Table I. Technical characteristics given for the two commercial grades of fibers VS 1304 (SF) and VS 1320 K (LF).

Fiber name	**VS 1304 (SF)**	**VS 1320 K[(2)] (LF)**	**Method**
Nominal fiber diameter[(1)] (μm)	16	16	*Cross section of the strand*
Average fiber length[(1)] (μm)	80	160	*Optic-Image analysis*
Average fiber diameter (μm)	11.9 ±1.5	12.3 ±1.7	*Optic-Image analysis*
Moisture content (wt%)	0.02	0.04	*TGA*
Bulk density[(1)] (g/cm^3)	~1.2	~0.65	-
density (g/cm^3)	2.73	2.73	*Experimentally-TGA*
Product appearance	Powdery	Lumpy powdery	-

[(1)]Technical characteristics given by the supplier
[(2)]K = lubricant in the formulation

B. Fiber size measurement

The estimation of the particle size distribution of fibers is not trivial. In this work, fiber size distribution analysis was performed by two methods, optic microscopy-coupled to image analysis and light scattering. On the one hand, particle size distribution (PSD) was determined by light diffraction in a Master sizer 2000 device (dry dispersion method, 2 bars). Master sizer 2000 uses the Mie theory to solve the equation of the interaction between matter and light [39]. The approximations and assumptions of this theory are explained elsewhere [39,40]. It is well known that diffraction size measurements give a volume distribution in which the characteristic size corresponds to the diameter of the equivalent sphere with the same volume of the particle. However, anisometric particles may adopt a random orientation during the measurement which in turn results in an average measure between the Length (L) and the diameter (D) of the fiber [41]. Thus, the size distribution measured via laser diffraction is expected to be wider and shifted towards smaller sizes compared to the PSD measured by Image analysis [26].

On the other hand, particle size distribution was quantified by optical microscopy coupled to Image-J analysis. For this purpose, a very dilute fiber suspension in ethanol has been prepared. Then, a few drops were deposited in between of two glass plates. After drying, they were observed using an optical microscope in transmission mode (Leica M205 A). The image processing was performed by a semi-automatic process. It includes image contrast, thresholding (image segmentation), filling holes and analyze particles (Fig. 2).

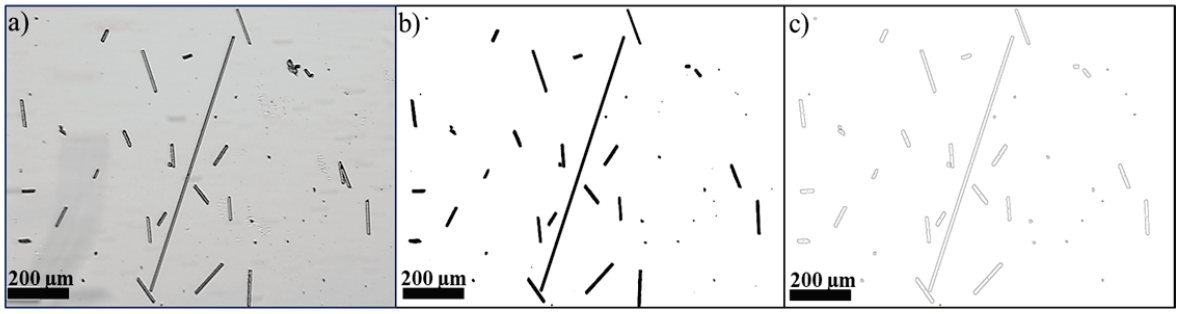


Fig. 2. Image processing performed by Image-J analysis software: (a) raw (b) binary and (c) outline images.

From the 2-D projections (Fig. 2(b)), the total weight-number distribution can be estimated. We propose a procedure that takes into account the shape factor of the particles. We assumed that the sample was constituted from two populations: one population of fibers and one of fragments (see Fig. 1). Each object was either model as a cylinder or as a sphere. The conditions used to calculate the total weight-number distribution are given in Table II. The statistical analysis was based on 200-230 images per sample. In order to compare both results, image analysis (IA) was transformed into volume-weighted distribution by using the method proposed and described by [42]. In short, D_{eq} was transformed to D_{eq}^3, together with two re-ordering steps (permutation from the highest to the lowest data). Unfortunately, such permutation may induce some inaccuracies to the largest part of the population due to the finite character of the measure. Both results will be discussed in Section III.A.

It is important to note that all the results presented here correspond to the initial size distributions (before processing). Since, it was previously demonstrated that the particle size distribution of such milled fibers were not much affected by the mixing process (see additional results N°1).

Table II. Image analysis conditions used in this work. The counting of objects was performed in a semi-automatic process by using Image-J software.

Population	**Equivalent diameter (D_{eq})**	**Measurement**	**n**
Fragments $l < d$ $l < 10$ µm	 $D_{eq} = \sqrt{\frac{4 \times A_p}{\pi}}$	Projected area (A_p)	SF = 4386 LF = 4154
Fibers $l \geq d$ $l \geq 10$ µm	 $V_c = \frac{\pi D^2 L}{4}$ $D_{eq} = \left(\frac{6V_c}{\pi}\right)^{1/3}$	Fit ellipse Minor = D Major = L	SF = 2722 LF =2329

C. Sizing quantification

Milled fibers always present lower sizing contents compared to chopped fibers [43], which makes very difficult its quantification. Fig. 3 shows SF's close-up along with a SEM-EDX analysis. From this analysis, we could not find any significant difference between the dissimilar chemical contrasts observed on the surface of the fibers, even under very low voltage. Results showed a normal chemical composition for E-glass fibers compared to what is presented in literature [14]. We also performed Time-of-Flight Secondary Ion Mass Spectroscopy (TOF-SIMS) analysis. Results showed evidence of silicone and nitrogen species (coupling agents), traces of saturated and unsaturated linear fatty acids (lubricant agents) and traces from a bisphenol epoxy compound (film former resin). Those are typical glass fiber compounds adding in conventional sizings. [44,45]. TGA/GC-MS and FTIR-ATR spectroscopy were also used to intend to characterize the sizing; however, due to the very low amount of sizing, we were unable to obtain reliable results. No concluding differences between the fibers were found.

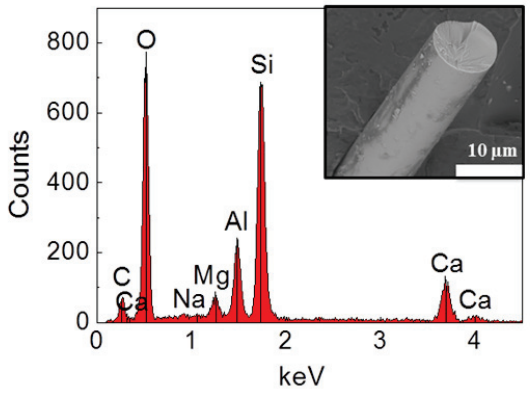


Fig. 3. Energy-dispersive X-ray spectroscopy (EDX) for SF sample, under 5 kV and Back-scatter electrons (BSE) detector.

The fiber sizing content was characterized by Thermogravimetric analysis (TGA) over a temperature range of 25 to 900 °C. The sample is monitored in a micro balance TGA/DSC 1, Mettler Toledo under nitrogen. The protocol used for this analysis consists in two steps. In step one; the sample is heated from 25 °C to 120 °C at 10 °C/min and held at this temperature for 10 min. Then, a ramp temperature is performed at 10°C/min from 120 to 900 °C and held again for 10 min (step 2). So that, step one removes the physically adsorbed water [46], whereas step two removes the organic components of the sizing.

Fig. 4 shows the TGA curves and Table III compiles the average results of three samples per grade. During TGA analysis, the initial weight of the sample is affected by buoyancy effects. As it can be seen in Fig. 4(a), the sample seems to gain weight at the beginning of the ramps until a significant loss is evidenced. This is attributed to convection currents due to differences in density of the gas in the furnace [47]. To solve this and perform an accurate measurement all the samples were summited twice to the same protocol. During the first run, the sizing was quantified (Fig. 4(a), left axis) and

during the second, the buoyancy effects of the sample plus the crucible were measured (Fig. 4(a), right axis). By subtracting both curves and by normalizing the weight (end of the step 1), the sizing was correctly quantified (Fig. 4(b)). We have thus reported a detailed protocol which enables us to measure such a low amount of sizing. Results in Table III showed that LF presented a higher amount of sizing compared to SF.

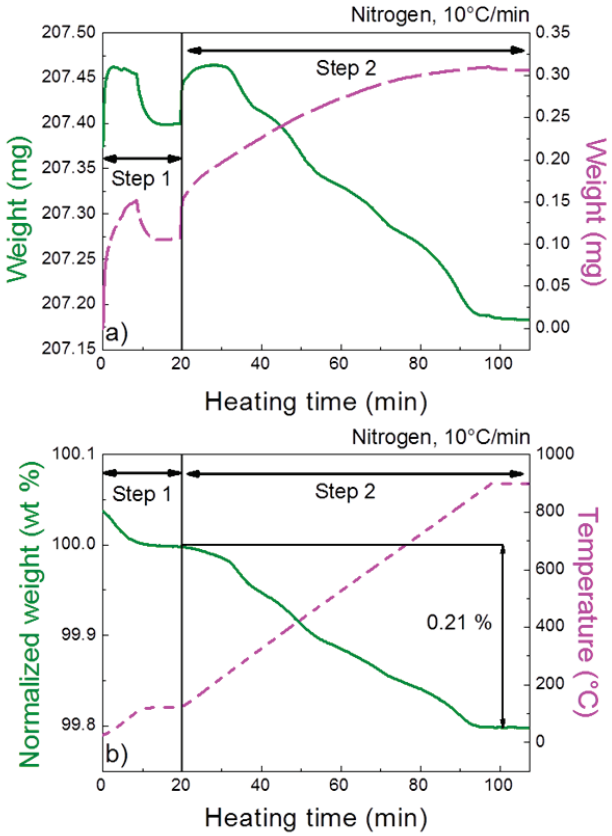


Fig. 4. TGA curves of a LF sample under step 1: Ramp 10°C/min, 25 to 120 °C, Iso 10 min, step 2: Ramp 10 °C/min, 120 to 900 °C, Iso 10 min under Nitrogen (a) weight sample loss (left) and buoyancy effect (dashed line, right) versus heating time. Subtraction both curves and normalization by the weight at the end of the step 1gives as a result (b) normalized weight and temperature (dashed line) versus heating time.

Table III. Comparison of the sizing content of the fibers.

Sample, n=3	Water content (%) (Step 1)	Sizing (%) (Step 2)	Total loss on ignition (%)
SF	0.02	0.12±0.01	0.14±0.01
LF	0.04	0.21±0.01	0.25±0.01

D. Mixing process

The fibers were incorporated into PP by melt mixing using a Haake Rheomix 600 (Thermo Fisher Scientific), equipped with two counter rotating roller rotors and a chamber volume of 69 cm^3. The set point temperature (*T*) was fixed at 190 °C and the chamber filling level at 62%. The blending was

divided into three steps: melting (1 min-30 rpm), incorporation (2 min-15 rpm) and mixing (10 min-50 rpm). After the mixing process, the samples were hot pressed at 190°C into disks of 1, 2 and 3 mm thickness and 25 mm diameter. The pressing protocol has been optimized in order to avoid air bubbles. It consists in increasing the pressure by steps from 0 to 250 bar. During this procedure, two gas releasing steps were performed. The total time of the molding procedure was 10 min.

E. Morphology characterization

The state of dispersion and orientation has been observed by Scanning Electron Microscopy (SEM) and optical microscopy. The observed samples were collected after the internal mixer process (IM), hot pressing step (HP) and rheometer loading. IM samples were molded by using a spatula into a flat shape just after the Haake was opened. SEM observations have been performed by means of a Quanta 250 SEM under high vacuum, an acceleration voltage of 10 kV with an Electron Backscatter Diffraction (EBSD) detector. Prior to observations, either flat or disklike samples were cryocut and metallized by using a BalTec MED 020 Coating System. Sputter coating was applied under 35 mA and a 10 nm layer copper was deposited. A quartz layer device was used for measuring the layer thickness.

Optical stereomicroscope (Leica M205 A) was used to quantify the particle size distribution in transmission mode (fibers deposited in between two glass plates). Also, it was used to observe the state of dispersion and orientation of low filled composites (5 vol%).

F. Dynamic rheology

The rheological measurements were performed in dynamic mode (small amplitude oscillatory shear) on a Discovery Hybrid Rheometer DHR, TA instruments stress controlled rheometer. All measurements were performed at 190 °C under nitrogen atmosphere, using a parallel plate geometry (diameter=25 mm). Different gaps were used to evaluate such effect on the results; it ranges between 700 and 2600 μm. The linear viscoelastic deformation was carefully determined for each fresh sample. A time sweep experiment showed that the samples were stable over time. Oscillatory strain sweeps were performed at a fixed frequency of 1 rad/s, from 3×10^{-6} to 6×10^{0} of strain. Frequency sweep experiments were performed by varying ω from 4×10^{2} to 10^{-2} $rads^{-1}$ at fixed strain. From an experimental point of view, the errors on the measurements of the complex shear modulus are lower than 10%.

III. Results and Discussion

A. Analysis of characteristics dimensions

Light scattering (LS) results are shown in Fig. 5. As it can be seen, SF presents a broader distribution with three different populations reflected by two maximum points and a shoulder (rather than a third maximum). We named these populations as fragments, short and long fibers. LF distribution is represented by a curve presenting a maximum and a shoulder: short and long population of fibers. It does not show any evidence of fragment population. LF presents a larger population of fibers compared to SF grade. These observations confirm the hypothesis of a more pronounced fragment population of SF due to the second milling process (see Fig. 1).

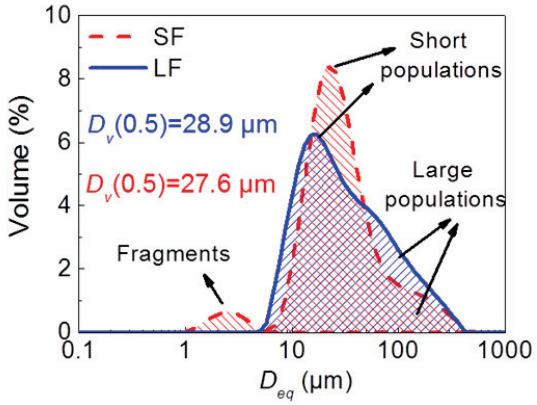


Fig. 5. Particle size distribution for SF and LF performed by light scattering by using a Master sizer 2000 device under the following conditions: dry method, 2 bars, particle Refractive Index (RI): 1.520, n=5.

Image Analysis (IA) results are depicted in Fig. 6. Fig. 6(a) shows the histogram and the cumulative probability of the total weight number distribution. Similar trends were found. First, both grades display a similar distribution. Second, LF reveals again a larger population of fibers in the range of D_{eq}>20 µm compared to SF. However, the median diameter by number D_n(0.5) is much lower compared to light scattering measurements. Thus, the crucial question becomes: What distribution represents in a better way the samples? In fact, to answer this question the physics of the system need to be considered. In this study, the volume occupied by the fiber is essential to describe the flow properties. Thus, the median diameter by volume D_v(0.5) may show us more where the volume of the system lies, being more representative in our case. For this reason, number weighted distribution (q_0) obtained by image analysis was transformed to volume weighted distribution (Q_3) and will be compared to LS results.

Fig. 6(b) presents the results obtained from the "$q_0 \rightarrow Q_3$ transformation". This transformation has been explained in detail by [42]. Thus from Fig. 6, it can be evidenced that, the equivalent diameters based on the number distribution shift to higher values on the volume distribution. This is expected because the majority of the total volume comes from the bigger particles. So, D_v(0.5) is estimated to be close

to~25µm for both samples, which is not that far from the LS results. It must be added that, due to cut off at a few µm of the measurable size by IA, it is not possible to characterize the fragments of the SF grade by this method. Fig. 7 compares the cumulative volume obtained by the two methods. From this, two interesting aspects can be noted. First, the $D_v(0.5)$ perfectly matches for both methods, hence light scattering results are validated by the image analysis method. Second, as expected, LS results depict broader distributions due to random orientations that particles may adopt on the measure unit. However, there is no shift to lower values contrary to what has been shown in literature [26].

Table IV compiles all the information and gives the estimated lengths and aspect ratio of each grade. Therefore, a complete description of the PSD was conducted and light scattering analysis was validated as a good approximation to estimate fiber lengths. Thus, light scattering results were used as the reference size in this work for two reasons. First, their $D_v(0.5)$ gives us a more discriminating value between both populations. Second, this method takes into account the whole population of fibers, while the image analysis represents a finite number of objects within the population. This is a very interesting result, which places light scattering as one the most effective method to quantify PSD, even for particles with a relative high aspect ratio ($P \approx 10$).

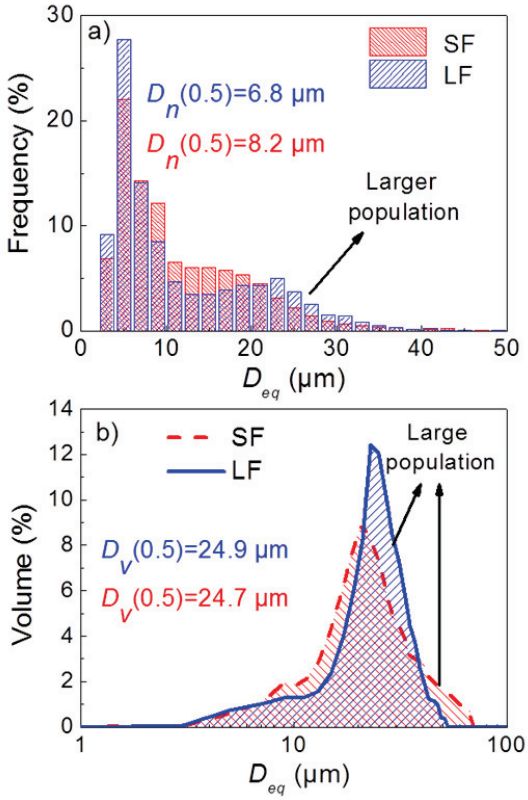


Fig. 6.Histograms of (a) total number-weighted distribution (fibers and fragments) and (b) total volume-weighted distribution for Short glass Fibers (SF) and Long glass Fibers (LF).

To conclude, both methods present similar results for both types of fibers. However, small differences in the distributions can be pointed out. LS results showed the presence of a fragment population in SF, while a large population of fibers either in LS or IA was evidenced for LF.

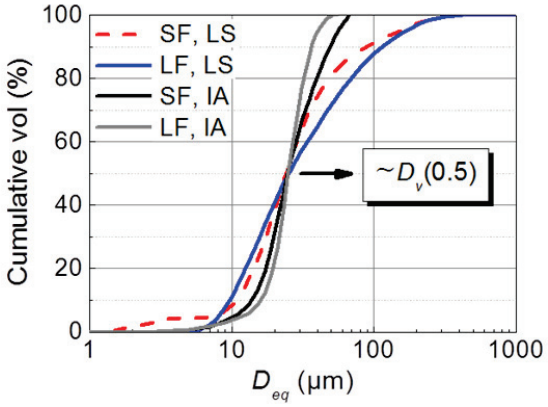


Fig. 7. Comparison between volume-weighted size distributions (cumulative curves) obtained by two different methods: Light Scattering (LS) and Image Analysis (IA).

Table IV. Sum up of particle size distribution obtained by two different methods: light scattering and image analysis. First column gives SF data (in gray) and second column presents LF results.

Method	**Distribution**	**D(0.1) (µm)**		**D(0.5) (µm)**		**D(0.9) (µm)**		**Equivalent Length[(1)] (µm)**		**Aspect ratio p=L/D**	
LS	*Volume*	12.4	11.1	27.6	28.9	102.2	131.0	97	112	8.1	9.3
IA	*Number*	3.3	3.1	8.2	6.8	21.4	23.8	3	1	0.3	0.1
IA	*Volume*	13.6	15.91	24.7	24.9	49.0	36.4	70	71	5.8	5.9

[(1)] $L = 4V_{eq(sphere)}/(\pi D^2)$, $D \sim 12\ \mu m$

B. Morphology, dispersion and orientation in composites

Fig. 8 displays the morphology of different composites after the mixing by internal mixer and after the hot pressing process for samples filled with SF. Fig. 8(a) and Fig. 8(b) show a sample filled with 5 vol% after hot pressing (HP) in both radial and normal direction of the pressed disk. As it can be seen, hot press induces alignment and thus a planar random orientation is evidenced. It is worth noting that fibers are well dispersed and distributed throughout the matrix phase. Next to these images, Figs. 8(c-f) shows on the contrary a concentrated composite with 45 vol% of fillers. The SEM images represent both steps of the process IM (c-d) and HP (e-f). From this, it can be stated that hot press induces strong alignment, while internal mixer shows both oriented and random orientation. Therefore, it becomes necessary to evaluate the effect of the process history on the rheological properties.

Fig. 9 shows the shear moduli as a function of the strain for pressed and not pressed samples with 25 and 45 vol%. First, no significant effect of gap on the non-linear viscoelastic behavior is observed at

high strain which confirms that there is no wall slip phenomenon at the plateau surface. Second, such preliminary experiments showed no influence of the process history on the flow properties. Thus, loading on the rheometer seems to be the preponderant factor on orientation. This step definitely induces planar orientation as shown by SEM image in Fig. 9(b). Third, the rheological measure is not perturbed by the gap even when this is close to the average length of the fibers (700 µm). It seems very likely that, as particles are oriented parallel to the disk surfaces, it is the diameter and not the length that has to be considered when relating fiber size to the gap [30]. Finally, for practical purposes, pressed samples were preferred to perform this study.

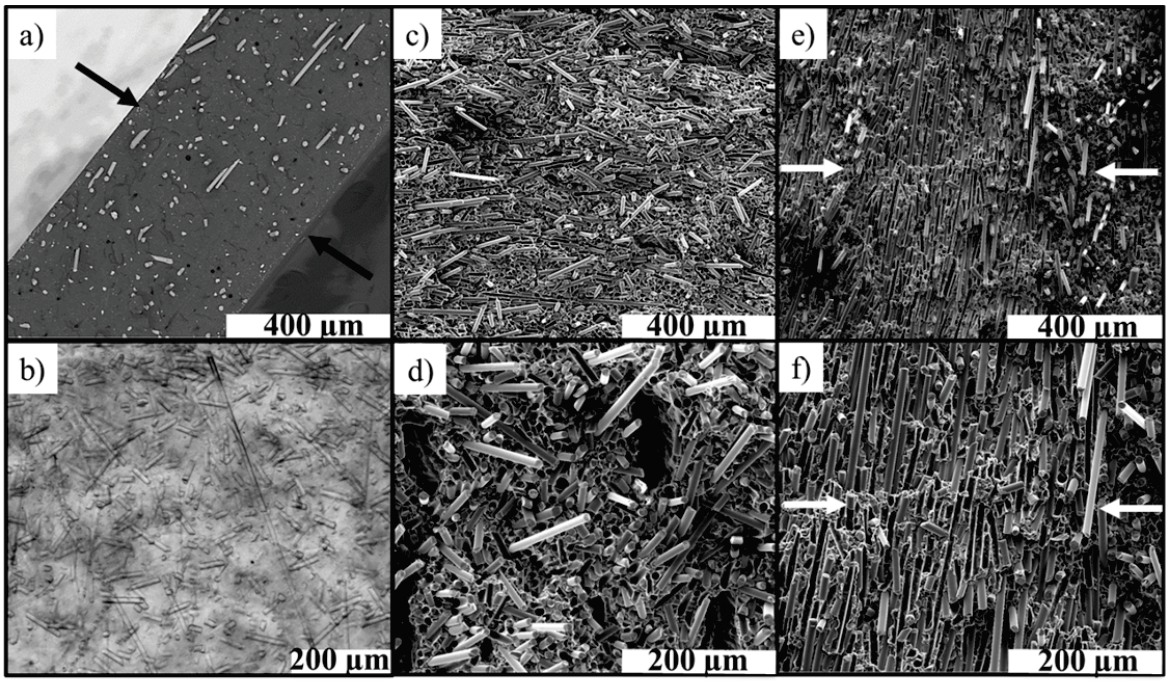


Fig. 8. SEM and optical images for SF filled polypropylene after internal mixer (IM) and hot pressing (HP). (a-b) SEM and optical picture of 5 vol%, after HP (c-d) 45 vol%, after IM (e-f) 45 vol%, after HP. Arrows indicate the direction in which the sample was pressed.

C. Dynamic rheological properties: effect on fiber concentration

As already discussed in the introduction, the concentration regime defines the flow properties of fibers suspensions. The characteristic sizes were $D \sim 12$ µm (for both types) and $L \sim 97$ and 112 for SF and LF, respectively. Hence, the onsets of concentration were calculated and are shown in Table V. It is thus expected that, the transition to concentrated regimes occurs at lower concentration for LF fibers compared to SF.

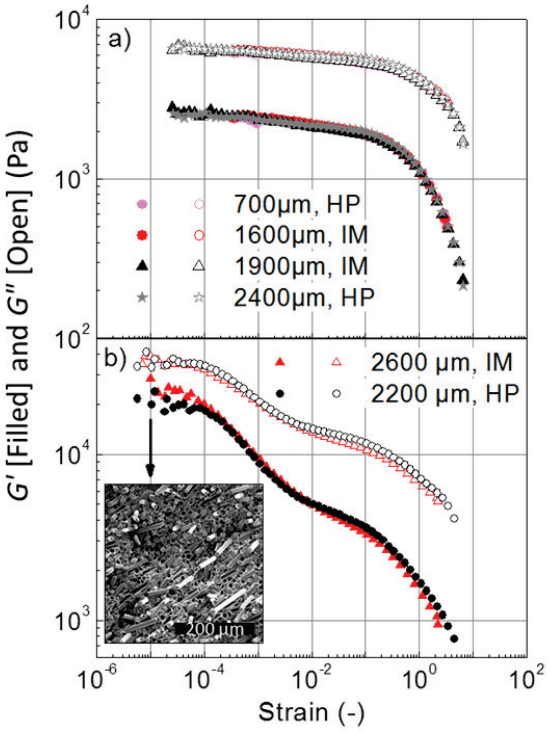


Fig. 9. Strain sweep experiments for SF composites filled with (a) 25 vol% and (b) 45 vol% at different gaps after internal mixer (IM) and hot pressing (HP). SEM image shows a sample obtained after rheometer loading. Arrows indicate the direction in which the sample was pressed during the loading.

Table V. Concentration regimes for SF and LF based on Doi-Edwards and Onsager's theories [25,42].

Aspect ratio (p)	**Dilute below $\phi < (1/p)^2$**	**Transition from semi-dilute to isotropic concentrated at $\phi < 1/p$**	**Maximum concentration of isotropic suspensions at $\phi < 3.3/p$**
8.1	0.02	0.12	0.41
9.3	0.01	0.11	0.35

1. Strain sweep experiments

Fig. 10 shows the strain sweep experiments performed for the both types of composites. As it can be observed, a very large range of filler levels was studied, covering all the regime of concentrations. A nonlinear viscoelastic behavior has been clearly found for these short fiber filled polymers. The storage modulus (*G'*) decreased markedly with increasing the strain amplitude. The linear viscoelastic domain decreases by increasing the fiber concentration, as usually shown in the literature of filled polymers [5,48,49]. Another interesting result concerns the change in the shape of the curve with increasing the filler level. A strain softening behavior is noticed by the presence of a pseudo plateau at intermediate strains for samples with filler levels $\phi \geq 0.25$. Upon continue increasing the strain amplitude, *G'* shows a shoulder and a final decrease at high strains. Such phenomenon has been already shown in the literature for SGF (ϕ=0.15) suspended in PE/PA6 (70/15 v/v) polymer blend [50].

Actually, the strain softening in SGF filled polymer melts arise from fiber alignment [38] together with the breakdown of fiber network and molecular disentanglement of the matrix [51,52]. However, chain disentanglement of the polymer chains are expected at much higher deformations.

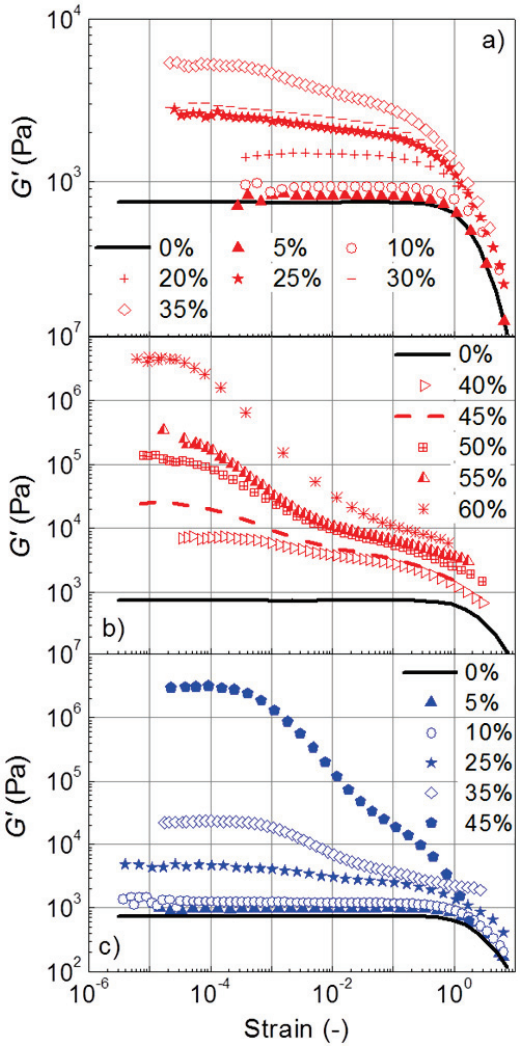


Fig. 10. Strain sweep experiments for samples filled with SF (a) from 0 to 35 vol% (b) from 40 to 60 vol% and LF (c) filled with 0 to 45 vol%, ω=1 rad/s, T= 190 °C.

2. *Shear moduli and viscosity*

Fig. 11 shows the rheological behavior of both types of composites. Fig. 11(a-d) display the moduli, the absolute value of the complex viscosity $|\eta^*|$ and the relative viscosity normalized by the matrix contribution, $|\eta_r^*(\omega)| = |\eta^*|/|\eta_{pp}^*(\omega)|$, as a function of the frequency for SF-based composites. Fig. 11(e-h) show the respective LF results. Common observed trends and other new interesting observations can be drawn from these results. First and as expected, the addition of glass fibers increases all

the dynamic material functions (*G'*, *G''*, $|\eta^*|$). However, LF presents a higher increase of such properties compared to SF at constant fiber content.

Second, the rheological behavior does not seem affected below $\phi \leq 0.1$ for both composites. Above $\phi = 0.1$, *G'* shifts to higher values. This onset of concentration corresponds to the transition between semi-dilute to concentrated isotropic regimes (Table V). Beyond this point, fibers start to get in contact and thus, particle interactions become dominant at low ω.

This leads us to the third observation. Thus, particle interactions start to appear in the concentrated regime. The latter is evidenced by the increase of the *G'* slope with increasing ϕ. This is in fact the rheological signature of the consolidation of the fiber network. On the one hand, SF-based composites continue keeping the same shape of *G'* and $|\eta_r^*(\omega)|$ until $\phi = 0.3$ as observed by [9]. On the other hand, LF-based composites start to show a network behavior at low frequencies. The onset of such fiber network arises at $\phi = 0.25$ for LF, while only up to $\phi = 0.45$ for SF, indicating that higher values of *p* promote the creation of the fiber network. Such phenomenon can be clearly evidenced in Fig. 11(d) and 11(h), in which the zero shear viscosity starts to diverge.

Further to this fiber contents, *G'* slope continue increasing until it does no longer depend on the frequency, representing a completely solidlike behavior. As expected, such behavior arises at lower concentration for LF (ϕ=0.45) than for SF-based composites (ϕ=0.6). This means that higher *p* hinders the flowability of the system.

The rheological behavior of both types of composites is very different; despite the particle size distribution shows a lot of similarity (see Fig. 7). Thus, in order to decoupling sizing effects from PSD, the fibers were burnt off (1h at 500 °C, air) and then compounded to the PP matrix, under the same conditions. Filler levels of ϕ=0.35 and 0.45 were chosen to perform the new composites.

Fig. 12 displays $|\eta^*|$ for composites filled with 35 and 45 vol% compared to the bare fibers (B-). It is clear that bare fibers composites results in lower viscosity values in all the range of frequency. However this viscosity decrease remains moderate. Moreover, it is clear that even after having removed the sizing, the behaviors for SF and LF remain different. These results suggest that the sizing is not the origin of the strong difference in the flow behavior between both grades. Additionally, it proves that burning the fibers decreases interparticle interactions, leading to a weaker fiber network and thus lower viscosities are evidenced.

Another interesting result seen in Fig. 11(b) and 11(f) is that, the crossover between the *G'* and *G''* shifts to lower frequencies with increasing the amount of fibers. Such crossover point corresponds to the characteristic elastic time of the composite, defined as [53]:

$$\lambda = \frac{G'}{G''\omega} = \frac{1}{\tan(\delta)\omega} \tag{1}$$

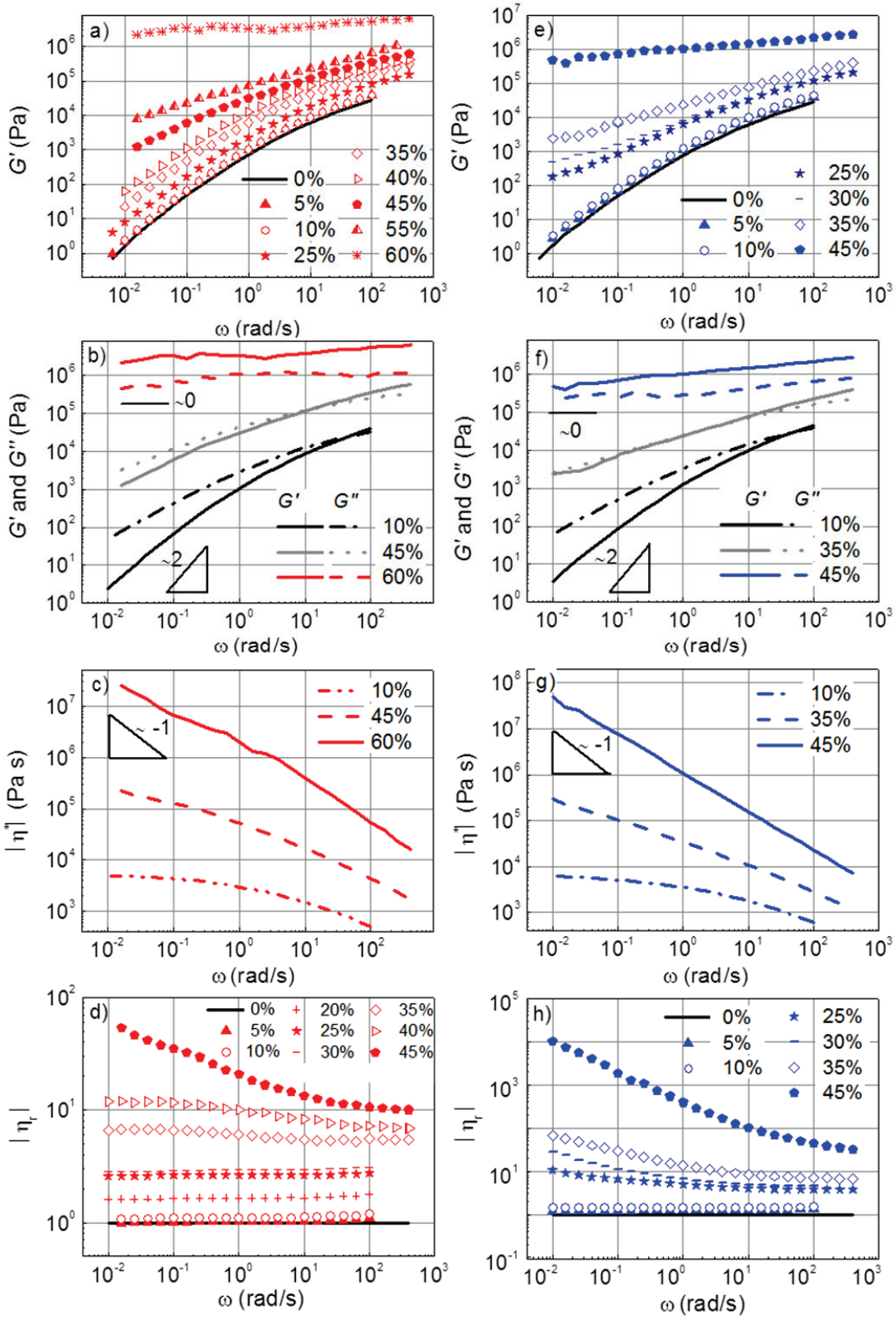


Fig. 11. Dynamic behavior of (a-d) SF and (e-h) LF under oscillatory frequency sweeps. Figures (d) and (h) show the relative viscosity defined as $|\eta_r| = |\eta^*|/|\eta^*_{pp}(\omega)|$ *as a function of the frequency.*

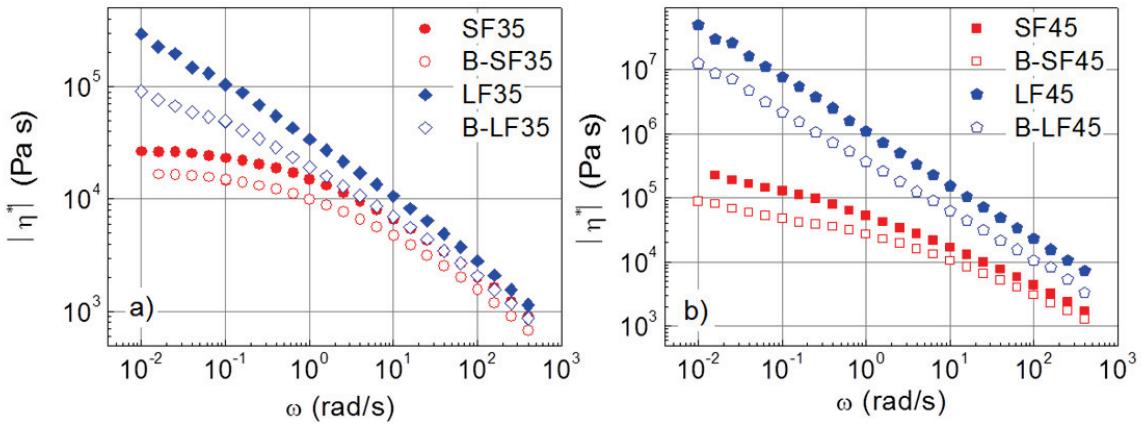


Fig. 12. Comparison between bare fibers and sized fibers. Complex viscosity as a function of frequency for SF and LF-based composites with 35 and 45 vol%. Bare fibers are named by B-SF and B-LF.

Fig. 13 shows the characteristic elastic time as a function of ϕ. The more the fiber content is, the higher is the characteristic elastic time of the mixture. Krieger and Dougherty model was used to fit the data, giving a good approximation. This means that, the crossover frequency decreases with increasing the fiber content until the completely solidlike behavior. In that point, *G'* and *G''* become parallel and the crossover does not occur at the studied range of frequencies. Thus, the critical concentration ϕ_c^*, makes allusion to the transition from liquidlike to solidlike behavior.

Fig. 14 displays the zero shear viscosity of the composites, $\eta_{0,c}$, normalized by the zero shear viscosity of the matrix, $\eta_{0,pp}$. The $\eta_{0,c}$ was estimated by the Carreau-Yasuda model. It can be clearly seen that, $\eta_{r,0}$ increases as a function of ϕ and diverges to infinity when the fibers form a network. Such fiber content corresponds to the mechanical percolation threshold, ϕ_c. Above ϕ_c, fiber interactions totally arrest the flow at very low deformations, indicating that $\eta_{0,c}$ does not exist. The Krieger and Dougherty model perfectly matches the experimental data and gives us an indication of ϕ_c and of the intrinsic viscosity $[\eta]$. On the one hand, ϕ_c was found to be much lower for LF ($\phi_{c,LF}$=0.3) than for SF-based composites ($\phi_{c,SF}$=0.45). Moreover, $[\eta]$ was found to be larger for LF ($[\eta]$=5.5) than for SF-filled composites ($[\eta]$=2.9). This parameter is related to the aspect ratio of the filler. Indeed, for the ideal rigid sphere case the intrinsic viscosity is $[\eta]$=2.5. Based on this value, the greater is $[\eta]$, the higher is the average aspect ratio of the filler. This is in good agreement with the $[\eta]$ values found for SF and LF and their respective aspect ratios p_{SF} =8.1, p_{LF} =9.3.

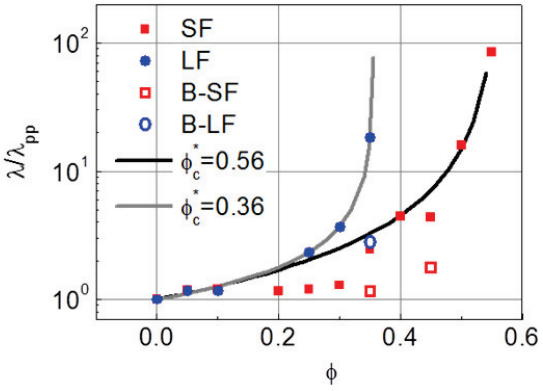


Fig. 13. Characteristic elastic time as a function of the filler level, λ_{pp}=0.017 (s).

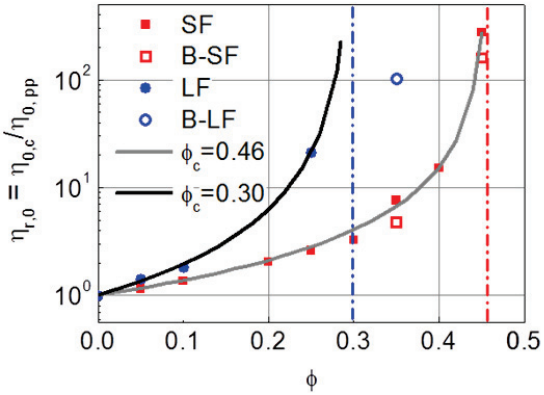


Fig. 14. Relative viscosity ($\eta_{0,r} = \eta_{0,c}/\eta_{0,pp}$) as a function of the filler concentration. The data is fitted by Krieger-Dougherty model.

Fig. 13 and Fig. 14 also include the bare filled composites data represented by unfilled symbols. When burning the fibers, lower characteristic elastic times and lower $\eta_{0,r}$ values were found. B-LF composite filled with 45 vol% presents a completely solidlike behavior, thus, in the same way as LF45% composite, any value of λ is displayed in Fig. 13. Regarding the relative viscosities, B-LF35% still shows a zero shear viscosity $\eta_{0,c}$, while the LF35% does not. The latter is slightly observed in Fig. 12(a). It seems clear that ϕ_c is delayed to higher values for bare fiber composites. This is in agreement with the decrement of fiber-fiber interactions.

Besides all this, the transition from concentrated isotropic to nematic regimes was estimated to be ϕ_{SF}=0.41 and ϕ_{LF}=0.35 (see Table V), fairly close to the calculated percolation thresholds. It seems possible that, above these concentrations, the fibers can no longer be packed isotropically. Hence, they might be forced to change its random planar orientation in order to accept a new fiber in its structure.

V. Conclusions

The objective of the current research is to get a better understanding of the effects of fiber size distribution and fiber content on the dynamic flow properties. This work confirms common observations and shows some other interesting new results. To achieve these objectives, particle size characterization was evaluated and compared by two methods. Light scattering results were compared to image analysis results, giving very good accordance between both techniques. This result places light scattering as the most attractive method to measure particle size distribution due to its versatility, fast acquisition of data, higher sensibility for small particles and highly reproducible results. This is in contrast to what has been shown in literature for systems with relative high p.

We have reported a rather complete rheological dynamic characterization of two commercial glass fiber reinforced polypropylene. Shear moduli and $|\eta^*|$ were found to increase with increasing both filler level and average aspect ratio. The linear viscoelastic domain decreases with increasing the filler content. The flow behavior was determined by the fiber content and thus, the transition from the semi-dilute to the concentrated regime was clearly evidenced by G', $|\eta^*|$ and $|\eta_r(\omega)|$ plots. It has been observed that, the probability that particles form a network depends on the interparticle distance, the aspect ratio and the particle interactions. The onset of semi-dilute to concentrated isotropic regimes corresponds to the shift to higher values of *G'* and $|\eta_r^*(\omega)|$, $\phi \sim 0.1$. The percolation threshold values (ϕ_c=0.46 for SF, ϕ_c=0.3 for LF) were found to be close to the onset of concentrated isotropic to nematic regimes (ϕ=0.41 for SF, ϕ=0.35 for LF). As a side result, it was shown that removing the sizing of the fibers leads to decrease the fiber-fiber interactions. Finally, it can be concluded that, the strong different flow behavior between both types of composites might be in part due to small variations in the distribution of the fibers. Indeed, LF presented a small amount of very large fibers that govern the rheological properties of the composite. However, this cannot completely explain such a strong difference in the rheological behavior.

References

[1] P. Brøndsted, H. Lilholt, A. Lystrup, Composite Materials for Wind Power Turbine Blades, Annu. Rev. Mater. Res. 35 (2005) 505–538.

[2] T. Sathishkumar, S. Satheeshkumar, J. Naveen, Glass fiber-reinforced polymer composites – a review, J. Reinf. Plast. Compos. 33 (2014) 1258–1275.

[3] S. Ranganathan, S.G. Advani, Fiber–fiber interactions in homogeneous flows of nondilute suspensions, J. Rheol. 35 (1991) 1499–1522.

[4] T. Malek, J. HASPEL, U. Dajek, R. Zimnol, G. Margraf, Lightweight component of hybrid, US8383242 B2, 2013.

[5] M.M. Rueda, M.-C. Auscher, R. Fulchiron, T. Périé, G. Martin, P. Sonntag, P. Cassagnau, Rheology and Applications of Highly Filled Polymers: A review of current understanding, Prog. Polym. Sci. 66 (2017) 22–53.

[6] T. Kitano, T. Kataoka, Y. Nagatsuka, Dynamic flow properties of vinylon fibre and glass fiber reinforced polyethylene melts, Rheol. Acta. 23 (1984) 408–416.

[7] J.-M. Charrier, J.-M. Rieger, Flow of short glass fibre-filled polymer melts, Fibre Sci. Technol. 7 (1974) 161–172.

[8] R.O. Maschmeyer, C.T. Hill, The Rheology of Concentrated Suspensions of Fibers: I. Review of the Literature, in: R.D. Deanin, N.R. Schott (Eds.), Fill. Reinf. Plast., AMERICAN CHEMICAL SOCIETY, WASHINGTON, D. C., 1974: pp. 95–105.

[9] R. Guo, J. Azaiez, C. Bellehumeur, Rheology of fiber filled polymer melts: Role of fiber-fiber interactions and polymer-fiber coupling, Polym. Eng. Sci. 45 (2005) 385–399.

[10] A.S. Doumbia, M. Castro, D. Jouannet, A. Kervoëlen, T. Falher, L. Cauret, A. Bourmaud, Flax/polypropylene composites for lightened structures: Multiscale analysis of process and fibre parameters, Mater. Des. 87 (2015) 331–341.

[11] S.K. De, J.R. White, Short Fibre-Polymer Composites, Woodhead Publishing, 1996.

[12] M. Kráčalík, L. Pospíšil, M. Šlouf, J. Mikešová, A. Sikora, J. Šimoník, I. Fortelný, Effect of glass fibers on rheology, thermal and mechanical properties of recycled PET, Polym. Compos. 29 (2008) 915–921.

[13] N.-J. Lee, J. Jang, The effect of fibre content on the mechanical properties of glass fibre mat/polypropylene composites, Compos. Part Appl. Sci. Manuf. 30 (1999) 815–822.

[14] D.M. Laura, H. Keskkula, J.W. Barlow, D.R. Paul, Effect of glass fiber surface chemistry on the mechanical properties of glass fiber reinforced, rubber-toughened nylon 6, Polymer. 43 (2002) 4673–4687.

[15] S. A. Ramazani, A. Ait-Kadi, M. Grmela, Rheology of fiber suspensions in viscoelastic media: Experiments and model predictions, J. Rheol. 45 (2001) 945–962.

[16] A. m. a. Huq, J. Azaiez, Effects of length distribution on the steady shear viscosity of semiconcentrated polymer-fiber suspensions, Polym. Eng. Sci. 45 (2005) 1357–1368.

[17] A.P.R. Eberle, D.G. Baird, P. Wapperom, Rheology of Non-Newtonian Fluids Containing Glass Fibers: A Review of Experimental Literature, Ind. Eng. Chem. Res. 47 (2008) 3470–3488.

[18] S.Y. Fu, B. Lauke, E. Mäder, X. Hu, C.Y. Yue, Fracture resistance of short-glass-fiber-reinforced and short-carbon-fiber-reinforced polypropylene under Charpy impact load and its dependence on processing, J. Mater. Process. Technol. 89–90 (1999) 501–507.

[19] R. von Turkovich, L. Erwin, Fiber fracture in reinforced thermoplastic processing, Polym. Eng. Sci. 23 (1983) 743–749.
[20] D.M. Bigg, Effect of compounding on the properties of short fiber reinforced injection moldable thermoplastic composites, Polym. Compos. 6 (1985) 20–28.
[21] A. Hassan, R. Yahya, A.H. Yahaya, A.R.M. Tahir, P.R. Hornsby, Tensile, Impact and Fiber Length Properties of Injection-Molded Short and Long Glass Fiber-Reinforced Polyamide 6,6 Composites, J. Reinf. Plast. Compos. 23 (2004) 969–986.
[22] J.E. O'Connor, Short-Fiber-Reinforced Elastomer Composites, Rubber Chem. Technol. 50 (1977) 945–958.
[23] M.S. Huda, L.T. Drzal, A.K. Mohanty, M. Misra, Chopped glass and recycled newspaper as reinforcement fibers in injection molded poly(lactic acid) (PLA) composites: A comparative study, Compos. Sci. Technol. 66 (2006) 1813–1824.
[24] F. Chinesta, G. Ausias, Rheology of Non-spherical Particle Suspensions, Elsevier, 2015.
[25] R.G. Larson, The Structure and Rheology of Complex Fluids, New York: OUP USA, 1999.
[26] W. Pabst, C. Berthold, E. Gregorová, Size and shape characterization of oblate and prolate particles, J. Eur. Ceram. Soc. 27 (2007) 1759–1762.
[27] C. Mobuchon, P.J. Carreau, M.-C. Heuzey, M. Sepehr, G. Ausias, Shear and extensional properties of short glass fiber reinforced polypropylene, Polym. Compos. 26 (2005) 247–264.
[28] R.O. Maschmeyer, C.T. Hill, Rheology of Concentrated Suspensions of Fibers in Tube Flow. III. Suspensions with the Same Fiber Length Distribution, Trans. Soc. Rheol. 21 (1977) 195–206.
[29] J.P. Greene, J.O. Wilkes, Steady-State and dynamic properties of concentrated fiber-filled thermoplastics, Polym. Eng. Sci. 35 (1995) 1670–1681.
[30] A. Abdennadher, M. Vincent, T. Budtova, Rheological properties of molten flax- and Tencel®-polypropylene composites: Influence of fiber morphology and concentration, J. Rheol. 60 (2016) 191–201.
[31] M. Keshtkar, M.C. Heuzey, P.J. Carreau, Rheological behavior of fiber-filled model suspensions: Effect of fiber flexibility, J. Rheol. 53 (2009) 631–650.
[32] N. Agarwal, Transient shear flow rheology of concentrated long glass fiber suspensions in a sliding plate rheometer, Citeseer, 2009. http://citeseerx.ist.psu.edu/viewdoc/download?doi=10.1.1.512.825&rep=rep1&type=pdf (accessed August 27, 2015).
[33] S. Goto, H. Nagazono, H. Kato, The flow behavior of fiber suspensions in Newtonian fluids and polymer solutions., Rheol. Acta. 25 (1986) 246–256.
[34] J. Thomasset, P.J. Carreau, B. Sanschagrin, G. Ausias, Rheological properties of long glass fiber filled polypropylene, J. Non-Newton. Fluid Mech. 125 (2005) 25–34.
[35] N.J. Mills, The rheology of filled polymers, J. Appl. Polym. Sci. 15 (1971) 2791–2805.
[36] L.A. Mondy, T.G. Morrison, A.L. Graham, R.L. Powell, Measurements of the viscosities of suspensions of oriented rods using falling ball rheometry, Int. J. Multiph. Flow. 16 (1990) 651–662.
[37] U. Saeed, K. Hussain, G. Rizvi, HDPE reinforced with glass fibers: Rheology, tensile properties, stress relaxation, and orientation of fibers, Polym. Compos. 35 (2014) 2159–2169.
[38] J.K. Kim, J.H. Song, Rheological properties and fiber orientations of short fiber-reinforced plastics, J. Rheol. 41 (1997) 1061–1085.
[39] Mastersizer 2000 user manual (English), (2017). http://www.malvern.com/en/support/resource-center/user-manuals/MAN0384EN.aspx (accessed April 21, 2017).

[40] N. Gabas, N. Hiquily, C. Laguérie, Response of Laser Diffraction Particle Sizer to Anisometric Particles, Part. Part. Syst. Charact. 11 (1994) 121–126.
[41] C. Berthold, R. Klein, J. Lühmann, K.G. Nickel, Characterization of Fibres and Fibre Collectives with Common Laser Diffractometers, Part. Part. Syst. Charact. 17 (2000) 113–116.
[42] W. Pabst, C. Berthold, E. Gregorová, Size and shape characterization of polydisperse short-fiber systems, J. Eur. Ceram. Soc. 26 (2006) 1121–1130.
[43] Energy Efficient Building Products & Fiberglass Composites | Owens Corning TM, (2017). https://www.owenscorning.com/ (accessed April 21, 2017).
[44] H.N. Petersen, Y. Kusano, P. Brøndsted, K. Almdal, Preliminary characterization of glass fiber sizing, in: 34th Risø Int. Symp. Mater. Sci., 2013: pp. 333–340.
[45] R.L. Gorowara, W.E. Kosik, S.H. McKnight, R.L. McCullough, Molecular characterization of glass fiber surface coatings for thermosetting polymer matrix/glass fiber composites, Compos. Part Appl. Sci. Manuf. 32 (2001) 323–329.
[46] R. Mueller, H.K. Kammler, K. Wegner, S.E. Pratsinis, OH Surface Density of SiO2 and TiO2 by Thermogravimetric Analysis, Langmuir. 19 (2003) 160–165.
[47] Buoyancy Phenomenon in TGA Systems, Thermal Analysis and Surface Solutions GmbH, (2017). http://www.thass.org (accessed January 9, 2017).
[48] H.A. Barnes, Review of the rheology of filled viscoelastic systems, Rheology Reviews, The British Society of Rheology, Br. Soc. Rheol. (2003) 49.
[49] T. Kaully, A. Siegmann, D. Shacham, Rheology of highly filled natural CaCO3 composites. I. Effects of solid loading and particle size distribution on capillary rheometry, Polym. Compos. 28 (2007) 512–523.
[50] P.G. Malchev, B. Norder, S.J. Picken, A.D. Gotsis, The strain dependence of the dynamic moduli of short fiber reinforced thermoplastic blends, J. Rheol. 51 (2007) 235–260.
[51] L. Zhao, H. Yang, Y. Song, Y. Zhou, G. Hu, Q. Zheng, Non-linear viscoelasticity of vapor grown carbon nanofiber/polystyrene composites, J. Mater. Sci. 46 (2011) 2495–2502.
[52] G.S. Shibulal, K. Naskar, Scrutinizing the influence of strain-induced fiber orientation on the melt rheological behavior of short aramid fiber/thermoplastic elastomer composite using rubber process analyzer, J. Appl. Polym. Sci. 128 (2013) 4151–4163.
[53] P.J. Carreau, D.D. Kee, R.P. Chhabra, Rheology of Polymeric Systems: Principles and Applications, Hanser Publishers, 1997.

Part III

Additional Results N°1

Extrusion process: short-glass fibers

This additional result section aims to show how the particle size distribution and thus the rheological properties were affected by the process conditions in an extruder.

I. Materials and Methods

The materials used in this section correspond to the systems Short glass Fibers SF/PP and Long glass Fibers LF/PP filled with 30 vol% by means of an extruder (Leistritz ZSE-18). The mixing protocol has been explained in detail in Chapter 2, Section 2.2.2. Two screw profiles were used: soft (profile A) and hard (profile B) screw profile as shown in Chapter 2, Fig 2.6. Thus, the raw materials were blended in the extruder, granulated and then shaped into rheometer disks by injection molding, Babyplast 610P, Alecop at 190 °C. Rotational and capillary rheometers were used to characterize the mixtures. The particle size distribution was characterized before and after mixing by light scattering. The PP was burnt in three stages: 1) 350 °C, 45 min, under N_2, 2) 450 °C, 15 min, under N_2, 3) 450 °C, 10 min, under air. Then, the particles were collected and measured.

II. Results and discussion

Fig. 1 shows the dynamic rheological behavior for the extruded composites under different screw speeds (*N*=200, 400, 600, 800 rpm) at 3 kg/h for the hard screw profile (profile B). Fig. 1(a) presents the results for SF30vol%, while Fig. 1(b) presents the behavior of LF30vol%. These results are in total agreement with the previous chapter. SF30vol% presents a Newtonian plateau, while LF30vol% display a divergence on the zero shear viscosity η_0. In other words, LF30vol% composite attains the percolation threshold, while SF30vol% still flows at low frequencies. The screw speed (*N*) slightly changes the rheological behavior; however the shape of all the curves is maintained invariant. Fig. 2 compares the η_0 and the $\left|\eta^*_{0.01rad/s}\right|$ for SF and LF-based composites for both screw profiles. It is clear that the soft profile affects to a less extent the PSD of the fibers, while the hard profile data shows a decrease of the viscosity with increasing *N*. Thus, as expected, the roughest shear conditions are evidenced for *N*=800 rpm, profile B. In addition, the mass flow rate was also evaluated (3, 5kg/h at 400 rpm), however no significant changes were found between both conditions.

Under the roughest shear conditions (*N*=800 rpm, 3 kg/h, profile 2), the shear viscosity of both composites were measured by capillary rheometry. Fig. 3 shows the shear viscosity as a function of the apparent shear rate for three different capillaries (*L*/*D*=10). Three major observations can be drawn from these results. First, wall slip phenomenon is not manifested under these conditions of shear rates. Second, no significant differences are observed between both composites. This is

principally due to the orientation of fibers in the flow direction, thus particle size distribution becomes less important in an align structure. Third, a strong fiber contribution is observed compared to the unfilled matrix.

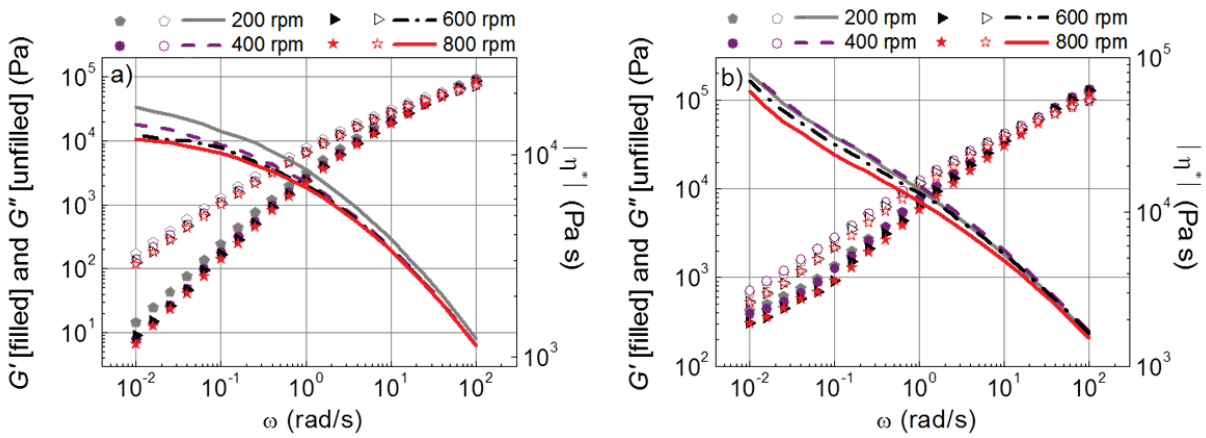


Fig. 1. Dynamic rheological behavior of samples filled with (a) SF30vol% and (b) LF30vol% for the hard screw profile (profile B).

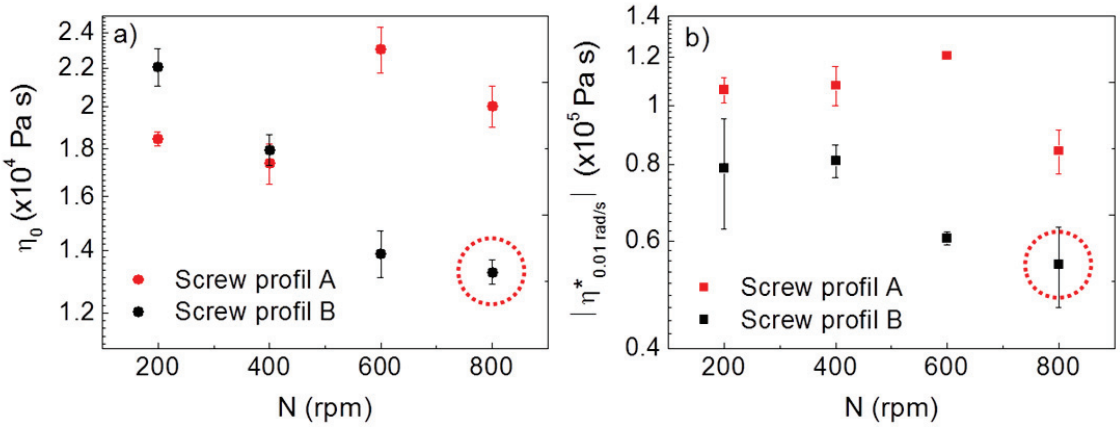


Fig. 2. (a) Zero shear viscosity for samples SF30vol% and (b) complex viscosity for LF30vol% for both soft (A) and hard (B) screw profile. Data is the average of three measurements. Circles depict the roughest shear conditions.

It is thus clear that, dynamic rheology allows the differentiation between small differences in the morphology of the filler, while capillary rheology smashes all the differences.

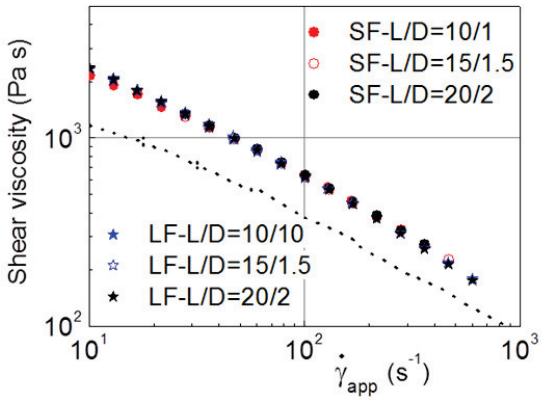


Fig. 3. Shear viscosity for samples filled with SF30vol% and LF30vol% at different L/D=10/1, 1.5/15, 2/20. Dash line represents the unfilled matrix. Operating conditions: 800 rpm, 3kg/h, 190 °C.

Moreover, the particle size distribution was measured after the capillary rheometry test. Thus, fibers had undergone the most severe shear conditions in the extruder together with the capillary measurements. Fig. 4 shows the PSD for both SF and LF before and after the process. Similar populations were found before and after processing (AP).Only a small decrease in the large population of AP-LF was noticed. Table I shows the three most common representative diameters. As it can be seen, $D_v(0.5)$ slightly decreases to lower values, while $D_v(0.9)$ is much affected for fibers collected after processing. Thus, the largest particles for the LF are cut during the extrusion process and capillary measurement.

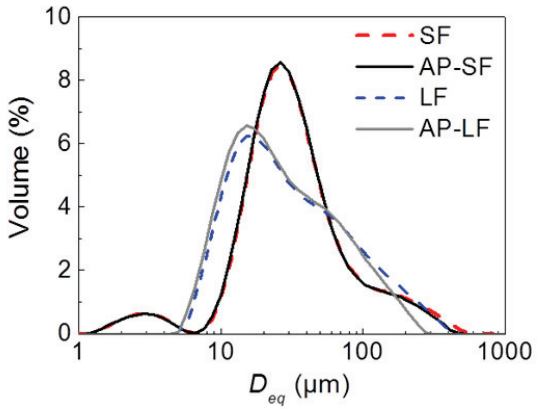


Fig. 4. Particle size distribution measured before and after processing (AP) for SF and LF grades. The results are the average of 5 measurements and were obtained by using a Master sizer 2000 device under the following conditions: dry method, 2 bars, particle Refractive Index (RI): 1.520.

Table I. Particle size distribution measured by light scattering (Master sizer 2000, 2 bars, dry method).

Sample	**$D_v(0.1)$**	**$D_v(0.5)$**	**$D_v(0.9)$**
SF	12.4	27.6	102.2
AP-SF	12.2	27.2	93.6
LF	11.1	28.9	131.0
AP-LF	10.4	26.0	101.4

To conclude, it is clear that the PSD is slightly changed by the process. During the extrusion, the highest shear conditions appear at the exit of the die ($\dot{\gamma} = 4Q/\pi r^3$), which can be estimated to be close to 230 s^{-1}. During the capillary measurement, the material is brought to flow into the die at shear rates $\leq$600 s^{-1}. Therefore, it can be expected that, the PSD was not much affected during the internal mixer mixing, as the average shear rate is$\sim$10 s^{-1} at 50 rpm (see Section 2.2.1).

Additional Results N°2

Limit of processability: Batch mixing process study

In this additional results section, we defined an original method to quantify the maximum packing fraction of solids, as well as, the limit of processability by a batch process approach. Thus, this section is an extension from the previous chapters and is situated in the non-linear regime.

I. Materials and Methods

The materials used in this section correspond on the one hand, to the systems ferrite/PP and ferrite/dispersant/PP and on the other hand, to the systems Short glass Fibers SF/PP and Long glass Fibers LF/PP. The mixing protocol has been explained in detail in Section 2.2.1. Sixty-two percent of the available volume of the mixing chamber was used. The mixing was carried-out in five steps for the ferrite/PP composites and three steps for fibers/PP composites.

II. Results and discussion

Fig. 1 shows the last value of the measured torque for composites ferrites/PP and ferrites/dispersant/PP during the mixing step. Fig. 1(a) shows the last value of torque and temperature for the composites ferrites/PP. It can be seen that, the torque and the temperature increase with increasing the filler level. The temperature set point is fixed at 190°C in the Haake device, however, self-heating is observed due to stress and friction between the components. In the same way, torque increases with increasing ϕ, indicating that more energy is required to perform the mixing process. Thus, both variables increase until reaching a maximum and then drastically drop. In this manner, two distinct zones can be identified by following the torque and the temperature variables with ϕ.

To explain this, we showed in Fig. 1(a) some pictures from the obtained mixtures. On the one hand, the composite filled with 65 vol% (hF65%) which corresponds to the maximum of torque and temperature was shown. It presented a smooth surface and a cohesive homogenous aspect. On the other hand, a sample filled with 70 vol% (hF70%) which corresponds to the data in the second zone was displayed. As it can be observed, the material is friable and its surface is constituted by multiple defects and cracks.

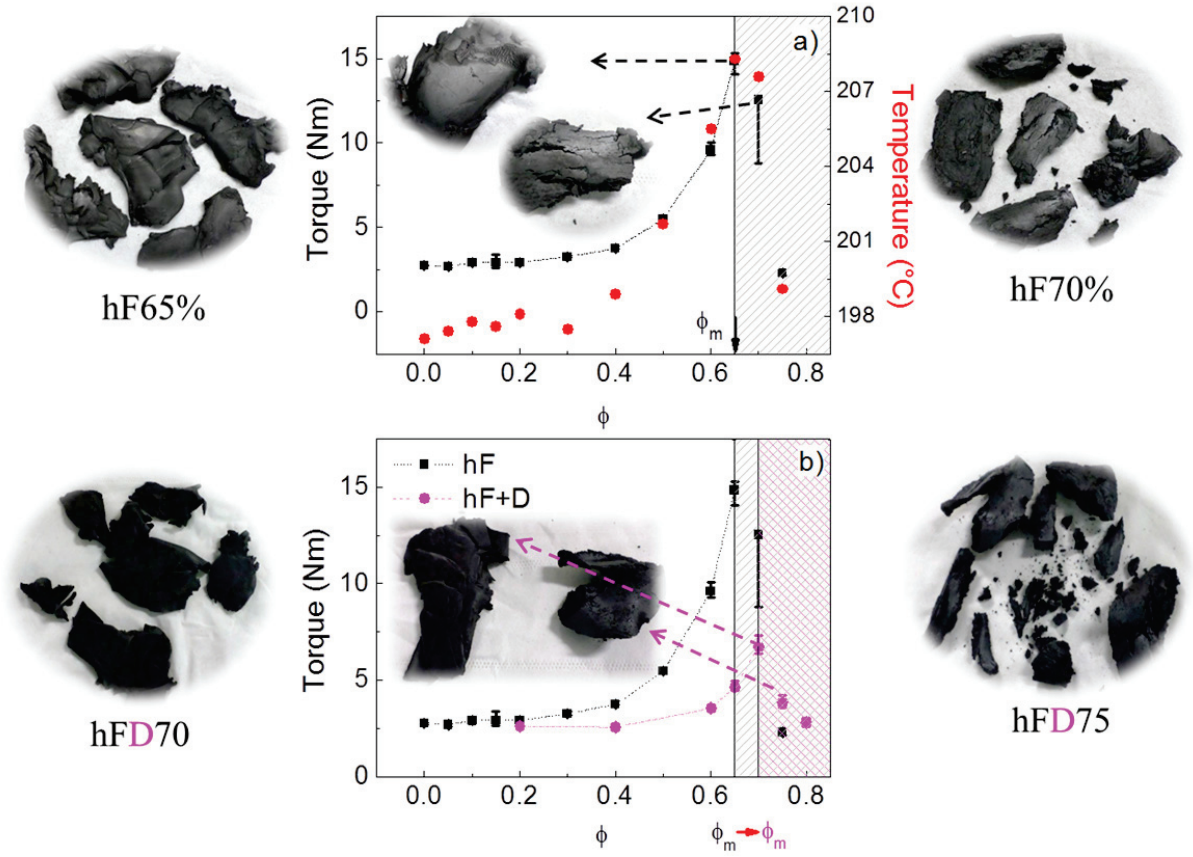


Fig. 1. (a) Last value of the measured torque and temperature for ferrites particles/PP composites and (b) comparison between both systems: ferrite/PP and ferrite/dispersant/PP. Error bars represent the minimum and the maximum value of torque during the last two minutes of the mixing. Here, H means internal mixer "Haake", F: ferrite and D: dispersant.

Therefore, the higher is the filler level, the more brittle the solid material is. The higher the filler level is, the hardest the incorporation of particles becomes. Thus, above the maximum of torque and temperature, the matrix can no longer ensure the cohesion of the whole material, resulting in a segregated material which cannot be shaped afterwards.

We thus consider such limit of filler amount (ϕ=0.65) as the maximum packing fraction of solids (ϕ_m) which the matrix is able to incorporate under these conditions. Fig. 1(a) also shows a striped zone which was considered as the zone-of no adhesion in which the material is no longer processable or shaped.

Fig. 1(b) shows the comparison between formulations ferrite/PP (hF) and ferrite/dispersant/PP (hF+D). From this figure, it is clear that dispersant agent aids the processability of these highly filled materials, by decreasing the torque and thus the energy required to perform the blending. It can be also observed that, ϕ_m was delayed from 0.65 to 0.7. This indicates, on the one hand, that particles-

particles interactions were reduced and on the other hand that, the addition of the dispersant had increased the wettability of the matrix. The latter is extremely important from an industrial point of view.

In Chapter 1, it was shown that ϕ_m depends on the characteristic of the particles (particles size distribution, aspect ratio), as well as on the process conditions. In this section, we can observe that ϕ_m does not only depend on such parameters but also depends on the species that can be adsorbed on the surface of the particles.

Fig. 2 shows the measured torque for samples filled with SF and LF. Similar observations were found which confirms our previous statements. As expected, LF-based composites showed a lower value of ϕ_m compared to SF filled composites.

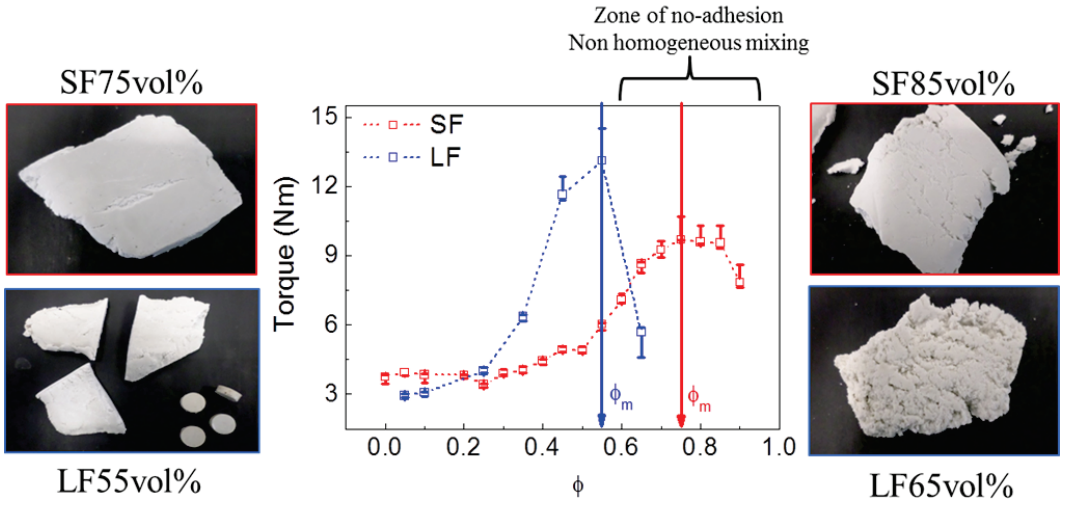


Fig. 2. Comparison between the last value of measured torque for SF and LF-based composites. Error bars represent the minimum and the maximum value of torque during the last two minutes of the mixing.

Table I presents the measured maximum packing fraction and the estimated ϕ_m for all the composites studied here. It is worth noting that, the composite which reached the highest ϕ_m was the SF-based composite. This is in contrast to what has been shown in Chapter 1. From literature, we know that the higher the aspect ratio is, the lower the value of ϕ_m is. However, this statement does not take into account the possible orientation that the particles may adopt during the mixing. Fibers may definitely align in the shear flow which may lead, for instance, to hexagonal close-packed structures. It is also important to remark that the calculated ϕ_m=bulk/true densities, well predicts the measured ϕ_m for the ferrite systems, while underestimate the fibers ϕ_m values. This is again due to the preferential orientation of the fibers in the mixing chamber. Moreover, the bulk density is a very important process indicator. The higher is the bulk density, the higher is maximum packing fraction of solids.

Table I. Maximum packing fraction and percolation thresholds measured in this work.

Composite	p	ϕ_m	***Estimated ϕ_m**	**Bulk density (g/cm^3)**	**True density (g/cm^3)**
ferrite/PP	0.25	0.65	0.72	3.2	4.5
ferrite/dispersant/PP		0.70			
SF	8.1	0.75	0.44	1.2	2.7
LF	9.3	0.55	0.24	0.65	2.7

ϕ_m=bulk density/true density

Conclusions and Outlooks

The aims of this thesis were to investigate from dynamic and capillary rheology experiments the flow behavior and the structural variations in highly filled polymers. This work was focused on two distinct anisometric fillers: oblate ferrite particles and prolate short-glass fibers. However, since the theory is general, the concepts clarified in this work are likewise relevant to other filled materials.

Therefore, the flow of ferrite particles dispersed in polypropylene and short-glass fibers dispersed in the same matrix were systematically investigated.

On the one hand, ferrite/polypropylene composites were studied under dynamic and steady state flows. Under dynamic flows, ferrite/PP composites showed a non-stable behavior which was manifested by an increasing of the storage modulus over time at very low deformations. We demonstrated that the shear external forces strongly affect such behavior. The higher the shear external force, the lower was the structuring for those materials. We also studied the effect of the addition of a dispersant agent (12-hydroxystearic acid) into the formulation. We found that this amphiphilic molecule was able to diffuse and be adsorbed onto the surface of the particles, leading to a decrease of the particle-particle interactions.

Under steady state flows, the rheological behavior of the composites filled with 10 to 40 vol% was studied. The steady state viscosity did not present any evidence of changes in the microstructure over time. Wall slip contribution was negligible in the present study as proved by the conventional Mooney method. The flow curves obtained by capillary results showed smaller differences between the composites compared to the results obtained by dynamic rotational flows. However, the steady state results led to other interesting observations. Three distinct zones were observed in the flow curves. Low, moderate and high shear rates promote different microstructures. At low shear rates, the particles interactions lead to the formation of a network structure as proved by the divergence of the zero shear viscosity. At moderate shear rates, the interactions between the particles are broken down and the particulate phase contribution is less observed. Finally, at high shear rates, an attenuation on the shear-thinning behavior was evidenced, which is in contrast to what is generally shown in the literature. This has been attributed to the fact that, particles may form local clusters which restrict the flow. Thus particles-particles interactions become dominant again, leading one more time to the divergence of the shear viscosity. When adding the fatty acid, similar trends were found. For the highest filled composite (40 vol%), the addition of the fatty acid decreases the shear viscosity in all the range of

shear rates. This confirms the ability of this compound to decrease the interparticle interactions, resulting in a lubricant effect between the charges.

On the other hand, short glass fibers composites were studied under dynamic conditions. The effect of particle size distribution, aspect ratio and sizing on dynamic flow properties has been investigated. Two commercial milled fibers were the object of this study. They presented similar particle size distribution, however, a very distinct flow behavior was found for both types of composites. Such a different behavior was attributed to the little population of large particles presented in the LF-based composites. Thus, large particles, even at low quantities change the rheological behavior to large extent. We also demonstrated that larger aspect ratio, lower interparticle distance and better interparticle interactions promoted the creation of a fiber network. As a side result, we found that burning the fibers decreases the interparticle interactions and thus the probability to create a network is also decreased. In addition, the flow behavior was determined by the fiber content. Thus, we investigate the relation between concentration transitions and the flow transitions. The latter has been neither well investigated nor well understood in the literature. We found that the transition from semi-dilute to concentrated regimes correspond to the shift of the moduli to higher values, while keeping the same shape in the flow curve behavior ($\phi \sim 0.1$). Concentrated isotropic to nematic transition was found to occur near the percolation threshold of the fibers. The percolation limit was found to be lower for LF (ϕ_c=0.3) than for SF (ϕ_c=0.46) due to the higher aspect ratio of LF.

We also proposed an original method to quantify the maximum packing of solids for these polymer-based composites. In Chapter 1, we showed from the open literature that the maximum packing of solids depends on the characteristic of the particles (particles size distribution, aspect ratio), as well as on the process conditions. However, we demonstrated that ϕ_m does not only depend on such parameters but also depends on the species that can be adsorbed on the surface of the particles.

Our research was motivated by the close relationship between the nature of the flow and the structure. We covered the most important aspects to take into account when considering the flow of such complex materials. This work showed that each system of study was very different, however, common tools and approaches come together to evaluate the behavior of highly filled polymers.

From an industrial point of view, the mixing process constitutes the biggest challenge in this material field. Mastering the mixing process is the key to obtain the better dispersion and thus better final properties. Several strategies can be considered to improve such step such as finding the best compromise in the particle size distribution, adding a dispersant agent, a sacrificial phase, using micro-sized particles and optimizing the matrix viscosity and its affinity with the particulate phase.

From a scientific point of view, the evaluation of the rheological properties of filled polymers reveals a large number of interesting phenomena which can vary according to the nature of the filler and the matrix. An experimental approach is therefore necessary to establish these physical trends which can be described by a phenomenological description. The main goal is to be able to predict a rheological behavior from parameters related to the physical interactions. For this purpose, the formulation of robust mathematical models that take into account the effect of the

nature of particles, shape factors and size distributions on the viscosity of the mixture is an indispensable task to look forward in future works. Therefore, using simulation to create such a table of multiple factors is a valid option. We strongly believe that future simulation works, based on experiments and models will be able to target material properties by using a data base of characteristics of the ingredients of the mixture.